ELECTRICAL AND MAGNETIC CHARACTERISATION OF A SERIES OF TCNQ SALTS

GRAHAM HUGH CROSS

BSc GRSC

SHEFFIELD CITY POLYTECHNIC

Collaborating Establishment; I.C.I Corporate Laboratory Runcorn

Submitted to the CNAA in partial fulfilment of the requirements for the award of the degree of Doctor of Philosophy

APRIL 1985

ACKNOWLEDGMENTS

I am sincerely grateful for the constant guidance and encouragement throughout this project by my Director of Studies, Dr. G.J.Ashwell and for the helpful and enjoyable discussions with my external supervisor, Mr. J.G.Allen of the ICI Corporate Laboratories, Runcorn.

I am indebted also to my parents who have supported me in every conceivable way throughout this time.

The typing of the original manuscript of this thesis was undertaken boldly and with skill by Miss J.P.D.Hewes to whom I extend many thanks and thanks also for allowing me almost exclusive use of the word processor.

Thank you D.A.S. for your patience with this thesis and for convincing me I could finish it.

ABSTRACT

The electrical and magnetic properties of a series of 12 isostructural TCNQ salts of bis-pyridinium cations are reported and these properties are related to the structural characteristics. The role of the cation lattice in stabilising a regular TCNQ stack in these salts is discussed. For comparison with this series, the electrical and magnetic properties of two TCNQ salts of bis-pyridinium cations with ordered structures and two salts of dialkyldiphenylphosphonium cations are reported.

Within the isostructural series of salts, the stoichiometry takes values of between 1:3 and 1:5, and the cation length determines the stoichiometry. In all these salts, the hydrated cation lattice is disordered and the TCNQs stack in regular columns. The room temperature conductivities, measured along the stacking axis, are in the range Ø.Ø5 to 5ØØ S/cm with the highest conductivities observed in dehydrated salts having the approximate stoichiometry, 1:4.5. The 1:5 salts possess the lowest conductivity of the series and in these salts the cation lattice is partially ordered. The 1:3 and 1:4 salts are small band gap semi-conductors whereas the conductivity of the 1:5 salts is not simply activated within the experimental range of temperatures. In these salts the conductivity obeys the empirical power law:

$$\sigma = AT^n \quad \text{where} \quad 4 > n < 7$$

The temperature dependence of the magnetic susceptibility of all but the 1:3 salts of the isostructural series is characteristic of a system of partially localised triplet excitons. The magnitude of the singlet-triplet exchange energy exhibits a stoichiometric dependence and is lower in the 1:5 salts where the spin concentration is lower. The magnetic susceptibility of the 1:3 salts varies with temperature according to the Curie-Weiss law:

$$\chi = C/(T + \theta)$$

The apparent low spin concentration supports the evidence found for alloy formation in these salts where the cation lattice is partially occupied by neutral or monoquaternised base.

CONTENTS

I INTRODUCTION

1.1: HISTORICAL PROGRESS

Interest in organic materials as being potentially highly conductive began in the late 1950s. Previously the materials studied for their electrical properties were mainly of biological interest such as DNA[1] or the fused ring hydrocarbons, and in particular, anthracene[2]. These systems are insulators or at best wide band gap semi-conductors and exhibit activation energies of a few eV. In 1960, however, Acker[3] reported the results of a study on a series of simple ionic and mixed valence salts of the newly synthesized electron acceptor tetracyano-p-quinodimethane (TCNQ) with a variety of cations.

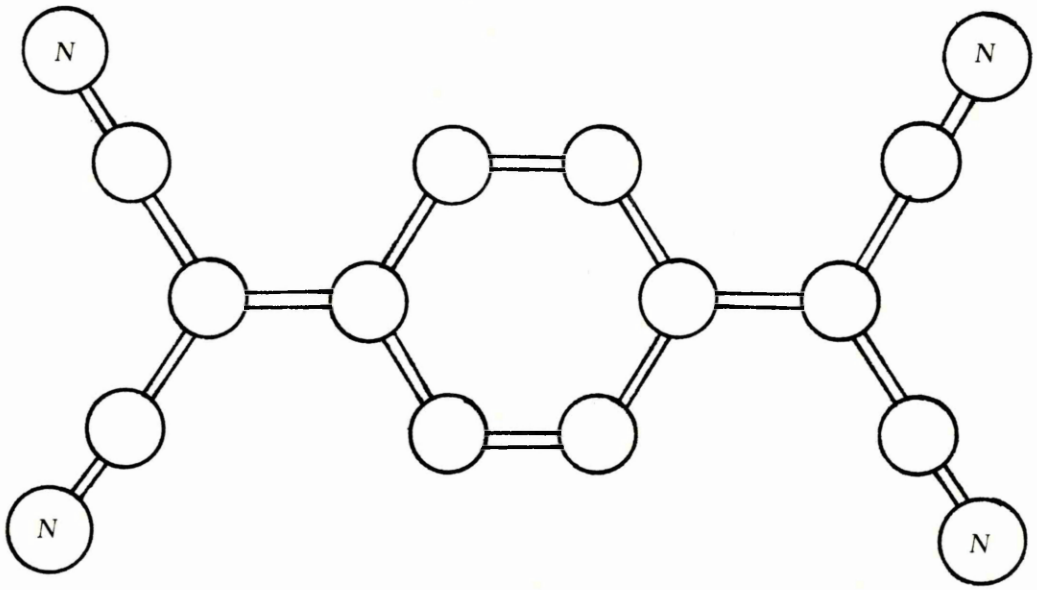

Fig.1.1 TCNQ owes its high electron affinity in part to the planarity of the molecule and in part to the quinone structure and to the electron - withdrawing cyano groups.

These salts have conductivities which span several orders of magnitude[3-6] and the values are dependent upon the stoichiometry and the stacking characteristics.

The simple salts are of the form $M^+(TCNQ)^-$, where M^+ is the cation, and, in general, these salts are of low conductivity. For example, the alkali metal TCNQ salts, Na^+TCNQ^- and K^+TCNQ^- have room temperature conductivities[4] of 10^{-6} and 10^{-4} Scm^{-1} respectively.

The mixed valence salts are of the form $M^+(TCNQ)_n^-$ where $n>1$. The common stoichiometry is 1:2 but n may take values as high as 5. Among the early examples of mixed-valence salts, quinolinium $TCNQ_2$, $Qn(TCNQ)_2$, was found to be highly conductive with $\sigma_{R.T.} = 100$ Scm^{-1}. In addition, the temperature dependence of the conductivity at high temperature was characteristically metallic. A study of the magnetic properties revealed that $Qn(TCNQ)_2$ exhibited a nearly temperature independent paramagnetic susceptibility within the range 300 to 50K[7]. This was ascribed to Pauli paramagnetism, characteristic of a degenerate electron gas.

Similar electrical properties have been observed for the 1:1 salt, N-methylphenazinium-TCNQ, NMP-TCNQ which has a room temperature conductivity of between 100 and 400 Scm^{-1}. It remains metallic down to 200K, at which point it undergoes a smooth metal-to-insulator transition. In fact, NMP salts of TCNQ may be formed as any one of three different phases, one metallic[8] with a stoichiometry of 1:1, possessing segregated

regular stacks and the other two semiconductive[9,40], one with a stoichiometry of 2:3 consisting of segregated distorted stacks[9], the other possessing mixed stacks of donor and acceptor[40](in this latter salt the nitrogen of the donor para to the N-Me group is protonated). The differences in TCNQ stacking are largely responsible for this diversity in behaviour.

For high conductivity it is necessary for the molecules involved in the conduction process to stack in infinite columns with a favourable overlap and an interplanar spacing shorter than the van der Waals distance. These features will be discussed later. The crystal structure of $Qn(TCNQ)_2$ as determined by Kobayashi et al.[10] shows the TCNQ lattice to be of this type and the high conductivity may be in part attributed to these favourable structural characteristics. The crystal structure of the semi-conductive NMP_2TCNQ_3 salt determined by Santz & Daly[9], reveals the conductive lattice to consist of isolated TCNQ triads whereas the metallic form consists of segregated, uniform stacks of TCNQ and NMP.

It is convenient at this stage to introduce a classification for the stacking characteristics introduced by Dahm et al.[11] which will be referred to later when describing the other systems. In this scheme, those structures in which molecules stack in segregated columns are termed "homosoric", those in which different molecules stack alternately "heterosoric" and those which are non-stacked, "non-soric". Thus the metallic form of NMP-TCNQ is homosoric and the mixed stack

semiconductive form is heterosoric. Although this classification may be used to describe the majority of systems, Ashwell et al.[12] later introduced the term "pseudosoric" to describe those systems in which the TCNQs stack in stoichiometric groups, such as triads, tetrads or pentads, but between each group there is no direct plane-to-plane overlap. The structure of the semiconductive 2:3 salt of NMP may be classed as pseudosoric.

These early studies revealed that high conductivity was possible in organic systems provided that (i) the mean charge on the TCNQ sites is non-integral and (ii) that the stacking is homosoric with favourable overlap and a short uniform spacing.

The suggestion of superconductivity in organic conductors was made in a theoretical paper by Little[13] in 1964. In spite of the fact that there was no experimental evidence to support these ideas, the arguments were convincing enough to generate a new effort in the field towards this goal.

In 1973 Ferraris et al.[14] and others[15] reported the first of a new series of highly conductive quasi-one-dimensional organic conductors. The material was a 1:1 complex formed between tetrathiafulvalene (TTF) as the electron donor and TCNQ as the acceptor. In this salt the degree of charge transfer from donor to acceptor[16] is Ø.59 e. TTF-TCNQ has a room temperature conductivity of between 2ØØ and 6ØØ Scm^{-1}, measured along the direction of stacking, which rises to a

maximum at 58 K. At this temperature it undergoes a transition to an insulating state. Many TTF derivatives have been synthesized and the TCNQ complexes were prepared with the aim of enhancing the conductivity further. In Table 1.1 the electrical and structural properties of some of the metallic and semiconductive charge transfer complexes are summarised. The relationship between structural and electrical properties are discussed in detail at a later stage but as an initial observation it is clear from Table 1.1 that these highly conductive charge transfer complexes have in common a structure consisting of segregated uniform stacks with a short interplanar spacing. It is likely that conduction occurs along both stacks. The majority of complexes listed are metallic but undergo metal-to-insulator transitions at some temperature between 20 and 100 K. An exception is the HMTSeF-TCNQ salt which remains highly conductive to below 1 K but even so it exhibits a decrease in conductivity at about 40 K.

The first successful stabilisation of a low temperature metallic state in organic materials was in the single chain conductor[51-53] $[DEPE][TCNQ]_{4.5}(H_2O)x$. This salt was previously reported to have a stoichiometry of 1:4 but this is now known to be erroneous. This complex salt exists in two forms, a hydrated form where x = 1, which is semiconductive and exhibits a conductor to insulator transition at 40 K, the other, a dehydrated form which remains metallic to below 0.03 K. The isostoichiometric and

SALT	$\sigma_{R.T.}(Scm^{-1})$	E_A(eV)	M-I(K)$^+$	A-A(A)*	D-D(A)*	A-D(A)*	Reference
TTF-TCNQ	200-600	0	58	3.17	3.47	3.2(S-N)	14,17-19
TSF-TCNQ	1000	0	40	3.21	3.52	3.16(Se-N)	20
TMTTF-TCNQ	350	0	34	3.27	3.53	3.45(S-N)	21,22
TMTSF-TCNQ	1000	0	57	3.26	3.60	3.36(Se-N)	23,24
HMTTF-TCNQ	400	0	50	3.23	3.57	3.25(S-N)	25
HMTSF-TCNQ	1500	0	-	3.20	3.6	3.1(Se-N)	26,27
TMTTF-DMTCNQ	120	0	51	-	-	-	28
TMTSF-DMTCNQ	300	0	50	3.31	3.64	3.48(Se-N)	29
HMTSF-TNAP	2500	0	47	-	-	-	30
TTT-$TCNQ_2$	100	0	90	3.18	3.52	-	31
t-TTF-TCNQ	200-400	0	81	3.2	3.58	3.11	32
MeEt-t-TTF-TCNQ	90	0	95	3.22	3.58	-	32
HMTTF-$TCNQF_4$	10^{-4}	0.21	-	3.27	3.62	3.42(S-N)	33
TMPD-$TCNQ_2$	2	0.14-0.1	-	-	-	-	34,35

TABLE1.1

The electrical and structural properties of some charge transfer salts of TCNQ and TCNQ derivatives with various open shell donors.

* A-A, D-D and A-D refer to inter-acceptor spacing, inter-donor spacing and to the shortest inter-stack (acceptor-donor) spacing, respectively.

\+ Metal-Insulator transition temperature.

isostructural salt [DEPA][TCNQ]$_{4.5}$(H_2O)x was later also shown to exhibit similar low-temperature metallic behaviour. The possible causes of this stabilisation will be discussed later, but as a general observation at this stage, the low temperature metallic state depends upon the retention of a uniform stack of TCNQ with short inter-site spacing. The two salts [DEPE][TCNQ]$_{4.5}$(H_2O)x and [DEPA][TCNQ]$_{4.5}$(H_2O)x are both examples of mixed valence TCNQ salts relying for conduction on a single chain. In Table 1.2 the properties of a number of TCNQ salts are listed in which the conductivity occurs predominantly along the TCNQ lattice. Differences in the conductivities might be ascribed to differences in the stacking characteristics and to differences in the mean charge on the TCNQ sites. These considerations are discussed in section 1.2.

Stabilisation of the metallic state at low temperatures has also been achieved when salts are subjected to moderate hydrostatic pressures. For example, in TMTSF-DMTCNQ, the metal to insulator transition which occurs at 5Ø K at ambient pressure[29] is suppressed when P > 1Ø kbar[95,96]. This material is of interest since it was found to be a predominantly single chain conductor with conduction occurring mainly along the TMTSF stack[96]. The room temperature thermopower has been determined to be[95] +11 μV/K in accordance with majority hole conduction.

TABLE 1.2

SALT	$\sigma_{R.T.}$ (Scm^{-1})	E_A (eV) (T range)	TCNQ lattice *	Reference
Salts with homosoric structures				
$Ad(TCNQ)_2$	100	0(300-140K)	Regular stack R/B o/lap d = 3.24	36, 49
$BAd_2(TCNQ)_3$			Regular stack	37
$Qn(TCNQ)_2$	100	0(300-200K)	Regular stack with R/B o/lap d = 3.2	3, 4, 10
NMP TCNQ (I)	140	0(300-200K)	Regular stack with R/B o/lap d = 3.241	5,8,38,39,110
$NPrQn(TCNQ)_2$	10		Distorted regular stack	111
$MEM(TCNQ)_2$	20	0(T>340K)	Regular stack with distorted O/lap (T>340K)	41
$Morph._2(TCNQ)_3$	0.2×10^{-3}		No R/B o/lap every third TCNQ as $NMP_2(TCNQ)_3$	42,4
$NEQn(TCNQ)_2$(I)	0.13(c)		Distorted regular stack with R/B o/lap	37,4
Ammonium TCNQ (II)	10^{-2}	0.21	Monads R/B o/lap d = 3.31	64
$Tetraethylammonium(TCNQ)_2$	0.5×10^{-4}(c)		As for $MEM(TCNQ)_2$	74,4

$TEA(TCNQ)_2$	6.5	0.09 (300-250K)	Pseudo regular stack	5, 45, 46
$TMPD(TCNQ)_2$	2		Regular stack d = 3.241	35
$NMAd(TCNQ)_2$	100	<0.01 (300-150K)	As $Ad(TCNQ)_2$	48, 49
N-ethyl-2-methylthiazolinium $(TCNQ)_2$			Distorted regular stack	50
$DEPE(TCNQ)_{4.5}(H_2O)x$	50-500	0(300-0.03K)	Regular stack d = 3.2	51-53
$DEPA(TCNQ)_{4.5}(H_2O)x$	100-500	0(300-10K)	As for $DEPE(TCNQ)_{4.5}(H_2O)x$	54, 55
$Me_2Ph_2P(TCNQ)_2$	0.05	0.2	Pseudo regular stack d = 3.28 (evidence of low-T distortion)	56
Na TCNQ (353K)	10^{-4}		Regular stack but no R/B o/lap d = 3.39	57,4
K TCNQ (T>298K)	0.2×10^{-3}		Regular stack with R/B o/lap	58,4
Rb TCNQ (II)	10^{-2}	0.16 - 0.19	Regular stack R/B o/lap d = 3.43	59, 60
Rb TCNQ (III)			As for (II) but d = 3.33	61
$Cs_2(TCNQ)_3$	10^{-3}	0.3	No R/B o/lap every third TCNQ	62, 186
$Rb_2(TCNQ)_3$(294K)			Isostructural with $Cs_2(TCNQ)_3$	63

N-methyl-N-ethyl benzimidazolium $(TCNQ)_2$(<100K)	24	0.09 (300-250K)	Pseudo regular stack, but Dimers below 100K where d = 3.28	75-77
Salts with Pseudosoric Structures				
$TMA_2(TCNQ)_3$	10^{-4}		Monads and diads alternating along b	65
3,3'-diethylthiacyanine TCNQ			Dimers Inter and intra-molecular R/B o/lap d = 3.23	66
3,3'-diethylthiacarbocyanine $(TCNQ)_2$			Dimers with distorted R/B o/lap	67
3,3'-diethylthiazolinecarbocyanine $(TCNQ)_2$	$6x10^{-4}$	0.21	Dimers R/B o/lap d = 3.11	68
N,N'-dimethyl-benzimidazolium $(TCNQ)_2$			Dimers R/B o/lap d = 3.5; inter dimer o/lap is "tail-to-tail"	70
$DMM(TCNQ)_2$			Dimers no R/B o/lap between TCNQs within the dimer	71
Morph. TCNQ	10^{-9}		As for $DMM(TCNQ)_2$ d = 3.28	72
N-methylphenanthrolinium $(TCNQ)_2$			Dimers R/B o/lap d = 3.03 (shortest spacing known)	37
$MEM(TCNQ)_2$ (T<340K)	20	0.6	Dimers form below 340K	42,173

$DEM(TCNQ)_2$			Dimers Two crystallographically independent sheets of TCNQ	74
Na TCNQ (298K)	10^{-6}	0.041-0.34 (300-100K)	Dimers no R/B o/lap d = 3.21	78, 79
$DHPA(TCNQ)_2$	10^{-7}		Dimers R/B o/lap d = 3.04	94
K TCNQ (<298K)			Dimerized stack with ring/ring o/lap	80
Rb TCNQ(I)(294-113K)	10^{-5}	0.4-0.5	Dimers with no R/B o/lap d = 3.16	81,74
$NMePy(TCNQ)_2$	2.07	0.35	Dimers d = 3.2	83, 84
1,1'-ethylene-2,2'-bipyridinium $(TCNQ)_2$			Two crystallographically independent dimers R/B o/lap d=3.22, 3.26 Inter dimer o/lap is "tail-to-tail"	86
$(NMP)_2(TCNQ)_3$			Triads with no R/B o/lap every third TCNQ	40, 9
Methyltriphenylammonium$(TCNQ)_2$			Tetramers R/B o/lap d = 3.2	87
$MePh_3P(TCNQ)_2$	10^{-3}	0.42 (T<314K)	Tetramers R/B o/lap d = 3.24 (294K), 3.32(326K)	88, 92
N,N'-dibenzyl-4,4'-bipyridinium			Tetramers R/B o/lap	89

1,2-di(N-benzyl-4-pyridinium)-ethane$(TCNQ)_5$	0.03		Pentamers	Cations 'end-to-end' o/lap to form "polymolecule"	90
1,2-di(N-benzyl-4-pyridinium)-ethylene$(TCNQ)_5$	0.1-0.01		Pentamers	Cations 'end-to-end' o/lap to form "polymolecule"	91
1,1'-bis-(p-cyanophenyl) 4,4'-bipyridinium$(TCNQ)_4$	0.1	0.1	Tetramers	inter tetramer R/B o/lap	93

TABLE 1.2

The electrical and structural properties of complex mixed valance and simple radical anion salts of TCNQ.

* Notes:

R/B represents the ring/bond overlap of neighbouring TCNQs in the stack (see Fig. 1.2)

d represents the plane-to-plane spacing (A) of the nearest neighbouring TCNQs.

(c) represents powder compaction conductivity.

Bechgaard[97] has studied a series of highly conductive salts of TMTSF of general formula $[TMTSF]_2X$, where X is, for example, PF_6^-, AsF_6^-, SbF_6^-, BF_4^- and NO_3^-.
At ambient pressures these all have high conductivities (σ_{RT} = 500 to 800 Scm^{-1}) and metallic temperature dependences to below 100 K. The series is isostructural and is characterised by uniform donor stacks, arranged in sheets and interleaved by the counter ions. At moderate pressures several of the series were found to superconduct [98-101]. Jerome et al.[98] first reported a superconducting transition at 0.9 K in $(TMTSF)_2 PF_6$ at 12 kbar. Confirmation that the material possessed bulk superconductivity came from the observation of flux expulsion due to the Meissner effect at temperatures below 1 K and a pressure of 12 kbar[102]. The properties of the TMTSF and other radical cation salts are given in Table 1.3.

Among the salts in the $[TMTSF]_2X$ series, the perchlorate was found to superconduct at ambient pressure and at a temperature of 1.2 K. Bechgaard et al.[103] has suggested that the use of the smaller counter ion mimics the effect of pressure necessary for superconductivity in the PF_6 salt. The greatest change in the TMTSF lattice dimensions which results from increasing the anion size from ClO_4, the smallest anion in the series, to TaF_6, the largest, is in the separation of the TMTSF sheets, the c direction. The parameters a and b vary by less than 0.1% whereas c increases with increasing anion size by about 5%[108]. Thus the

TABLE 1.3

SALT	$\sigma_{R.T.}(Scm^{-1})$	M-I(K)	$T_c^*(K)$	Reference
$(TMTSF)_2PF_6$	540	19	0.9 (12kbar)	97,98,107
$(TMTSF)_2ClO_4$		-	1.2 (1bar)	103,107
$(TMTSF)_2AsF_6$	430	15	1.1 (12kbar)	97,99
$(TMTSF)_2SbF_6$	500	17	0.38 (10.5kbar)	100
$(TMTSF)_2TaF_6$		-	1.35 (<11kbar)	100
$(TMTSF)_2BF_4$	540	39	X	97
$(TMTSF)_2NO_3$	780	12	X	97
$(TMTSF)_2FeSO_3$		87	>2 (5kbar)	101,104
$(BEDT\text{-}TTF)_4(ReO_4)_2$	200	81	<2 (4kbar)	106

Table 1.3 : Electrical properties of some radical cation salts.

*superconducting transition temperature

superconducting transition temperature depends in part on the degree of inter-stack coupling which, in turn, depends on the inter-chain separation. The salt $(TMTSF)_2TaF_6$ requires a minimum pressure of 9 kbar to induce a three dimensional superconducting state at 1.35 K. The inference is[136] that the c axis compresses according to 0.5 $\%kbar^{-1}$ to reach an inter-chain separation, at 9 kbar, equivalent to that in $(TMTSF)_2ClO_4$ which becomes superconducting at 1.2 K at ambient pressure. This pressure induced c-axis compression would agree well with values ranging from 0.5 to 0.27 $\%kbar^{-1}$ measured previously for TTF-TCNQ.[136]

More recently, a new series of organic conductors have been found to be superconductive. These are based on the sulphur-donor molecule, bis-(ethylenedithiolo) tetrathiofulvalene, BEDT-TTF[106]. The salt $[BEDT\text{-}TTF]_4\ (ReO_4)_2$ undergoes a metal-to-superconductor transition at about 2 K and a pressure of 4 kbar, whereas at ambient pressure, the material is an insulator below 81 K. The salt $[BEDT\text{-}TTF]_2I_3$ has recently been shown to be superconductive at ambient pressure[85]. The transition to a superconductive state occurs at 1.4 to 1.5 K. The metal-to-insulator transition in the ReO_4 salt is thought to arise as a result of anion ordering. In the case of a non-centro-symmetric anion such as ReO_4^- there is the possibility of alternate ordering which would give rise to a periodicity of the electron potential and the opening of a gap at the Fermi level. The use of centro-symmetric anions such as PF_6^- or AsF_6^- may result in superconductors of

BEDT-TTF with higher critical temperatures[106].

Since the discovery of the first conductive organic systems based upon TCNQ, there have been many hundreds of salts prepared having segregated stacks. Of these, however, only a relatively small percentage have appreciably high conductivity and metallic character. The major unifying features of these salts have been established and will be discussed in the following sections. The structural and chemical requirements are reviewed as are some conduction mechanisms and the special conditions imposed by the inherent one-dimensionality are discussed. The magnetic properties are discussed in Section 1.3.

1.2 : Electrical Conductivity.

The organic conductors may be classified in a general way into three groups: (I) the simple ionic salts and charge transfer complexes with a neutral or ionic ground state, and a low conductivity ($\sigma_{R.T.} < 10^{-4}$ Scm^{-1}) and a wide band gap; (II) the mixed valence salts with intermediate conductivity of 10^{-4} to 10 Scm^{-1} at room temperature and (III) materials with a high conductivity and metallic temperature dependence.

There are inevitably exceptions to this scheme but for the majority of materials the classification can be made. By looking for certain unifying features in the chemical and physical properties, an understanding can develop of the relationship between the electrical, magnetic and structural properties. In Sections 1.2.1 to 1.3.3 these are reviewed.

1.2.1: Structure.

The fundamental requirement of the structure of an organic conductor is that the molecules are arranged to form a suitable conduction pathway. This is usually provided by planar molecules forming regular stacks to allow charge transport along the columns under the influence of an applied field.

In the case of two chain conductors, such as the charge transfer salts of Table 1.1, the contribution to the conductivity is from electron and hole transport along the anion and cation stacks, respectively. The bis-pyridinium

TCNQ salts, which are discussed in this work, rely for conduction on charge transport along the TCNQ stacks only. An example of a highly conductive salt in which the conduction arises primarily on the TCNQ stack, is NMP-TCNQ. The structure of the highly conductive form of this salt[110] consists of segregated stacks of NMP and TCNQ moieties. The TCNQs stack in uniform columns with a short interplanar spacing of 3.26 Å. The overlap between adjacent TCNQs is of an exocyclic double bond-to-ring type, illustrated in Figure 1.2, providing favourable π orbital overlap.

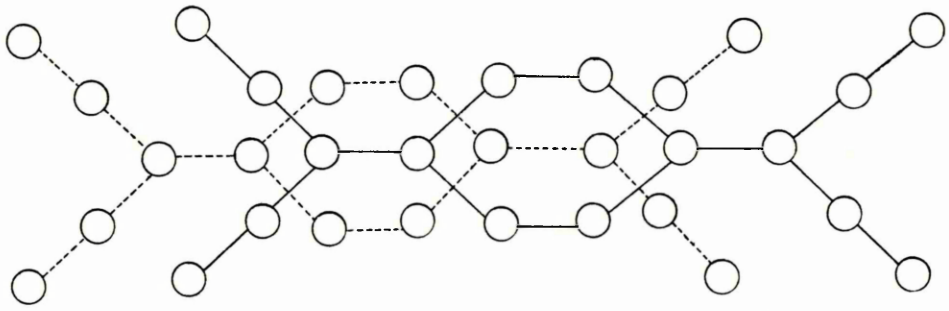

Figure 1.2: Exocyclic double bond-to-ring overlap of adjacent TCNQs.

The optimum interplanar separation is 3.2 +/- Ø.1 Å and reference to the parameter 'A-A' in Table 1.1 shows that all the highly conductive salts possess a TCNQ separation which is comparable to this value.

In the two chain conductors, an analogous arrangement of molecules arises for the cation species. The sulphur-donor or selenium-donor molecules also stack regularly in columns with a short interplanar spacing and ring/bond overlap.

In TTF TCNQ[19], the inter-TTF and inter-TCNQ spacings are 3.47 Å and 3.17 Å respectively. The TTF overlap is as illustrated in Figure 1.3 and the TCNQ overlap is of the ring to external double bond type.

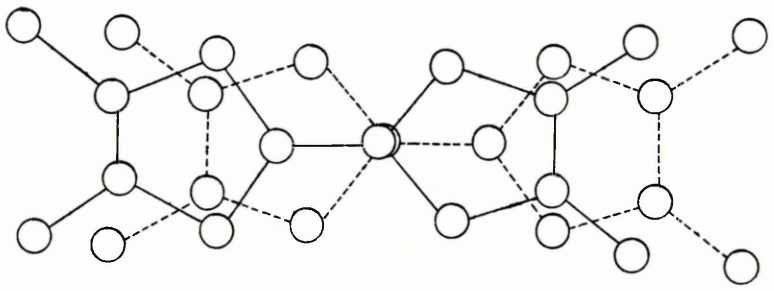

Figure 1.3: Ring/bond overlap of adjacent TTF molecules.

Analogous overlaps occur in the corresponding selenium-donor congeneric salts with an attendant increase in the separation.

Table 1.1 (Section 1.1) lists a series of highly conductive charge transfer complexes some of which are isostructural with TTF-TCNQ. In these salts the structure is characterised by segregated anion and cation stacks. Dahm et al.[11] describes infinite stacking of like species as homosoric but subdivides such systems into classes where the stacks may consist of diads, triads, tetrads or higher groupings. Between these groups, there is a discontinuity of the regular short spacing which generally results in a lower conductivity. Some examples of homosoric structures with such groupings are given in Table 1.2 and are listed among the pseudosoric salts.

The majority of systems that may be classified in groups II and III (moderate to high conductivity) possess either homosoric or pseudoric structures.

Two other types of structure where the molecules are either stacked alternately (heterosoric) or do not form columns (nonsoric) are also described by Dahm et.al.[11]. The periodic change in potential in the heterosoric complexes causes the materials to have low conductivities and the properties are characteristic of Group I. Examples of salts with heterosoric structures may be found in references 111-114 or in van Bodegom's thesis of reference 74.

The discussion of the structural features has so far been confined to a one dimensional description with no mention of the consideration of inter chain interactions. The importance of these will become apparent as the discussion progresses as will the importance of modifications to the molecular structures of the donor and acceptor species.

1.2.2: One Dimensional Effects.

The chain-like structures of the organic conductors leads to quasi-one-dimensional electrical and magnetic behaviour. There are normally strong interactions along the chains due to the intermolecular overlap, but weak transverse interaction. As a result, the electrical conductivity is highly anisotropic. The conductivity is often of the order

of a few hundred times greater parallel to the chains ($\sigma_{\parallel}$) than perpendicular ($\sigma_{\perp}$). As examples, if $\alpha = \sigma_{\parallel}/\sigma_{\perp}$; then α for TTF-TCNQ is 500 [115,116], for TMTSF-DMTCNQ 200[95], and for $[(Me(Ph_3)P][TCNQ]_2$ α = 450(ref.117). The degree of transverse conductivity depends greatly on the extent of interchain interactions. These have a direct effect on the critical temperature of the conductor-to-insulator transition which is observed in many one-dimensional systems.

Peierls[118] predicted that a one-dimensional metallic system was liable to undergo a periodic lattice distortion leading to a localisation of charge and an insulating state. The charge density in one dimension is coupled to the lattice modulation and condenses to form a charge density wave having wavelength equal to the lattice period and an amplitude proportional to the magnitude of coupling of the charges to the lattice sites.

In the classical picture of a one-dimensional metal [Fig. 1.4(a)][121] the overlap integral of electron wave functions (t) on neighbouring sites is large enough to form a conduction band of width 4t. In the tight binding model for one-dimensional conductors, the conduction band which results is as shown in Figure 1.4(b). The occupied states lie in the shaded region below E_F, the Fermi energy.

If n conduction electrons are present in the unit cell of lattice constant b (Fig. 1.4(a)), the Fermi wave vector of

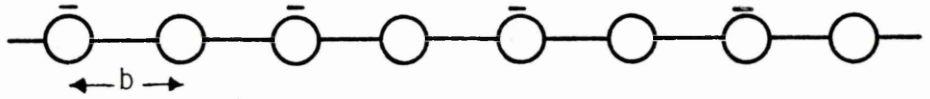

(a)

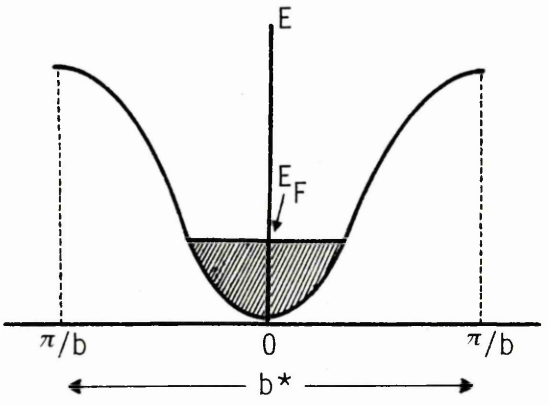

(b)

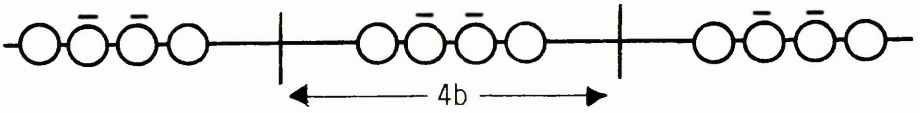

(c)

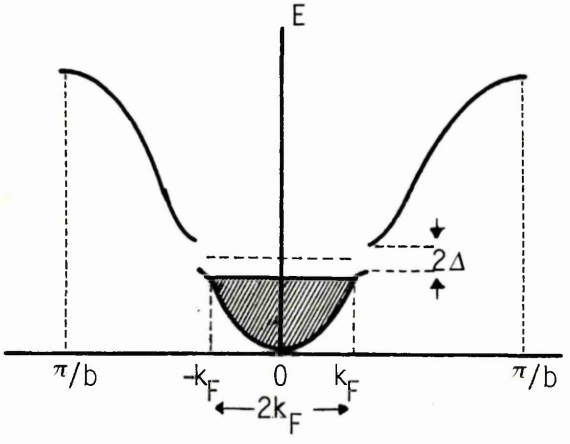

(d)

FIGURE 1.4 : Energy-wave vector diagram and stacking models of a quasi-one-dimensional conductor with uniform lattice and a $\frac{1}{4}$-filled conduction band[(a) and (b)] (c) and (d) denote a distortion of period 4b with a gap opening at the Fermi level.

the system of electrons within the band is given by

$$k_F = b^* n/4$$

Where b^* is the reciprocal lattice vector and is equal to $2\pi/b$. When n is 2, $k_F = \pi/b$ and the conduction band is full. However, when $n < 2$ the band is partially filled [Fig. 1.4(b)] and, if Coulomb interactions are neglected, metallic conduction may occur. At low temperatures many quasi-one-dimensional conductors undergo a lattice distortion with a loss of metallic behaviour. The distortion occurs with wave vector $2k_F$ [Fig. 1.4(d)].

There is an energy lowering of the electron system of which opens up a gap of 2Δ at the Fermi level. Classically this is illustrated in Figure 1.4(c). The lattice is modulated and the charge localisation on the lattice sites forms a charge density wave (CDW) with wavelength $2\pi /2k_F$.

The CDWs on neighbouring chains will be of opposite phase thus minimising the Coulomb interaction between regions of high charge density[122]. This phase ordering is found[123] below the transition temperature in, for example, the single chain one-dimensional conductors $K_2(CN)_4PtBr_{0.33}$ (refs.124,125) and in $K_2(CN)_4PtCl_{0.33}$ (refs.124,125).

Below the transition temperature the material exhibits an activated conductivity or, depending on the ratio $2\Delta/kT$, becomes insulating. There are numerous examples of this type of distortion and its attendant conductivity transition. Reference to Table 1.1 (Sec. 1.1) shows that the charge

transfer complexes based upon TTF and its analogues often exhibit a metal to insulator (M-I) transition at some temperature below 1ØØK.

The temperature at which the Peierls transition occurs is usually dependent upon the strength of the three dimensional couplings present. These may be due to the transverse overlap between wave functions on neighbouring chains or to direct Coulomb interaction between charge density waves. It would be expected that the greater the coupling the higher the transition temperature. This has been shown for a series of single conductive chain TCNQ salts studied by Coulon et al.[8Ø] The compounds consisted of TCNQ and I_3^- chains with quaternary ammonium cations. The cation size was progressively increased with a resultant increase in the separation of the TCNQ chains, confirmed in the X-ray structural analysis of the salts. A reduction of the M-I transition temperature was associated with a reduction in interchain coupling.

Disorder Stabilisation.

The metal to insulator transition temperature may also be reduced and in some cases smeared out completely by the introduction of disorder into the lattice. Since the Peierls modulation and condensation of the charge density wave depend upon commemurability, any disruption of this will inhibit the periodic ordering. There are a number of ways in which the degree of disorder may be modified.

Etemad et al.[86] have studied the effect on the M-I transition in TTF-TCNQ by doping with tetraselenafulvalene, TSF. The inclusion of TSF into the donor stack forms an alloy system with a random occupation by TTF and TSF of the lattice sites. The coupling of the donor chain to the TCNQ chain may now vary randomly in strength along the stacks due to the differences in the interstack S-N and Se-N contacts (see Table 1.1). The M-I transition in the alloy salts shifts to lower temperatures than in pure TTF-TCNQ (58K) reflecting the enhanced stabilisation against 3-dimensional ordering.

The effect of cation lattice disorder and solvent inclusion are thought to be responsible for the sample dependent electrical properties of the complex salt $[DEPE][TCNQ]_{4.5}(H_2O)_x$. These range from metallic to semiconductive. The semiconductive crystals undergo a semiconductor to insulator transition at 40 K whereas the conductivity of the metallic crystals increases monotonically upon cooling to at least 30 mK. The differences may be attributed to differences in the degree of cation disorder and the 40 K transition is thought to be due, in part, to an ordering of the cation lattice upon cooling. The role of the water is interesting because metallic behaviour has only been seen in crystals which have been dehydrated by vacuum annealing. Such crystals posses a contracted unit cell and increased cation disorder[127]. Also significant is the unusual stoichiometry of 1:4.5[128] and it is important to note that this cation to TCNQ ratio may vary slightly from a

commensurate value (see Table 3.1, p 86). In section 3.1, a series of twelve isostructural salts [129] formed between TCNQ and the diquaternised 1,2-bis-(4-pyridyl)ethylene, 1,2-bis-(4-pyridyl)ethane and 1,2-bis-(4-pyridyl)propane cations are discussed. For these the stoichiometry is dependent upon the cation length and varies from 1:3 to 1:5. Only the 1:4.5 salts have shown metallic properties.

Non-stoichiometry and anion disorder in the tetrathiotetracene, (TTT) salts,[130] $(TTT)_{1.1}Br_{0.5}$ and $(TTT)_{1.1}Br_{0.7}$, are important in stabilising metallic behaviour down to 30 K. The transition is suppressed at higher temperatures by the lack of long range ordering and thus by the long commensurability coupling period.

In the series of organic metals $(TMTSF)_2X$ where X = ReO_4, NO_3, PF_6, AsF_6, SbF_6, TaF_6 and $FeSO_3$, the metal - insulator transitions at ambient pressure arise as a result of anion ordering[137].

The presence of tetrahedral anions such as ReO_4^-, BF_4^-, and ClO_4^-, which possess no inversion symmetry, makes the conductivity sensitive to the degree of anion order[137].

As the lattice orders interchain coupling will ultimately result in a distortion of the quasi-one-dimensional conductive chains and a periodic distortion will cause a gap to open at the Fermi level with the loss of metallic behaviour[136]. In fact, anion ordering has been clearly

observed in $(TMTSF)_2ReO_4$ at 18Ø K, where it coincides with a metal - insulator transition[137]. $(TMTSF)_2BF_4$ also exhibits a relatively high transition temperature and it can be expected that anion alternate ordering occurs in this salt. Centrosymmetric anions such as PF_6^-, AsF_6^- and SbF_6^- cannot lead to this doubling in cell length upon ordering. The metal - insulator transitions of the TMTSF salts of these anions are below 2Ø K (see Table 1.3, p 14).

Radiation Induced Defects.

The introduction of radiation induced defects into a crystal can provide the disorder necessary to suppress charge or spin density wave condensation[131]. Both require coupling between neighbouring chains although a charge density wave coupling is a stronger interaction and is reflected by higher temperature metal - insulator transitions. Defects act to disturb the coherence needed for a transition to occur and thus the transition is smeared out and shifted to a lower temperature. The metal - insulator transitions in TTF-TCNQ and TMTSF-DMTCNQ (see Table 1.1, p 6) both result from CDW coupling and irradiation with X-rays produces shifts to lower temperature in the metal - insulator transition equivalent to 15ØK per % of defects for TTF-TCNQ[94] and 11ØK per % of defects for TMTSF-DMTCNQ[135]. In $(TMTSF)_2PF_6$, the metal - insulator transition is due to the formation of a spin density wave state[132,133]. The interstack interactions between SDWs, and the transitions which result from them, occur at lower temperatures. The effect of radiation induced

defects is to reduce the transition temperature by 50 K per % of defects[135].

Pressure Stabilisation.

The metallic state in TMTSF-DMTCNQ is stabilised[95,96,135] to below 90 mK by modest pressures of up to 13 kbar. Similarly, the metal - insulator transitions of the $(TMTSF)_2X$ salts are also suppressed (see Table 1.3, p 14) and transitions to a superconductive state have been observed[98-101,106].

In TMTSF-DMTCNQ the enhanced conductivity and suppression of the metal - insulator transition may arise from two possible effects. It is known that CDW condensation and interchain coupling are responsible for the transition, the CDW wavelength, $2k_F$, being commensurate with the lattice period. If the wavelength of the Peierls modulation can be varied under the influence of pressure, $2k_F$ may become incommensurate with the lattice period and the phase of the CDW may vary freely. This translational motion allows the charge density wave to carry a current under the influence of an electric field. This collective effect is known as the Fröhlich conductivity. It is a zero energy process characterised by being totally anisotropic and therefore contributes to the total longitudinal conductivity ($\sigma_{//}$). The remainder being composed of the longitudinal single particle contributions. Thus Jerome and Shultz[138] give the approximate relation;

$$\sigma_{//} = \sigma^F + \sigma_{//}^{sp}$$

where σ^F is the Fröhlich contribution and $\sigma_{//}^{sp}$ is the single particle contribution to the longitudinal conductivity.

The relevance of Fröhlich conduction to the present discussion is that the application of pressure may sufficiently modify the lattice in the direction of stacking in TMTSF-DMTCNQ to an incommensurate state where the CDWs are released. The experimental evidence which supports this proposal is the observation of an increase in the anisotropy at ambient temperature[95] of 25% as the pressure is increased from Ø to 13kbar. The increase in $\sigma_{//}$ reflecting the greater contribution from the de-pinned CDWs. By contrast, in TTF-TCNQ the anisotropy falls by about 25% as pressures up to 19kbar are applied[139] suggesting that the charge density wave is driven to commensurability. The metal-to-insulator transition temperature of TTF-TCNQ is increased[140] under these pressures.

An alternative explanation given by Andrieux et.al.[95] for the pressure enhanced conductivity in TMTSF-DMTCNQ is that there is a gradual development of superconductive fluctuations, the effects of which would be to override the Peierls transition. There is, however, no transition to a superconducting state within the experimental ranges of temperature and pressure.

The position remains unclear for TMTSF-DMTCNQ but there is evidence to support the latter hypothesis in the experimentally observed superconducting transitions in $(TMTSF)_2PF_6$ and related salts.

The superconductivity in these salts may be of the BCS type in which the electrons interact with lattice vibrations (phonons) to form attractively bound pairs. If so, the superconducting transition temperature would vary with the efficiency of the pair forming electron-phonon interaction. In $(TMTSF)_2PF_6$ the superconducting transition was initially found at 0.9K under 12kbar[98]. A subsequent study in which the pressure was reduced revealed a shift in the transition temperature of -0.08K/kbar[141]. The T_c depression could be explained[101] on BCS theory by a hardening of the phonon modes as the pressure is increased.

As mentioned already in Section 1.1, the value of T_c in the $(TMTSF)_2X$ series is related to the separation of the cation sheets. An increase in pressure modifies the lattice in this direction most markedly and suggests that the formation of superconducting pairs relies greatly on the magnitude of the interstack transfer integral.

1.2.3: Conduction.

In order to discuss the various conduction mechanisms in organic salts and compounds it is helpful to refer back to the three general classes of materials described in the introduction to Section 1.2. Classes II and III are of most interest in this work and the majority of materials studied here are semiconductors which belong to class II. Conduction depends upon charge transport along a linear chain of closely

packed molecules and the stacking arrangement results in anisotropic properties.

Many of the salts in Table 1.I such as TTF-TCNQ are examples in which conduction may occur in both the donor and the acceptor stacks and these salts are described as two-chain linear conductors. Many of the examples show metallic behaviour at high temperatures and upon cooling, a metal-to-insulator transition.

Coulomb Interactions and Charge Density

The discussions presented so far on the factors affecting conductivity have been limited to relating the lattice structure to the observed properties. Salts exhibiting high conductivity invariably possess closely packed homologous stacks of donors or acceptors. Salts with non stacked or non segregated stacked structures are generally poor conductors. Although this is a useful observation, the limitations it has as an explanation for the observed properties become apparent when considering certain Class I salts which have otherwise favourable structural characteristics. Examples are Na and Rb(PhaseII)-TCNQ [57,59,60], and HMTTF-$TCNQF_4$ [33] which have low conductivities although the TCNQ chains are uniform at least over part of the temperature range.

An explanation might be found in the consideration of the energetics of conduction for single particles in linear chain compounds. Electronic Coulomb interactions govern the ease with which carriers can migrate along the conductive chains.

This may be illustrated by recourse to a model of single particle hopping conduction in one dimension, which is shown schematically in figure 1.5 (overleaf). Each potential well represents a lattice site such as TCNQ and the conduction electrons reside, under zero applied field, in the lowest unoccupied energy levels. In the simple ionic salts [Figure 1.5(a) and (b)] it is necessary to place two electrons on the same TCNQ lattice site during the conduction process and the conductivity is limited by the high on-site electron-electron Coulomb repulsion energy. The difference, U, between the on-site electron-electron Coulomb repulsion energy (U_o) and the neighbouring site repulsion energy (V_1);

$$U = U_o - V_1 \quad \text{.....Eqn. 1.1}$$

is typically 1 eV for TCNQ salts. To overcome this problem, it is necessary to reduce the mean ionic charge on the lattice sites. This may be achieved by forming salts with a cation to TCNQ ratio greater than 1:1 (for example the complex TCNQ salts) or, in the 1:1 complexes, by selecting a suitable electron donor with an intermediate ionisation potential of 6 - 7 eV in order to obtain partial charge transfer. Many of the materials of Class II are complex mixed valence salts (where $\rho<1$) having a higher conductivity and a smaller activation energy than their corresponding simple ionic salts[4,148]. In such systems conduction may occur without the need to place two electrons on the same lattice site [see Figure 1.5(c) and (d)]. Torrance[144] has proposed that the Coulomb interactions (U_o and V_1) are the dominant

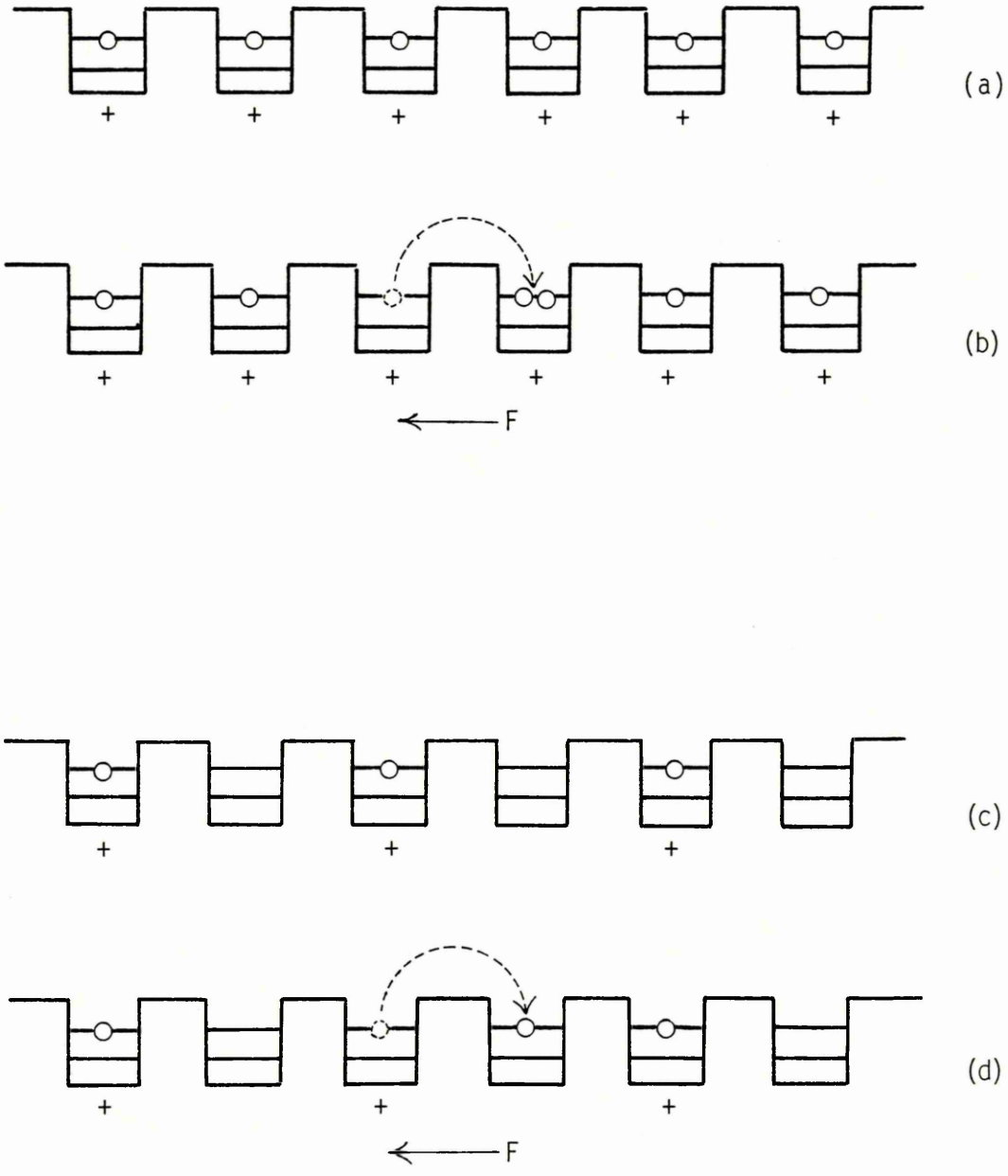

FIGURE 1.5 : Schematic representation of single particle hopping in one dimension. (a) and (b) represent a salt in which $\rho = 1$; (c) and (d) represent a salt in which $\rho < 1$.

interactions and that the variations in the conductivity may be related to the number of electrons per site.

Mazumdar and Bloch[143] have discussed the effects of band filling on the short range Coulomb interactions, U_o and V_1. Conduction electrons are known to experience short range Coulomb screening through the long range interactions which are also those responsible for collective motion of electrons. Since the screening depends on the number of electrons involved in the long range interactions, it will be sensitive to the degree of band filling. Mazumdar and Bloch report that the screening is least effective for a commensurate charge on the lattice sites that is for $\rho = 1$ and $\rho = 1/2$ and increases from both these limits to a maximum at around $\rho = 0.75$.

For the highly conductive 1:1 salts of Table 1.1, the effective Coulomb repulsion energy is reduced by having $\rho < 1$ due to incomplete charge transfer. The degree of charge transfer depends on the difference (I-A) between the donor ionization potential (I) and the acceptor electron affinity (A) as well as the Madelung binding energy[73]. Thus the 1:1 TCNQ charge transfer complexes of donors of low ionization potential (such as TMPD and the alkali metals) are ionic with $\rho = 1$, whereas the complexes of high ionization potential donors (e.g. anthracene) have a neutral ground state with $\rho = 0$. Only those donors with an intermediate ionization potential in the range 6-7 eV (e.g. TTF, $I_o = 6.8$ eV) form

highly conductive TCNQ complexes. Increasing the electron affinity of the acceptor[33], for example by fluoro substitution on the ring, results in an ionic ground state for the TTF complexes and a lower conductivity (see Table 1.4, overleaf).

The conductivity is dependent upon the degree of charge transfer and is highest when ρ is incommensurate, that is, when it is not a simple fraction. When $\rho = 1/2$ the long range interactions cause the electrons to order on alternate sites to give a so-called Wigner crystal [157]. For charge transport in these $\rho = 1/2$ systems the electrons have to overcome the smaller gap arising from V_1, the nearest neighbour interactions[158]. If ρ is incommensurate the electrons can correlate their movement to avoid both the U_o and V_1 interactions and the conductivity will be high. The relationship between commensurate and incommensurate ρ and the conductivity are clearly seen in Table 1.4 .

The Temperature Dependence of Conductivity.

The temperature dependence of conductivity can be described in terms of both the carrier concentration and the carrier mobility. Recent descriptions[149] of the conductivity for a wide range of organic conducting materials can be made by assuming an activated carrier concentration and a strongly temperature - dependent mobility . The relationship;

$$\sigma(T) = AT^{-\alpha} \exp(-\Delta/T) \quad \text{.....Eqn. 1.2}$$

forms the basis of a mobility model proposed by Epstein et al. and is found to be a good fit to the observed

SALT	ρ	$\sigma_{R.T.}$	Ref.
TMPD(TCNQ)$_2$	Ø.5	2	34, 35
TEA(TCNQ)$_2$	Ø.5	6.5	5
MEM(TCNQ)$_2$	Ø.5	2Ø	41, 143
Qn(TCNQ)$_2$	Ø.5	1ØØ	3, 144
TMTSF-TCNQ	Ø.57	1ØØØ	23, 143
TTF-TCNQ	Ø.59	2ØØ-6ØØ	14, 16
TSF-TCNQ	Ø.63	1ØØØ	2Ø, 143
HMTTF-TCNQ	Ø.72	4ØØ	25, 145
HMTSF-TCNQ	Ø.74	15ØØ	26, 143
NMP-TCNQ	Ø.91	1ØØ	8,47
NMAd-TCNQ	1	*$1Ø^{-5}$	38
NMQn-TCNQ	1	*$1Ø^{-7}$	4,73
TEA-TCNQ	1	*$1Ø^{-9}$	4,73
Rb TCNQ (II)	1	$1Ø^{-2}$	99, 1ØØ
Na TCNQ	1	$1Ø^{-6}$	78, 79
HMTTF-TCNQF$_4$	1	$1Ø^{-4}$	33
HMTSF-TCNQF$_4$	1	$1Ø^{-4}$	156

* denotes powder conductivity.

TABLE 1.4 : The relationship between ρ and the room temperature conductivities of a number of TCNQ salts.

conductivity over a wide temperature range for many salts.

Some of the models used to describe conduction in quasi-one-dimensional TCNQ salts are reviewed in the following sections for the Class II and Class III salts.

Class II Salts

Most materials in Class II exhibit a positive conductivity temperature dependence below room temperature and may be classed as semiconductors. It is important to note however that plots of log σ versus reciprocal temperature are rarely linear over a wide range of temperatures, say 300 to 70 K, but either exhibit curvature or two intersecting lines. These may be attributed to a temperature dependence of the pre-exponential factor or to the onset of extrinsic behaviour at low temperature.

There have been attempts to ascribe the activation energy observed to an intrinsic semiconductor gap within simple band model theory[150,151]. A combination of electrical conductivity and themoelectric data yields a mobility temperature dependence of $T^{-1.5}$ to $T^{-2.5}$, consistent with a simple scattering mechanism. The simple band model approach is supported by the observation of a thermoelectric power (TEP) temperature dependence which is similar to that observed in germanium[152].

Activated hopping has been proposed for several Class II salts. The activation energies derived from the log σ versus

reciprocal temperature plots for ethyltriphenylphosphonium $(TCNQ)_2$, ETPP$(TCNQ)_2$ and (DEPE)$(TCNQ)_{4.5}(H_2O)_x$ (semiconductive form), for example, are thought to be due to hopping[153]. The evidence comes primarily from the observation of a temperature independent TEP in the range 100 to 370 K suggesting that the carrier population is not determined by thermal activation. Similar TEP behaviour has led to a hopping description for the conductivity in methyltriphenylphosphonium $(TCNQ)_2$, MTPP $(TCNQ)_2$, for T > 314 K[154], and in TEA$(TCNQ)_2$[155,156] for T>200 K. In these salts, the observed activation energy is thought to be derived from a gap due to Coulomb interactions.

Although not a typical Class II material, NMP-TCNQ exhibits a positive temperature dependence of conductivity below 200 K. The low temperature (T < 70 K) conductivity has been correlated with a model of variable range phonon-assisted hopping. Bloch[157] shows that the conductivity of NMP-TCNQ obeys the relationship, $\ln \sigma \propto T^{-1/2}$ within the limited temperature range 20 to 70 K.

Shante[158] has found reasonable agreement for the conductivity of NMP-TCNQ, at temperatures below the metallic regime, with a model of phonon assisted hopping in two and three dimensions. At very low temperatures where the interchain hopping distances are large, the hopping is three dimensional and follows the form $\ln \sigma \propto T^{-1/4}$. At higher temperatures, the hopping becomes two dimensional with interchain hopping only possible between nearest neighbour chains. The

conductivity varies as $\ln \sigma \propto T^{-1/3}$. This model only fits the conductivity of NMP-TCNQ well between 18 and 140 K.

Similar temperature dependences of the conductivity have been proposed to fit a model of interrupted conductive strands[159,160]. In a system of parallel linear strands, the conductivity is activated as a result of insulating defects within the strands. The conductivity is given by $\ln \sigma \propto T^{-n}$ where n is related to the energy required to add another electron to the strand. In a similar discussion, Lenahan and Rowland[161] have found that the non-ohmic behaviour of crystals of methyltriphenylarsonium$(TCNQ)_2$, $MPh_3As(TCNQ)_2$ can be explained by assuming a scheme in which the conductivity is activated as a result of electrostatic barriers caused by charge imperfections between conductive strands. The activation energy is related to the Coulomb gap due to the interaction between electrons on the chain and electrons on the imperfections.

The presence of a Peierls gap in some TCNQ salts might explain the observed activation energy. In methylethyl morpholinium$(TCNQ)_2$, $MEM(TCNQ)_2$ [41,162] in the temperature range 340 - 250 K, the TCNQ stack is dimerized and the gap may be attributed to non-uniformity of spacing. Above 340 K the TCNQ molecules are uniformly spaced and the conductivity has a value of 30 Scm^{-1} and is temperature independent.

It has been suggested that the anomalous temperature dependence observed in the conductivity of $MEM(TCNQ)_2$ at

temperatures below 314 K may be due to a temperature dependent gap[163]. The conductivity exhibits an anomaly at about 314 K which may signify an increasing gap. However recent measurements of the electron and hole mobilities by the thermoelectric power[82] suggest that below this temperature there is a significant decrease in the electron mobility due to polaron binding of the conduction electrons to the cation which is a consequence of an increasing restriction in the cation motion. The possible effects of an increase in the gap are thus only of secondary importance.

The observation of curvature in the ln σ vs reciprocal temperature plot for $TEA(TCNQ)_2$ above 300 K has been attributed to the onset of a semiconductor to metal transition[135]. This implies a gap in the low temperature state which is renormalized to zero around 300 K. Such a scheme has been previously proposed for the apparent semiconductor to metal transition for NMP-TCNQ at 200 K[166] although a more acceptable theory developed by Epstein et al.[149], and discussed later, proposes a gap which persists throughout the range 70-400 K. Curvature in the conductivity plot above 300 K in $DMBP(TCNQ)_4$[167] has been explained by assuming a temperature dependence of T^{-2} of the pre-exponential factor in the relationship;

$$\sigma = \beta T^{x} \exp(-Eg/2kT) \quad \ldots\ldots \text{Eqn 1.3}$$

with this value for the exponent reflecting a mobility temperature dependence of $T^{-3.5}$. This is inconsistent with purely accoustic phonon scattering ($\mu \propto T^{-1.5}$) and could

imply some admixing of optical phonon scattering giving rise to a greater temperature dependence. The difference to note between this explanation and that for the TEA salt is that a gap of Ø.21 eV is assumed to persist throughout the experimental range of temperatures.

Class III Salts

The materials in Class III are metallic conductors at room temperature and exhibit an increase in conductivity as the temperature decreases. Figure 1.6 depicts the typical shape of conductivity curves for Class III salts and identifies two distinct types of behaviour. The salts of Class III(i) which includes TTF-TFNQ, TSF-TCNQ and HMTSF-TCNQ, for example, generally have high conductivities with $\sigma_{R.T.} = 4x10^{2}$ to $10^{3} Scm^{-1}$ (see Table 1.1, p 6) and upon cooling the majority undergo metal-to-insulator transitions at T_m. In most cases $\sigma (T_m)/\sigma (295K) > 2$.

Class III(ii) salts have room temperature conductivities of about $10^{2} Scm^{-1}$ and include materials such as NMP-TCNQ, $Qn(TCNQ)_2$ and acridizium$(TCNQ)_2$ (see Table 1.2, pp 8-12). The conductivity increases as the temperature is lowered with a slightly negative curvature and passes through a broad maximum around T_m. Usually, $\sigma (T_m)/\sigma (285) < 2$.

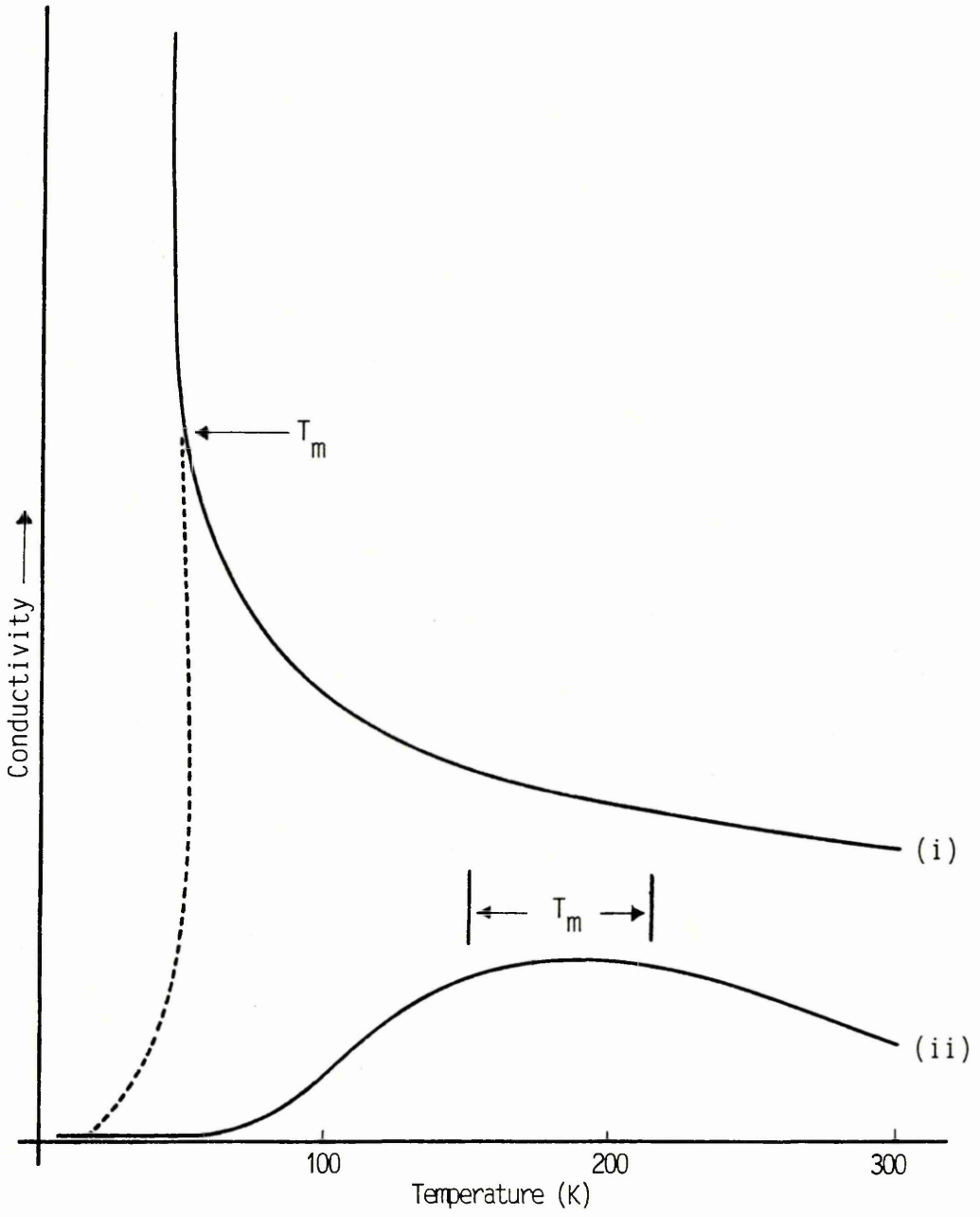

FIGURE 1.6 : The conductivity temperature dependence of the Class III salts ; the dashed line denotes the conductivity below a transition at T_m which is seen in many Class III(i) salts.

In the metallic region the conductivities of the highly conductive Class III(i) salts often give a reasonable fit to the expression[168];

$$\sigma = (A + BT^{\alpha})^{-1} \quad \ldots\ldots \text{Eqn 1.4}$$

where the exponent, α, reflects the mobility temperature dependence of carriers. Groff[169] has determined α to be between 2.23 to 2.40 for a number of high purity samples of TTF-TCNQ with a value of 2.33 representing the majority of samples. Similarly in HMTSF-TCNQ α = 2.39(ref.171). A mobility temperature dependence greater than the $T^{-1.5}$ dependence suggests that carriers are scattered by the higher energy, optical phonons [170]. This proposal would seem to apply to many of the 1:1 charge transfer complexes in Table 1.1 where the exponent is greater than 2.

The existence of a one-dimensional Fröhlich conductivity at lower temperatures has been discussed for salts in this class and in particular for TTF-TCNQ[136]. The conductivity anisotropy in TTF-TCNQ rises strongly above the 59K transition as the temperature is lowered below 150K suggesting an increasing contribution to the parallel component of the conductivity. The temperature exponent for this mechanism (α = 0.5) calculated from theory[172] is not, however, in agreement with the experimental data.

There is good evidence for the presence of superconducting pairs created by fluctuations providing the observed temperature dependences in $(TMTSF)_2PF_6$[136]. Such

paraconductivity may be present well above the superconducting transition temperature. The conductivity anisotropy of $(TMTSF)_2PF_6$ is constant from room temperature down to 50 K and has a magnitude of between 1000 and 700. The anisotropy decreases rapidly to low temperatures as a three dimensionally ordered state is approached at a temperature, T_3. Shulz[183] has shown that for one dimensional systems well above T_3, the conductivity varies as $T^{-3.2}$. Near T_3 the exponent reduces to 0.5, characteristic of a three dimensional superconductor.

For the less conductive (Class III(ii)) salts, for example NMP-TCNQ, $Qn(TCNQ)_2$, $acridizium(TCNQ)_2$ etc., the conductivity in the metallic region may not be fit by such simple temperature exponents.

NMP-TCNQ has been described as a Mott-Hubbard semiconductor in the range 20 to 70 K[168]. The activation energy due to on site Coulomb interactions. The high temperature behaviour of the salt in this proposed model is that of a correlated metal with the gap renormalized to zero at T_m. The description does not give a good fit to the observed conductivity up to 300 K, but Coleman[174] was able to fit the region 300 to 400 K with a T^{-4} law.

The negative temperature dependence above T_m may in fact result from the combined effect of a small band gap and a negative pre-exponential factor. The best fit for the conductivity of Class III(ii) salts has been made using the

'mobility model' of Epstein[149]. A good fit to the observed conductivity of NMP-TCNQ, Qn$(TCNQ)_2$ and acradizium$(TCNQ)_2$ within the range 70 to 400 K has been made using the relationship;

$$\sigma(T) = AT^{-\alpha}\exp(-\Delta/T) \qquad \text{(Eqn 1.2)}$$

The parameters α and Δ are sample dependent constants of the mobility where $\mu \propto T^{-\alpha}$ and the energy gap, persistent throughout the range 70 to 400 K, respectively. Where $\Delta > 0$ the carrier concentration is activated according to $n \propto \exp(-\Delta/T)$. Assuming that the mobility of carriers at high temperatures is limited by optical phonon scattering, μ is a monotonically decreasing function of temperature while n monotonically increases with temperature. The product gives $\sigma(T) = n(T)e\,\mu(T)$ where the conductivity exhibits a maximum at $T_m = \Delta/\alpha$.

For NMP-TCNQ, a computerised fit of the conductivity to equation 1.2 gives $\alpha = 3 - 4$ and $\Delta = 900$ K. The higher values of α are correlated with samples of higher purity. There is some deviation below 65 K from the curve which is ascribed to a contribution from electrons in localized states. This is borne out by the observation of poorer fit at low temperatures seen for samples of poorer quality.

The high mobility temperature dependence is considered to arise from optical phonon scattering of carriers which for TCNQ, implies electron phonon coupling in the frequency range 120 cm^{-1} to 600 cm^{-1}.

The conductivity of TTF-TCNQ (Class III(i)) can also be fit to equation 1.2 where $\Delta = 0$ and $\alpha = 2.3$

The differences in the conductivity temperature dependences illustrated in figure 1.6 can now be explained if it is assumed that there is an energy gap, Δ , persistent at all temperatures for the less conductive salts of Class III(ii) and a zero gap for the highly conductive salts of Class III(i). In both classes the mobility is governed by majority optical phonon scattering.

The model may also be extended to account for the conductivities of Class II materials where the activation energy is generally greater than 1500K. With α of 4 or less, the maximum (Δ/α) will occur at temperatures much greater than 300 K, and the exponential will dominate the temperature dependence.

1.3 : Magnetic Properties

1.3.1 : Introduction

Magnetic susceptibility studies of organic salts compliment those of the electrical conductivity by providing evidence of the state of the conduction electron system[175].

The fact that the same electrons determine both the electrical and magnetic properties in organic salts was shown in early studies by, for example, Kepler[7] and Siemons[5] et al. A close correlation between these properties was found. It was seen[7] that the highest conductive complexes such as Qn(TCNQ)$_2$ exhibit a nearly temperature independent susceptibility between 40 and 300 K with a large low temperature upturn. The less conductive complexes such as TEA(TCNQ)$_2$ and trimethylammonium(TCNQ)$_2$, TMA (TCNQ)$_2$ exhibit an activated magnetic susceptibility with an activation energy, J, which, in general, is higher for salts of lower conductivity.

The very weak temperature dependence of the susceptibility for Qn(TCNQ)$_2$[7] and others[175] such as Ad(TCNQ)$_2$ and phenazinium (TCNQ)$_2$ at high temperatures might be explained as arising from a system of non-interacting spins in a degenerate electron gas, characteristic of a metallic system. Certainly the high conductivity and high temperature metallic properties in these salts would support this idea but the low temperature upturn in the susceptibility which is observed is

inconsistent with the Pauli susceptibility expected for metals and would have to be explained as being extrinsic in origin. An alternative explanation which fits the high temperature data and explains the low temperature upturn as an intrinsic feature, is a one-dimensional system of localised spins possessing an antiferromagnetic interaction[175] which decomposes into a system of virtually isolated spins at very low temperatures. This is discussed later.

Temperature independence of susceptibility occurs in, for instance, the tetraphenyl-dithiapyranilidene iodides[176] where the susceptibility is constant between 100 and 300 K. The salts are metallic at room temperature and the susceptibility could interpreted as Pauli paramagnetism. The conductive organic alloy[177] $(2,2\text{-DHPE Cl})_x(2,2\text{-DPE})_{1-x}$ (TCNQ) also exhibits a temperature independent susceptibility which may be interpreted as Pauli paramagnetism. The electrical studies of this alloy show the conductivity to be high, and recent studies of the temperature dependence of conductivity of single crystals suggest the salt is metallic. In section 3.2 this salt is discussed. Potassium chloranil [178] exhibits a quasi temperature independent susceptibility in the region 100-200 K. This material is a semiconductor and the susceptibility is not, therefore, Pauli paramagnetism. The authors suggest that the observed properties are due to van Vleck paramagnetism. TTF-TCNQ exhibits a quasi temperature independent susceptibility above 280 K, but calculations of

the bandwidth[179] yield a value too small (0.085 eV) to account for the metallic character. The high temperature susceptibility of TTF-TCNQ and the metallic salts given in Table 1.1 and 1.3 is not fully understood. In these salts the susceptibility rises quasi-linearly with temperature over most of the temperature range up to 300 K.[182,183]. Similarly anomalous behaviour is the observed susceptibility in the metal (DEPE)$(TCNQ)_{4.5}(H_2O)_x$ (I) which exhibits a weak temperature dependence of the susceptibility (see section 3.4) and not the Pauli susceptibility expected for a band model metal.

The preceding examples show that it is not always possible to ascribe models of magnetism which are founded on simple band theory, to the magnetic properties of organic metals.

In the 1:1 charge transfer complexes, the susceptibility must be considered to be the weighted susceptibilities, χ_D and χ_A, of the donor and acceptor stacks, respectively. By a susceptibility deconvolution technique developed by Tomkiewicz et al.[184], the separate contributions to the susceptibility from the donor and acceptor stacks may be determined. Analysis of the susceptibility of TTF-TCNQ[185] and HMTTF-TCNQ[186] by this technique reveals that χ_D is nearly temperature independent above the conductivity transition temperature while χ_A is strongly temperature dependent. Scott et al.[183] had suggested earlier a two chain model for TTF-TCNQ based on the observation of a metallic

contribution to the optical conductivity above 60K[187], co-existing with an energy gap of 1000 cm^{-1} , determined from optical studies [188]. The model proposes that the TTF chains behave as a simple one-dimensional metal with a Pauli susceptibility χ_p, while the TCNQ chains possess an activated susceptibility fitting the Lee, Rice, Anderson, (LRA) susceptibility[189] for a distorted chain, χ_{LRA}.
The spin susceptibility, χ_s, in this model for T > 60 K is:

$$\chi_s = \chi_p + \chi_{LRA}$$

and χ_s is thus not Pauli-like.

The activated behaviour observed for the less conductive complexes is interpreted by Kepler[7] as arising from localised triplet excitons by which a fit to the susceptibility might be made from Equation 1.5;

$$\chi = [2Ng^2 \mu_B{}^2/kT][3 + \exp(J/kT)]^{-1} \quad \text{.....Eqn 1.5}$$

Woodward[180] uses the above expression to correlate a conduction model of hopping among localised states with the observed activated susceptibility for certain bipyridinium TCNQ salts. For systems in which the spins possess some degree of delocalisation, an alternative expression[181] (equation 1.10, p 62) has been fit by Woodward[180] for a number of bipyridinium TCNQ salts. This model is discussed in section 1.3.2 .

Strong evidence for the existence of mobile spins is derived from the abscence of zero-field splitting lines in the low temperature esr spectrum of organic salts[206]. Chesnut and Phillips suggest that the abscence of these lines indicates

the existence of a mutual spin-exchange of partially delocalised spins.

The degree of localisation of electrons is of relevance to discussions of the electrical conductivity and low temperature esr studies may be of value in determining, qualitatively, this property.

The susceptibility can give additional information in identifying the nature of the metal to insulator transitions of organic salts [30,183].

One of the essential differences between the insulating states of NMP-TCNQ and TTF-TCNQ is that the former material possesses a magnetic ground state[190] and becomes a Mott insulator with the electrons localised by Coulomb interactions, whereas TTF-TCNQ below 60 K possesses a non magnetic ground state[183]. The Peierls transition opens a gap in the electronic density of states and the magnetic system becomes an activated singlet-triplet system with a singlet ground state. The magnetic gap is found to be comparable to the activation energy of conduction[191] below the transition.

The metal to insulator transitions in the salts of the $[TMTSF]_2X$ series have been shown to be not of the Peierls-Frohlich type. For $[TMTSF]_2PF_6$, the magnetic susceptibility shows no sharp drop at the temperature (ambient pressure) at which the salt undergoes a metal to insulator transition[30]. Instead, it is proposed[30] that the insulating state is due to

a condensation of spin density waves [spin density waves are discussed in the literature (for example, see reference 133) and will not be discussed here].

Many of these salts undergo a superconductive transition and the magnetic susceptibility has confirmed the transition temperature and the bulk nature of the superconductivity. The observation of complete flux expulsion (Meissner effect) is seen at the superconductive transition temperature in a number of these salts [102,192-194].

The above discussion presents some examples of how the magnetic susceptibility may be correlated with conclusions drawn from conductivity work. In section 3 the results of a study of the magnetic susceptibility of 19 simple ionic and complex mixed valence salts of TCNQ are reported, and the principles of magnetism as they relate to the discussion of the results are outlined below.

1.3.2 : Principles of Magnetism

Non Interacting Spins

The volume magnetic susceptibility, χ, is defined as the magnetization induced per unit applied field;

$$\chi = M/H$$

M is the magnetization per unit volume and H is the applied field.

All systems possessing unpaired electrons will have a

positive contribution to the susceptibility, χ_s, the spin susceptibility. The electons in closed shells will contribute a negative component to the susceptibility, χ_{DIA}, the diamagnetic susceptibility. The total susceptibility is therefore;

$$\chi_{tot} = \chi_s - \chi_{DIA}$$

The diamagnetic susceptibility has been determined for most atoms and the molar diamagnetic susceptibility may be calculated by summing the atomic values. The χ_s values reported in section 3 are derived by adding χ_{DIA}, (obtained from Pascal's constants) to χ_{tot}; χ_{DIA} is assumed to be temperature independent.

When a magnetic field is applied to a paramagnetic system, the individual magnetic moments tend to orient themselves to the field and a magnetization results. Thermal disorder tends to resist this orientation. If there is no interaction between spins, then $\chi \propto T^{-1}$ and the Curie law is obeyed;

$$\chi = N\mu_B{}^2 g^2 J(J+1)/3k_B T = C/T \quad \text{..... Eqn 1.6}$$

J is the angular momentum quantum number. For a half filled shell with the total spin quantum number S = 1/2, then J = S = 1/2.

g is the gyromagnetic ratio and for 'spin half' systems, g = 2.

μ_B is the spin magnetic moment, the Bohr magneton.

N is the number of spins.

C is the Curie constant

Curie law behaviour has been observed[195-197] at low temperatures in certain TCNQ salts. The spins responsible are typically of low concentration (0.07% per mole in TTF-TCNQ [196]) and are assumed to be extrinsic in origin. In a series of charge transfer complexes based on quinones and p-phenylenediamines[208], the spins obey a Curie-law dependence. The spins in these salts arise from free radicals formed in these strongly ionic salts and the spin system may be described as consisting of non-interacting doublets.

Curie law behaviour is not commonly found in organic conductors and in the majority of salts the spins interact with each other with the interaction possessing some degree of anisotropy.

Many inorganic metals exhibit a temperature independent paramagnetism known as Pauli paramagnetism. The susceptibility is only 1/100th that of the expected Curie value.

In Curie paramagnetism the energy resisting spin alignment to the field is kT (eqn 1.6) whereas in Pauli paramagnetism the energy is the Fermi energy, kT_F, where T_F is the Fermi temperature which is a constant;

$$\chi_p = N\mu_B^2 / kT_F$$

Examples of salts which exhibit quasi temperature independent susceptibility have been mentioned in 1.2.1. The interpretation of this behaviour as being Pauli paramagnetism, indicating a metallic system of spins as an

electron gas has to be excercised with caution[178]. If this assumption is made however, then experimental χ_p values may be used to determine the transfer integral, t and therefore the electron bandwidth, 4t . The Pauli susceptibility has been given as[176,197];

$$\chi_p = N\mu_B^2 / \pi t \, Sin(1/2\pi\rho) \quad \ldots\ldots \text{Eqn 1.7}$$

ρ is the charge-to-site ratio.

Interacting Spins

An antiferromagnetic interaction i.e. one which favours the alignment of spins antiparallel to one another is found in many organic systems.

The susceptibility of a classical antiferromagnet passes through a maximum at a critical temperature, T_N, as the temperature is lowered. T_N is known as the Néel point.
The susceptibility above the Néel point varies according to the Curie-Weiss relationship;

$$\chi = C/(T + \theta) \quad \ldots\ldots\ldots \text{Eqn. 1.7}$$

where θ is the Weiss constant.
Below the Néel point, a magnetically ordered state exists in which spins adjacent in the lattice are alternatly "spin up" or "spin down".
The magnitude of θ is related to the strength of the antiferromagnetic exchange interaction, thus in a Curie paramagnet $\theta = \emptyset$. The Weiss constant is equal to T_N only in isotropic antiferromagnets that is, in materials in which all the interactions are antiferromagnetic and three dimensional.

The complex 1:3 salts, discussed in section 3.2, exhibit Curie-Weiss behaviour and the low values of θ reflect only a weak spin-spin interaction in these salts. Similar behaviour is observed in the susceptibility of 1,1-bis(p-cyanophenyl)4,4-bipyridinium$(TCNQ)_4$, CPP-$TCNQ_4$ in the temperature range 100 to 300 K (see section 3.6).

The susceptibility of many salts at low temperature increases sharply but the temperature dependence often exhibits deviations from true Curie law behaviour due to spin - spin interactions[175,196,198-203]. The susceptibility usually varies as $\chi \propto T^{-\alpha}$ where $\alpha < 1$. Qn$(TCNQ)_2$, in particular, has been studied[202] in order to establish the nature of the interactions and to describe the low temperature spin state.

Kepler[7] first suggested that the large Curie tail in the susceptibility of Qn$(TCNQ)_2$ may be an intrinsic property of the salt rather than a susceptibility due to impurities or defects. Bulaevskii[175] has subsequently fit the observed data at all temperatures (0.1 to 400 K) to a model where the spins are localised on alternate TCNQs in the stack and experience an antiferromagnetic interaction between them. At high temperatures the linear spin system is homogeneous in respect of the antiferromagnetic interaction. As the temperature is lowered, the spin system is decomposed into weakly interacting sub-systems which determine the low temperature susceptibility. Within this model the general conditions giving a $T^{-\alpha}$ law[204] are that there is a random distribution

of spins along the chains and that Jm, the exchange interaction between neighbouring magnetic sites, decays exponentially with distance between spins. The random distribution of the spins creates a random Jm in a chain with a probability distribution of;

$$P(Jm) = A\ Jm^{-\alpha}$$

The source of the random variations in Jm have been proposed to be a result of random variations in site energy leading to a random spin distribution along the chain[205]. Only sites within a certain energy range will be singly occupied and thus possess a magnetic moment. This magnetic model which applies to one-dimensional magnetic systems refers to a Random Exchange Heisenberg Antiferromagnetic Chain, (REHAC).

In attempts to explain the thermodynamic properties of the REHAC more fully, Clark et al.[199] and Miljak et al.[200] have proposed models for the spin system in which the interaction between pairs of spins only are considered. In the exchange coupled pair (ECP) model of Clark[199] every alternate Jm in a linear chain of randomly distributed localised spins is set (arbitrarily) to zero, thus splitting up the chain into a system of interacting pairs. The susceptibility of a pair is determined by a singlet triplet energy level system to give;

$$\chi_{ECP} = 2\mu_B{}^2 g^2 / kT[3+ \exp(J/kT)] \quad .....\text{Eqn 1.8}$$

The total susceptibility is obtained by integrating over the probability distribution of the susceptibility of exchange coupled pairs χ_{ECP}.

Exciton Magnetism

In many semiconductive TCNQ salts, the susceptibility exhibits a temperature dependence which may be fit to an activation law. The susceptibility passes through a maximum at a temperature which is related to the magnitude of the magnetic gap. It has been shown by esr[206] and static susceptibility measurements[7] that the susceptibility is activated due to a pairwise interaction of spins in which a singlet ground state and a thermally accessible triplet excited state (triplet exciton) are separated in energy by an interaction, J.

The presence of radicals in strongly ionic charge transfer salts was discovered in the early 1950s[207]. In the complexes formed between the p-phenylenediamines and halogenated quinones, the large differences in the electron affinities between each moiety allows charge transfer to be complete and an ionic ground state exists. An e.s.r. absorption occurs due to the presence of free radicals. In these salts the spins are non-interacting and follow the Curie law but Bijl, Kainer and Rose-Innes, (BKR)[208], suggested that in certain salts the radicals could interact to produce magnetic states of higher multiplicity than the doublet state of single unpaired spins. The radicals were proposed to interact in pairs to form a singlet (antiparallel) state and a triplet (spin parallel) state. BKR gave the expression for the

e.s.r. intensity versus temperature as;

$$I \propto I/T[\exp(J/kT)+3]^{-1}$$

where I is the e.s.r. signal intensity and J is the singlet-triplet (S-T) exchange energy. The expression refers to a singlet ground state system since J is negative. Chesnut and Phillips[206], in a study of $TEA(TCNQ)_2$, $(MePh_3P)(TCNQ)_2$, $(MePh_3As)(TCNQ)_2$ and morpholinium(TCNQ) subsequently found such an interaction and fit the above expression to the e.s.r. susceptibility of these semiconductive TCNQ complexes. The slopes of the ln IT versus reciprocal temperature plots for these salts yield J values ranging from between Ø.Ø34 - Ø.41eV .

Equation 1.5 (given in the introduction to this section and recalled here) is analogous to the expression given above. Kepler[7] has determined the static molar susceptibility of $TEA(TCNQ)_2$ and finds a good fit to the following equation;

$$\chi = [2Ng^2\mu_B^2 / kT][3 + \exp(J/kT)]^{-1} \quad ....(eqn.1.5)$$

The model is one in which the spins interact in pairs only and the spins are localised. The susceptibility possesses a maximum at some temperature, kT_{max}, and it may be shown[7] that $J = 1.61(kT_{max})$. The expression is only valid over temperatures at which $J >> kT$.

In a one-dimensional system of spins there is the possibility of an exchange interaction between the spins of adjacent pairs. For a regular chain of spins with an antiferromagnetic interaction, Bonner and Fisher[226] have

calculated the susceptibility of the spin system described by the Hamiltonian;

$$\mathcal{H} = \sum_{m}[2JmSmSm+1 - g\,\mu_B HSm^z]$$

where Jm is the exchange interation and Sm and Sm+1 are the spins of a pair on the magnetic sites m and m+1.

The system of spins is homogeneous in respect of the exchange interaction as shown in Figure 1.7;

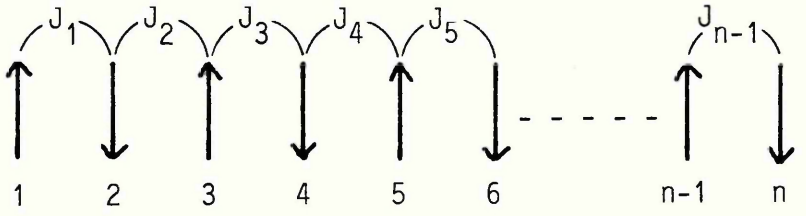

$$J_1 = J_2 = J_3 = J_4 = J_5 = J_{n-1}$$

Figure 1.7 : One-dimensional chain of n spins with a homogeneous exchange.

Since J is dependent on the separation of spins, the precondition for a homogeneous spin system is that the spins are spaced equally along the chain.

Bonner and Fisher[226] calculate that the susceptibility will possess a maximum whose magnitude is related to the temperature at which it occurs by;

$$\eta = \chi kTmax \,/\, g^2\mu_B{}^2N = 0.095$$

Bulaevskii et al.[175] find that the maxima in the susceptibility of $Qn(TCNQ)_2$ and $Ad(TCNQ)_2$ may be fit with the above expression, with η = 0.1 +/- 0.01. If these materials possess homogeneous one-dimensional spin systems, this may be

attributable to the TCNQ lattice structure. In both salts, the TCNQs stack in homologous columns with a short, regular inter-site spacing[10,36]. It must also be asumed that the charge is distributed evenly on the TCNQ lattice sites. The susceptibility given by equation 1.5 represents a spin system in which the interaction between adjacent spin pairs is negligible and thus alternate values of J are zero.

Many of the salts discussed in Section 3 possess spin systems in which there is some interaction between adjacent pairs and thus non-zero values of alternate J. The Hamiltonian which describes such systems is[209];

$$\mathcal{H} = \sum_{m} J(Sm.Sm+1 + \gamma Sm.Sm-1) \quad \text{..... Eqn 1.9}$$

The right hand set of terms describes the interaction between spins on site m with spins on neighbouring sites (m-1) where the exchange interaction is $J\gamma$. Thus γ represents the degree of alternation between adjacent spin pairs and is known as the alternation parameter.

For systems in which the spins possess some degree of delocalization $\gamma > 0$. A description of non-localised triplet excitons is required which can provide solutions to the Hamiltonion (Eqn 1.9) over the range of γ of 0 to 1.

Such a model, known as the exciton gas model, has been proposed by Etemad[181] and has been successfully used[180] to describe the esr susceptibility of some bipyridinium TCNQ salts. The applicability of the model is restricted,

however, since it cannot be applied in cases where $\gamma > 0.5$. Hibma[210] has proposed a model based on classical band theory in which the excitonic state has some of the characteristics of a strongly bound exciton (Frenkel exciton) or a weakly bound exciton (Wannier exciton). The model proposes intermediate degrees of localisation and the excitons may be described as 'extended Frenkel' excitons. This model has limited applicability, however, since it does not provide a solution to the Hamiltonian (eqn 1.9) in the localised limit, that is, where $\gamma = 0$.

The model which is applied to the results in this work is that developed by Bulaevskii[209] who has determined the susceptibility for a linear chain of spins with values for the alternation parameter of 0 to 0.9. This is preferred over the two models mentioned previously for its range of applicability and its relevance to descriptions of one-dimensional spin systems. The susceptibility varies as;

$$\chi = 2N\mu_B{}^2 g^2 \, a(\gamma)/kT \exp(-J\,\Delta(\gamma)/kT) \quad \text{....Eqn 1.10}$$

$a(\gamma)$ and $\Delta(\gamma)$ are functions of the alternation parameter which result from the finite triplet bandwidth. Figure 1.8 depicts the results of the calculations made by Bulaevskii and shows the variation of a and Δ vs γ for $\gamma = 0$ to 0.9. In a system with strong alternation i.e. where alternate J are zero, $a(\gamma)$ and $\Delta(\gamma)$ are both unity and equation 1.10 reduces to the form of equation 1.5 where the condition; $\exp(J/kT) >> 3$ applies.

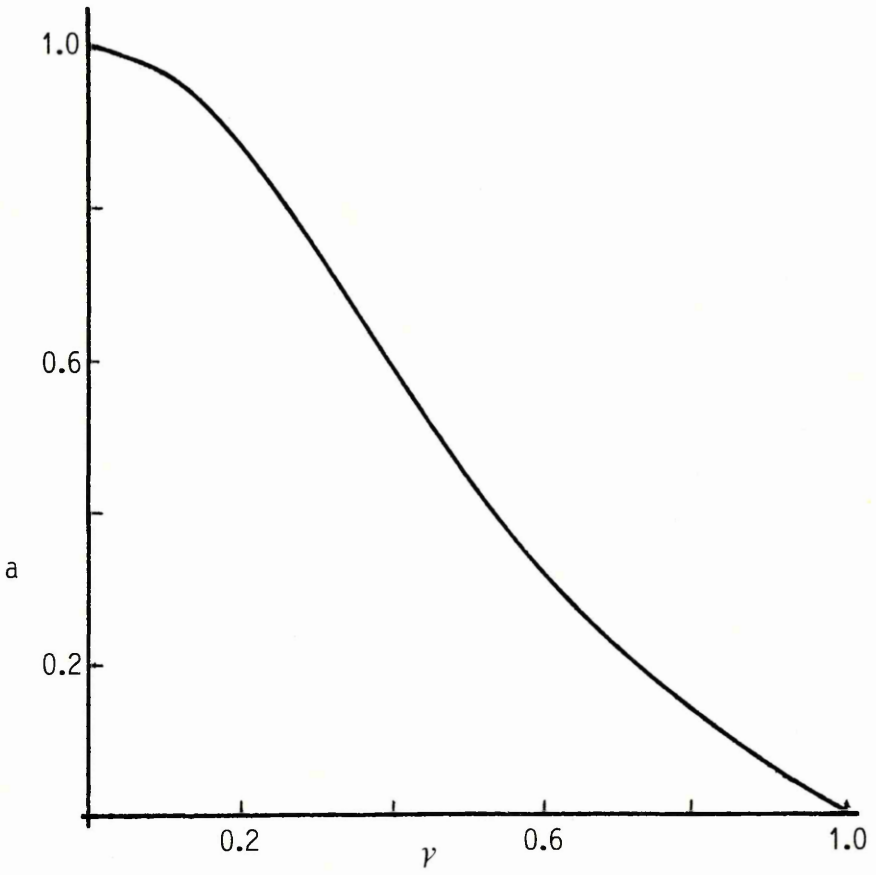

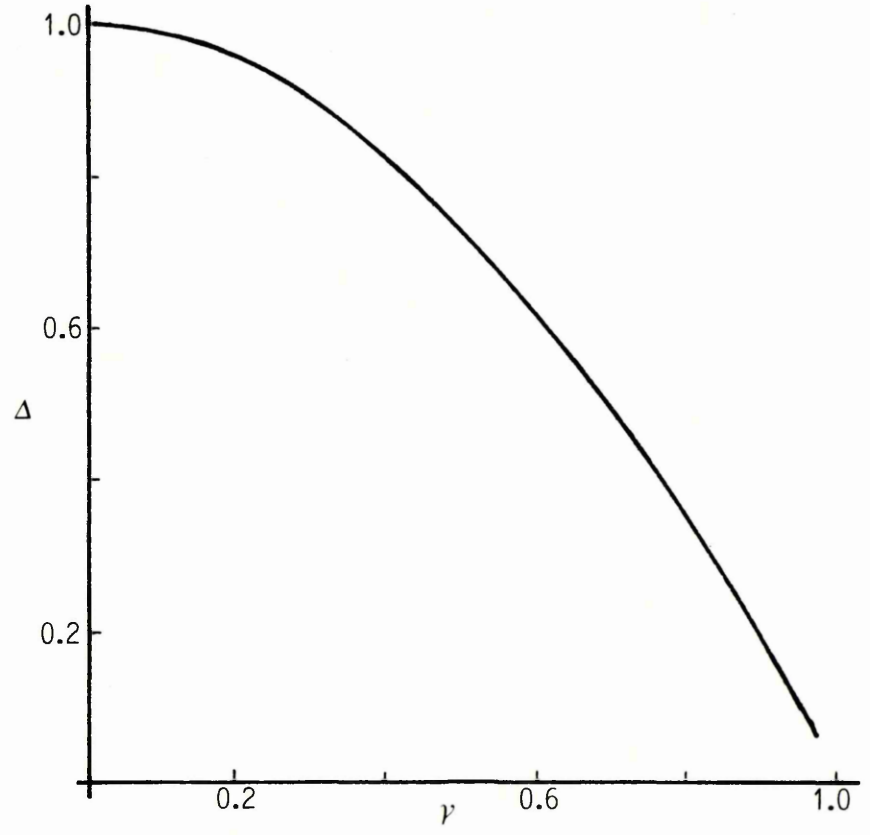

FIGURE 1.8 : Data plotted from reference 209

1.4 : Optical Studies

To determine the stoichiometry of the complexes studied in this work we have employed a spectrophotometric method first used by Rembaum et al.[211] in a study of back charge transfer in certain bipyridinium TCNQ salts.

$TCNQ^{o}$ absorbs strongly in the uv/vis region at 395 nm whereas $TCNQ^{-}$ shows strong absorption peaks at 842 nm as well as 395 nm. Rembaum et al. have plotted the ratio of $TCNQ^{-}$ to neutral TCNQ, made up in acetonitrile solution, versus the peak height $R = A_{395\ nm}/A_{842\ nm}$, where A is the absorbance. Their results are reproduced in Figure 1.9 where it is seen that Beer's law is obeyed for only a limited range of composition. However it is possible to use the technique in support of other methods of determining the stoichiometry and of ρ.

From the curve of Figure 1.9 the R values expected for salts of particular stoichiometry may be obtained. For the salts, which are discussed here, the values of R expected for the stoichiometry of the salts are given overleaf in table 1.5.

In the analysis of the complexes, the samples were finely ground to ensure that the bulk properties were represented. A few mgs were dissolved in spectroscopic grade acetonitrile (10ml) with dilution as necessary to bring the largest peak on scale.

Analysis was made using a Perkin-Elmer 550s uv/vis spectrophotometer coupled to a Perkin-Elmer 561 recorder. Heterosil cells (10mm path length, range 190-1000nm) contained the samples.

CATION : TCNQ	R ($A_{395\ nm}/A_{842\ nm}$)
DICATIONS	
$[CAT]^{2+}[TCNQ]_2^{2-}$	0.6*
$[CAT]^{2+}[TCNQ]_3^{2-}$	1.45
$[CAT]^{2+}[TCNQ]_4^{-2}$	2.1
$[CAT]^{2+}[TCNQ]_{4.5}^{2-}$	2.35
$[CAT]^{2+}[TCNQ]_5^{2-}$	2.55
MONOCATIONS	
$[CAT]^{+}[TCNQ]^{-}$	0.6
$[CAT]^{+}[TCNQ]_2^{-}$	2.1

* by the ratio of the molar absorption coefficients for the peaks at 395 nm and 842 nm for $TCNQ^-$ in acetonitrile.

Table 1.5: The ratio of solution spectra absorbance peaks at 395nm and 842nm for TCNQ salts of divalent and monovalent cations, derived from the data represented in Figure 1.9.

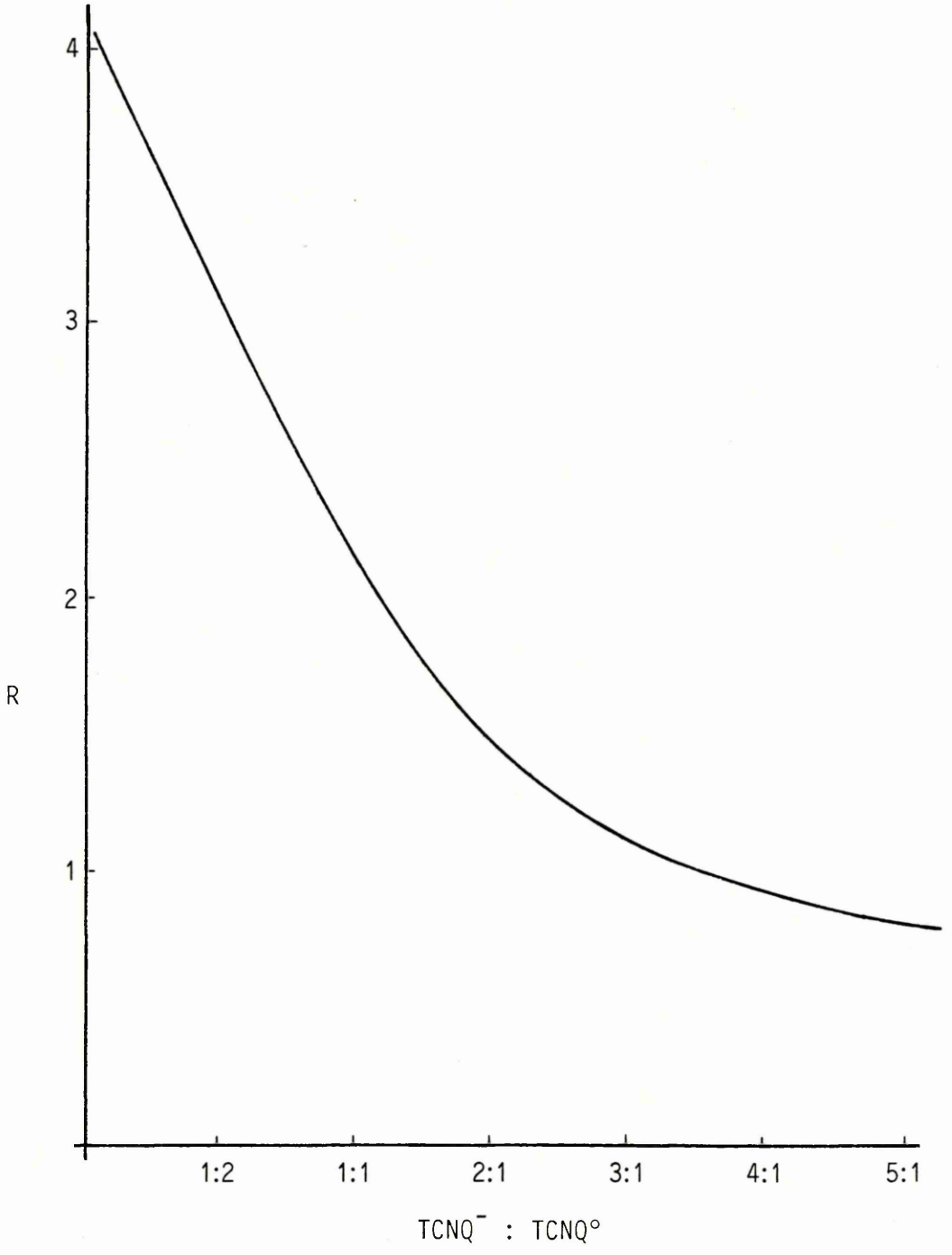

FIGURE 1.9 : The ratio of neutral TCNQ to $TCNQ^-$ versus the ratio of the absorption peak intensities at 395 nm and 842 nm in acetonitrile solution. $R = A_{395} / A_{842}$

2 EXPERIMENTAL

2.1 : Synthesis and Characterisation.

The synthesis and characterisation of the TCNQ salts discussed in sections 3.1 to 3.7 are given below. The analyses are by microanalytical techniques, conducted outside the department by contract and by the author using the spectrophotometric method described in section 1.4

2.1.1 : Salts of Section 3.2

2.1.11 Preparation of 1,2-bis(4-pyridinium)ethane][TCNQ]$_2$, [DHPA][TCNQ]$_2$

To a boiling solution of LiTCNQ (Ø.523g) in acetonitrile (2ØØml) was added a solution of [DHPA]Cl_2 (Ø.28g) in water (5ml). The mixture was refluxed for 5 minutes then allowed to cool to room temperature.

Purple parallelipiped plates were obtained from solution after 24 hours, the crystals were then washed with acetonitrile and ether.

Elemental Analysis: Calc (%) C 72.72, H 3.73, N 23.55

Found (%) C 72.99, H 3.9Ø, N 23.82

uv/vis A_{395}/A_{842} = Ø.6

2.1.12 Preparation of [1,2-bis(4-pyridinium)ethane][TCNQ]$_3$, [DHPA][TCNQ]$_3$

To a boiling solution of LiTCNQ and TCNQ was added a solution of [DHPA]Cl_2 in water, (molar ratios, LiTCNQ: TCNQ: [DHPA]Cl_2, 2:2:1) The mixture was allowed to cool and black needles were obtained. These were washed in acetonitrile and toluene until the washing were colourless.

Elemental Analysis: Calc (%) C 72.17, H 3.28, N 24.55

Found (%) C 71.76, H 3.33, N 24.25

uv/vis : A_{395}/A_{842} = 2.7 - 3.Ø (The expected value by the 1:3 stoichiometry is 1.45 and this anomalous value suggests alloy formation and is discussed later.)

2.1.13 Preparation of [1,2-bis(4-pyridinium)ethylene]$_{Ø.4}$ [1,2-bis-(4-pyridyl)ethylene]$_{Ø.6}$(TCNQ)$_3$, [4,4-DHPE]$_{Ø.4}$ [4,4-DPE]$_{Ø.6}$(TCNQ)$_3$

To a hot solution of LiTCNQ (Ø.266 g) and TCNQ (Ø.134 g) in acetonitrile (2ØØ ml) was added a solution of [DHPE]Cl_2 (Ø.129 g) in water (< 5 ml). The solution was refluxed briefly then left to cool to room temperature.

A blue feathery product was obtained. This was washed with water, then toluene to obtain a black microcrystalline powder.

Elemental Analysis: Calc (%) C 71.81, H 2.96, N 24.43

Found (%) C 72.28, H 3.Ø7, N 24.68

uv/vis: A_{395}/A_{842} = 3.Ø - 3.3

2.1.14 : Preparation of [1,2-bis(2-pyridinium)ethylene chloride]$_{0.7}$[1,2-bis(2-pyridyl)ethylene]$_{0.3}$(TCNQ), [2,2-DHPE Cl]$_{0.7}$ [2,2-DPE]$_{0.3}$[TCNQ]

To a boiling solution of LiTCNQ (0.5227 g) in acetonitrile (150 ml) was added a solution of [DH2,2PE]Cl_2 (0.3 g) in water (5 ml). The mixture was refluxed for 5 minutes then allowed to cool to room temperature.

Filtration of the solution yielded black, fine hair crystals.

Elemental Analysis:Calc (%)C 67.79, H 3.98, N 19.76, Cl 5.84

Found (%)C 67.28, H 4.02, N 19.76, Cl 5.95

uv/vis: A_{395}/A_{842} = 1.4

2.1.2 Salts of Section 3.3

2.1.21 Preparation of [1,2-bis(N-methyl-4-pyridinium) ethylene][TCNQ]$_4(H_2O)_x$, [DMPE][TCNQ]$_4$, (H_2O)x

To a boiling solution of TCNQ (0.402 g) in acetonitrile (200 ml), was added a solution of [DMPE]Cl (0.286 g) in water (5 ml). The mixture was refluxed for two minutes and then left to cool slowly to room temperature over 24 hours. Black microcrystals were recovered from solution after filtration, these then washed with cold toluene to remove excess TCNQ. The stoichiometry is confirmed by the ratio of two sets of layer lines seen in the oscillation photographs (section 3.1).

uv/vis: A_{395}/A_{842} = 1.84 - 1.86

2.1.22 Preparation of [1,3-bis(4-pyridinium)propane][TCNQ]$_4$ (H_2O)x, [DHPP][TCNQ]$_4$ (H_2O)$_x$

To a boiling solution of LiTCNQ;TCNQ (1:1, 0.5 g) in acetonitrile (200 ml) was added a solution of [DHPP]Cl_2 (0.63 g) in water (5 ml). The mixture was refluxed for 15 minutes then left to cool to room temperature.

Black needle crystals were recovered from solution and then washed with toluene.

Elemental Analysis: Calc.(%)C 70.79, H 3.31, N 24.36, O 1.55

Found (%)C 70.52, H 3.58, N 24.23, O 1.68

uv/vis: A_{395}/A_{842} = 2.1

There is no evidence here of the alloy formation which occurs in the salts of H-quaternised cations of Section 3.2

2.1.23 Preparation of [1,2-bis(N-methyl-4-pyridinium) ethane][TCNQ]$_4$(H_2O)x, [DMPA][TCNQ]$_4$(H_2O)x

A solution of [DMPA]Cl_2 (0.29 g) in water (5 ml) was added to a boiling solution of TCNQ (0.4 g) in acetonitrile. The mixture was refluxed for 5 minutes and then allowed to cool.

Black parallelipiped crystals were recovered from solution and washed with acetonitrile and ether to remove unreacted TCNQ.

Elemental Analysis: Calc(%) C 70.99, H 3.44, N 24.05, O 1.53

Found (%) C 71.01, H 3.23, N 24.80, O 1.36

uv/vis: A_{395}/A_{842} = 1.75

2.1.3 Salts of Section 3.4

2.1.31 Preparation of [1,3-bis(N-methyl-4-pyridinium)propane] $[TCNQ]_{4.5}(H_2O)_x$, $[DMPP][TCNQ]_{4.5}(H_2O)_x$

To a boiling solution of TCNQ (Ø.4 g) in acetonitrile (25Ø ml) was added a solution of $[DMPP]I_2$ (Ø.217 g) in water (5 ml). The mixture was refluxed for 3Ø mins and left to cool slowly to room temperature.

Black plate crystals were recovered from solution.

Elemental Analysis: Calc.(%) C 71.13, H 3.45, N 24.Ø4, O 1.37

Found (%) C 71.64, H 3.59, N 23.93, O 1.15

uv/vis: A_{395}/A_{842} = 1.95 - 2.Ø3

2.1.32 Preparation of [1,2-bis(N-ethyl-4-pyridinium)ethylene] $(TCNQ)_{4.5}(H_2O)_x$, $[DEPE][TCNQ]_{4.5}(H_2O)_x$

A hot aqueous acetonitrile solution of $[DEPE]I_2$ (Ø.25 g) and TCNQ (Ø.4 g), (1:4 molar ratio) was allowed to cool to room temperature. Black needle-shaped crystals were recovered from solution and washed in acetonitrile and ether.

Elemental Analysis: Calc.(%) C 71.65, H 3.52, N 23.51, O 1.31

Found (%) C 71.9Ø, H 3.5Ø, N 24.Ø3, O 1.2Ø

uv/vis: A_{395}/A_{842} = 2.2

2.1.4 Salts of Section 3.5

2.1.41 Preparation of [1,3-bis(N-ethyl-4-pyridinium)propane] $[TCNQ]_5(H_2O)$ $[DEPP][TCNQ]_5(H_2O)$

To a hot solution of TCNQ (Ø.4 g) in acetonitrile (15Ø ml) was added a solution of $[DEPP]I_2$ (Ø.199 g) in water (5 ml) and the mixture left to cool to room temperature.

Needle crystals in clumps were recovered from solution. Twinned crystal samples were isolated.

Elemental Analysis: Calc.(%) C 71.4Ø, H 3.58, N 23.79, O 1.24

Found (%) C 71.78, H 3.54, N 23.78, O 1.34

uv/vis: A_{395}/A_{842} = 2.4

2.1.42 Preparation of [1,3-bis(N-propyl-4-pyridinium) propane] $[TCNQ]_5(H_2O)$, $[DPPP][TCNQ]_5(H_2O)$

To a boiling solution of TCNQ (Ø.4 g) in acetonitrile (15Ø ml) was added a solution of $[DPPP]I_2$ (Ø.211 g) in water (5 ml). The mixture was swirled and left to cool slowly to room temperature.

Black needle crystals were recovered from the solution, these were then washed with toluene.

Elemental Analysis: Calc.(%) C 71.7Ø, H 3.81, N 23.28, O 1.21

Found (%) C 71.33, H 3.77, N 23.33, O 1.3Ø

uv/vis: A_{395}/A_{842} = 2.35 - 2.48

2.1.43 Preparation of [1,2-bis(N-propyl-4-pyridinium) ethylene][TCNQ]$_5$ [DPPE][TCNQ]$_5$(H_2O)

To a boiling solution of TCNQ (Ø.399 g) in acetonitrile (2ØØ ml) was added a solution of [DPPE]I_2 (Ø.211 g) in water (< 5 ml). The mixture was left to cool slowly to room temperature.

A black microcrystalline product was recovered after filtration of the solution. This was washed with toluene until the filtrate was clear of yellow excess TCNQ.

Elemental Analysis: Calc.(%) C 71.66, H 3.55, N 23.57, O 1.22

Found (%) C 71.89, H 3.49, N 23.64, O 1.Ø2

uv/vis: A_{395}/A_{842} = 2.6

2.1.44 Preparation of [1,2-bis(N-butyl-4-pyridinium)ethylene] [TCNQ]$_5$(H_2O), [DB$_u$PE][TCNQ]$_5$(H_2O)

A microcrystalline sample was provided by G.J.Ashwell and purified for this study by recrystallisation from acetonitrile.

2.1.5 Salts of Section 3.6

2.1.51 Preparation of [1,1-dimethyl-4,4-bipyridinium][TCNQ]$_3$, [DMBP]TCNQ]$_3$

To a boiling solution of TCNQ (Ø.4 g) in acetonitrile (25Ø ml) was added a solution of [DMBP]I_2 (Ø.215 g) in water (5 ml). The mixture was left to cool slowly to room temperature over 12 hours.

Large black crystals (Av. length, 2mm) were obtained after filtration of the solution.

The crystal structure has been determined by Ashwell and Wallwork[227] and is discussed in Section 3.6.

uv/vis: A_{395}/A_{842} = 1.36 - 1.42

2.1.52 Preparation of [1,1-bis(p-cyanophenyl)-4,4-bipyridinium][TCNQ]$_4$, [CPP][TCNQ]$_4$

To a boiling solution of TCNQ (Ø.2 g) in acetonitrile (15Ø ml) was added a hot solution of [CPP]I_2 (Ø.275 g) in water (5 ml). The mixture was left to cool slowly to room temperature.

Small black crystals were recovered from the filtered solution.

Elemental Analysis: Calc.(%) C 73.45, H 2.75, N 23.8

Found (%) C 73.2Ø, H 2.9Ø, N 23.7

uv/vis: A_{395}/A_{842} = 1.76 - 2.1

2.1.6 Salts of Section 3.7

2.1.61 Preparation of [dimethyldiphenylphosphonium] $[TCNQ]_2$, $[Me_2Ph_2P][TCNQ]_2$

To a boiling solution of TCNQ (Ø.2 g) in acetronitrile (1ØØ ml) was added a solution of $[Me_2P]I$ (Ø.17 g) in water (5 ml). The mixture was refluxed briefly and left to cool to room temperature. Black plate crystals (av. l = 4mm, w = 2 mm) were recovered from solution. These were washed with toluene.

The stoichiometry is confirmed by the X-ray structure determination in Section 3.7.

2.1.62 Preparation of [diethyldiphenylphosphonium] $[TCNQ]_2$, $[Et_2Ph_2P][TCNQ]_2$

To a boiling solution of TCNQ (Ø.2ØØ9 g) in acetonitrile (75-9Ø ml) was added a solution of $[Et_2Ph_2P]I$ (Ø.1767 g) in acetonitrile (minimum quantity). The solution was allowed to cool for 48 hours.

Thick black crystals were recovered after filtration of the solution.

Elemental Analysis: Calc.(%) C 73.75, H 4.33, N 17.19, P 4.74

Found (%) C 73.96, H 3.97, N 17.44, P 3.93

2.2 Crystal Structure Determination of [DHPA][TCNQ]$_2$

Crystal data: Monoclinic, space group C2/c, a = 29.517(15), c = 13.528(6) Å, β = 93.98(5)°, U = 2958 Å^3, D_m = 1.34 Mg m^{-3}, Z = 4, D_C = 1.34 Mg m^{-3}, F (000) = 1232, (Mo Kα) = 0.048 mm^{-1}, λ = 0.71069 Å.

The space group and unit cell parameters of (DHPA)(TCNQ)$_2$ were obtained from precession and Weissenberg photographs. Intensities were collected, in the range $1^o < \theta < 25.0^o$, from a crystal of approximate dimensions 0.40 x 0.25 x 0.15 mm, mounted with its b axis coincident with the ω axis of a Stöe Stadi-2 two-circle diffractometer, using Mo Kα radiation and the background-ω-scan-background technique. 2347 unique reflections were measured of which 1884 had significant counts [$I > 2\sigma(I)$] and were used in the subsequent refinement. Lorentz and polarisation factors were applied but no absorption correction was made.

Multisolution direct methods using SHELX enabled the positions of all non-hydrogen atoms to be readily located. The hydrogens were included in positions calculated from the molecular geometry (C--H = 1.08 Å). Scattering factors were taken from International Tables for X-ray Crystallography and the weighting scheme; $w = [\sigma^2(F_o) + 0.03816(F_o)^2]^{-1}$ adopted. Full matrix refinement with isotropic and anisotropic temperature factors for the hydrogen and non-hydrogen atoms respectively gave the final R = 0.042 and R_w = 0.052. The final difference map

showed no peaks greater than 0.18 $e\text{Å}^{-3}$. The final atomic coordinates are listed in Appendix I.

2.3 Electrical Measurements

DC conductivity measurements were made on compactions or single crystals of the salts, usually within the temperature range 10 - 300K. Electrical contact to the samples was made by a pseudo 4 - contact technique using Acheson 915 Electrodag silver paint as electrodes. The contact geometry is shown in figure 2.1

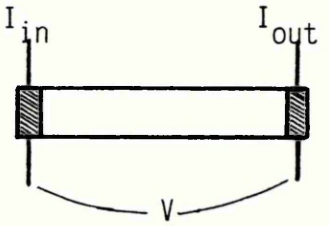

Figure 2.1 Sample contact geometry. The 4-contact technique minimises the effects of lead resistance.

A constant current of 100 μA was supplied. Compacted samples were prepared from microcrystals or powders previously dried for 24 hours at room temperature in an evacuated drying chamber. Samples were ground and compressed at 75MPa in a 3mm evacuated die for 2 minutes. The compactions were cut into slices of typical dimensions 2mm x 1mm x 0.5mm and measurements were made along the cross section.

The conductivity of the single crystal samples was measured parallel to the direction of highest conductivity.

All samples were mounted at the 4 K station of the expander

module in an Air Products 'Displex' closed cycle helium refrigerator system. The sample contact wires were wound tightly around the length of the 'cold finger' to ensure good thermal contact for the sample.

Temperature control was made with an Oxford Instruments sweep generator and temperature controller. Temperature sensing was made using an Oxford Instruments platinum sensor, linear in response in the range 15-400 K. The temperature was swept at a rate of approximately 0.5 K/min.

The analogue voltage signals from the sensor and the sample were received and converted to digital output by a Solartron 7055 microprocessor voltmeter coupled to a 16 channel Solartron 'Minate' 7010 scanner. The voltmeter was interfaced to, and controlled from, a Teletype Model 43 printer. The data from the voltmeter was processed using a BASIC programme, written for this project and listed in Appendix II, to give tabulated data for temperature, resistance, 1000/T, normalized conductivity and the logarithmic normalized conductivity. Programmes analogous to that in Appendix II were used to give the results in units of absolute conductivity and to process data from the magnetic studies.

2.4 Magnetic Measurements.

The magnetic susceptibility was determined by the Faraday method using a CI Robal microbalance with a rated sensitivity of 1 μg.

The samples were contained in a Teflon bucket suspended from the balance beam by silica and aluminium rods. Samples of between 20 and 100 mg were used in the susceptibility determinations. The temperature control was provided by an Air Products 'Displex' closed cycle helium refrigerator equipped with a vacuum shroud and copper sample shroud. Figure 2.2 shows the cold head cross section and sample position.

The balance and sample were pumped to 10^{-5} mbar for between 14-16 hours to remove residual oxygen and water vapour. The system was then backfilled with helium exchange gas to 0.1 bar (at room temperature). The helium supply was maintained throughout the experiment and the pumping and backfilling rates were controlled by an in-line leak valve. An Oxford Instruments temperature controller and sweep generator controlled the cooling cycle to a rate of 0.5 K/min. At this rate, the temperature difference between the sensor at the 4 K station of the cold head and that in the sample chamber was no more than +/- 2 K. At temperatures below 35 K it was found necessary to pump off some of the exchange gas to achieve a minimum temperature at the sample of 25 K. The effects of thermomolecular pressure and adsorption of gas were cancelled by sweeping the field up and down at each temperature. A magnet supply of 10 A was supplied by a KSM type SCT stabilised power supply. Figures 2.3 and 2.4 show the Faraday Magnetic balance which was constructed as part of this project.

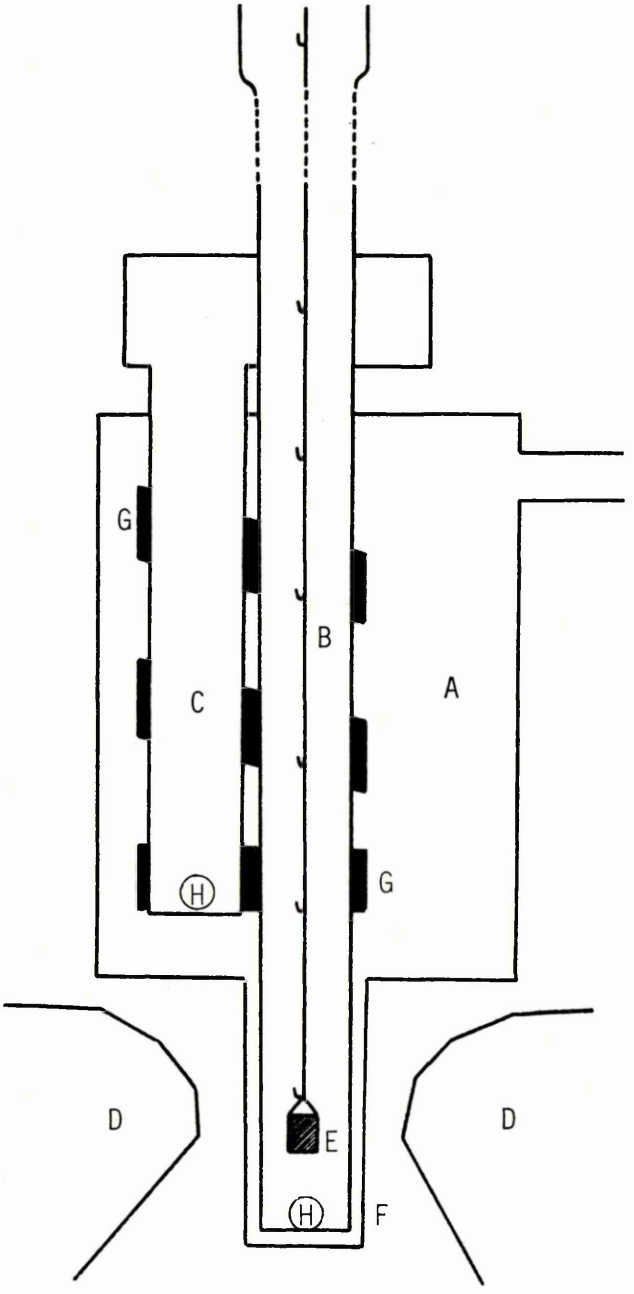

FIGURE 2.2 : Faraday magnetic balance; cold head and sample position

KEY : A ... Vacuum shroud (pumped to 10^{-5}mbar)
B ... Sample tube (dry He gas at 0.1bar)
C ... Cold head
D ... Magnet pole piece
E ... Sample bucket(PTFE)
F ... Diamagnetic casing (copper)
G ... Thermal tape
H ... Platinum sensor

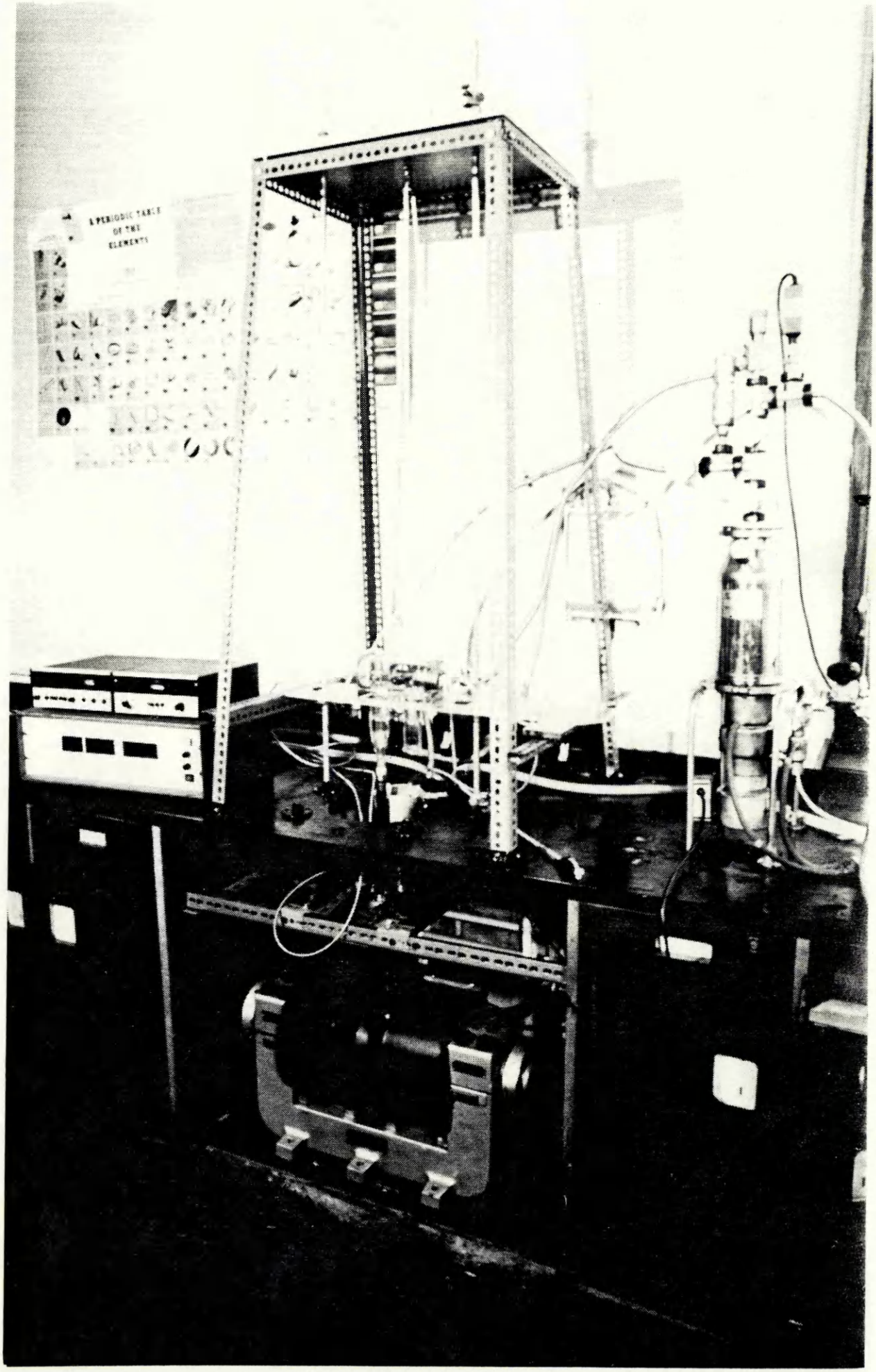
A PERIODIC TABLE
OF THE
ELEMENTS

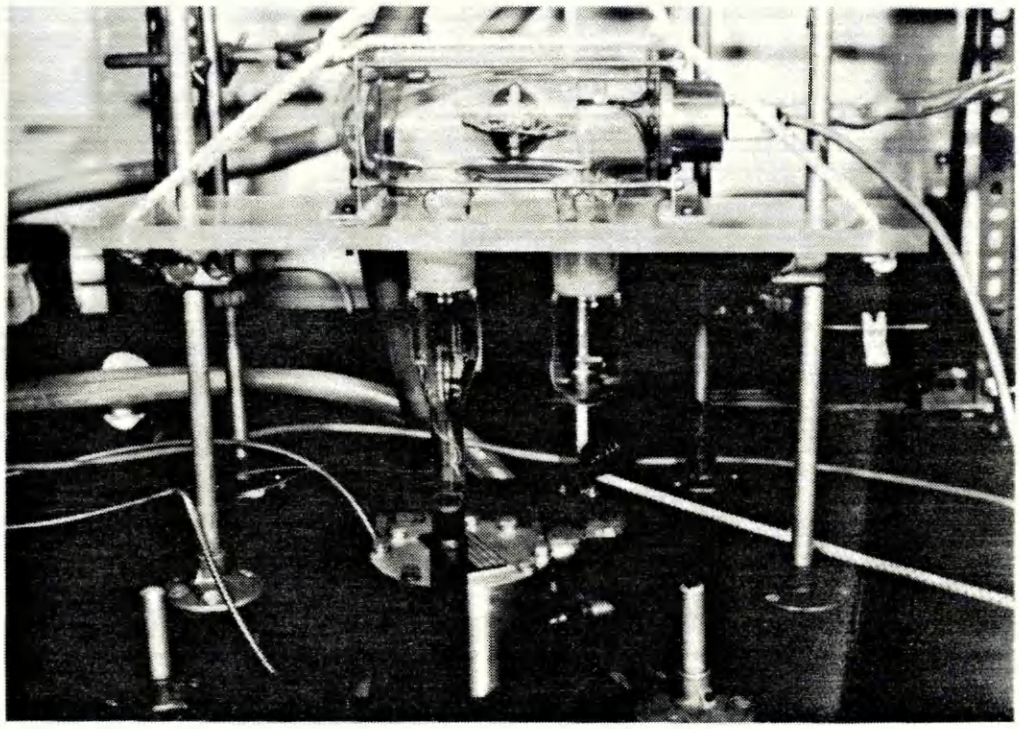

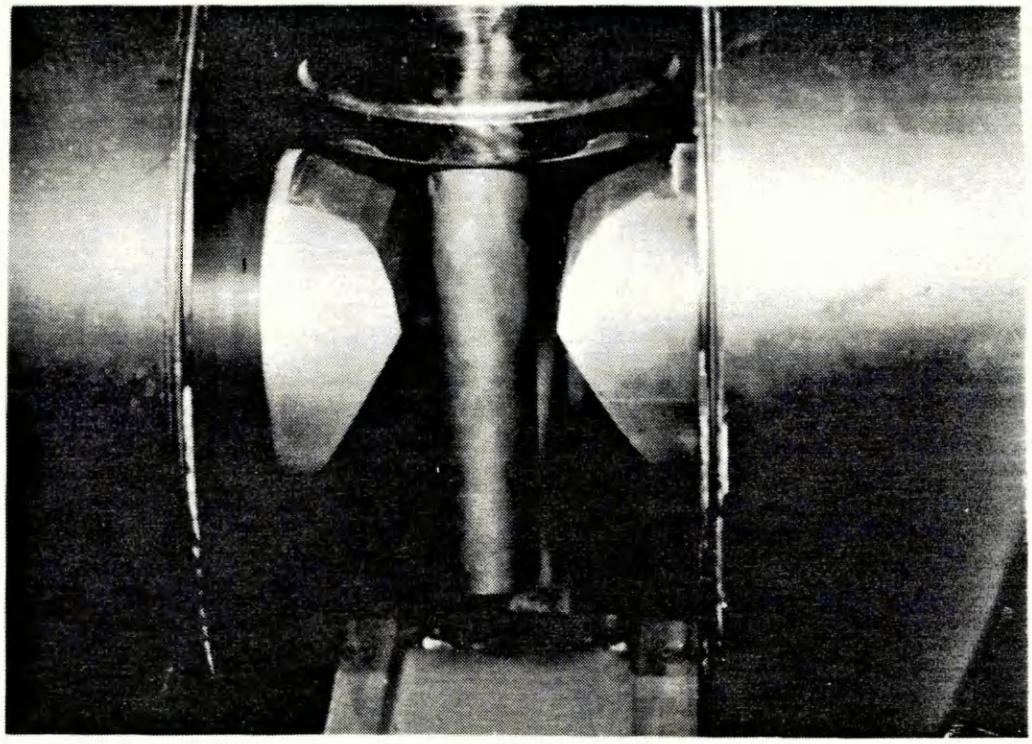

FIGURE 2.4 : (TOP) Microbalance assembly : (ABOVE) Faraday pole pieces and copper vacuum shroud of closed cycle helium refrigerator

The magnetic susceptibility is related to the force exerted on a sample by a magnetic field of constant field x field gradient by[212];

$$g\,\Delta m = m\,\chi_g[H(dH/dz)] \quad \ldots\ldots \text{Eqn 2.1}$$

where **g** is the acceleration due to gravity (981 cms^{-2}), H is the field strength, **z** is the axis perpendicular to the field, χ_g is the gramme susceptibility and **m** is the weight of the sample. Δm is the apparent weight change of the sample when the field is applied.

The Δm values were corrected for the diamagnetism of the bucket by subtracting from the weight change observed of the sample and bucket the value obtained for the empty bucket.

A study of the empty bucket (washed in acetone and dried) showed a temperature independent weight change, throughout the range 25-300 K, of -1.20 +/- 0.03 mg .

The position of the sample was adjusted to maximise H(dH/dz). The product of field and field gradient was calibrated using a sample of pure, dry $HgCo(CNS)_4$ for which;
$\chi_g = 206.67 \times 10^{-6}\ cm^3 g^{-1}$.

The total molar susceptibilities were then calculated from;

$$\chi_{TOT} = Mg\,\Delta m \,/\, m[H(dH/dz)] \quad \ldots\text{Eqn. 2.2}$$

Where M is the molecular weight. χ_{TOT} is in units of $cm^3 mol^{-1}$

The molar spin susceptibility is derived from the total susceptibility by;

$$\chi_S = \chi_{TOT} + \chi_{DIA}$$

with χ_{DIA}, the molar diamagnetic susceptibility calculated from Pascals constants (cm^3mol^{-1})

The susceptibility values were converted to acceptable c.g.s. units using the conversion factor[213];

$$\chi_S(c.g.s.) = \chi_S(S.I.) / 4\pi$$

The reliability of the technique was determined by measuring the susceptibility of a sample of ferric acetyl acetonate, by the Gouy method.The experimental value determined by this technique (χ_{TOT} = Ø.181 cm^3mol^{-1}) is in close agreement with the result obtained by the Faraday method (χ_{TOT} = Ø.2Ø8 cm^3mol^{-1}) and using the experimental details described here. The absolute accuracy of the susceptibility is limited by paramagnetic impurities. The contribution to the susceptibility from paramagnetic impurities is usually determined by an analysis of the low temperature susceptibility. The Curie component due to impurities may be calculated and subtracted from the susceptibility over the complete experimental range of temperatures. Such corrections have not been applied to the results in this work since the low temperature limit set by the experimental constraints is 25 K. Measurements to below 1 K are generally required.

3 Results and Discussion

3.1 A Series of 12 Isostructural Salts of TCNQ with Bis-pyridinium Cations.

The TCNQ complex salts of bis-pyridinium cations have stoichiometries of 1:3, 1:4, 1:4.5, and 1:5 and these values are determined by the length of the cations. Sections 3.2-3.5 present the experimental results for the electrical conductivity and magnetic susceptibility for the isostoichiometric TCNQ salts of the isostructural series. The electrical and magnetic properties are related to the stoichiometry.

In Table 3.1 the relationship between cation length and stoichiometry is shown. Also presented are the space groups and unit cell parameters, the room temperature conductivities and the magnetic properties. The space group and unit cell parameters of the TCNQ salts in this series were determined from X-ray oscillation and Weissenberg photographs[129]. The oscillation photographs of crystals mounted about the needle axis (b axis) show, in addition to the strong layer lines, attributable to the TCNQ lattice, a set of weak layer lines which have been attributed to the hydrated cation lattice[127,177]. The lines are seen to weaken in intensity and may become unobservable after annealing the crystals[127] and this indicates an increase in disorder of the cation lattice. The d spacing of the weak layer lines (d_w) have been used to determine the stoichiometries of the salts

R	R'	b:d_w	Space Group	a	b	c	β	d_w	σ_{300K}	Magnetic Susceptibility
H	CH = CH	1:3	$P2_1/c$	12.79	3.84	27.67	108.0	11.8	10	Curie-Weiss
H	CH_2-CH_2	1:3	$P2_1/c$	12.91	3.93	27.62	109.9	11.8	10	
H	$(CH_2)_3$	1:4	$P2_1/c$	12.93	3.86	27.48	109.1	15.4	1 - 10	Activated
CH_3	CH = CH	1:4	$P2_1/c$	12.73	3.82	27.19	107.8	15.4	1 - 10	
CH_3	$(CH_2)_2$	1:4	$P2_1/c$	12.90	3.84	27.34	107.4	15.4	1 - 50	
CH_3	$(CH_2)_3$	1:4.44	$P2_1/c$	12.93	3.85	27.50	108.1	17.1	10-100	Weak Temperature Dependence
CH_3-CH_2	CH = CH	1:4.53	$P2_1/c$	12.72	3.84	27.67	107.8	17.4	50-500	
CH_3-CH_2	$(CH_2)_2$	1:4.53	$P2_1/c$		3.84			17.4	100-500	
CH_3-CH_2	$(CH_2)_3$	1:5							1 - 10	Weak Temperature Dependence
CH_3-CH_2-CH_2	CH = CH	1:5							0.1 - 1	
CH_3-CH_2-CH_2	$(CH_2)_3$	1:5	$P2_1/c$	12.73	3.87	28.47	107.9	19.4	0.05	
$CH_3(CH_2)_3$	CH = CH	1:5							0.05-1	

TABLE 3.1: Crystal data and electrical and magnetic properties of the isostructural series of TCNQ salts. For key to columns, see overleaf.

given in Table 3.1, i.e. by the ratio $\underline{b}:d_w$. Where unit cell parameters are not listed X-ray powder diffraction studies have confirmed that these materials are isostructural. The stoichiometry has been determined by elemental analysis and spectrophotometric analysis. The series of 12 salts are isostructural and the X-ray crystal structure of 2 congeners have been determined[177,214]. The TCNQs stack plane-to-plane in columns with the hydrated cations occupying narrow channels between the TCNQ stacks with each channel surrounded by six stacks. The channels show no long range order as indicated by the weakness of the layer lines on the oscillation photographs.

KEY TO TABLE 3.1 (previous page)

R .....the quaternary group of the bis-pyridinium cation

R' .....the linking group between pyridinium rings

d_w .....the spacing (Å) of the weak layer lines

$\underline{a},\underline{b},\underline{c}$ ....the unit cell parameters of the TCNQ lattice

All 12 salts have moderate to high conductivities in the range 0.02 to 500 Scm^{-1} at 300 K and Table 3.1 shows that those salts in which the stoichiometry is non-integral have higher conductivities.

The relatively high conductivity of all 12 salts may be attributed in part to the TCNQ stacking characteristics and in part to the condition, $\rho < 1$, where ρ is the mean ionic charge per TCNQ. In the TCNQ columns the overlap is of the exocyclic double bond to ring type and the interplanar spacing is uniform[177,214].

The inherent disorder of the cation lattice favours the homologous TCNQ stacking to provide a favourable conduction pathway[215]. The periodic cation potential is smeared out throughout the channels and inhibits a periodic three dimensional ordering by electrostatic interstack interactions.

The variation in the conductivities (four orders of magnitude at 300 K) of these isostructural salts may have a number of physical origins.

The slight variations which may be found in the TCNQ interplanar spacings (varying from 3.84 to 3.93 Å) are not expected to be a dominant consideration in this case. There is a strong stoichiometric dependence, for example the 1:4.5 salts have conductivities of 10 to 500 Scm^{-1} at 300 K whereas the 1:5 salts have corresponding values of 0.05 to 1 Scm^{-1}.

These differences may reflect differences in the charge density on the TCNQ lattice sites and indeed the 1:4.5 salts may be non-stoichiometric and the charge incommensurate [for convenience in this thesis, these salts are discussed as having a stoichiometry rounded off to the nearest 1/2 integer].

Torrance[144] and Mazumdar and Bloch[143] have suggested that commensurate charge densities of ρ (ρ = 1 or 1/2) result in a reduced conductivity. When ρ = 1/2, the electrons have to overcome the nearest neighbour interaction V_1 and in addition the self consistent screening of the conduction electrons is minimised. On these considerations alone, the 1:4 salts (ρ = Ø.5) in the present study would be expected to have the lowest conductivities in the series, which is clearly not the case (see Table 3.1).

The degree of band filling is not thought to be of primary importance and we propose that the observed trends in the conductivity of the series depend upon the degree of cation disorder and hydration in these salts.

The degree of hydration has been shown to be important in determining the conductivity of the non-stoichiometric salts. This was first shown for $(DEPE)(TCNQ)_{4.5}(H_2O)_x$ in which the conductivity is enhanced and occasionally becomes metallic, after dehydration by vacuum annealing. We have shown in this work that the properties of $(DEPA)(TCNQ)_{4.5}(H_2O)_x$ and $(DMPP)(TCNQ)_{4.5}(H_2O)_x$ also depend upon the annealing process

(see Section 3.4). When annealed the crystals no longer give the weak layer lines on the X-ray oscillation photographs and this indicates an increase in disorder along the cation channels. Thus we may relate the conductivity enhancement to the disordering process but other factors should be considered. Upon annealing, the crystals dehydrate and there is a slight contraction (ca. Ø.6%) of the unit cell[216]. It is not clear to what extent these small structural changes affect the conductivity. Also the process may introduce states into the band gap[217]. However after considering these possibilities the degree of disorder is believed to have the greatest effect on the conductivity. As a guide to the disorder the cation layer lines are considered for the isosructural salts. For the highly conductive TCNQ salts (1:4.5) the layer lines are very weak and thus indicate a disordered lattice whereas for the less conductive 1:5 salts the cation layer lines are stronger and show some structure[214] and thus indicate a partially ordered cation lattice.

All of the salts in this series show transitions in the electrical conductivity at about 4Ø K. The non-metallic crystals undergo conductor to insulator transitions at this temperature (see sections 3.4 and 3.5) whereas the metallic crystals show a smeared out, or suppressed, transition. If the transition is attributed to a lattice distortion then in the metallic case the suppression of the phase change may be attributed to greater disorder within the lattice. The

metallic crystals of $(DEPE)(TCNQ)_{4.5}(H_2O)_x$ and $(DEPA)(TCNQ)_{4.5}(H_2O)_x$ remain highly conductive to below 10 K. Metallic behaviour is a property of the 1:4.5 salts and disorder associated with a non-stoichiometry might play an important role.

It has been reported that the conductivity in $(DEPE)(TCNQ)_{4.5}(H_2O)_x$ may be fit with a $T^{-0.5}$ law, consistent with a model of Fröhlich CDW conduction with accoustic phonon scattering[52]. The high conductivity in the dehydrated 1:4.5 salts might be due to CDWs whose phase is allowed to vary freely due to the incommensurability. In TMTSF-DMTCNQ, the pressure enhancement of the conductivity is possibly due to a release of a CDW contribution to the conductivity. In this salt, the pressure drives the lattice to incommensurability and the M-I phase transition is suppressed.

However, the description of the conductivity of these salts in terms of Fröhlich conduction is not complete since although it would explain the differences in the conductivity of the 1:4.5 salts and the stoichiometric salts, the phase transitions seen in the stoichiometric salts would be expected to be at a higher temperature. In fact the phase transitions exhibited by salts in this series all occur at about 40 K.

The phase transitions are not of the incommensurate-to-commensurate type, instead we attribute the phase transitions, in part, to an ordering of the cation lattice

upon cooling and the electrical properties in general for the series to the degree of cation lattice disorder. In this scheme, the disorder, inherent in the cation lattice above the phase transition temperature, may have an additional contribution from the incommensurability in the 1:4.5 salts.

3.2 The 1:2 and 1:3 Salts

3.2.1: Introduction

Two factors determining the low conductivity in TCNQ simple salts are, (i) integral charge on the TCNQ moiety and, (ii) the TCNQ stacking characteristics. Most TCNQ simple salts are insulating[4,79,94]. The integral charge on each TCNQ moiety means that for conduction to occur, by electron migration between sites, two electrons must occupy the same site. This is energetically unfavourable due to on-site electron-electron Coulomb repulsion. The introduction of charge vacant TCNQ sites generally enhances the conductivity and such mixed valence complex salts may be highly conductive[218] or even metallic[52,55]. A mean non-integral charge on the TCNQ lattice sites as well as favourable TCNQ stacking are necessary for high conductivity[144]. The structural features necessary for high conductivity in TCNQ salts are (i) infinite stacking of TCNQs with regular, short spacing and (ii) favourable overlap between TCNQs of the exocyclic double-bond to ring type (Figure 1.2,p 18)[10,45,59]

In this section, contrasts and comparisons are made between the simple (1:2) and complex (1:3) salts of the bis-pyridinium cations and evidence of alloy formation in salts of H-quaternised dications is reported.

3.2.2: (DHPA)$(TCNQ)_2$; a Simple Salt

The structure of (DHPA)$(TCNQ)_2$ was determined as part of this project. It consists of TCNQ diads in sheets parallel to the bc plane, successive sheets being interleaved along a by the DHPA cations. Fractional positional parameters bond lengths and bond angles are listed in Appendix I.

The overlap between TCNQs within each diad is of the favourable exocyclic double bond to ring type (see figure 1.2,p 18) and the mean interplanar spacing is 3.Ø4Å. It should be noted that this spacing is one of the shortest known for a TCNQ salt. However there is no direct overlap between succesive diads (see Figure 3.1).

The cations adopt a gauche configuration with a C(15)-C(18) C(18')-C(15') torsion angle of 56^{o} (Figure 3.2). It is of interest to note that in (DMPA)$(TCNQ)_4$ and $(DEPA)_2(TCNQ)_5$, the cations are extended[219].

The closest non-hydrogen cation to TCNQ contacts, N(2)-N(5') = 2.894Å and N(4)-C(17') = 3.175Å, are less than the Van-der-Waals distances of 3.ØÅ and 3.2Å, respectively. The N(5) - H - N(5') distance is 2.Ø6Å and the atoms are co-linear. These close contacts are significantly shorter than the corresponding distances in the 1,2-bis(1-alkyl-4-pyridinium)ethane TCNQ salts[54,220] and the possible instability of the cation in solution, to be discussed, may arise as a result of this strong interaction.

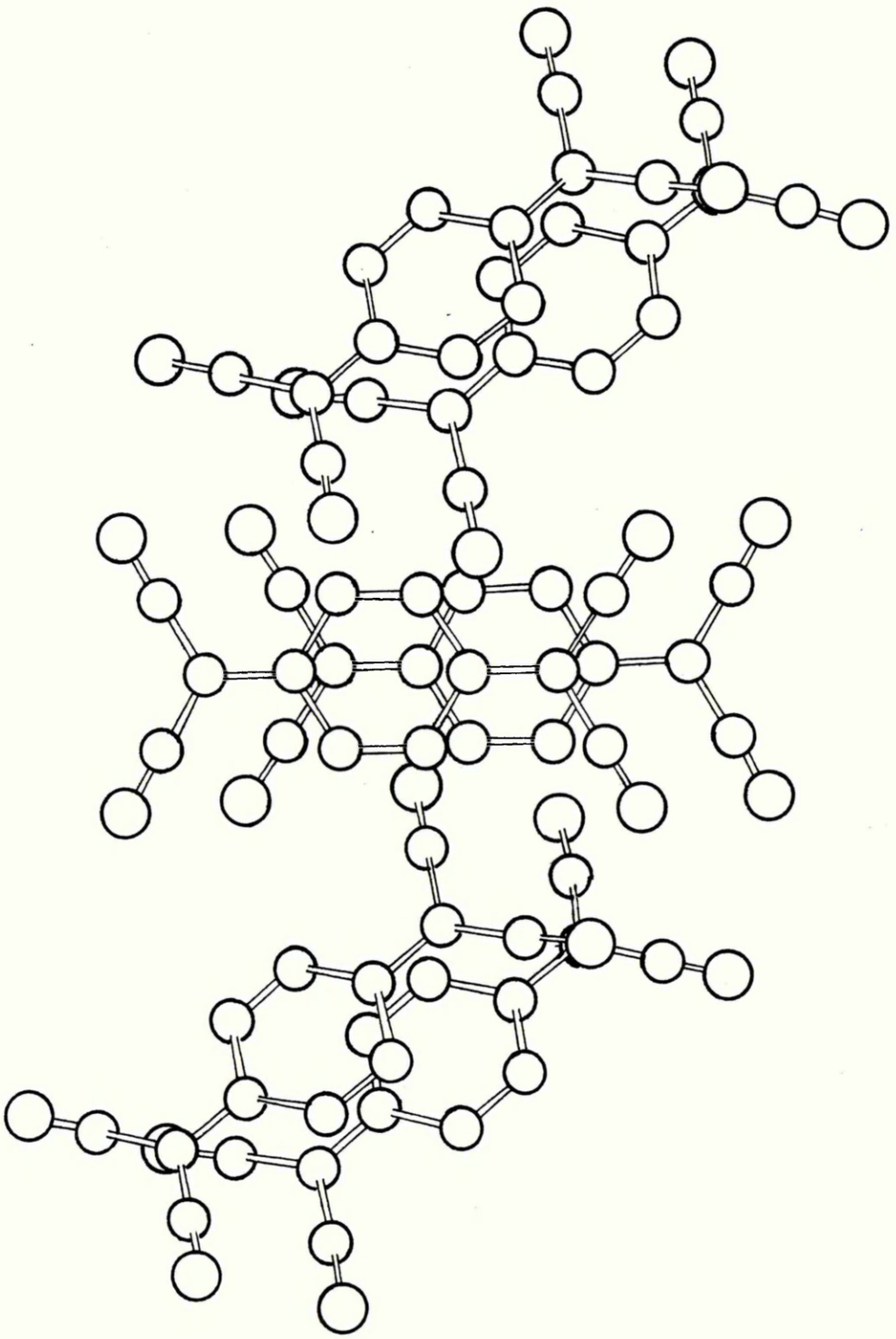

FIGURE 3.1 : The structure of $(DHPA)(TCNQ)_2$; cations not shown.

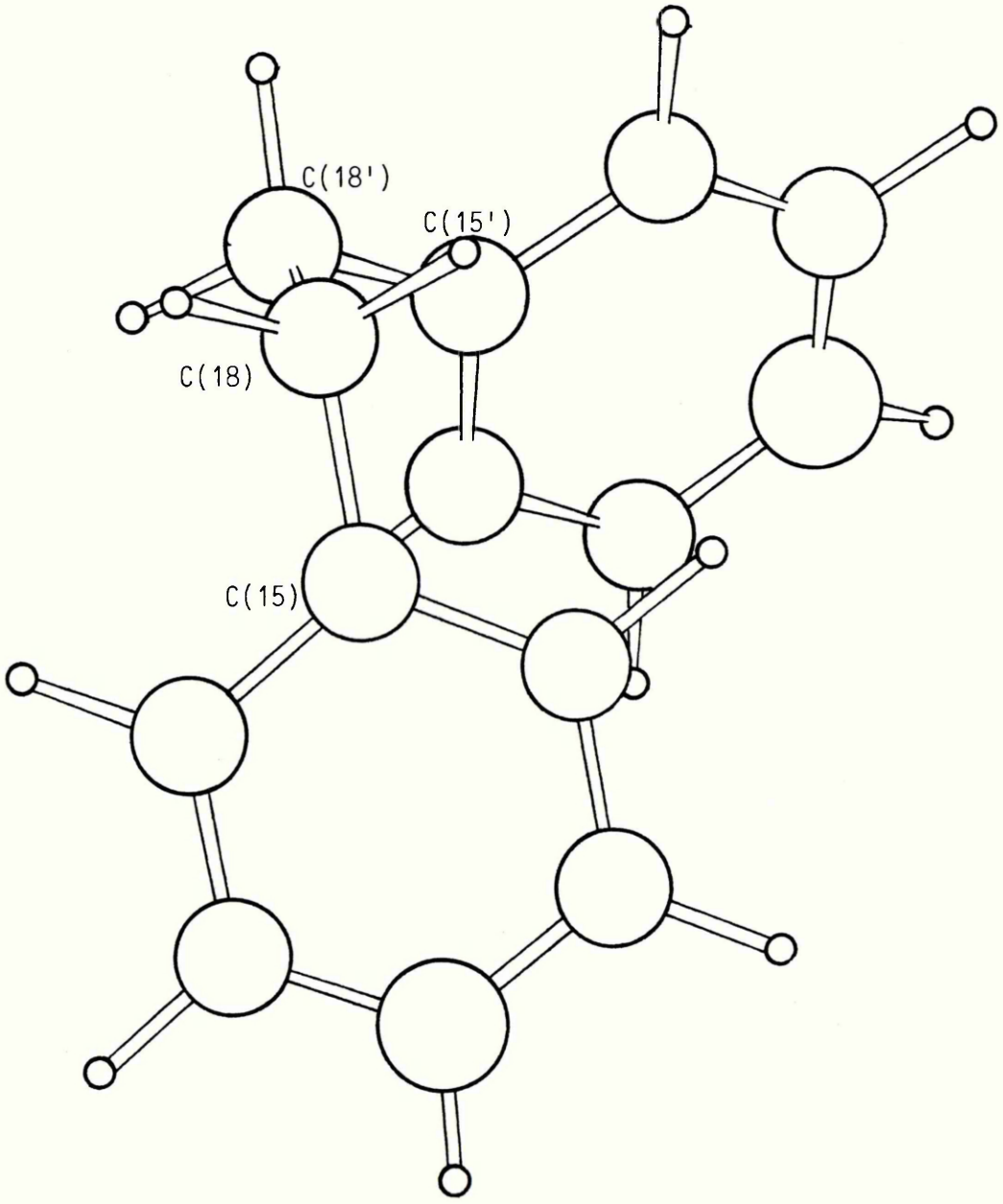

FIGURE 3.2 : The DHPA cation

Flandrois and Chasseau[221] have developed a scheme whereby the charge density on the TCNQ moiety may be determined from a study of the TCNQ bond lengths.

The bonds that are most important in the analysis are shown in Figure 3.3

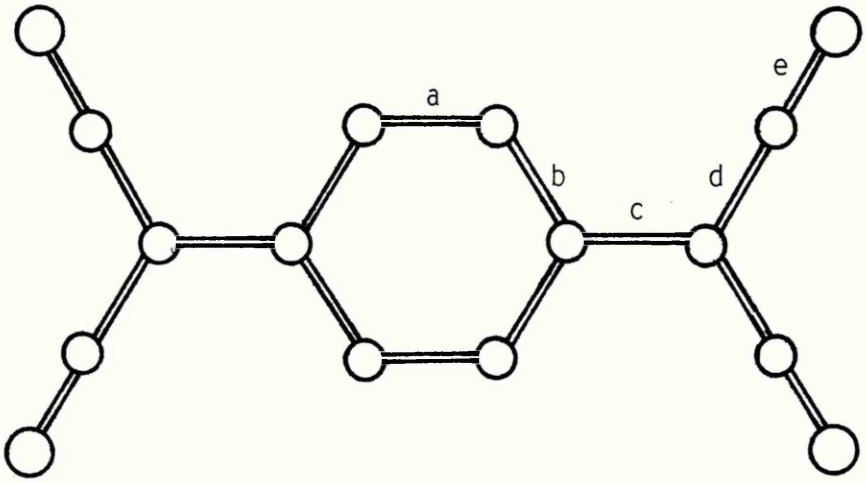

FIGURE 3.3

In neutral TCNQ, the lengths of the labelled bonds are; a = 1.344, b = 1.442, c = 1.373, d = 1.435 and e = 1.138 Ångströms(ref.222). In general, bonds a,c and e are found to lengthen when the molecule accepts an electronic charge whereas bonds b and d shorten. In the simple ionic salts Rb-TCNQ and Na-TCNQ where the charge on TCNQ is expected to be le, the lengths of the bonds b,c and d become nearly equal in length. Flandrois and Chasseau have evaluated the parameters, b-c and c-d, and have assumed a linear variation in these factors between neutral TCNQ (b-c = Ø.Ø69 and c-d = - Ø.Ø62) and the radical anion (b-c, c-d = Ø). For example, in TTF TCNQ [19], the parameters are; b-c = Ø.Ø31 and c-d = - Ø.Ø21. These values give the degree of charge transfer in

TTF-TCNQ to be 0.55 and 0.66 based on (b-c) and (c-d) respectively. The mean value of 0.61 compares very well with other methods of determination of this parameter, such as, for example, neutron diffraction[16]. Flandrois and Chasseau use the agreement to justify their assumption of a linear relationship between the charge on the TCNQ and the bond length parameters.

In $(DHPA)(TCNQ)_2$, b-c = 0.008 Å and c-d = 0.004 Å and within experimental error, these values correspond to a charge on the TCNQ moiety of 1e. It is of interest to note that the bond lengths of TCNQ in $(DHPA)(TCNQ)_2$ are very similar to those found for Na-TCNQ[78] and K-TCNQ[58].

The electronic absorption spectra of the crystals of $(DHPA)(TCNQ)_2$ dissolved in acetonitrile show maxima at 842, 824, 762, 745, 728, 679, 666, 436, 420, 410, and 395 nm with A_{395}/A_{842} = 0.6. According to the results of Rembaum et al.[211] this corresponds to an average charge of 1e per TCNQ, in agreement with the conclusion drawn from the structural analysis. However it may be unwise to compare the results obtained from the solid state and solution studies.

As expected, on the grounds of poor stacking and complete charge transfer, the conductivity of this salt is low (Table 3.2,p 100) and the material is diamagnetic. The molar susceptibility of $(DHPA)(TCNQ)_2$ is -3.2×10^{-4} emu mol^{-1} and temperature independent and is in close agreement to the diamagnetic value determined from Pascal's constants (-3.53×10^{-4} emu mol^{-1}).

3.2.3 : Complex Salts $(DHPA)(TCNQ)_3$ and $(DHPE)(TCNQ)_3$

The room temperature conductivities and magnetic properties for the salts $(DHPA)(TCNQ)_3$ and $(DHPE)(TCNQ)_3$ are given in Table 3.2. The conductivities of both salts are high, suggesting a structure possessing infinite TCNQ columns and uniform interplanar spacings. The temperature dependence of conductivity for the salts are shown in Figures 3.4 and 3.5. Within a limited temperature range between 300-200K, the log σ versus reciprocal temperature plots are linear but at lower temperatures, they exhibit curvature. All attempts to fit the experimental data to the expressions commonly used to describe the conduction process in quasi-one-dimensional materials[149,223] have been unsuccessful. In this case the curvature is attributed to the onset of extrinsic behaviour due to impurities or defects. The activation energies, derived from the log σ versus reciprocal temperature plots at high temperature, are given in Table 3.2. Both salts may be classified as small band gap semiconductors.

SALT	$\sigma_{R.T.}(Scm^{-1})$	$E_A(eV)$	Magnetic Susceptibility
$(DHPA)(TCNQ)_2$	10^{-7}	-	Diamagnetic
$(DHPA)(TCNQ)_3$	10	0.12	Curie-Weiss θ = 15K, μ_{eff} = 1.68
$(DHPE)(TCNQ)_3$	10	0.11	Curie-Weiss θ = 30K, μ_{eff} = 1.31
$(DHPE\ Cl)_{0.3}$ $(DPE)_{0.7}(TCNQ)$	10 - 70	-	Temperature independent $\chi_s(300K) = 1.3 \times 10^{-4}$emu/mole

TABLE 3.2 : The electrical and magnetic properties of simple ionic, complex and alloy TCNQ salts of H-quaternised bis-pyridinium cations.

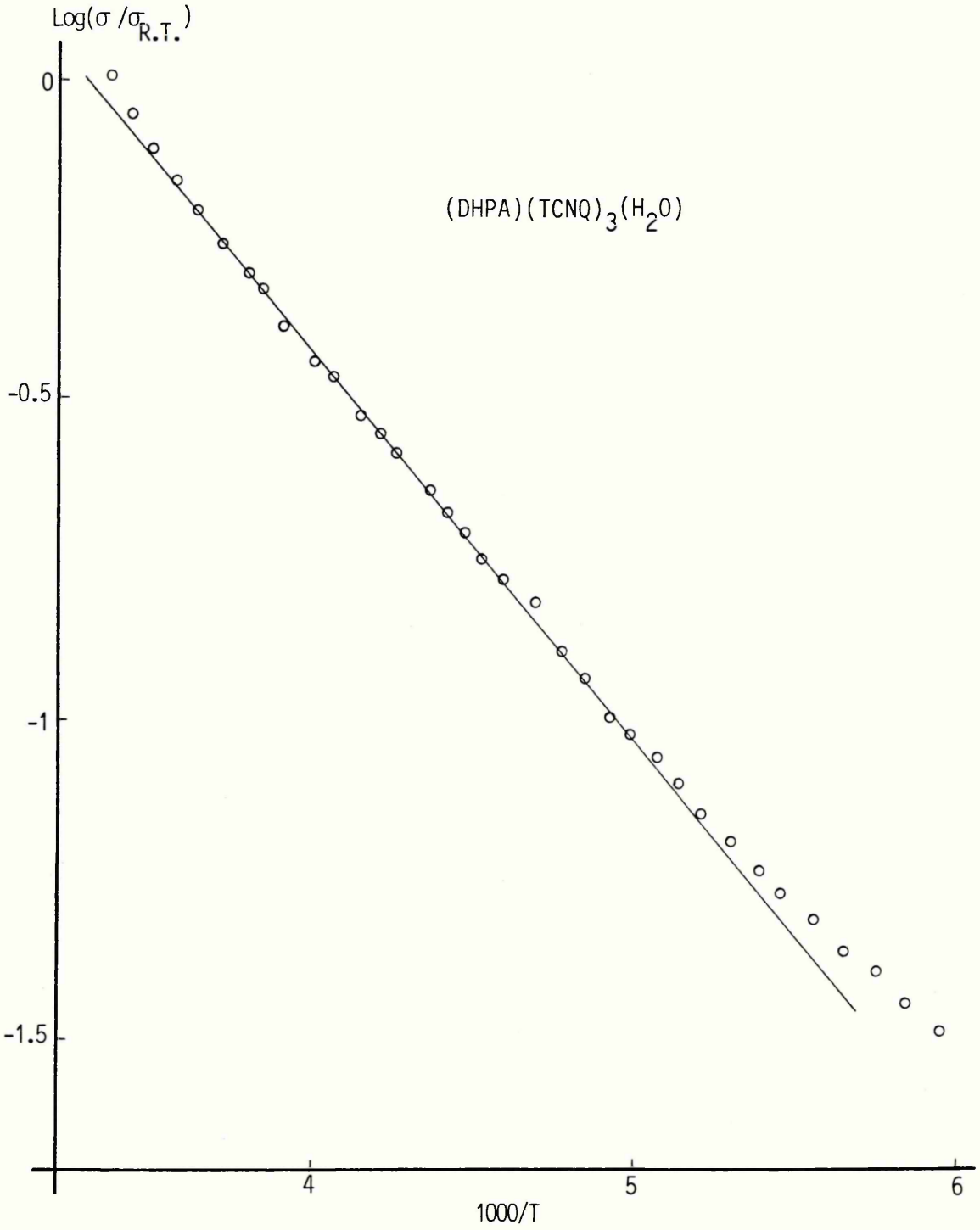

FIGURE 3.4 : Log normalised conductivity versus reciprocal temperature of $(DHPA)(TCNQ)_3(H_2O)$

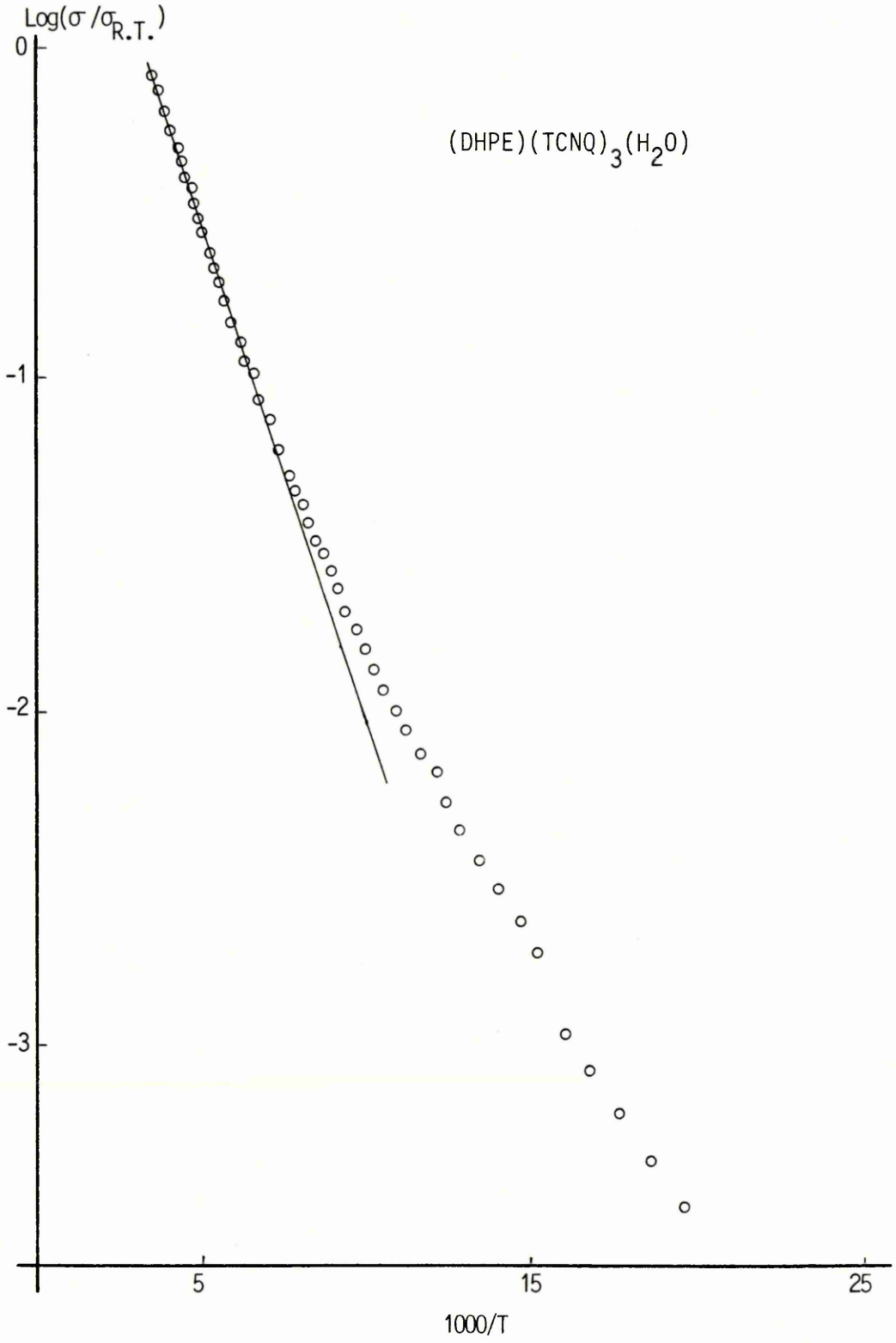

FIGURE 3.5 : Log normalised conductivity versus reciprocal temperature of $(DHPE)(TCNQ)_3(H_2O)$

The temperature dependence of the magnetic susceptibility, corrected for core diamagnetism, for the 1:3 salts are given in Figures 3.6 and 3.7. The $1/\chi$ versus T plots are linear in the range 300 to 25K, showing both salts to be Curie-Weiss paramagnets where the susceptibility varies as $\chi = C/(T + \theta)$.

From the slope of Figure 3.8 (p 106), for $(DHPA)(TCNQ)_3$, $C = 0.35$ emu $mol^{-1}K$ and $\theta = 15$ K.

The effective magneton number, μ_{eff} may be determined from;

$$\mu_{eff} = (3k/N\ \mu_B{}^2)^{1/2}C^{1/2} = 2.84C^{1/2}$$

For the experimental value , C = 0.35, $\mu_{eff} = 1.68$.

Using the "spin only" formula;

$$\mu_{eff} = [n(n + 2)]^{1/2}$$

where n is the number of free spins per mole, $\mu_{eff} = 1.73$ for one free spin (electron) per mole and agrees well with the experimental value. Thus the mean ionic charge on each TCNQ moiety in $(DHPA)(TCNQ)_3$ is of the order of 0.33 e. This is an anomalous value when compared with the expected mean ionic charge of 0.66 e from the formula; $(DHPA)^{2+}(TCNQ)_3{}^{2-}$.

The absorbance ratio A_{395}/A_{842}, derived from the visible spectrum obtained from crystals dissolved in acetonitrile, is 2.7 to 3.0. This corresponds to a mean ionic charge of 0.3 to 0.4e on the TCNQs and is in agreement with the magnetic result. In addition, the value of ρ obtained from thermoelectric power measurements[94] is between 0.4 and 0.5.

In solution, the H-quaternised cations are susceptible to deprotonation as shown by Somoano et.al.[34]. The dications

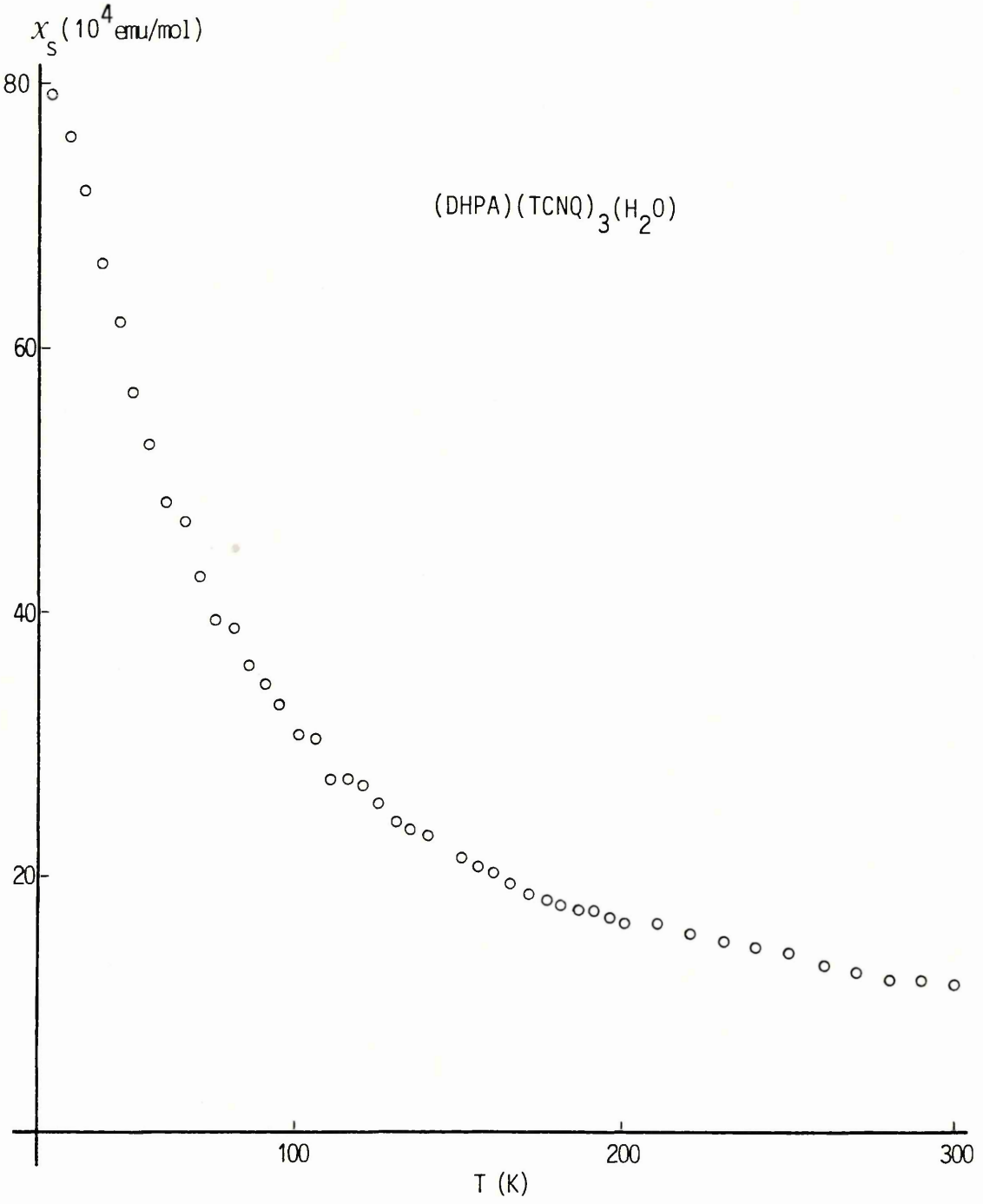

FIGURE 3.6 : The susceptibility, corrected for core diamagnetism versus temperature of (DHPA)(TCNQ)$_3$(H_2O)

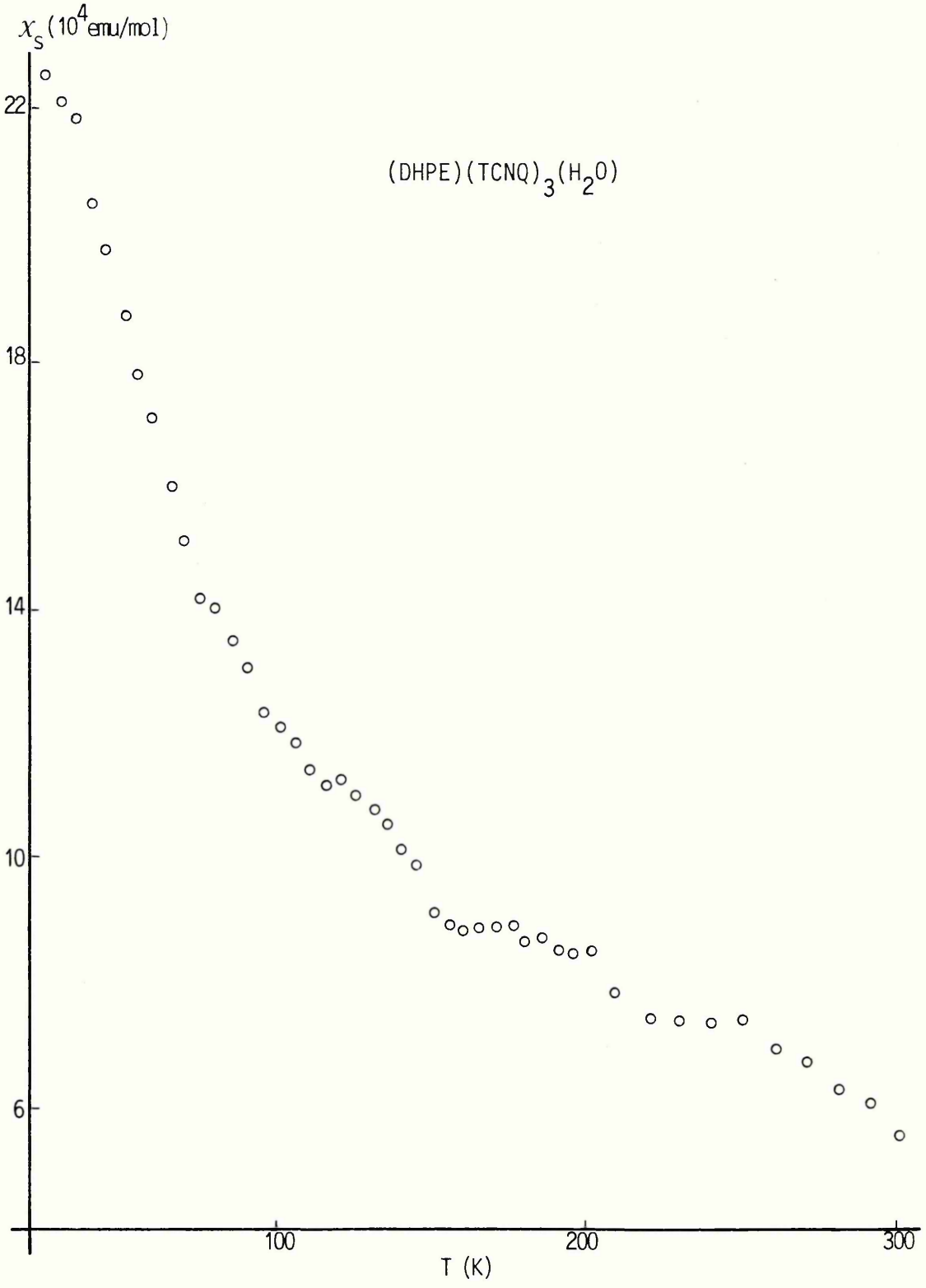

FIGURE 3.7 : The susceptibility, corrected for core diamagnetism versus temperature of (DHPE)(TCNQ)$_3$(H$_2$O)

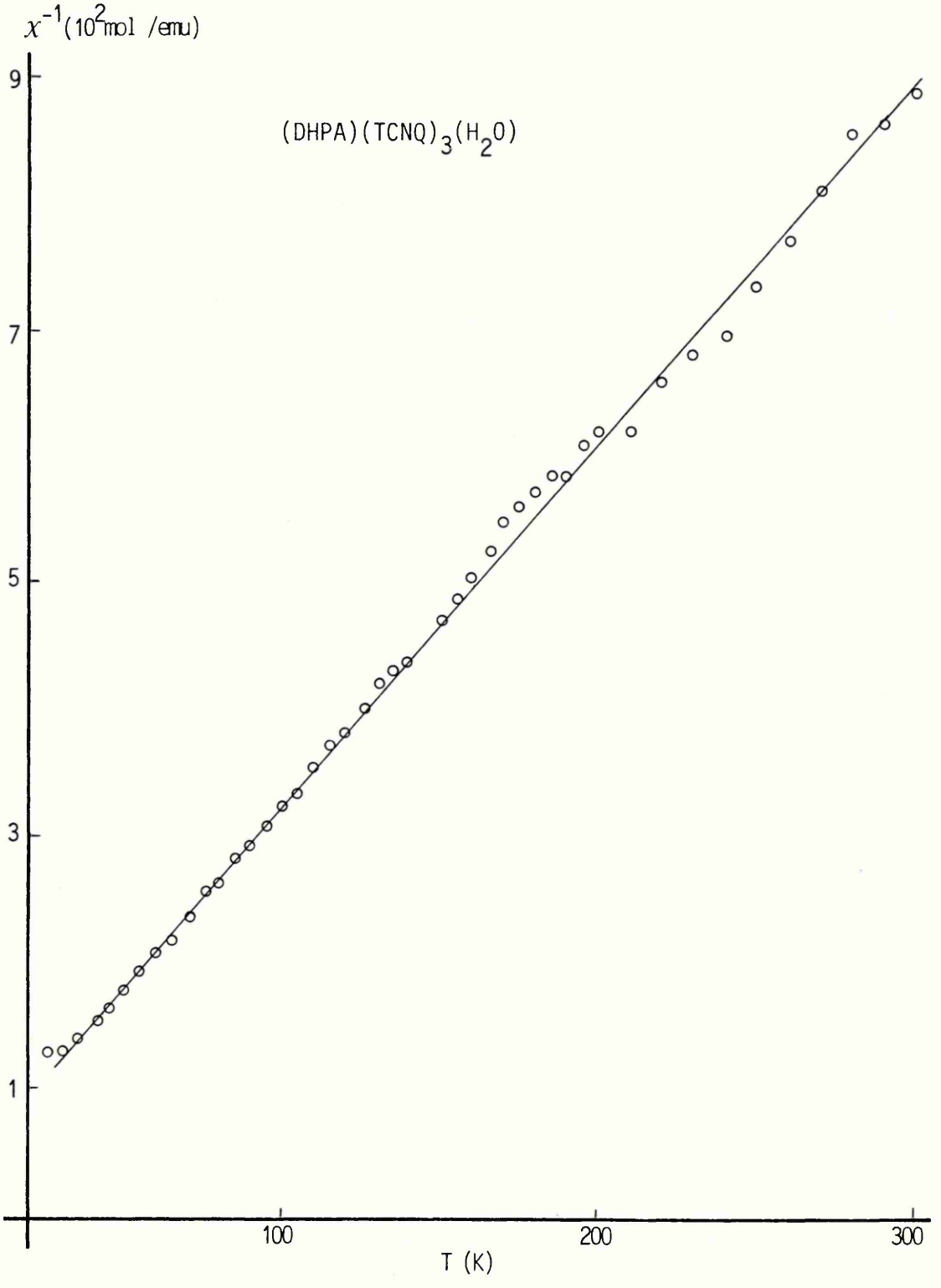

FIGURE 3.8 : The reciprocal susceptibility versus temperature of (DHPA)(TCNQ)$_3$(H$_2$O)

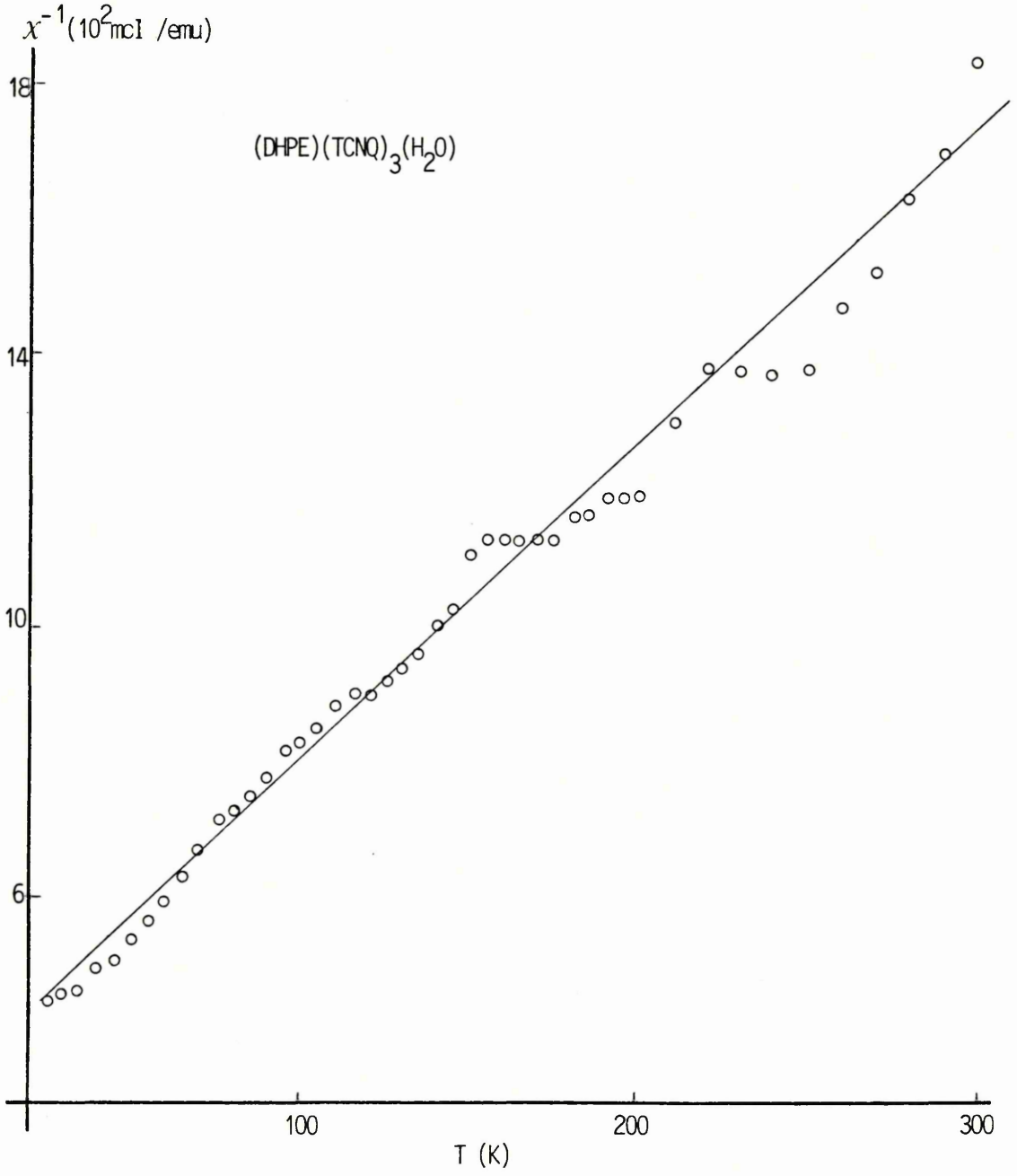

FIGURE 3.9 : The reciprocal susceptibility versus temperature of (DHPE)(TCNQ)$_3$(H$_2$O)

react with $TCNQ^-$, losing their quaternary protons with the subsequent formation of H_2TCNQ and $TCNQ^o$. If this process is occurring in the preparation of $(DHPA)(TCNQ)_3$ then the observed reduction in the mean ionic charge from that expected may be explained by the inclusion of either, monoquaternised cation (HPA) or, neutral 1,2-bis(4-pyridyl)ethane, (DPA), in the structure. This is supported by the fact that the dication and neutral base are of similar size which would favour the replacement of one by the other to give an alloy of general formula; $(DHPA)_x(DPA)_{1-x}(TCNQ)_3$. For simplicity, only the neutral base is considered.

The occupancy of DPA determined from the experimental data varies between 33% to 50%. A higher occupancy (90%) has been obtained when neutral 1,2-bis(4-pyridyl)ethane was added to the reaction mixture. This result supports the hypothesis of alloy formation in this 1:3 complex salt.

The slope of Figure 3.9 (p 107) for $(DHPE)(TCNQ)_3$ gives a Curie constant of C = 0.213 and hence μ_{eff} = 1.31. From the spin-only formula n, the number of free spins per mole, is 0.7. This gives the mean ionic charge per TCNQ in $(DHPE)(TCNQ)_3$ to be 0.23 e. From the electronic absorption spectrum, A_{395}/A_{842} = 3 which corresponds to a mean ionic charge of 0.4e per TCNQ. It is possible that alloy formation is occurring in the preparation of this salt by a similar mechanism to that in the DHPA salt. Recently the X-ray

crystal structure for $(DHPE)(TCNQ)_3$ has confirmed the overall stoichiometry of 1:3 (ref.177). From the elemental analysis, spectroscopic data and the magnetic susceptibility results the salt analyses as;

$(4,4\text{-DHPE})_x(4,4\text{-DPE})_{1-x}\ (TCNQ)_3$ where x = Ø.4.

In both of these salts the Curie-Weiss behaviour, persistent to low temperatures, suggest a magnetically dilute spin system with the dilution possibly due to the alloy formation.

3.2.4 : $(DHPE\ Cl)_{Ø.3}(DPE)_{Ø.7}$ TCNQ, An Alloy System.

In the attempts to prepare a simple salt of TCNQ with the cation $(DHPE)^{2+}.2Cl^-$, fine, black needle crystals were obtained. From the elemental and spectroscopic analysis the formula was determined as $(DHPE\ Cl)_{Ø.3}(DPE)_{Ø.7}TCNQ$.

The room temperature conductivity of this salt (Table 3.2, p 1ØØ) is high. Crystals suitable for temperature dependence measurements were not available at the time of the study.

The total susceptibility is independent of temperature in the range 3ØØ to 25 K, with a value χ_{TOT} = - $9.6x1Ø^{-5}$emu $mole^{-1}$ When the correction is made for the molar diamagnetic susceptibility of this salt (χ_{dia} = - $2.3x1Ø^{-4}$emu $mole^{-1}$), a value of χ_s = 1.34 x $1Ø^{-4}$emu $mole^{-1}$, is obtained. This small positive value, independent of temperature within the experimental temperature range could be interpreted as the Pauli paramagnetism for this material. If this is so, then

the bandwidth may be calculated from[176];

$$\chi_{pauli} = N \mu_B^2 / \pi t \ Sin \ (1/2 \pi \rho)$$

Using the room temperature susceptibility value obtained experimentally and $\rho = 0.7$, determined from the electronic absorption spectrum method, the bandwidth is calculated to be; $4t = 0.52$ eV

Many organic metals have bandwidths of the order of 0.3 to 0.5 eV(ref.176). The conductivity temperature dependences of single crystals of the salt have recently shown metallic behaviour. I propose that the high conductivity is due, in part, to a reduction of the mean ionic charge per TCNQ moiety by random occupation of neutral DPE in the cation sites. Thus the role of disorder in determining the conductivity in these salts, which has already been discussed, is again shown to be significant.

3.2.5 Summary

$(DHPA)(TCNQ)_3$ and $(DHPE)(TCNQ)_3$ are members of an isostructural series of twelve TCNQ salts. In these salts, the TCNQ molecules stack plane-to-plane in columns with the cations occupying narrow channels among the stacks. The channels can accommodate cations of widely differing lengths (see Section 3.1). This evidence, combined with the fact that the quaternised or neutral donors are of similar size, gives support to the postulation of alloy formation in these salts due to variable occupation of the cation sites by the neutral species. The magnetic susceptibility measurements support the determinations of mean ionic charge on the TCNQ species made from spectral and thermoelectric methods. The similarities in the electrical and magnetic properties between the two salts is noted in support of the observations made in the following sections of a relationship between stoichiometry and the general features of these properties.

In $(DHPE\ Cl)_{\emptyset.3}(DPE)_{\emptyset.7}$ and $(4,4\text{-}DHPE)_{\emptyset.4}(DPE)_{\emptyset.6}(TCNQ)_3$ direct evidence has been obtained, from the elemental analysis and spectral data, of the alloy character of these salts.

In (DHPA)$(TCNQ)_2$, the electrical and magnetic properties are as expected for a simple ionic salt and no evidence for alloy formation has been found. The structural characteristics are of a type unfavourable for electrical conduction.

3.3 The 1:4 Salts: $(DMPA)(TCNQ)_4$ and its Isostructural Congeners

The electrical and magnetic properties of the 1:4 salts are given in Table 3.3. All three salts possess moderate room temperature conductivities as expected from salts in which the TCNQ stack is regular and in which the ionic charge per site is less than 1. The cell constants of $(DMPA)(TCNQ)_4(H_2O)$ and the isostoichiometric congeners with the cations DMPE and DMPP indicate favourable stacking. A 1:4 DMPA-TCNQ salt has been synthesised previously by Ashwell et.al.[220] in which the TCNQs stack in stoichiometric groups of four with no direct overlap between adjacent tetrads. The conductivity of this salt in the general direction of stacking is 2×10^{-3} Scm^{-1} at 300K compared with 10 to 50 Scm^{-1} for the alternative structural phase reported here.

The log σ versus reciprocal temperature plot for $(DMPA)(TCNQ)_4(H_2O)$ (Figure 3.10,p 115) is linear for most of the range 100 - 300 K and only deviates at the extremes. The activation energy derived from the linear region is 0.04eV. Similar results have been obtained for the isostoichiometric DMPE and DHPP salts (see Table 3.3). Attempts have been made to fit the conductivity data of the 1:4 salts in the temperature range 40 - 300 K to the common conductivity expressions. The model of variable range phonon assisted hopping in one dimension[223], that is;

$$\sigma = \sigma_o \exp(-\Delta/T)^{1/2}$$

SALT	$\sigma_{R.T.}$ (Scm^{-1})	E_A(eV)	$\chi_{s(300K)}$ ($x10^4$emu/mole)	χ_{dia}	a(γ)	γ	$\Delta(\gamma)$	J(eV)
$(DMPE)(TCNQ)_4H_2O$	1.0	0.06	10	5.96	0.346	0.56	0.65	0.049
$(DHPP)(TCNQ)_4H_2O$	1.26	0.06	9.3	5.89	0.217	0.71	0.47	0.049
$(DMPA)(TCNQ)_4H_2O$	10	0.04	10.7	6.02	0.287	0.64	0.56	0.048

TABLE 3.3: The electrical and magnetic properties of the 1:4 salts.

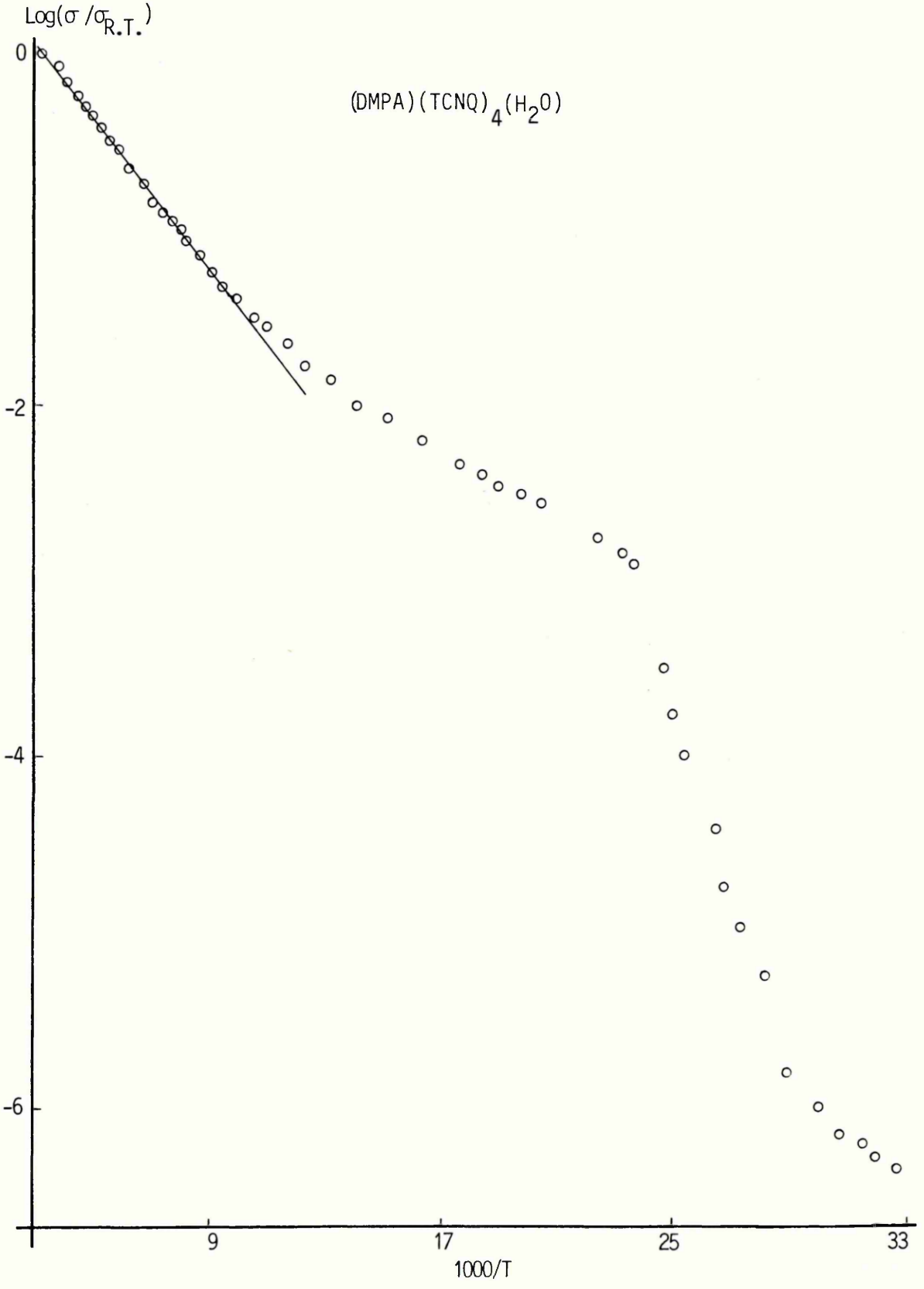

FIGURE 3.10 : Log normalised conductivity versus reciprocal temperature of $(DMPA)(TCNQ)_4(H_2O)$

has been used without success. Similarly a temperature dependent pre-exponential factor in the semiconductor equation;

$$\sigma = \sigma_o \exp(-E_A/kT)$$

does not adequatly describe the conductivity over the complete temperature range. From these results, we assume that the deviation observed at high temperatures does in fact arise as a result of a slight temperature dependence of the pre-exponential factor but at low temperatures may be attributed to the onset of extrinsic behaviour. Evidence of an intrinsic/extrinsic transition in $(DMPA)(TCNQ)_4(H_2O)$ at about 120 K has been obtained from thermoelectric power measurements[224]. The thermoelectric power changes from n-type to p-type at this temperature. Ashwell et.al.[167] have fit the conductivity data of N,N-dimethyl-4,4-bipyridinium $(TCNQ)_4$ with reasonable success to the expression;

$$\sigma = \beta T^x \exp(-E_A/kT)$$

where $x = -2$ and $E_A = 0.21$ eV. The temperature exponent in the pre-exponential factor suggests a temperature dependent mobility of carriers scattered by optical phonons[149]. Attempts to fit the data for the 1:4 salts discussed here have been unsuccessful except over a limited temperature range.

Below 40 K $(DMPA)(TCNQ)_4(H_2O)$ exhibits a conductor to insulator transition (Figure 3.10). This is attributed to a lattice distortion which may arise as a result of a partial ordering of the cation lattice upon cooling. There is evidence of a conductivity anomaly in the log normalised

conductivity versus reciprocal temperature plot of $(DMPE)(TCNQ)_4(H_2O)$ (Figure 3.11, overleaf) at 38 K which could also signify a phase transition. It should be noted that the DMPE studies were carried out on a pellet of a microcrystalline specimen.

The magnetic properties of the 1:4 salts are given in Table 3.3. In all these salts the susceptibility increases with increasing temperature in the range 90 to 300 K (Figures 3.13 - 3.15) and the semilog plot, log χT versus 1000/T (Figures 3.16 - 3.18) are linear in this temperature range. In $(DMPA)(TCNQ)_4H_2O$ and $(DHPP)(TCNQ)_4H_2O$ there is evidence of a Curie tail in the susceptibility below 90 K whereas in $(DMPE)(TCNQ)_4H_2O$ the susceptibility is temperature independent between 25 K and 80 K with no evidence of an upturn. In many salts, the low temperature Curie law behaviour has been attributed to paramagnetic impurities[7,180,183]. If the impurity susceptibility follows a Curie law, it is possible to subtract this contribution from the experimental data over the whole experimental temperature range. This analysis has been performed for TTF-TCNQ where the low temperature upturn follows a T^{-1} dependence. This has not been done for 1:4 salts, since there are insufficient results in this low temperature region to allow a valid Curie plot to be made. However it is of interest that the susceptibility of $(DHPP)(TCNQ)_4H_2O$ in this limited temperature range may vary as $\chi \propto T^{-0.5}$ as determined

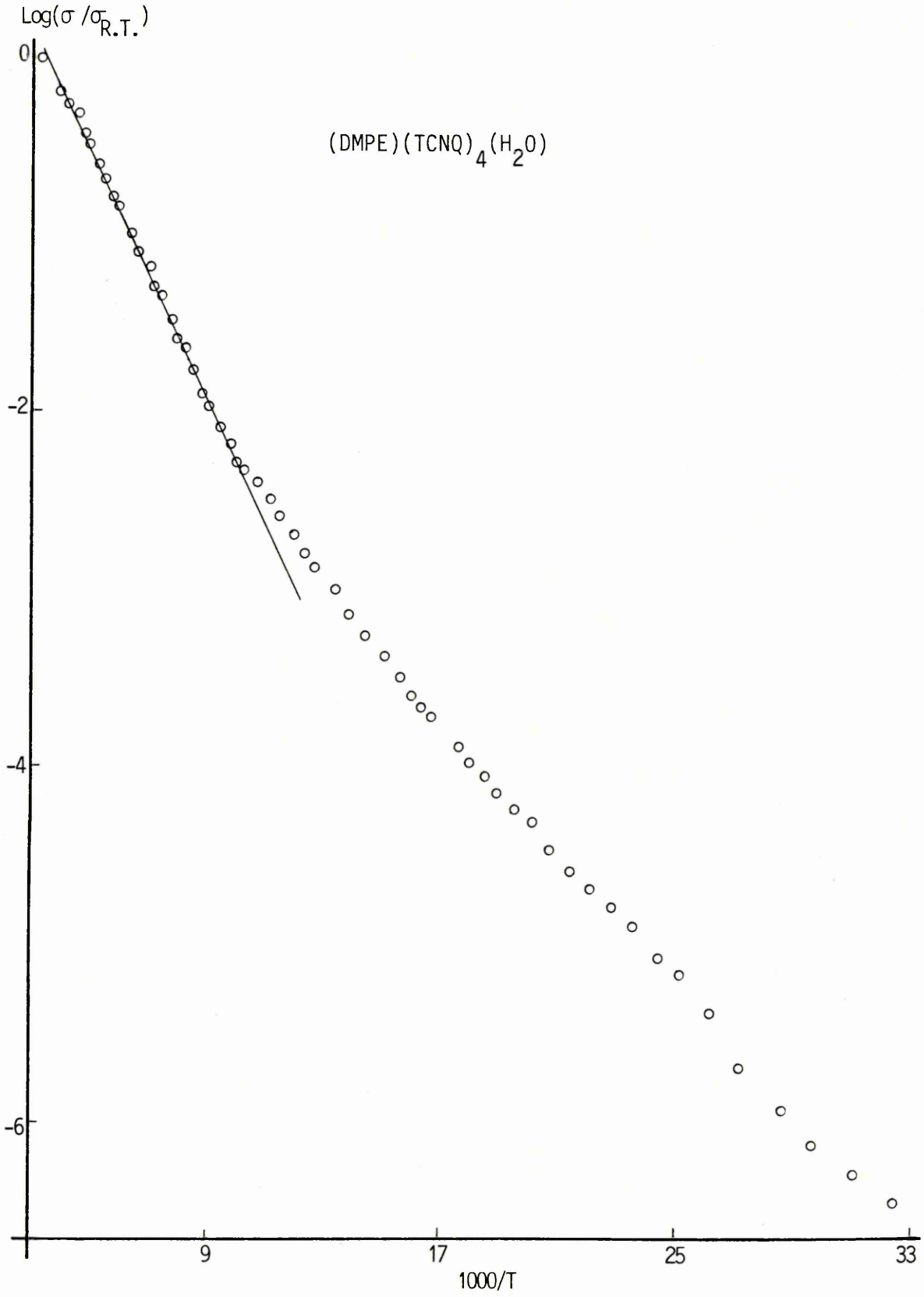

FIGURE 3.11 : Log normalised conductivity versus reciprocal temperature of $(DMPE)(TCNQ)_4(H_2O)$; powder sample

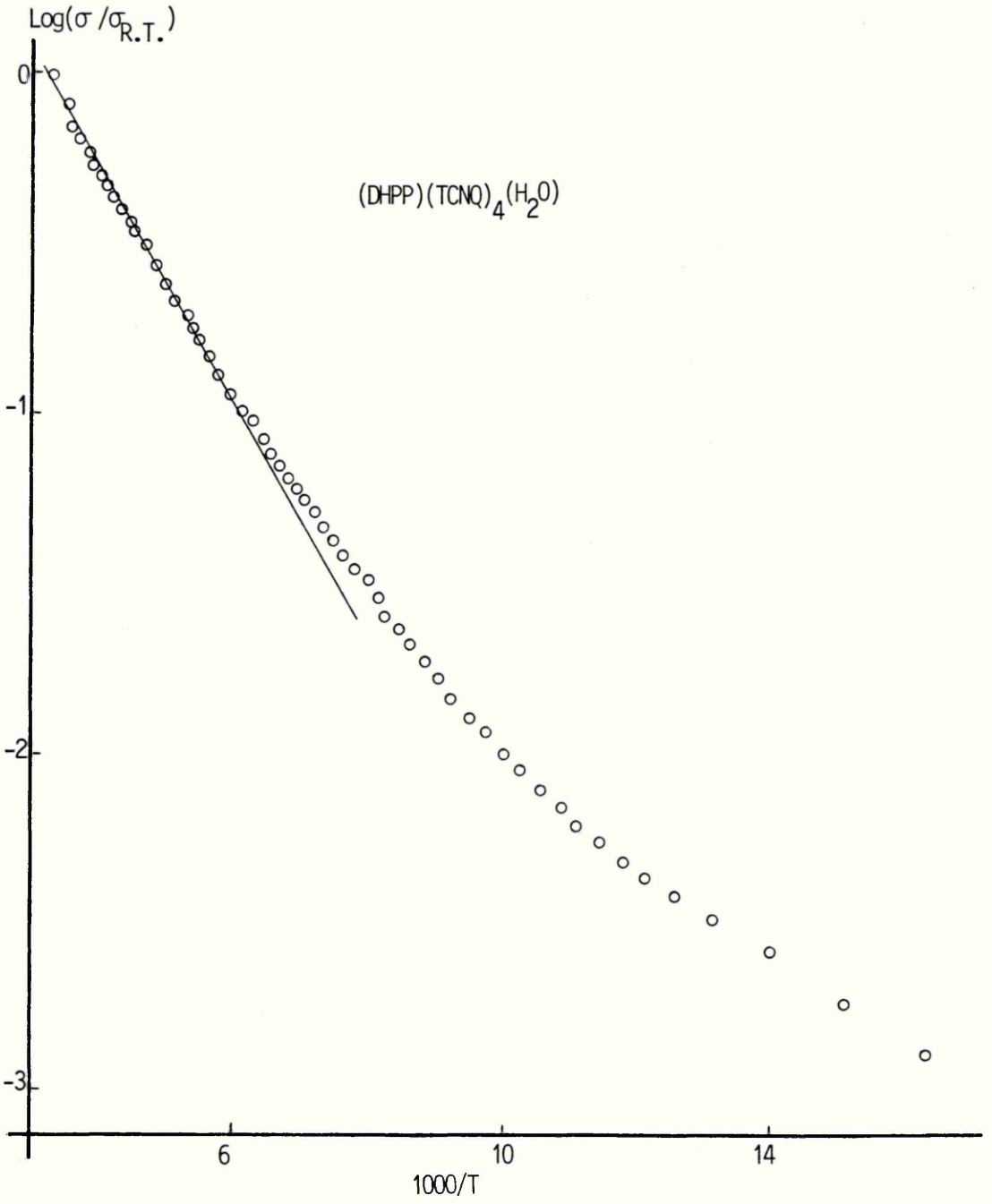

FIGURE 3.12 : Log normalised conductivity versus reciprocal temperature of $(DHPP)(TCNQ)_4(H_2O)$

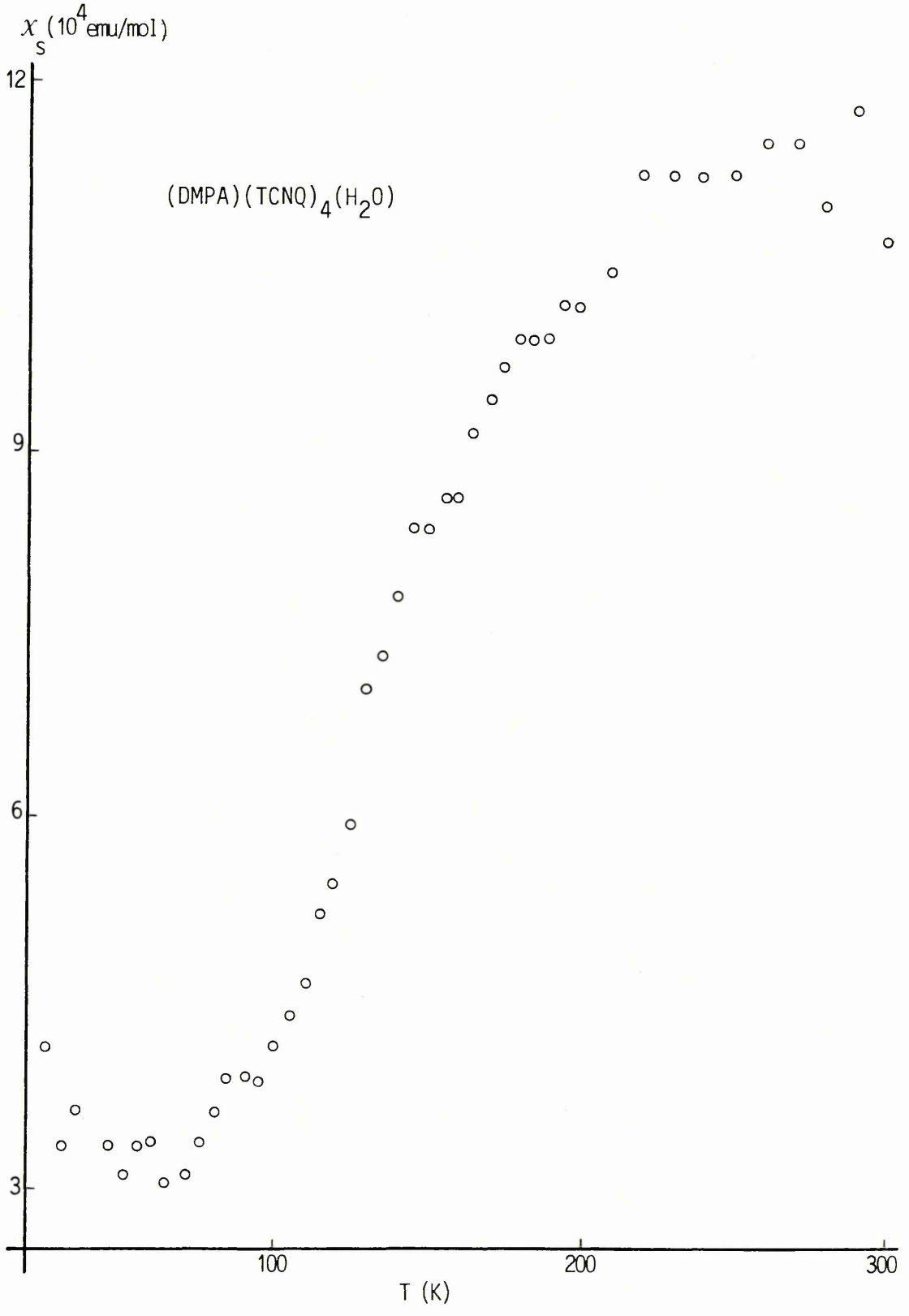

FIGURE 3.13 : The susceptibility, corrected for core diamagnetism versus temperature of (DMPA)(TCNQ)$_4$(H$_2$O)

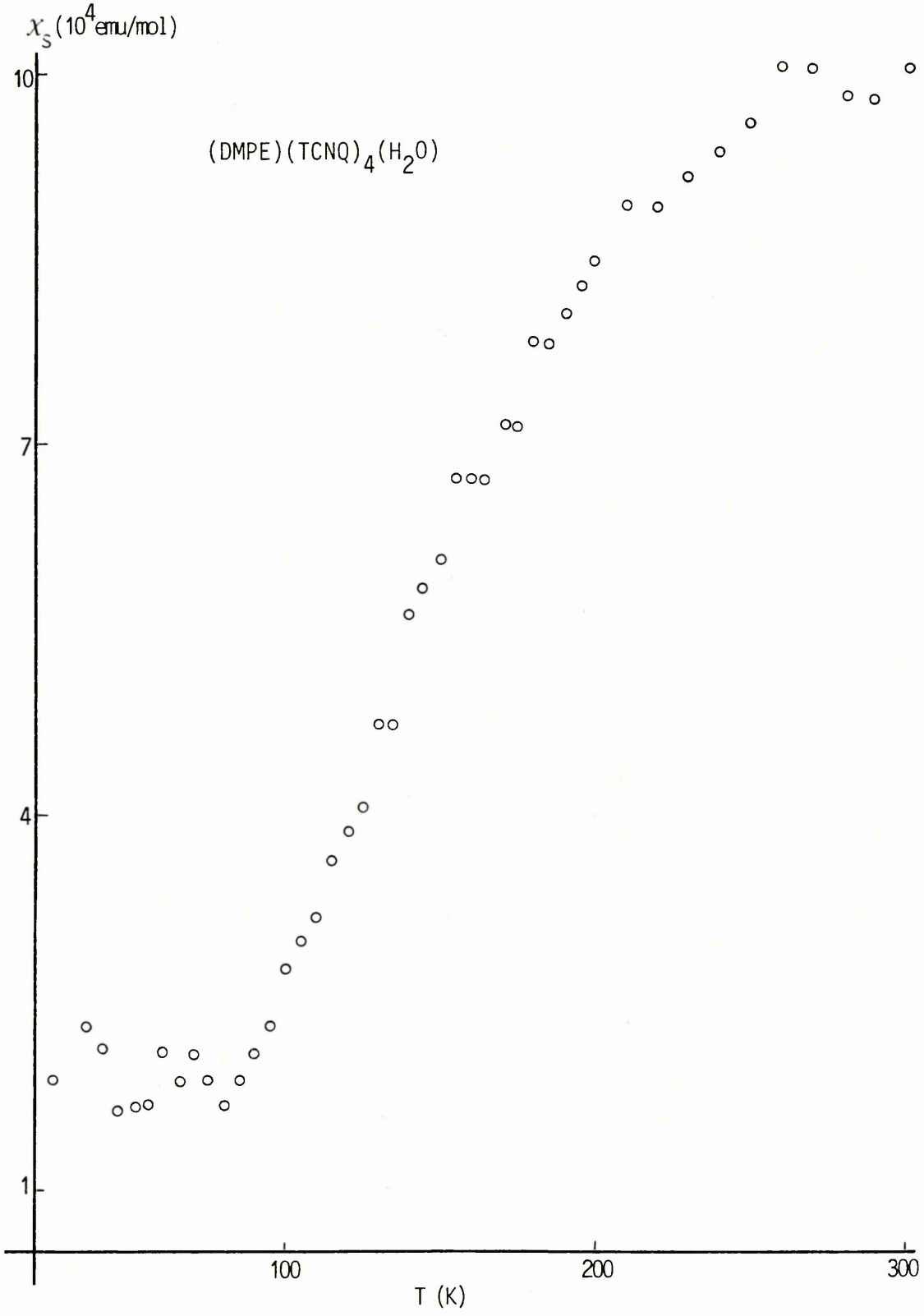

FIGURE 3.14 : The susceptibility, corrected for core diamagnetism versus temperature of (DMPE)(TCNQ)$_4$(H_2O)

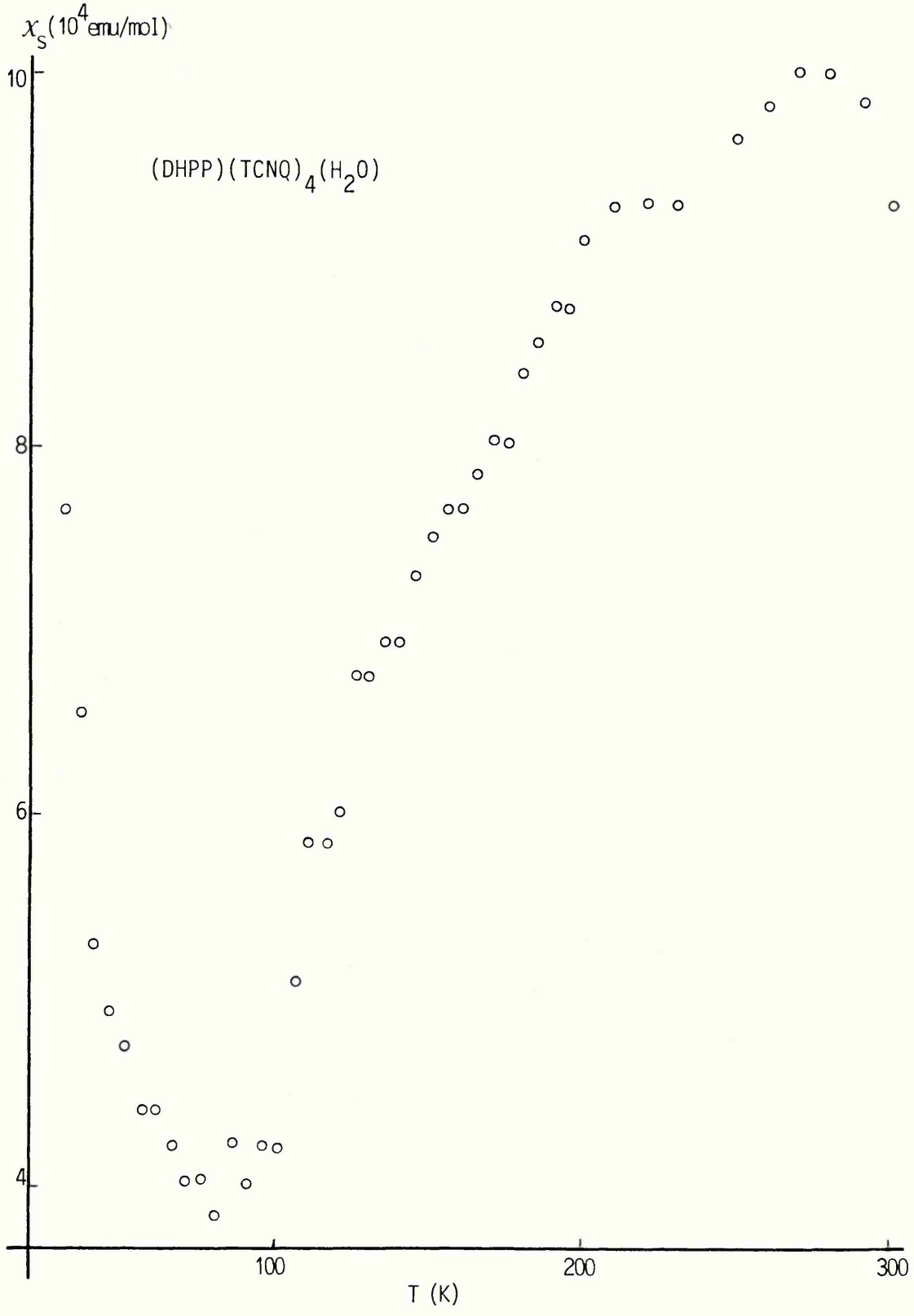

FIGURE 3.15 : The susceptibility, corrected for core diamagnetism versus temperature of (DHPP)(TCNQ)$_4$(H_2O)

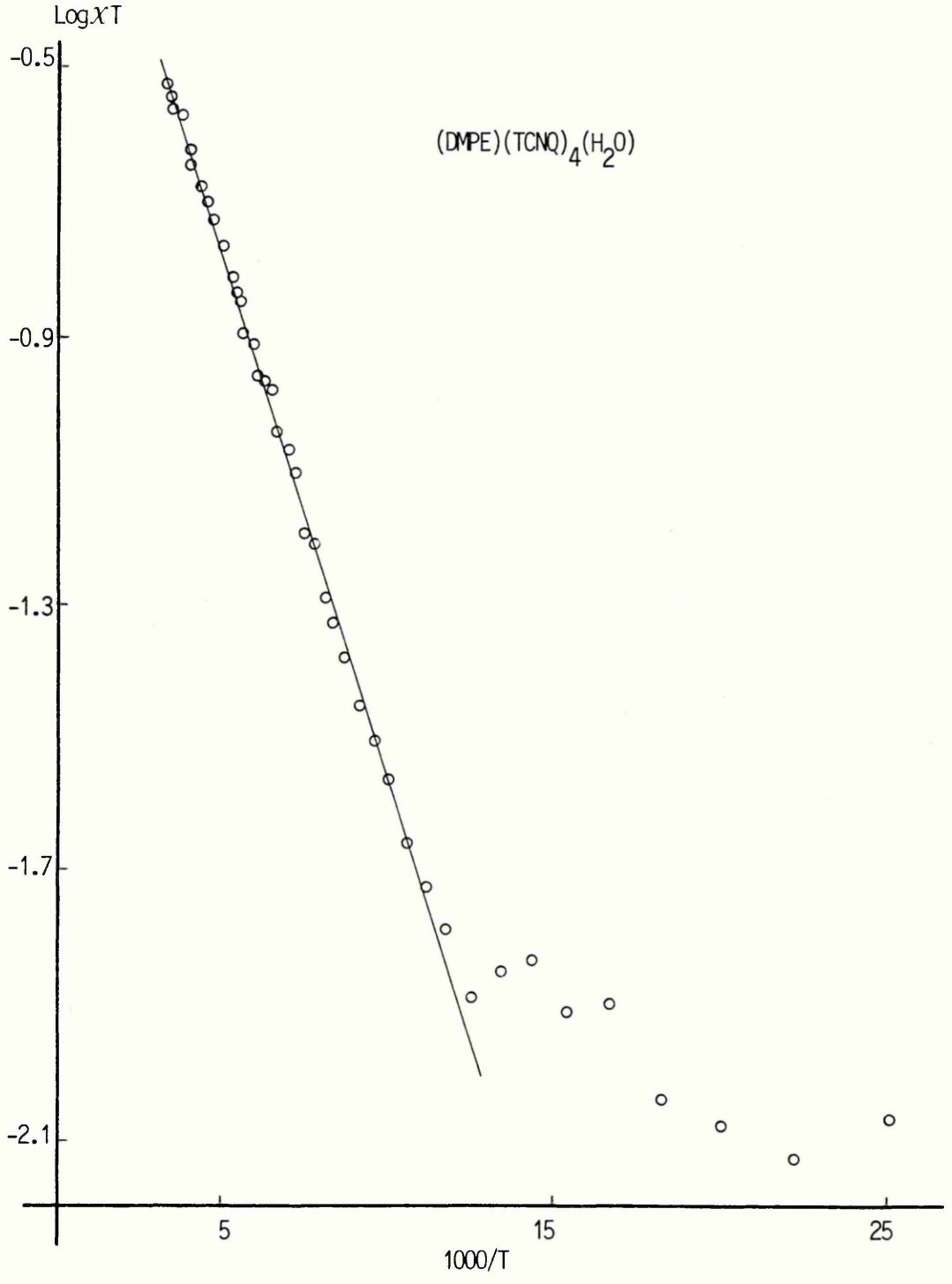

FIGURE 3.16 : The product of susceptibility and temperature versus reciprocal temperature of $(DMPE)(TCNQ)_4(H_2O)$

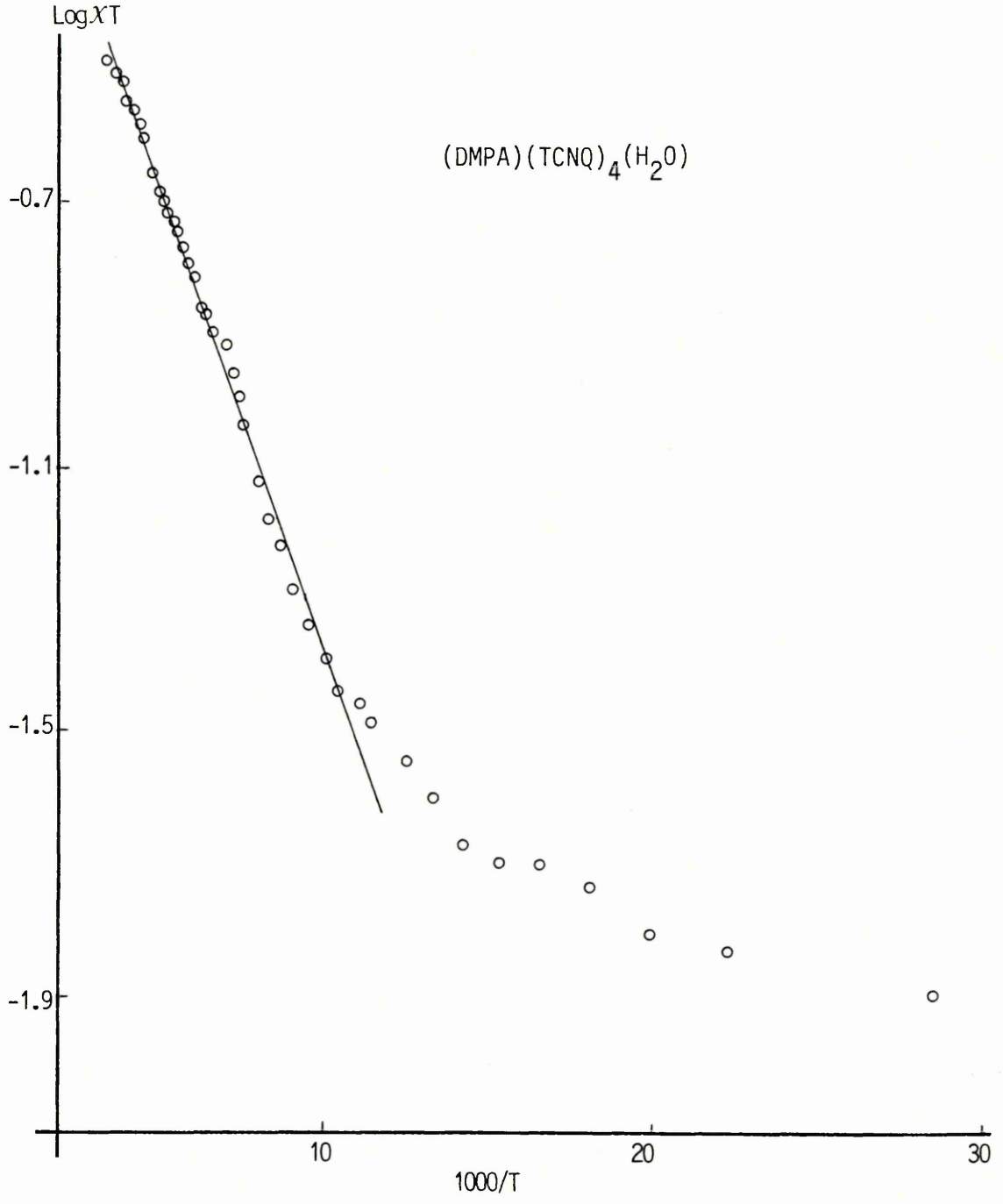

FIGURE 3.17 : The product of susceptibility and temperature versus reciprocal temperature of (DMPA)(TCNQ)$_4$(H$_2$O)

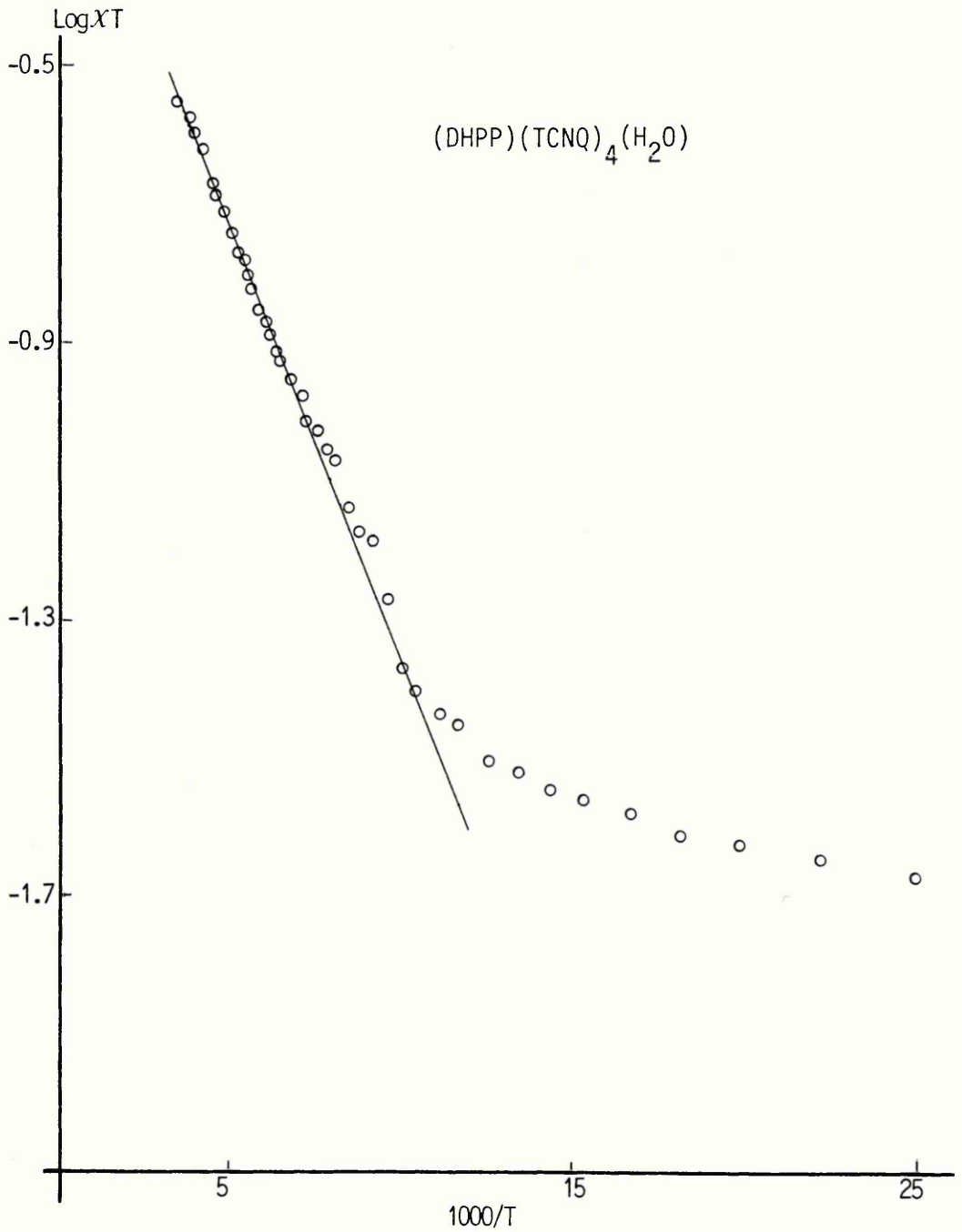

FIGURE 3.18 : The product of susceptibility and temperature versus reciprocal temperature of (DHPP)(TCNQ)$_4$(H$_2$O)

from a log/log plot. A similar temperature dependence has been obtained for certain other TCNQ salts.[175,196,198-203] In these salts, lattice irregularities may decompose the linear spin system into a number of subsystems, some of which may possess an odd number of spins. The strong antiferromagnetic interaction present in the regular spin system would be reduced and the spin 1/2 subsystems would behave as nearly free spins with weak interactions only between subsystems. In the studies where this explanation has been given, susceptibility measurements are made to below 1K.

It is of interest that the susceptibility at low temperature in (DMPE)(TCNQ)$_4$H$_2$O (see p 121) is lower than in the other two salts and that a Curie tail is not observed at 25 K. This may indicate a lower concentration of paramagnetic impurities or lattice defects in this salt.

The magnetic susceptibility above 90 K in the 1:4 salts is activated. In (DMPE)(TCNQ)$_4$H$_2$O the slope of Figure 3.16, is equivalent to 0.032 eV. The results do not fit the commonly used singlet-triplet model for localised spins;

$$\chi = [2Ng^2 \mu_B^2 / kT][3 + \exp(J/kT)]^{-1}$$

For J greater than a few kT the slope of Figure 3.16 (p 123) for (DMPE)(TCNQ)$_4$(H$_2$O) would approximate to J/k in the above expression. However, when the value of J obtained (J = 0.032) is substituted into the expression, the theoretical susceptibility at 300 K, χ_s = 1.5x10^{-3}emu mol^{-1}, is inconsistent with experiment where, χ_s = 1x10^{-3}emu mol^{-1}.

Poor agreement is also obtained for the DHPP and DMPA salt.

An alternative approach may be made by assuming a system of partially delocalised spins using the Bulaevskii model;

$$\chi = 2Ng^2 \mu_B{}^2 a(\gamma)/kT \exp[-J \Delta(\gamma)/kT]$$

In this equation, $a(\gamma)$ and $\Delta(\gamma)$ are functions of the alternation parameter, γ , and result from the finite triplet bandwidth. From the slope and intercept of Figure 3.16 for $(DMPE)(TCNQ)_4(H_2O)$, $J\,\Delta(\gamma) = 0.032$eV and $a(\gamma) = 0.346$. From the data of Figure 1.7, taken from reference 209 values of $\gamma = 0.56$ and $J = 0.049$eV are obtained. Similar results have been obtained by Woodward[180] by using an esr technique and the same interpretation applied.

The DHPP and DMPA salts show similar behaviour. For $(DHPP)(TCNQ)_4\ H_2O$, the susceptibility at 300 K calculated using the singlet-triplet expression is 1.8×10^{-3} emu mol^{-1} whereas the experimental value is 0.9×10^{-3} emu mol^{-1}. Using the Bulaevskii model as above, for a system of partially delocalised spins, $\gamma = 0.71$ and $J = 0.049$ eV.

For $(DMPA)(TCNQ)_4\ H_2O$, the suceptibility at 300 K calculated using the singlet-triplet model is 1.715×10^{-3} emu mol^{-1} and the experimental value is 1.1×10^{-3} emu mol^{-1}. Using the Bulaevskii model and assuming a system of partially localised spins, $\gamma = 0.64$ and $J = 0.048$ eV. These results are summarised in Table 3.3.

The close agreement of the values of J gives some justification to the use of this method for these salts but it should be noted that relatively small changes in χ(experimental) can cause significant variations in these parameters.

It is of interest that the 1:4 salt N,N-dimethyl-4,4-bipyridinium $(TCNQ)_4$ also possesses a singlet-triplet system of delocalised spins[167] with J = Ø.Ø48 eV similar to the results obtained here. The structure of this salt has not, however been determined.

It is known that the exchange interaction is dependent upon the separation of the spins. The dependence of J on the lattice constant for Cs_2TCNQ_3, for example, has been determined by Chesnut and Arthur[225], who observe that J decreases with increasing temperature as the lattice constant increases.

For the isostructural 1:4 salts it may be assumed that the separation of spins is roughly equivalent in each, to give an exchange interaction which is common to all three salts. The unit cell parameter (b axis) is roughly constant at 3.84 Å for all three salts and the distance between the positive charges on the dications is also similar.

3.4: $(DEPE)(TCNQ)_{4.5}(H_2O)_x$ and the Isostoichiometric Salts

The electrical and magnetic properties of the 1:4.5 salts $(DEPE)(TCNQ)_{4.5}(H_2O)_x$ and $(DMPP)(TCNQ)_{4.5}(H_2O)_x$ are given in Table 3.4. Both salts possess high conductivities and the properties are dependent on the degree of hydration and cation lattice disorder. The salts are isostructural and possess uniform columns of TCNQ with a short uniform interplanar spacing. The cations occupy narrow channels which run parallel to the TCNQ stacks. The isostructural congener $(DEPA)(TCNQ)_{4.5}(H_2O)_x$ also is highly conductive and has shown metallic behaviour (Figure 3.19,from reference 55).

$(DEPE)(TCNQ)_{4.5}(H_2O)_x$ was the first complex radical anion salt to remain metallic to very low temperatures[52] (less than 30 mK). The disorder and the metallic properties are dependent upon the degree of hydration and only the dehydated phase has shown metallic behaviour. The less conductive hydrated crystals are partially ordered and at 40 K undergo a conductor to insulator transition[55]. The conductivities of crystals of each form are shown in Figure 3.20.

An important observation is that upon annealing in vacuum at 370 K, the weak layer lines which correspond to the cation lattice are no longer seen[216]. This may show an increase in the cation lattice disorder. It is also important to note that under these conditions the crystals frequently show conductivity enhancement and in some cases metallic behaviour.

SALT	$\sigma_{R.T.}(Scm^{-1})$	$\chi_{s}(300K)$ (x10^{4}emu/mole)	χ_{dia}*	a(ν)	ν	$\Delta(\nu)$	J(eV)
$(DEPE)(TCNQ)_{4.5}(H_2O)_x$	50-500	15	6.8	0.24	0.68	0.5	0.024
$(DMPP)(TCNQ)_{4.5}(H_2O)_x$	10-100	32.5	7.2	0.46	0.48	0.73	0.012

* Calculated on the basis of x = 1

TABLE 3.4: The electrical and magnetic properties of the 1:4.5 salts.

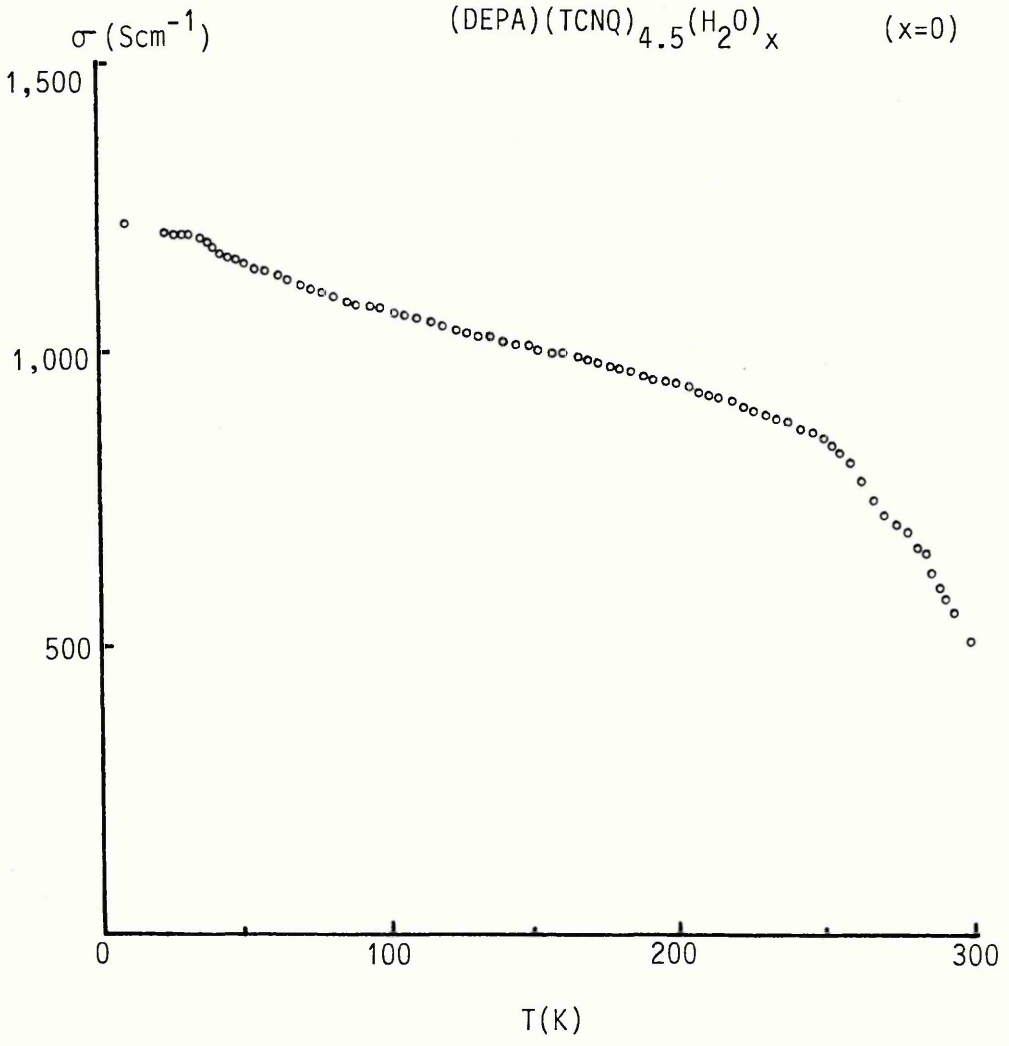

FIGURE 3.19 : The conductivity versus temperature of annealed $(DEPA)(TCNQ)_{4.5}(H_2O)_x$

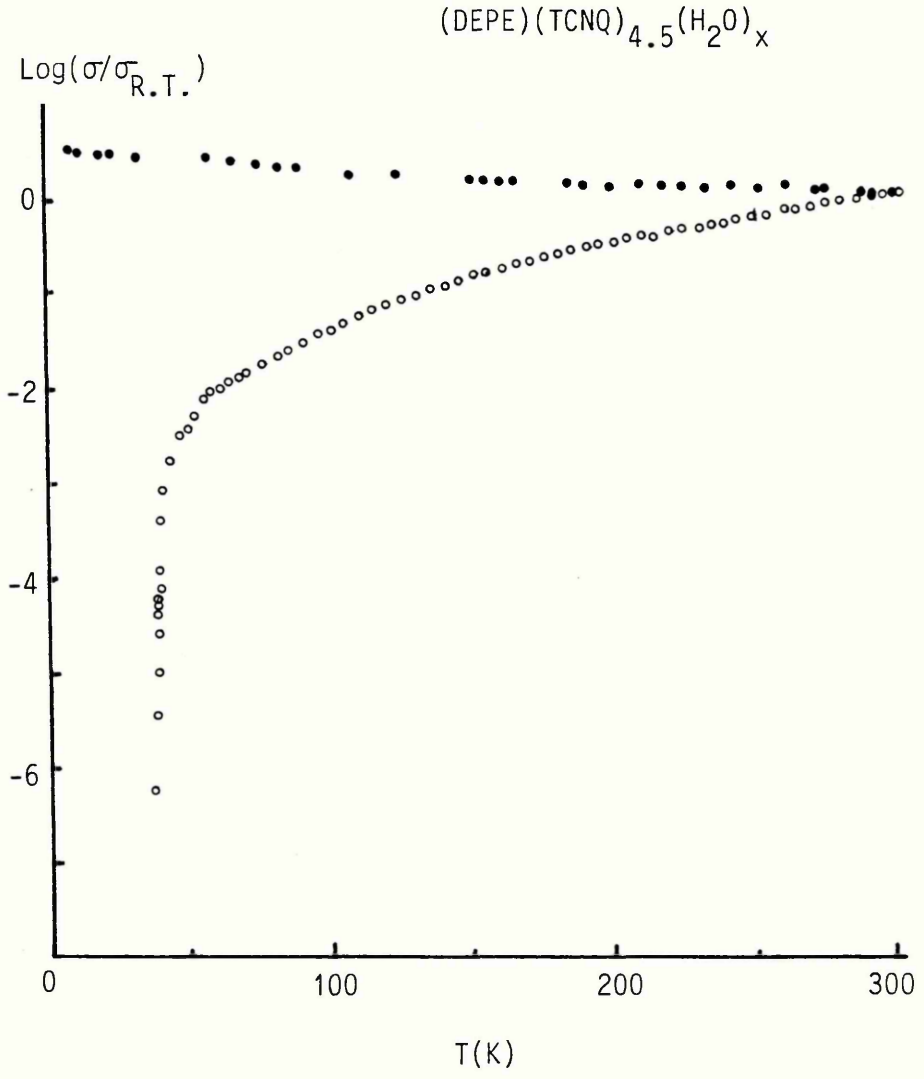

FIGURE 3.20

KEY : Closed circles represent dehydrated samples (x=0)

Open circles represent hydrated samples (x=1)

The conductivity temperature dependence of $(DMPP)(TCNQ)_{4.5}(H_2O)_x$ is shown in Figure 3.21. These crystals are frequently bowed and this may reflect a weaker than normal interchain coupling. This has also been observed in crystals of $(DEPE)(TCNQ)_{4.5}\ (H_2O)_x$.

Figure 3.21 shows the single crystal conductivity temperature dependence of the hydrated salt. Two features of the log σ versus reciprocal temperature plot are (i) the transition at 40 K and (ii) the curvature above this temperature.

The transition is a common feature of this isostructural series and it has been discussed previously. It has been attributed to a lattice distortion. The curvature is unusual. An attempt to fit the experimental data to the commonly used semiconductor models has been unsuccessful. By assuming a temperature dependent pre-exponential factor in the semiconductor equation;

$$\sigma = AT^n \exp(-E_A/kT)$$

a fit may be obtained but only if $E_A << kT$. In this limit, the equation approximates to;

$$\sigma = AT^n$$

A plot of log σ versus log T for the conductivity in the range 40 - 250 K is linear and the temperature exponent derived from the slope is n = 0.7. Thus the salt may be classed as a non-metal with a zero gap. The positive temperature dependence of the conductivity may be attributed to the mobility temperature dependence only. Similar

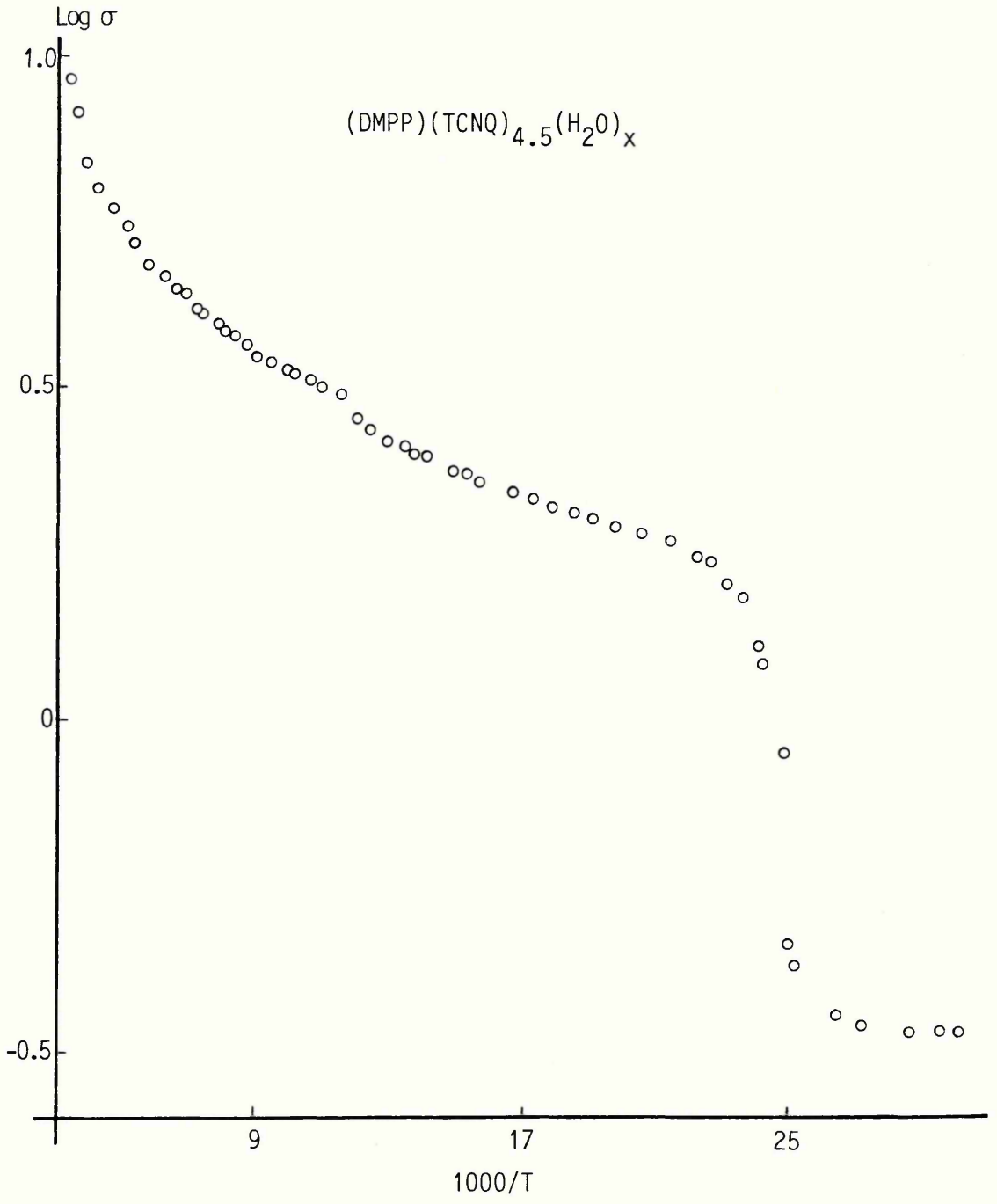

FIGURE 3.21 : Log conductivity versus reciprocal temperature of $(DMPP)(TCNQ)_{4.5}(H_2O)$

behaviour has been observed in the 1:5 salts and the unusual properties are discussed in section 3.5.

Annealed crystals of $(DMPP)(TCNQ)_{4.5}(H_2O)_x$ have not shown metallic behaviour. The annealing process does however enhance the conductivity and reduce the value of n to below Ø.7. As is observed for the DEPE salt, the X-ray oscillation photographs of crystals annealed in vacuum do not show the weak layer lines characteristic of the cation lattice and similarly the coductivity enhancement is attributed to an increase in cation disorder.

Most of the organic metals (listed in Table 1.1) possess a conductivity which varies as $\sigma \propto T^{\alpha}$, where α = -2.23 to -2.4Ø (refs.149,169,171). The conductivity of the metallic form of $(DEPE)(TCNQ)_{4.5}(H_2O)_x$ varies as $T^{-Ø.5}$ (ref.52). In these salts, the temperature dependence of the mobility of carriers is determined by phonon scattering. The positive temperature dependence of the mobility observed here for $(DMPP)(TCNQ)_{4.5}(H_2O)_x$ is anomalous but may be attributed to ionized impurity scattering. Such a mechanism would predict a mobility temperature dependence of $T^{1.5}$ which is not too dissimilar from the value obtained here. Such behaviour has been observed in inorganic semiconductors at low temperatures[164]. In these materials, the presence of ionic impurities causes a deflection of electrons as they pass through the Coulomb field of the ion. At higher temperatures the electrons have higher energies and the scattering diminishes.

The temperature dependence of the magnetic susceptibility of the 1:4.5 salts is shown in Figures 3.22 and 3.23 (p 137,138). The susceptibility exhibits a weak temperature dependence in the range 25 to 300 K and passes through a maximum (T_c), at 140 K for (DEPE)$(TCNQ)_{4.5}(H_2O)_x$ and 115 K for (DMPP)$(TCNQ)_{4.5}$ $(H_2O)_x$. The log χT versus reciprocal temperature plots (Figures 3.24 and 3.25) are linear in the range 110 - 300 K and deviation from linearity at lower temperatures may be attributed to a Curie law contribution from paramagnetic impurities. The activated susceptibility has been subtracted from the low temperature results, and attempts have been made to fit the residual susceptibility to a Curie law but without success. It is of interest that the temperature dependence of the susceptibility for the two salts are comparable.

Woodward has studied the esr susceptibility of the metallic form of (DEPE)$(TCNQ)_{4.5}(H_2O)_x$ and has reported that the normalised intensity is nearly constant in the range 60 to 300 K with a decrease below 60 K. It should be noted that this temperature is only 20 K greater than the observed conductivity transition. Since the material has shown metallic behaviour, the assumption was made that the high temperature susceptibility was characteristic of Pauli paramagnetic behaviour.

The present data is inconsistent with this hypothesis and instead an activated susceptibility has been observed. The temperature dependence of the paramagnetic suceptibility of

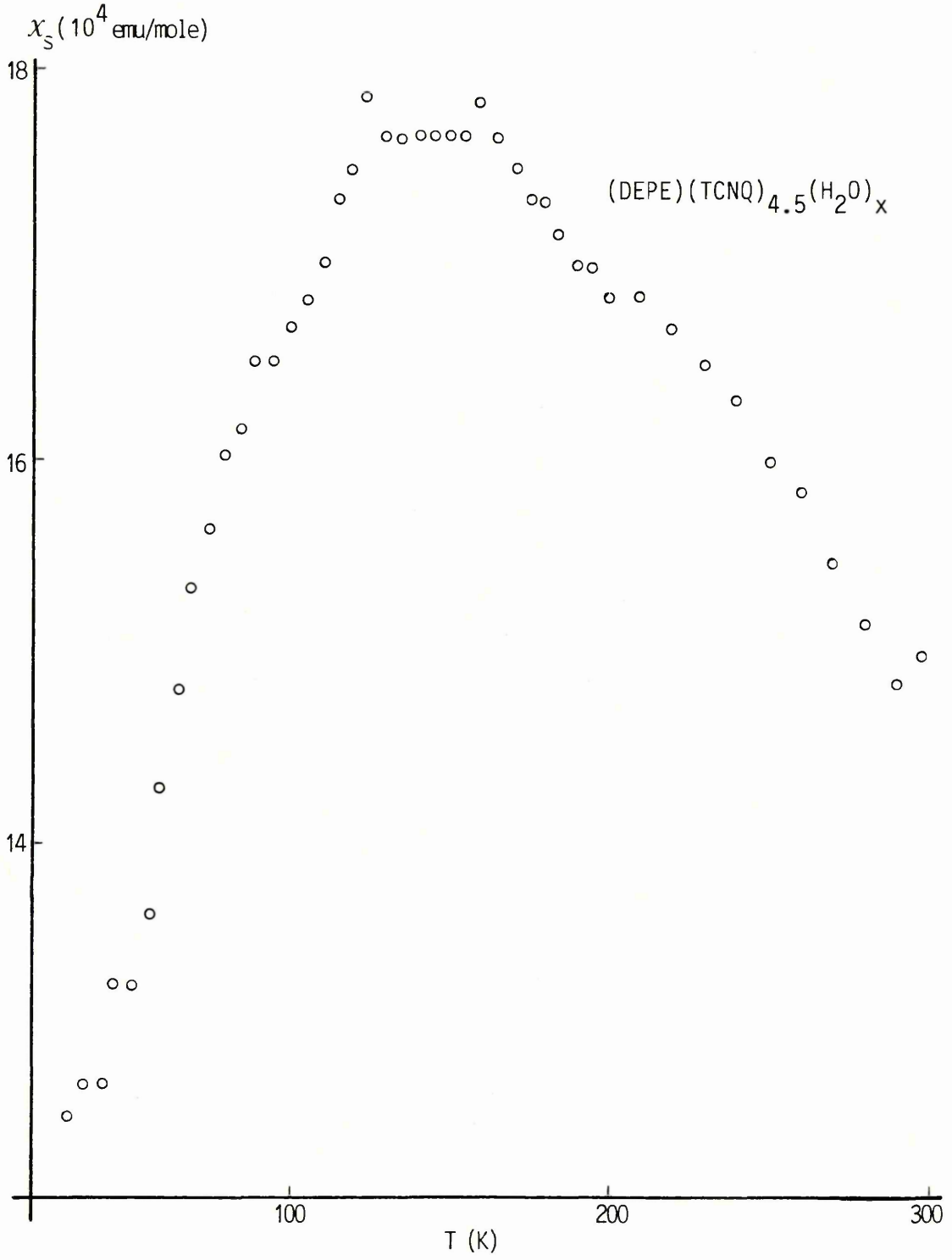

FIGURE 3.22 : The susceptibility, corrected for core diamagnetism versus temperature of (DEPE)(TCNQ)$_{4.5}$(H_2O)$_x$

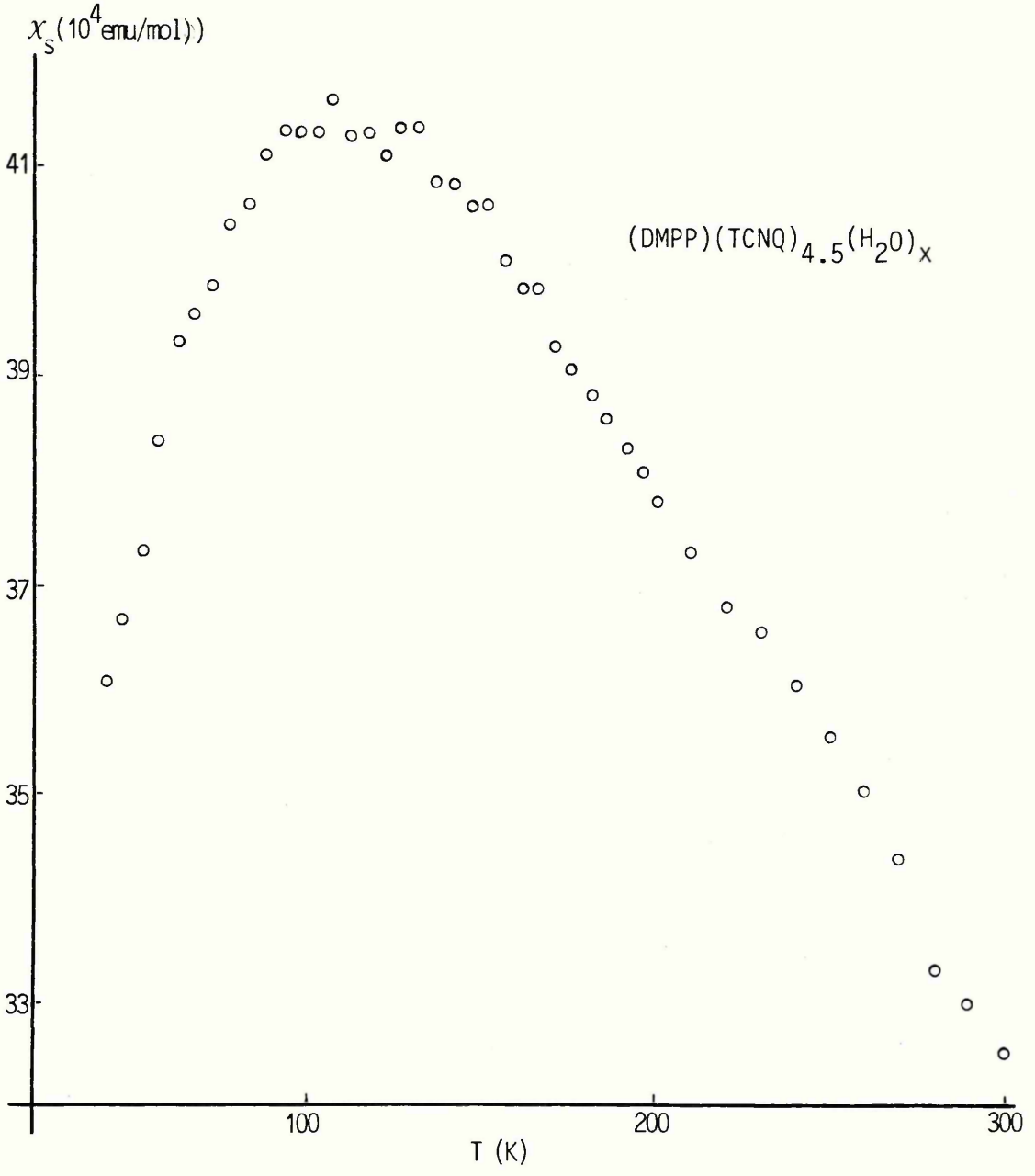

FIGURE 3.23 : The susceptibility, corrected for core diamagnetism versus temperature of $(DMPP)(TCNQ)_{4.5}(H_2O)$

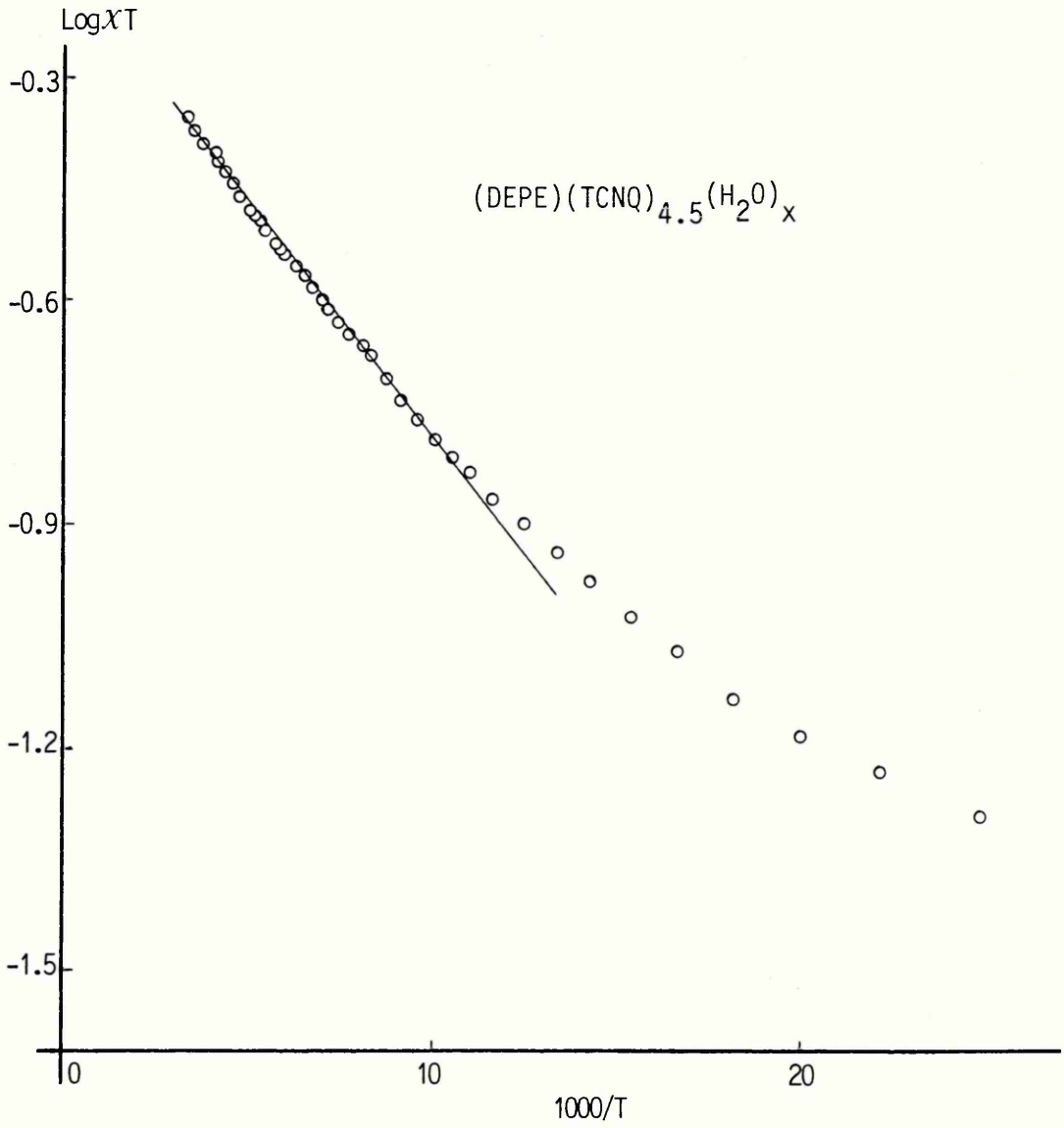

FIGURE 3.24 : The product of susceptibility and temperature versus reciprocal temperature of (DEPE)(TCNQ)$_{4.5}$(H_2O)$_x$

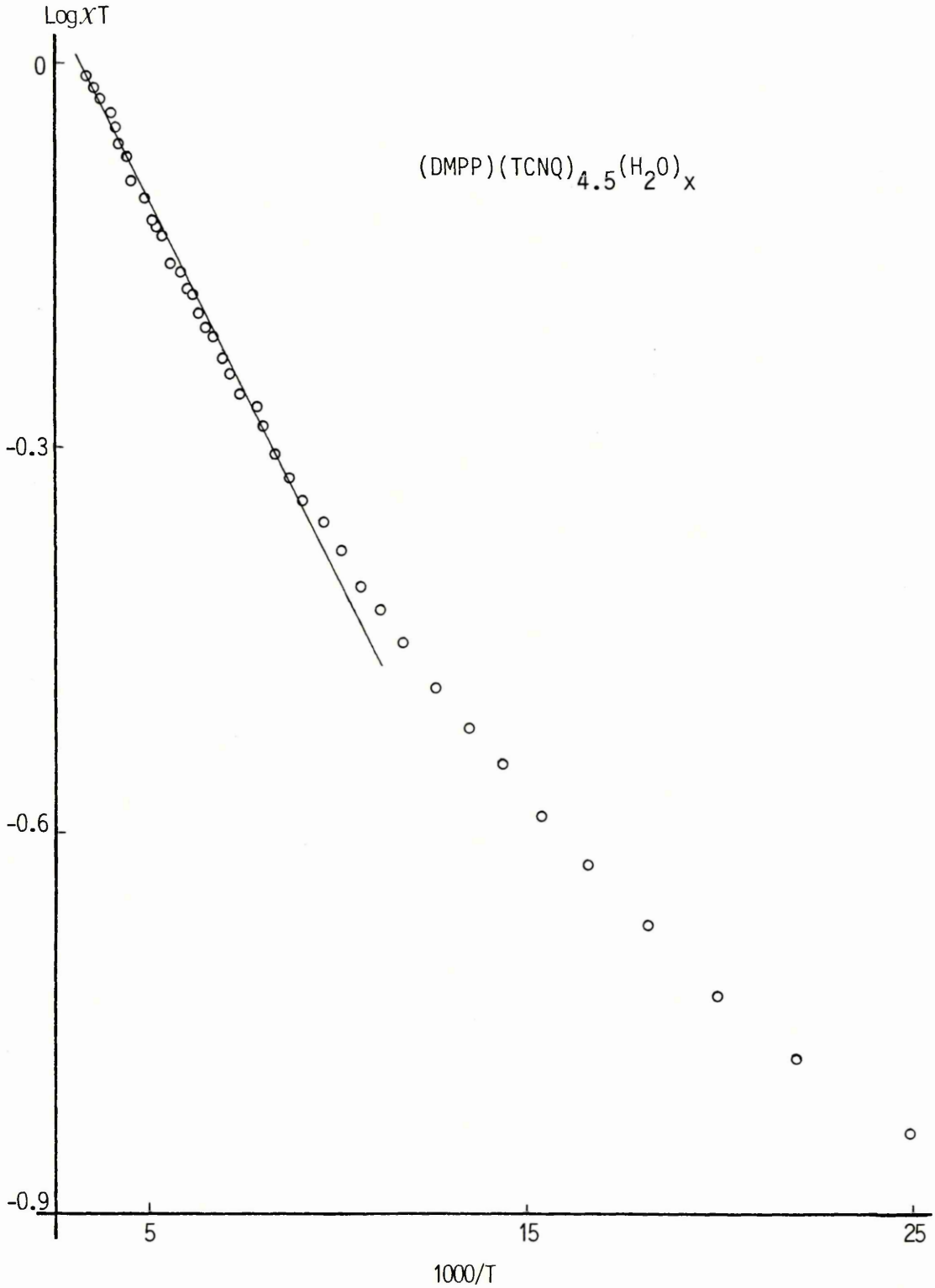

FIGURE 3.25 : The product of susceptibility and temperature versus reciprocal temperature for $(DMPP)(TCNQ)_{4.5}(H_2O)_x$

$(DEPE)(TCNQ)_{4.5}(H_2O)_x$ and of the isostoichiometric congener $(DMPP)(TCNQ)_{4.5}(H_2O)_x$ are compared in Figure 3.26.

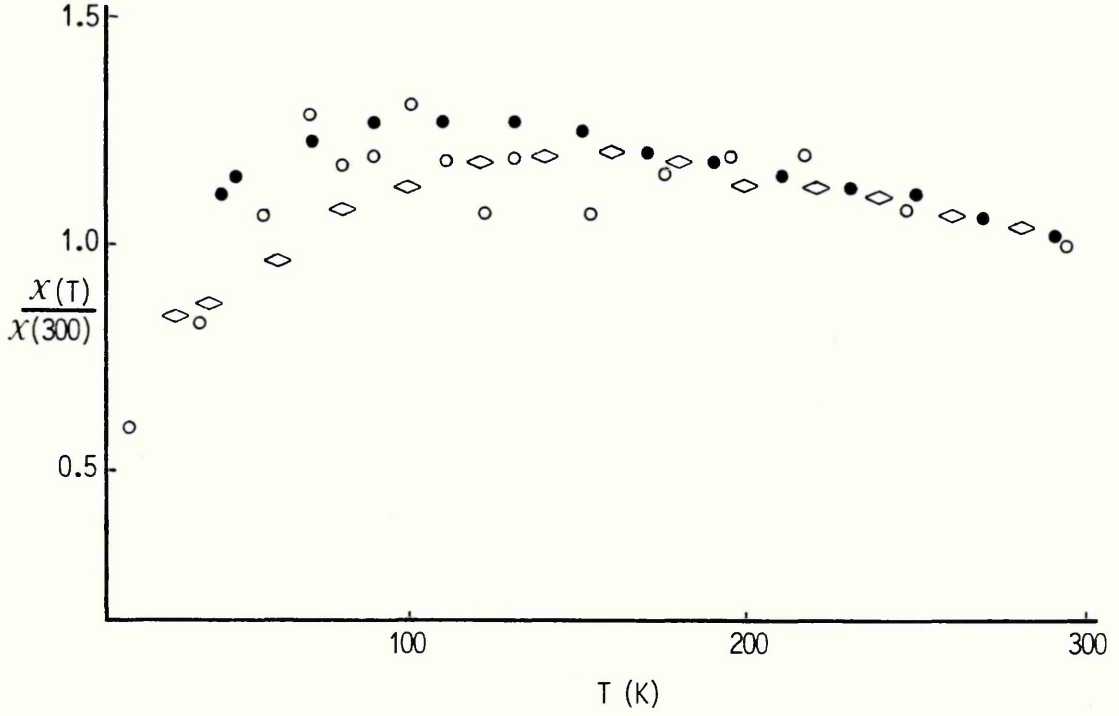

Figure 3.26 : The normalised susceptibility of two microcrystalline samples of $(DEPE)(TCNQ)_{4.5}(H_2O)_x$ (o◇) and of $(DMPP)(TCNQ)_{4.5}(H_2O)_x$ (●)

The temperature dependence of the magnetic susceptibility of these samples is weak and over the same temperature range a similar weak temperature dependence has been observed for the metallic salts $Qn(TCNQ)_2$ and $Ad(TCNQ)_2$. In these salts, the spin system may be described equally well by either one of two models.

The 'Mott' insulator model is realised when the spins are localised along the chain with a regular separation and a uniform antiferromagnetic interaction[175]. Bonner and Fisher [266] have calculated that for a homogeneous system of spins ($\mathcal{V}$= 1), the susceptibility maximum and the corresponding temperature may be related by;

$$(\chi kT)max \; / \; g^2 \mu_B{}^2 N \; = \eta \; = 0.095$$

The metallic model of non-interacting electrons, discussed by Bulaevskii[175], can also be fit to the weak temperature dependence of the susceptibility. The calculations show that the susceptibility tends to the Pauli value and passes through a maximum such that η = 0.089, for systems in which ρ = 0.5.For Qn$(TCNQ)_2$ and Ad$(TCNQ)_2$ it is found[175] that η = 0.10 .

For the 1:4.5 salts, $\eta >> 0.1$ and thus neither description may be applied.

The magnetic gap calculated from the slope of Figure 3.24 (p 139) for (DEPE)$(TCNQ)_{4.5}(H_2O)_x$ corresponds to an activation energy of 0.012 eV. From the position of the susceptibility maximum the strongly alternating singlet-triplet exciton model for localised spins gives[7] J = 1.61kT(max) = 0.02 eV. The magnetic activation energy determined experimentally for (DMPP)$(TCNQ)_{4.5}(H_2O)_x$ is 0.009eV and a corresponding treatment using the susceptibility maximum gives 0.015 eV. Thus this model is considered to be inappropriate to the description of the spin system in these salts.

The model of delocalised excitons (Bulaevskii model) has been applied to the experimental data, and the results are given in Table 3.4. Unlike the isostoichiometric series discussed in Section 3.3, there is little agreement between the values of J for the two salts. The absolute susceptibilities of the

salts are not comparable, and the discrepancy is considered to be outside the limits of experimental error. This discrepancy cannot be explained and the model may not be appropriate for the 1:4.5 salts.

3.5 The 1:5 salts.

The electrical and magnetic properties of the 1:5 salts are given in Table 3.5. The conductivities are representative of single crystals except for (DBuPE)$(TCNQ)_5(H_2O)$, for which only a microcrystalline sample was available. The salts are isostructural with the 1:3, 1:4 and 1:4.5 salts discussed previously but it should be noted that the conductivities at 300K are up to four orders of magnitude lower than the highest conductivities so far observed for the series.

The temperature dependence of conductivity of the 1:5 salts is shown in Figures 3.27 - 3.30 (pp 146-149). The log σ versus reciprocal temperature plots exhibit considerable curvature throughout the temperature range 130 to 400K. This behaviour is unlike the majority of other salts in this series with the exception of the 1:4.5 salt of DMPP.

For the 1:4 salts (section 3.3) a corresponding plot shows a well defined semiconductor gap. The 1:3 salts also show activated behaviour but over the narrower temperature range of 200 to 300 K. Only the salt of the DMPP cation shows curvature throughout this temperature range in the Log o versus reciprocal temperature plot, but this is less pronounced than the curvature shown in figures 3.27 to 3.30. For the DMPP salt discussed previously, the empirical fit gives;

$$\sigma = AT^n \qquad \text{;where } n = 0.7$$

SALT	$\sigma_{R.T}(Scm^{-1})$	n	$\chi_{s(300K)}$ ($x10^4$emu/mole)	χ_{dia}	a(γ)	γ	$\Delta(\gamma)$	J(eV)
$(DEPP)(TCNQ)_5H_2O$	1-10	5.5	18.3	7.48	0.26	0.53	0.53	0.017
$(DPPE)(TCNQ)_5H_2O$	0.1-1	4.3	13.6	7.54	0.2	0.72	0.45	0.02
$(DPPP)(TCNQ)_5H_2O$	0.02	6.7	18.1	7.72	0.26	0.53	0.53	0.017
$(DBuPE)(TCNQ)_5H_2O$	0.04	7	23.8	7.79	0.35	0.67	0.52	0.02

TABLE 3.5: The electrical and magnetic properties of the 1.5 salts.

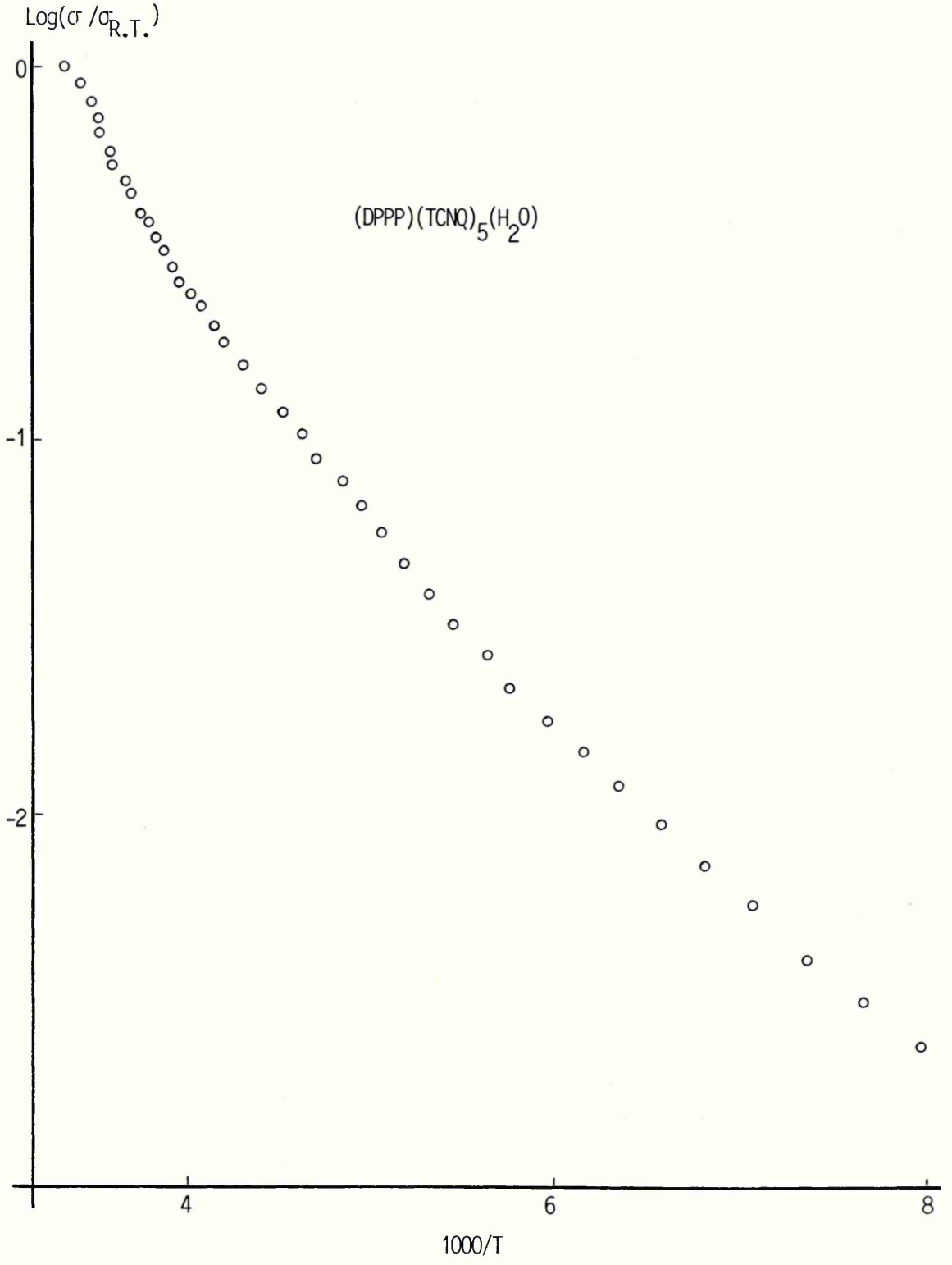

FIGURE 3.27 : Log normalised conductivity versus reciprocal temperature for $(DPPP)(TCNQ)_5(H_2O)$

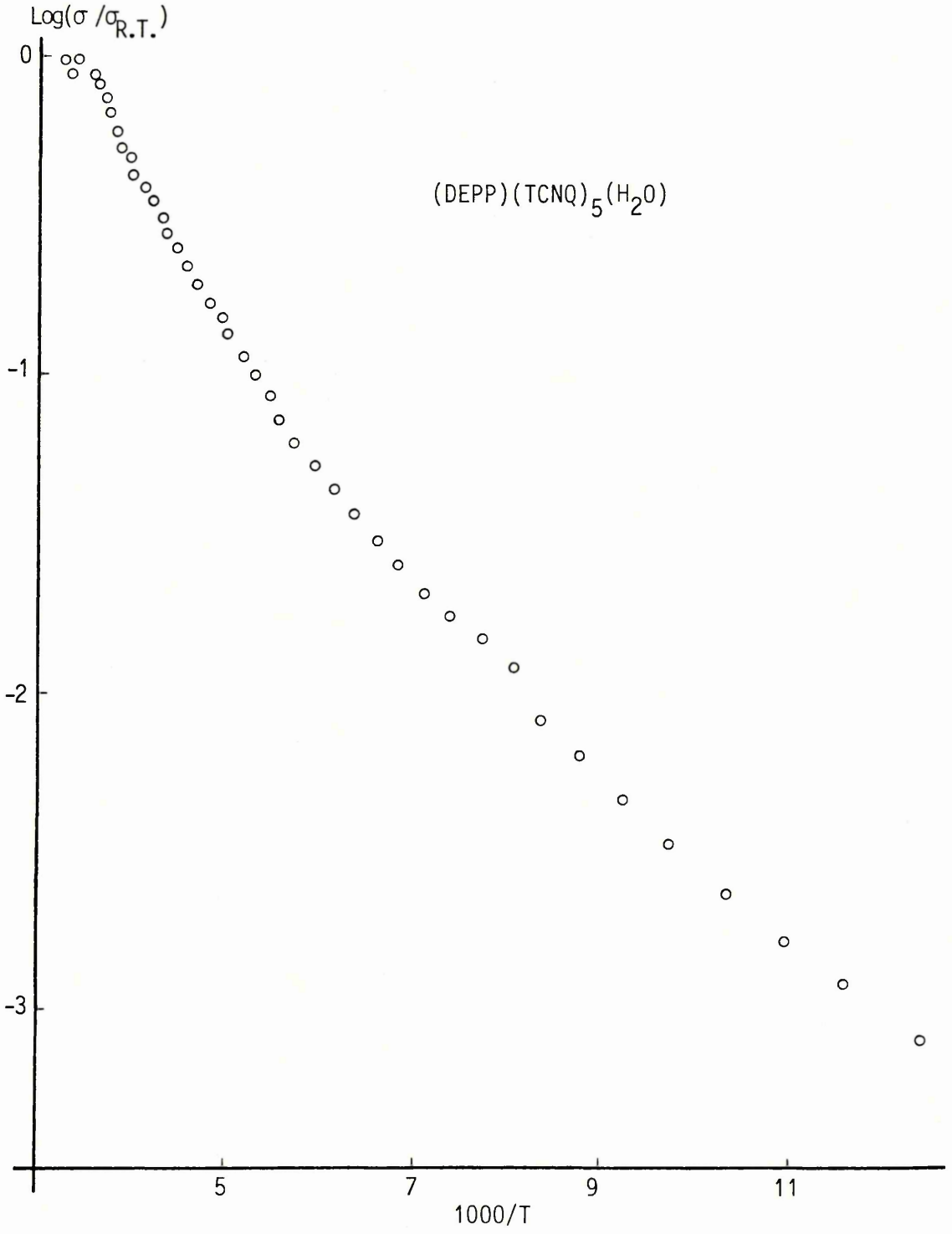

FIGURE 3.28 : Log normalised conductivity versus reciprocal temperature for $(DEPP)(TCNQ)_5(H_2O)$

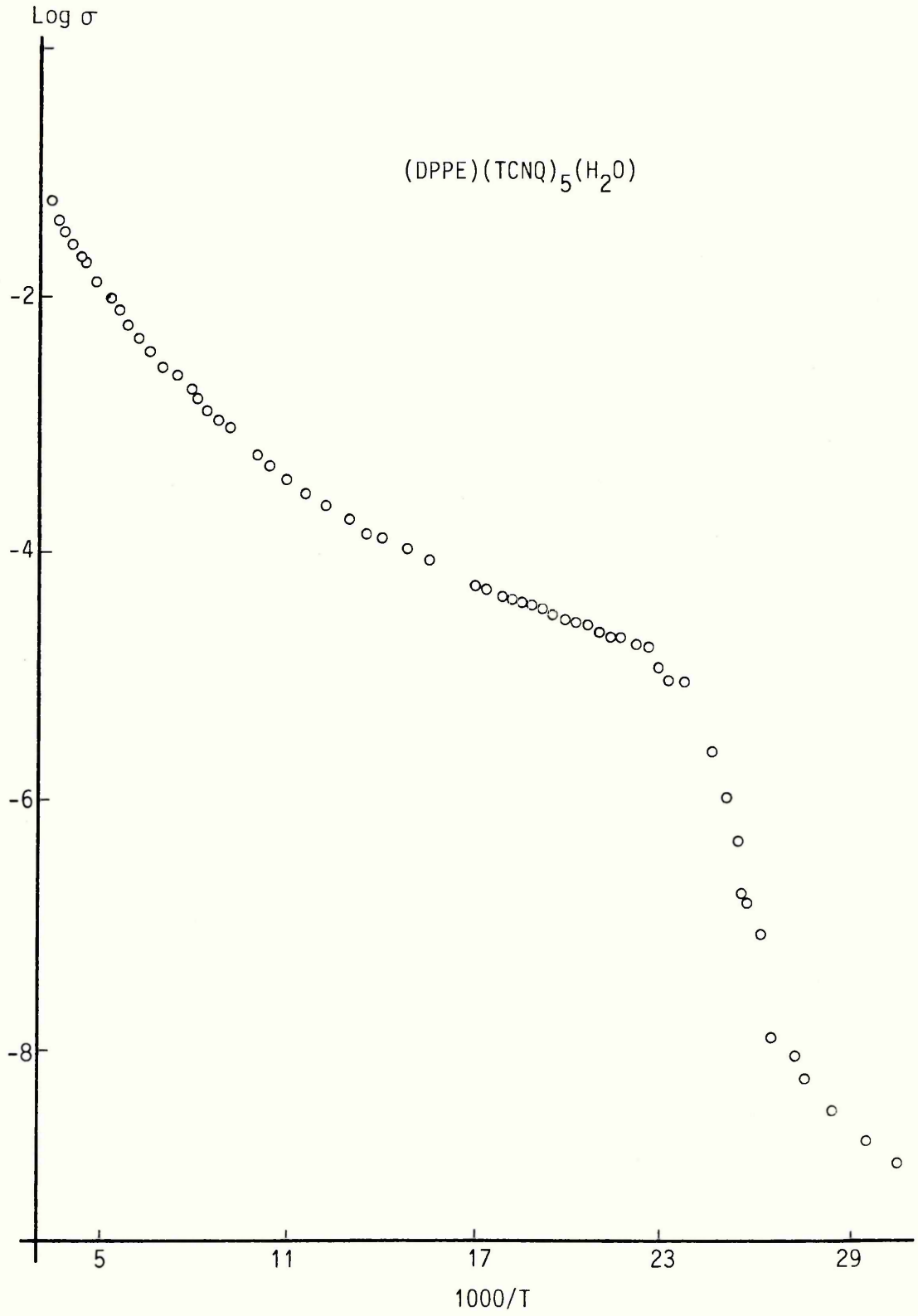

FIGURE 3.29 : Log conductivity versus reciprocal temperature of $(DPPE)(TCNQ)_5(H_2O)$

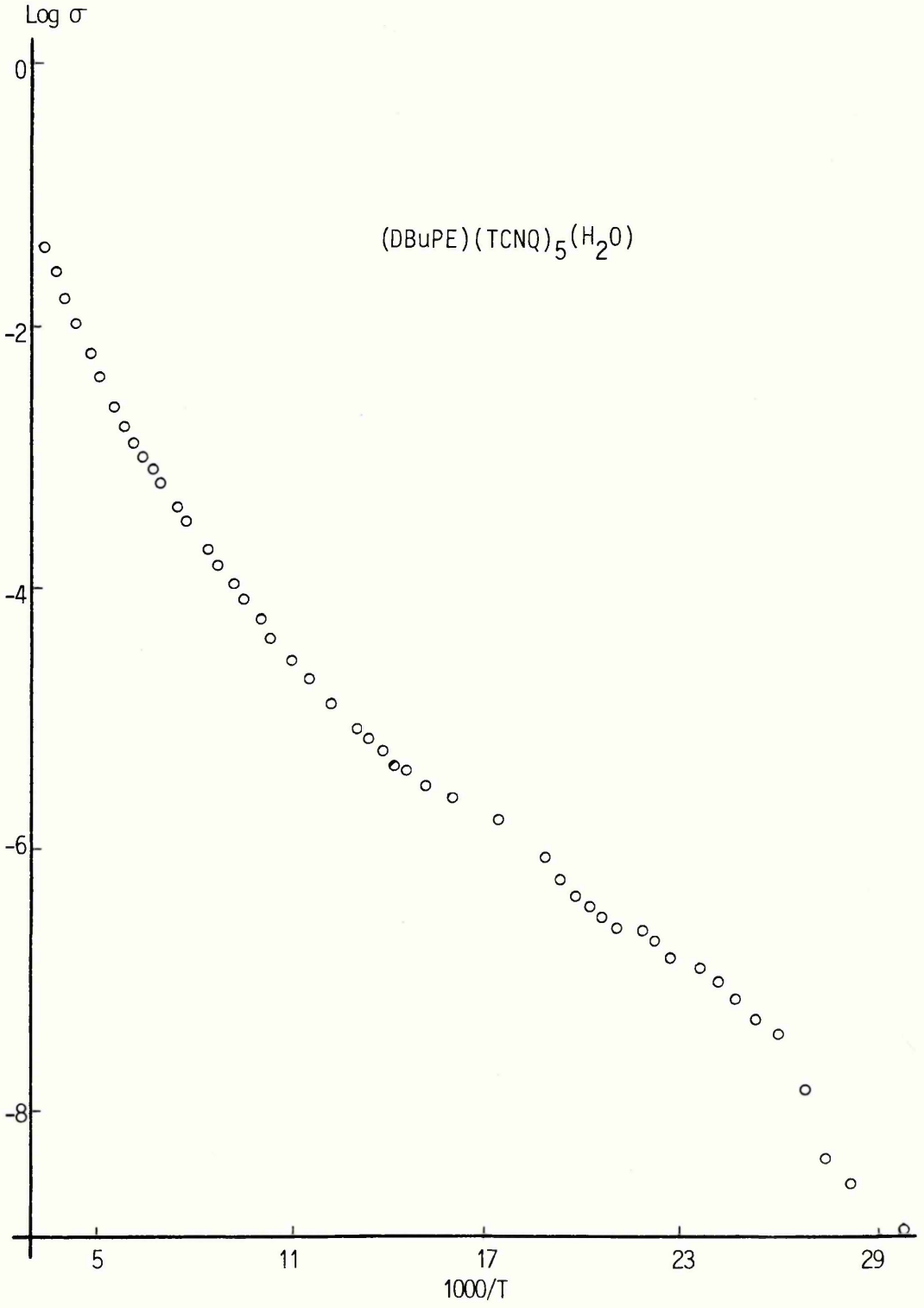

FIGURE 3.30 : Log conductivity (powder) versus reciprocal temperature for $(DBuPE)(TCNQ)_5(H_2O)$

The 1:5 salts also obey this simple relationship but with higher exponents of $4 < n < 7$. As expected the Log σ versus Log temperature plots (Figures 3.31 to 3.34, pp 151-154) are linear. The results are reproducible for 80% of the crystals studied with twenty crystals from each batch being examined.

The apparent absence of an activation gap in these salts suggests that the observed conductivity temperature dependence originates from a strong temperature dependence of the mobility of carriers and not from carrier generation across a gap. The observed temperature dependence of the conductivity is inconsistent with the temperature dependence predicted by the models normally used to describe conduction in one-dimensional systems. It is important to note that the conductivity in the 1:5 salts is not strongly anisotropic[43] and the power law dependence may not be a consequence of a strongly one-dimensional system.

Thus the salts may not be classified as semiconductors. In view of the moderate conductivity, a zero activation gap and positive temperature dependence of conductivity, the 1:5 salts may be described as 'non-metals' with the electrical properties determined by the mobility.

Two recent suggestions[44] which may account for the unusual temperature dependence in these salts involve considerations of (i) the effects of thermal expansion and (ii) optical phonon assisted hopping which is not simply activated in the experimental range of temperatures.

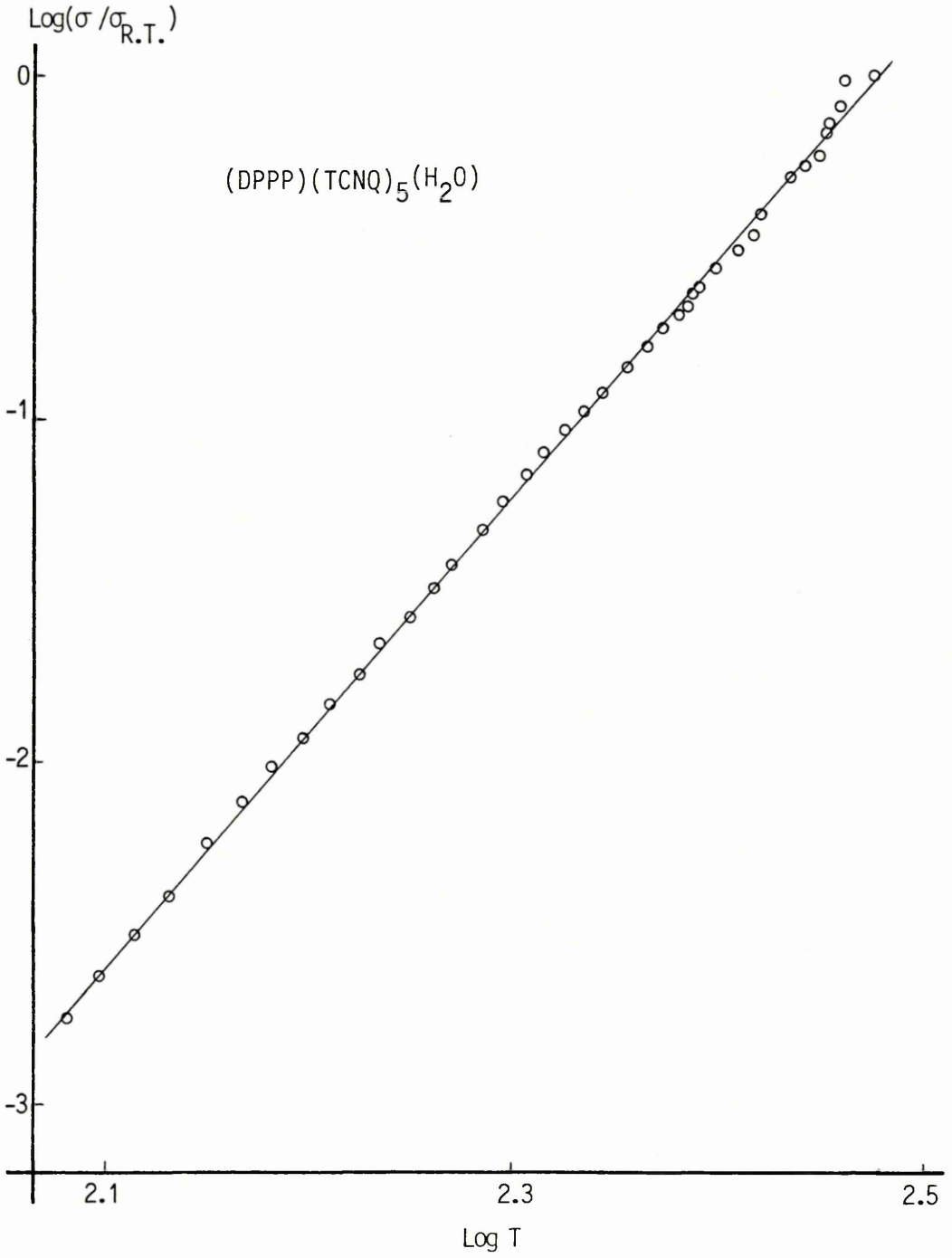

FIGURE 3.31 : Log normalised conductivity versus Log T for $(DPPP)(TCNQ)_5(H_2O)$

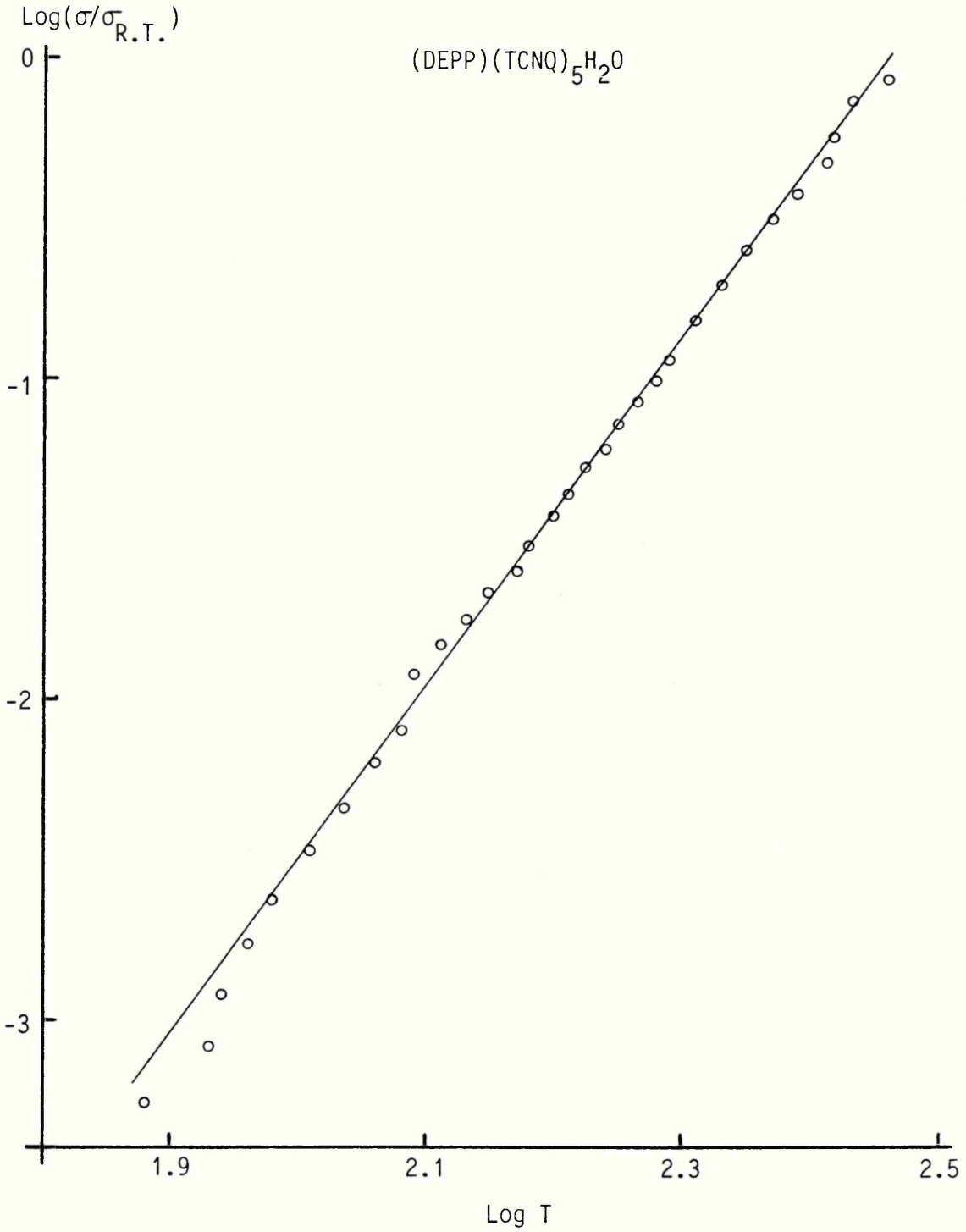

FIGURE 3.32 : Log normalised conductivity versus Log T of $(DEPP)(TCNQ)_5(H_2O)$

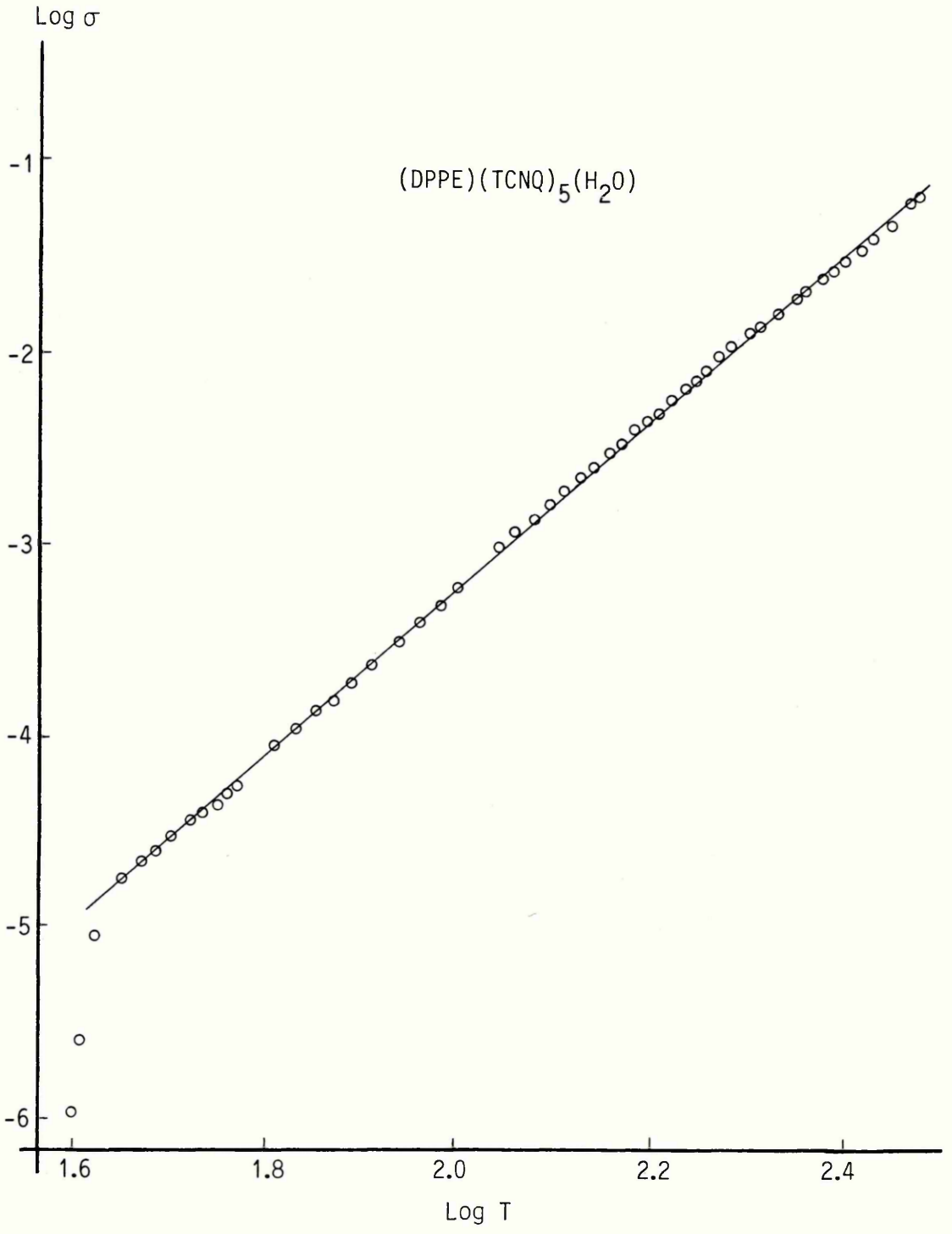

FIGURE 3.33 : Log conductivity versus Log T of $(DPPE)(TCNQ)_5(H_2O)$

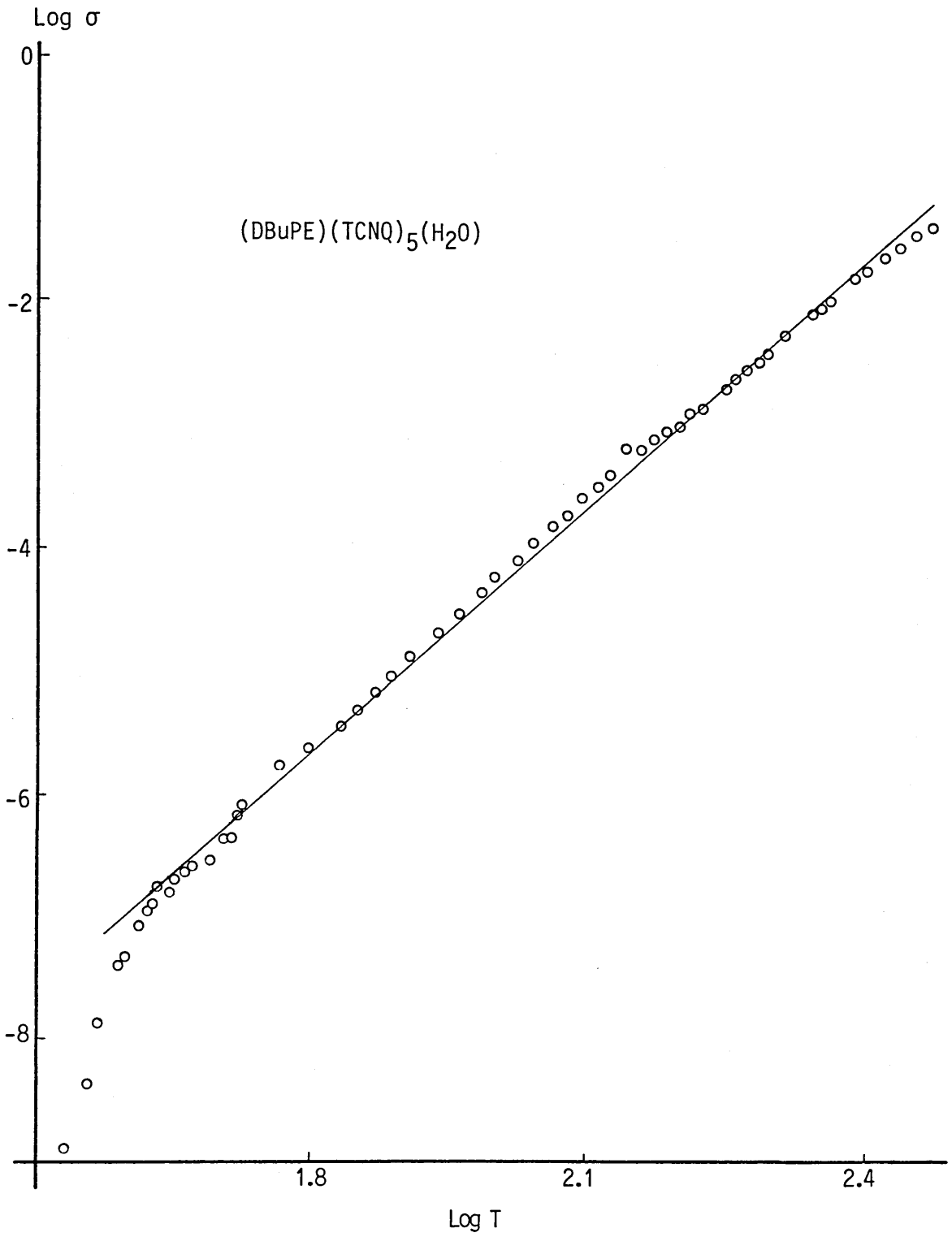

FIGURE 3.34 : Log conductivity (powder) versus Log T for $(DBuPE)(TCNQ)_5(H_2O)$;the slope is equivalent to 7

The arguments concerning the former consideration (that of the thermal expansion) are based on the expected discrepancies between the observed and calculated conductivity in materials which possess a large coefficient of thermal expansion.

The conductivity is usually calculated assuming **constant volume.** In materials which possess a large coefficient of thermal expansion this assumption may not be valid. Since measurements of the conductivity are normally made at **constant pressure** such materials may exhibit anomalous behaviour[235]. These materials are characterised as having an anomalously large pressure dependence of the conductivity since the conductivity is enhanced as the overlap on neighbouring sites is increased with increasing pressure. In the 1:5 salts it is proposed[44] that the power law dependence may be attributed to these effects assuming that the orbital overlap between sites increases as the temperature is lowered. By these arguments it was shown[44] that the **constant volume** conductivity should be;

$$(\delta \ln\sigma \ / \delta \ln T)_V = n + 6 \times 10^{-3} T \quad ....(1)$$

where n is the exponent in the empirical expression, $\sigma = AT^n$ and the second term includes the estimated contributions to the conductivity from the effects of thermal expansion. Equation (1) suggests that the constant pressure conductivity, which obeys the empirical expression $\sigma = AT^n$, possesses an exponent n which increases by a factor of between one or two in the temperature range $45 < T < 300$ K.

The experimental results however show that the exponent is constant in this temperature range.

An alternative explanation is that the power law dependence arises from optical phonon assisted hopping among localised states in a temperature range where the hopping rate is not simply activated[44].

It has been shown by Emin[236] that the optical phonon assisted hopping rates in solids are activated only within certain temperature ranges which are determined by the optical phonon frequency. In the low temperature limit the hopping rate is activated due to an interaction with a single phonon whereas in the high temperature limit, the hopping is also activated, but with a larger activation energy and the process dominated by multiphonon interactions. Between these limits the hopping rate is not simply activated and Ashwell and Care[44] suggest that the observed conductivity in the 1:5 salts is due to optical phonon assisted hopping in this temperature range.

A proposal has been made previously that the power law behaviour in the conductivity of $(DMPP)(TCNQ)_{4.5}(H_2O)_x$ may be due to ionised impurity scattering. This proposal does not apply to the 1:5 salts discussed here where the exponent n is much greater than that expected (n = 1.5) for this mechanism.

The proposals given in the above discussion and those in Section 3.4, concerning the conduction mechanism, remain tentative.

A conductor-to-insulator transition is seen in the conductivity of compacted samples of (DPPE)$(TCNQ)_5(H_2O)$ at 40K (see figure 3.29, p 148) and is attributed to a distortion of the quasi-one-dimensional TCNQ lattice, driven by a partial ordering of the cation lattice upon cooling. It is of interest that the transition occurs at a similar temperature to that observed in (DMPA)$(TCNQ)_4(H_2O)$ (Section 3.3) (DMPP)$(TCNQ)_{4.5}(H_2O)_x$ (Section 3.4), and in the non-metallic crystals of (DEPE)$(TCNQ)_{4.5}(H_2O)_x$ (ref.55).

In (DBuPE)$(TCNQ)_5(H_2O)$ the conductivity temperature dependence of a compacted microcrystalline sample (Figure 3.30, p 149) exhibits an anomaly at about 40 K also signifying the existence of a transition at this temperature.

The single crystal resistances of (DEPP)$(TCNQ)_5(H_2O)$ and (DPPP)$(TCNQ)_5(H_2O)$ were too high to allow measurements below 77 K and 125 K, respectively.

The temperature dependence of the magnetic susceptibility of the 1:5 salts is shown in Figures 3.35-3.38 (pp 160-163). The susceptibilities exhibit weak temperature dependences with maxima occurring between 100 and 150 K. The magnetic susceptibility is activated and the magnetic gap, determined from the slopes of the semilog plots ofthe 1:5 salts, (Figures 3.39-3.42, pp 164-167) is approximately 0.01 eV. The deviation from linearity at low temperatures is possibly due to the susceptibility of paramagnetic impurities, although none exhibits a low temperature 'Curie tail' sometimes associated with impurities[183,197].

Attempts to fit the susceptibility to the model of a homogeneous one-dimensional spin system[226] and to the localised singlet-triplet exciton model[7] have been unsuccessful.

For a homogeneous system of spins;[226]

$$\eta = \chi k T_{max} / g^2 \mu_B{}^2 N = 0.095$$

For all the 1:5 salts, $\eta >> 0.01$. The singlet-triplet activation energies (J) calculated from; $J = 1.61 k T_{max}$; are considerably higher than those obtained from the slopes of the Log χT versus reciprocal temperature plots. In the discussion of the susceptibility of the 1:4 and 1:4.5 salts (Sections 3.3 and 3.4) the data have been applied to the delocalised exciton model of Bulaevskii[209]. The spin system in these salts has been described as a linear chain of partially localised spins with a weakly alternating

antiferromagnetic exchange. The model is applied to the results for the 1:5 salts and the singlet-triplet exciton parameters are given in Table 3.5 (page 145). There is reasonably good agreement between the parameters, $a(\gamma)$, γ, $\Delta(\gamma)$ and J within this isostoichiometric group of salts which suggests that the features of the spin system are common to the salts. The spins are partially localised and form an antiferromagnetic chain of triplet excitons in which the triplet excited state lies about 0.017-0.02eV above a singlet ground state. The degree of alternation is low and varies only marginally among the salts.

The close agreement between the J values supports the suggestion made in Section 3.3 that the similarities in the unit cell dimensions of the salts of the isostoichiometric group would be reflected in similarities in the exchange interaction.

The exchange energy is lower in the 1:5 salts than that observed for the 1:4 salts, where J = 0.05eV. This is expected since the separation of spins on the TCNQ lattice, which is isostructural between the groups, should be larger in the 1:5 salts than in the 1:4 salts since ρ for the 1:5 salts is 0.4 and ρ for the 1:4 salts is 0.5.

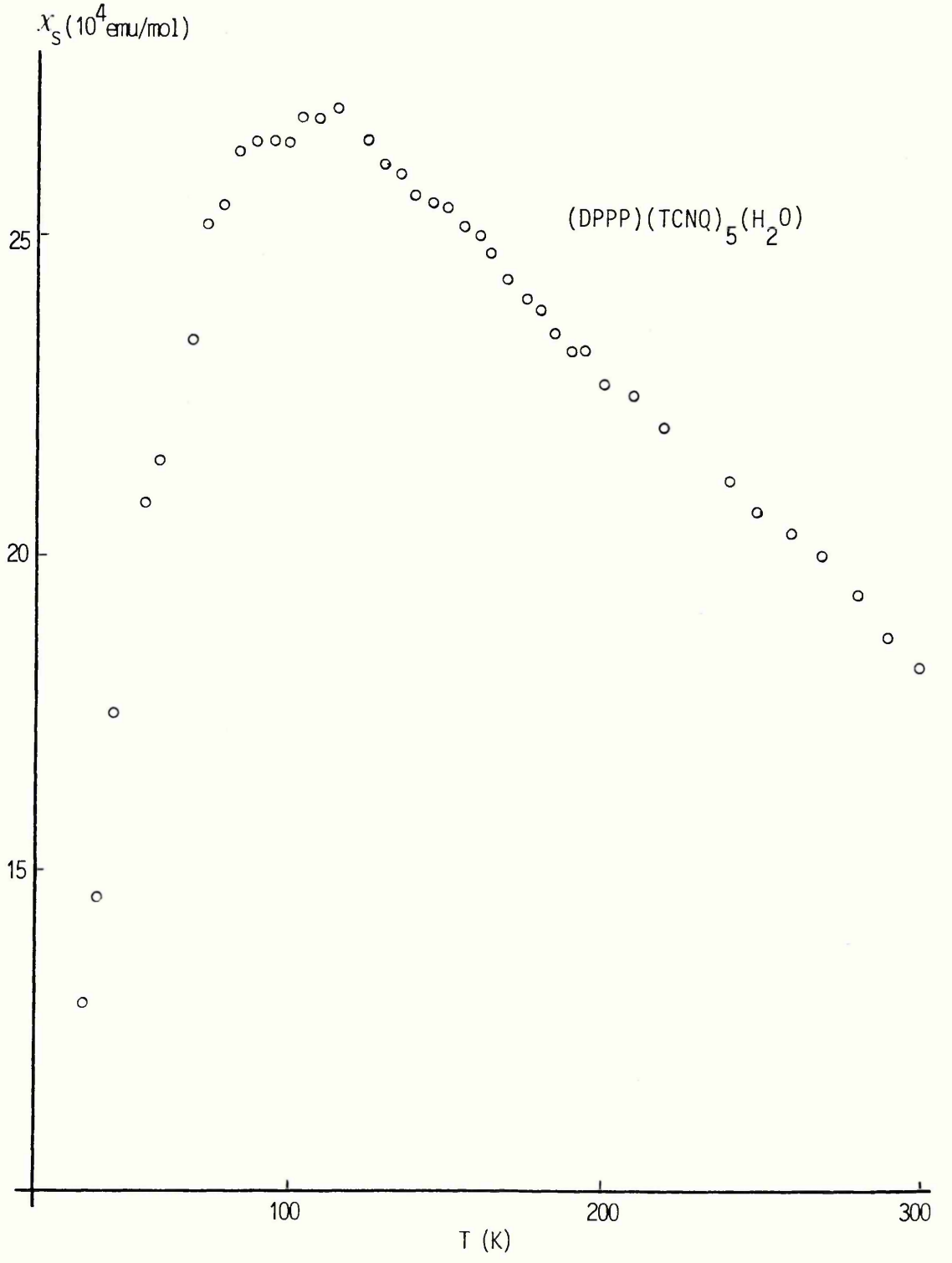

FIGURE 3.35 : The susceptibility, corrected for core diamagnetism versus temperature for (DPPP)(TCNQ)$_5$(H$_2$O)

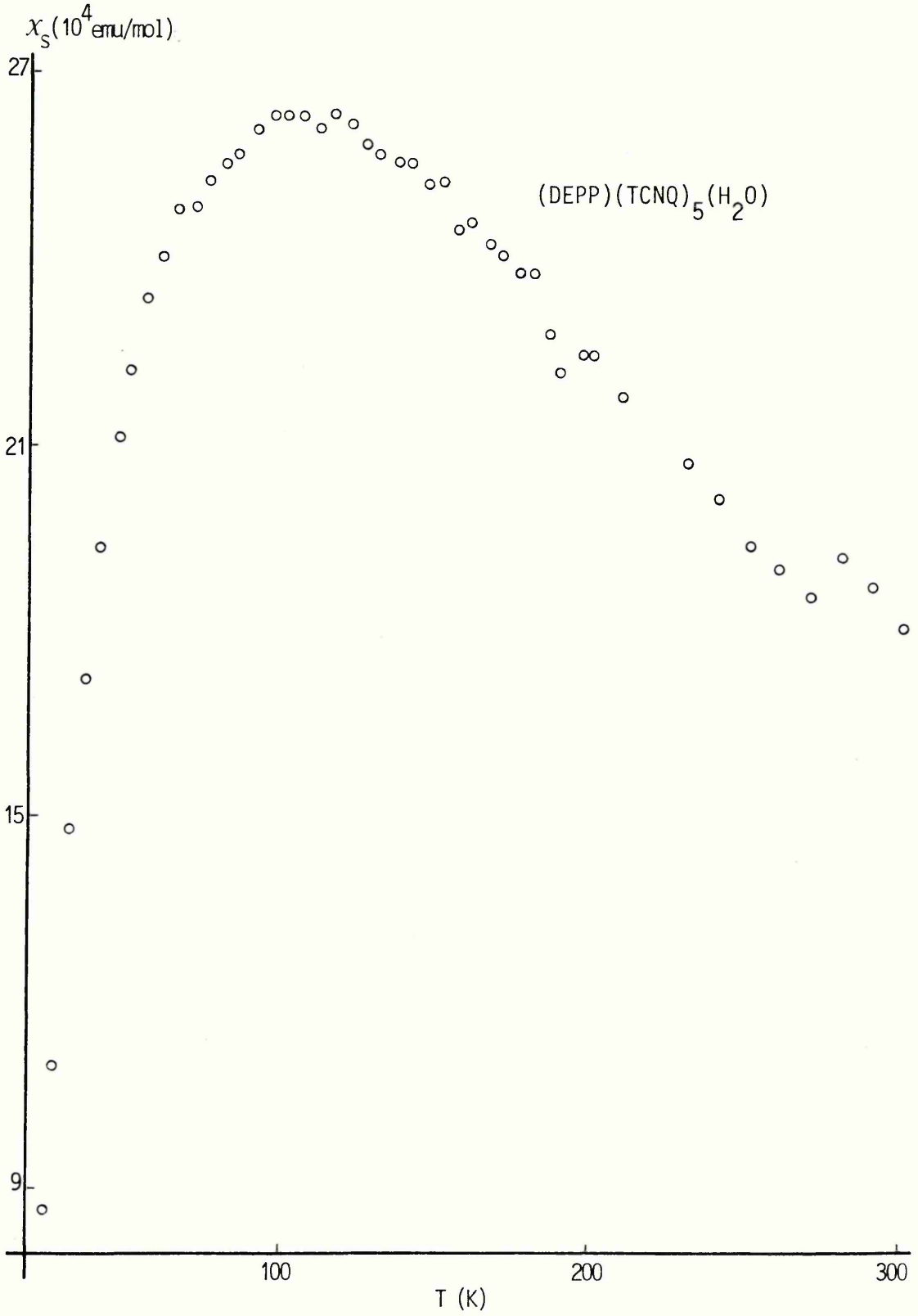

FIGURE 3.36 : The susceptibility, corrected for core diamagnetism versus temperature for (DEPP)(TCNQ)$_5$(H$_2$O)

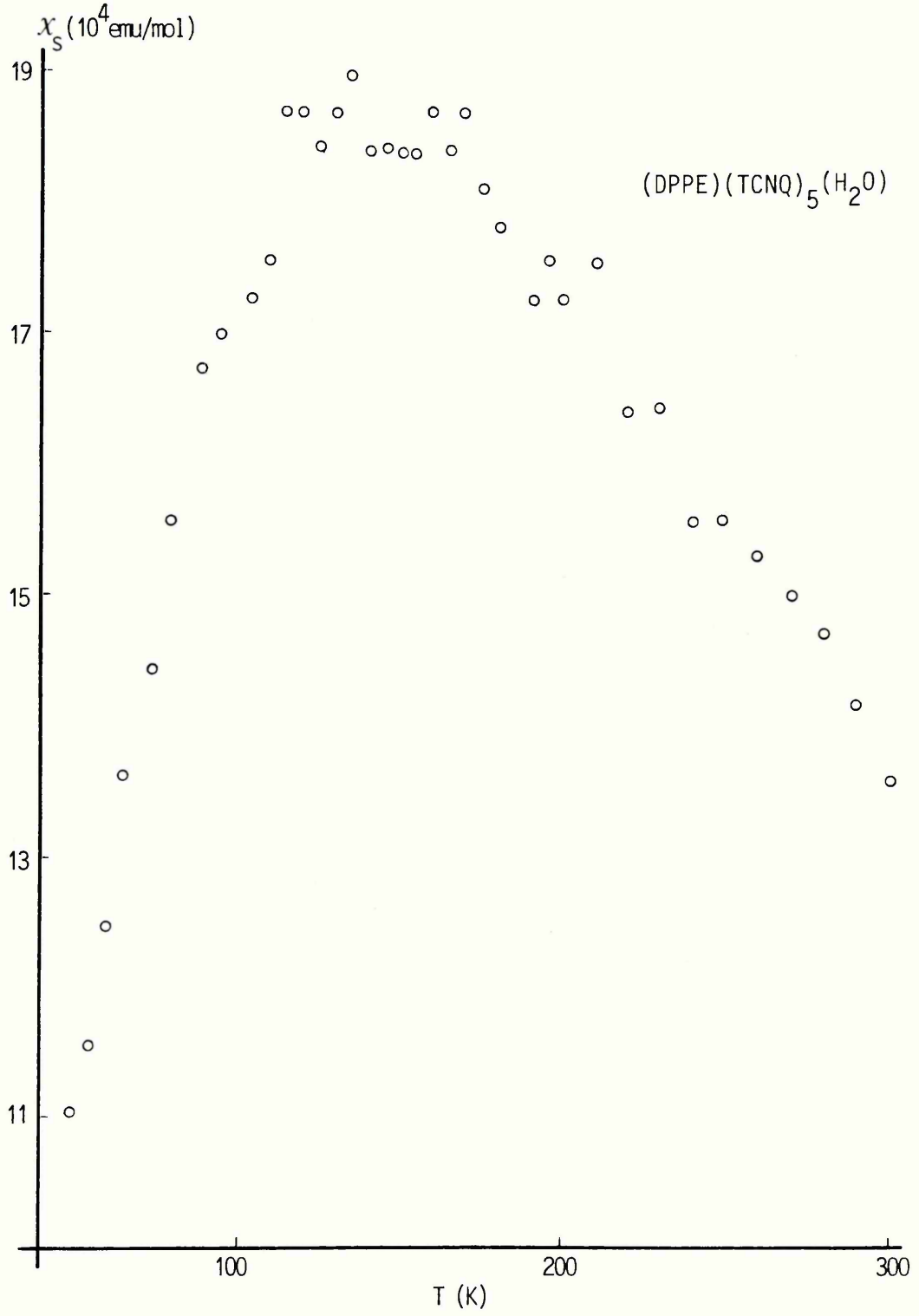

FIGURE 3.37 : The susceptibility, corrected for core diamagnetism versus temperature for (DPPE)(TCNQ)$_5$(H$_2$O)

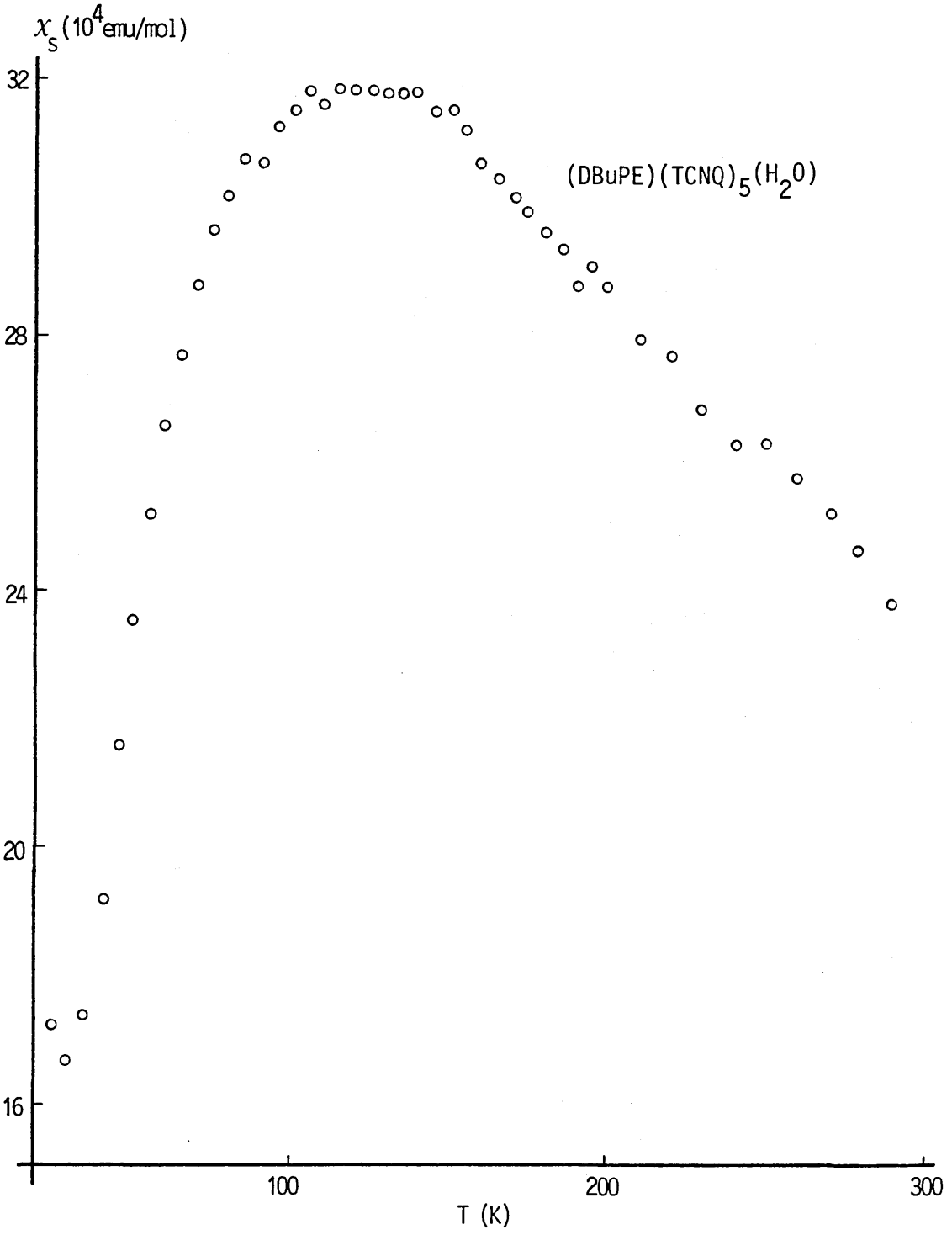

FIGURE 3.38 : The susceptibility, corrected for core diamagnetism versus temperature for (DBuPE)(TCNQ)$_5$(H$_2$O)

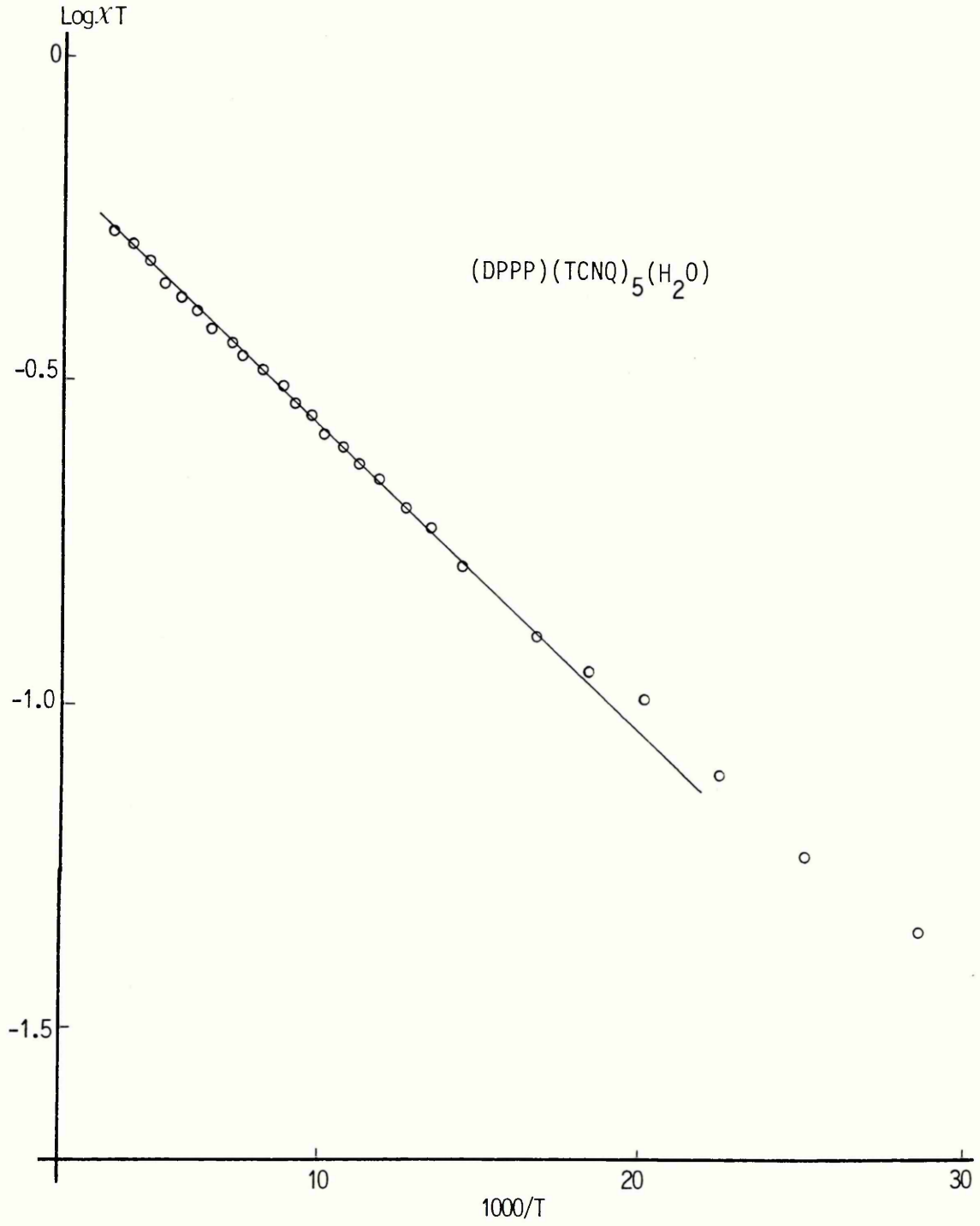

FIGURE 3.39 : Log of the product of susceptibility and temperature versus reciprocal temperature for $(DPPP)(TCNQ)_5(H_2O)$

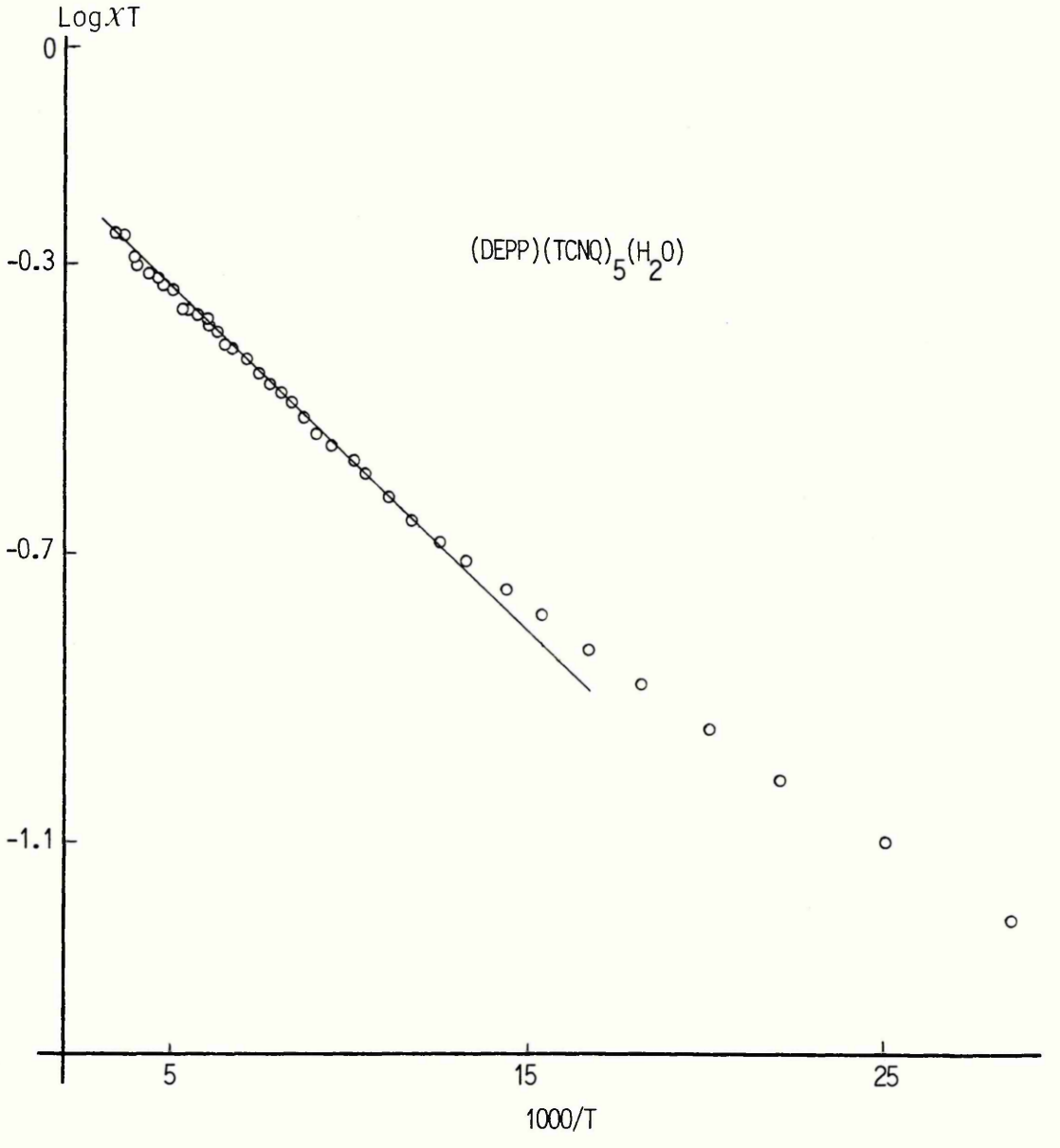

FIGURE 3.40 : The product of susceptibility and temperature versus reciprocal temperature for (DEPP)(TCNQ)$_5$(H$_2$O)

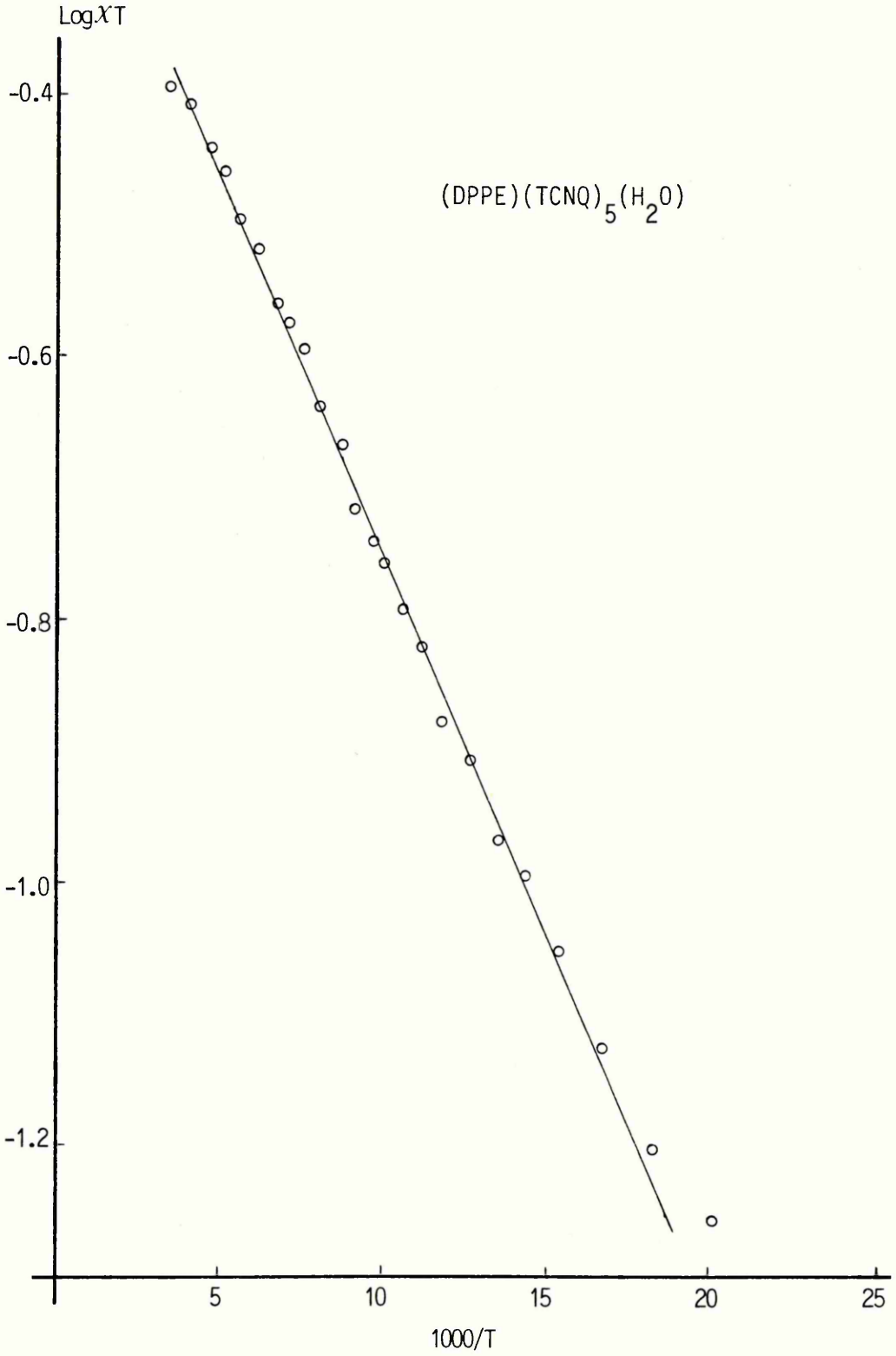

FIGURE 3.41 : The product of susceptibility and temperature versus reciprocal temperature for $(DPPE)(TCNQ)_5(H_2O)$

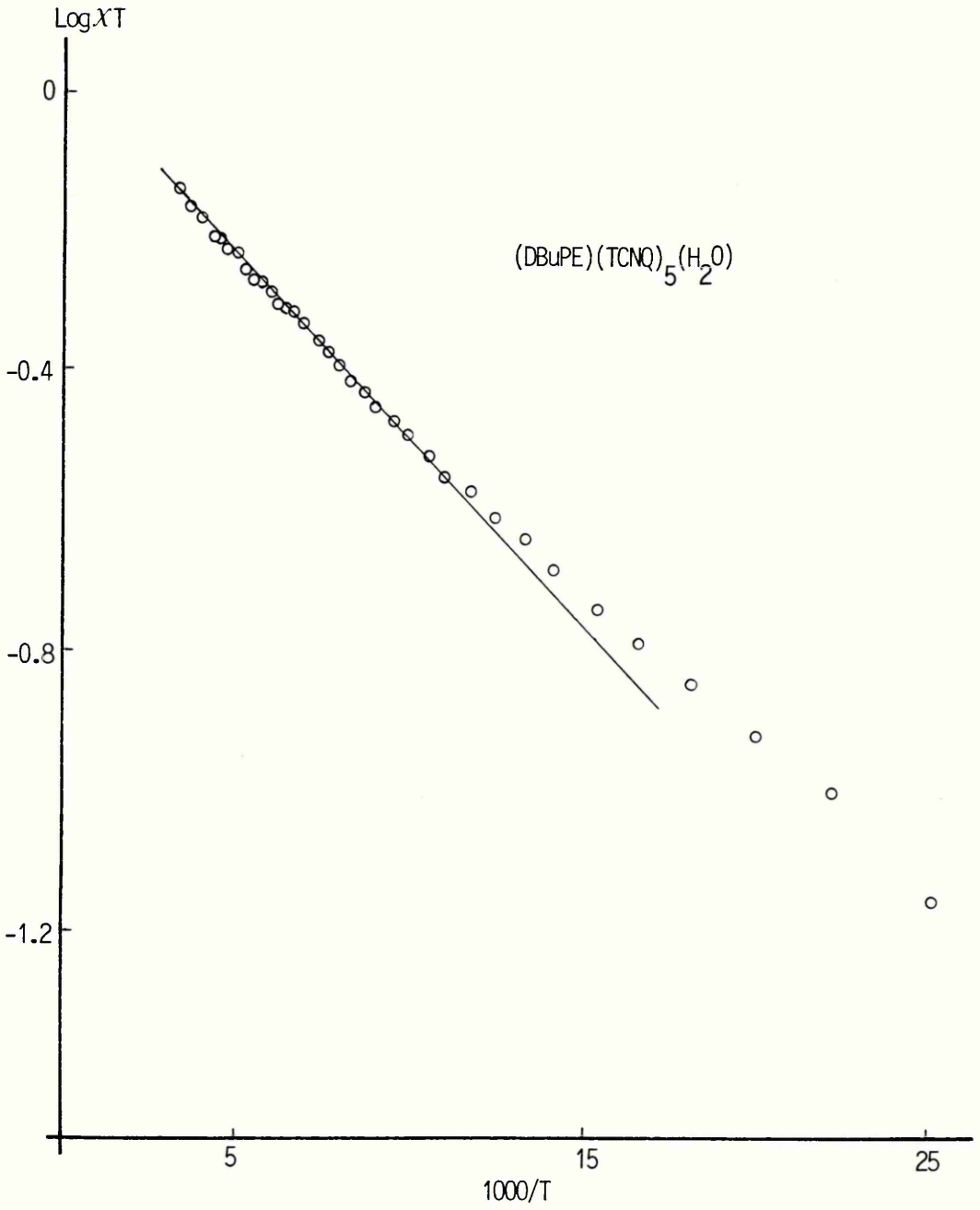

FIGURE 3.42 : Log of the product of susceptibility and temperature versus reciprocal temperature for $(DBuPE)(TCNQ)_5(H_2O)$

3.6 : Ordered bis-pyridinium TCNQ Salts

3.6.1: 1,1′-bis-(p-cyanophenyl)-4,4′-bipyridinium$(TCNQ)_4$, CPP - $TCNQ_4$

The crystal structure of CPP-$TCNQ_4$ has been determined as part of this study[93]. A general view of the structure is shown in Figure 3.43. The TCNQs are stacked in columns parallel to be b axis and are arranged in sheets parallel to the ab plane. The cation lattice is ordered with the cations interleaved between the TCNQ sheets. The molecules stack plane-to-plane in columns with mean interplanar spacings of 3.28, 3.36 and 3.00Å respectively between TCNQ(A) - TCNQ(A′), TCNQ(A) - TCNQ(B) and TCNQ(B) - TCNQ(B′). The corresponding overlaps are shown in Figure 3.44. Between TCNQ(A) and TCNQ(A′), the overlap is of the exocyclic double bond to ring type whereas between TCNQ(B) and TCNQ(B′) there is a minimal side-to-side overlap.

By applying the method of Flandrois and Chasseau[221] to the mean bond lengths of TCNQ(A) and TCNQ(B), the charges on each moiety may be estimated. In neutral TCNQ, the bonds a,b,c,d and e, shown in Figure 3.45 (p 171) are, respectively, 1.344, 1.442, 1.373, 1.435 and 1.138 Å (ref.222) and so; (b - c) = 0.069A and (c - d) = 0.062Å. In the radical anion, the lengths of the bonds b, c and d are such that;

$$(b - c) = (c - d) = 0$$

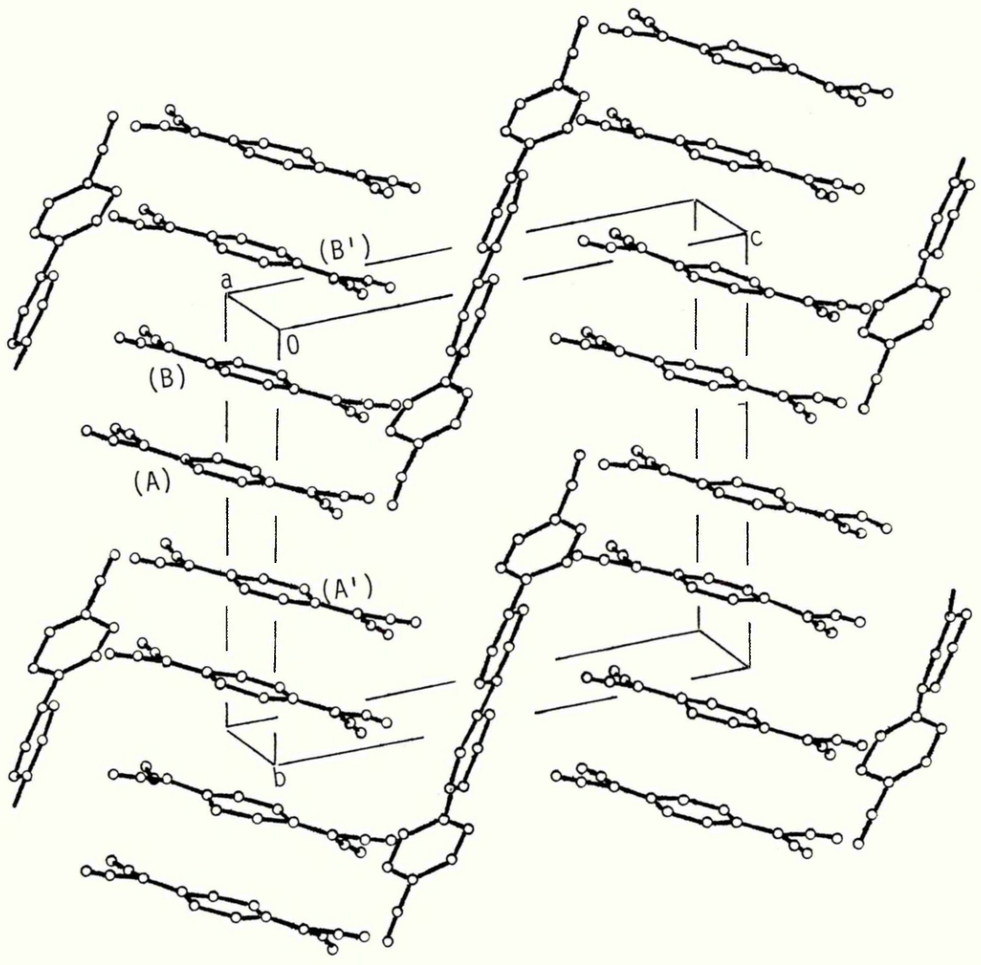

FIGURE 3.43 : The structure of CPP-$TCNQ_4$

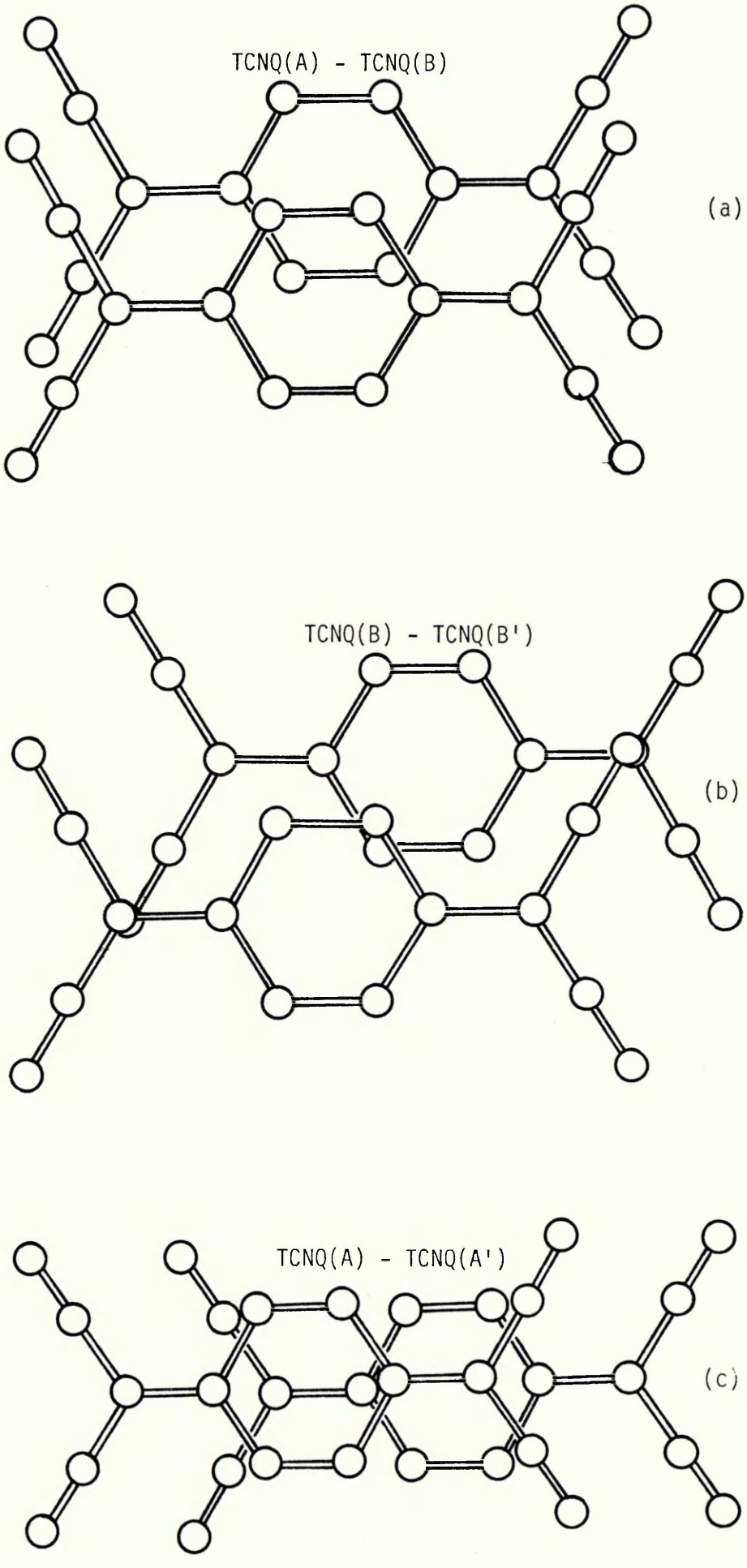

FIGURE 3.44 : Overlap types in CPP-$TCNQ_4$

A linear relationship exists between these factors[221] and the charge density on the TCNQ moiety.

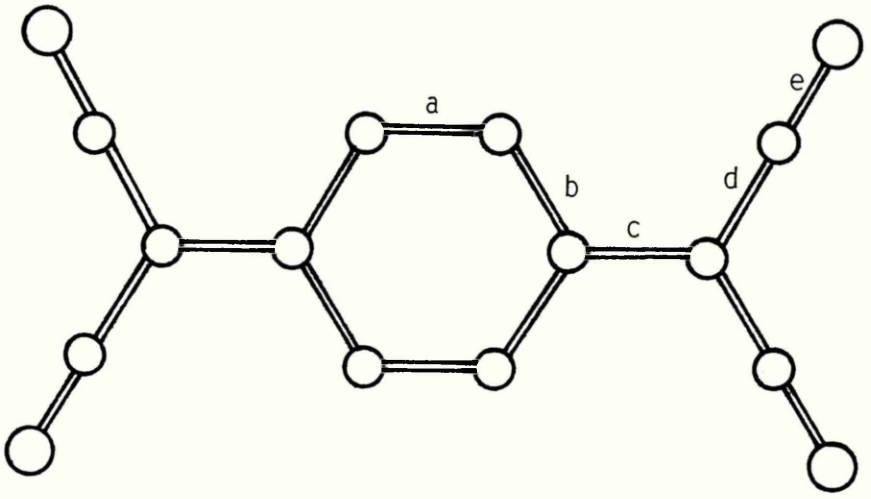

Figure 3.45

The corresponding bond lengths and estimated charge for TCNQ(A) and TCNQ(B) in the structure of CPP-$TCNQ_4$ are shown in Table 3.6 (overleaf). The estimated charge on TCNQ(B) is approximatly Ø.6 e whereas on TCNQ(A) the charge is estimated as Ø.3 e. This result provides tentative evidence that the charges are partially localised on specific sites in this salt. It is of interest that TCNQ(B) makes the closest contact with the cation. The closest non-hydrogen TCNQ to cation contact is 3.Ø62 Å for the terminal nitrogen on TCNQ(B) to the α carbon of the pyridinium ring.

The results of a similar analysis of the TCNQ bond lengths of a series of 1,1'-dialkyl-4,4'-bipyridinium salts[12,93,151,227] are consistent with the observation made for CPP-$TCNQ_4$. In each the charge is localised on the TCNQs with the closest cation contacts. Table 3.6 lists the bond lengths, the closest contacts and the calculated charge densities on the

Salt	TCNQ moiety	a	b	c	d	e	Charge	Closest * Contacts	Ref.
1,1'-Bis(p-cyanophenyl)-4,4'-bipyridinium(TCNQ)$_4$	B	1.357	1.429	1.398	1.422	1.149	0.58	3.062	93
	A	1.346	1.437	1.389	1.434	1.145	0.29	3.329	
1,1'-Dimethyl-4,4'-bipyridinium (TCNQ)$_3$	½A	1.372	1.423	1.415	1.413	1.151	0.96	3.085	238
	B	1.361	1.430	1.405	1.426	1.143	0.61	3.282	
1,1'- Diethyl-4,4'-bipyridinium (TCNQ)$_4$	A	1.351	1.431	1.410	1.424	1.143	0.73	3.231	161
	B	1.353	1.436	1.388	1.422	1.145	0.37	3.347	
1,1'-Di-n-propyl-4,4'-bipyridinium (TCNQ)$_4$	A	1.355	1.434	1.405	1.422	1.142	0.65	3.205	239
	B	1.346	1.433	1.394	1.428	1.142	0.44	3.322	
1,1'-Dibenzyl-4,4'-bipyridinium (TCNQ)$_4$	A	1.359	1.425	1.404	1.421	1.147	0.71	3.276	240
	B	1.350	1.433	1.384	1.432	1.139	0.26	3.338	

TABLE 3.6: Mean TCNQ bond lengths (Å) estimated charge on each of the TCNQs within the asymmetric unit and closest non-hydrogen TCNQ to cation contacts (Å) inCPP-TCNQ$_4$ and related salts.

* All are N-C contacts to the α-position of the pyridinium ring.

TCNQ moieties within the asymmetric unit for some salts in the series. The conclusions drawn from these observations can only be tentative because the method of Flandrois and Chasseau is very sensitive to minor changes in the bond lengths, however the magnetic properties of this salt support the conclusions regarding the distribution of charge.

The temperature dependence of the magnetic susceptibility of CPP-$TCNQ_4$ is shown in Figure 3.46 (overleaf).

In the range 100 to 300 K the susceptibility varies as;

$$\chi = C / (T = \theta)$$

(see Figure 3.47, p176) with C = 0.62 and θ = 26 K. The effective magneton number, μ_{eff}, calculated from;

$$\mu_{eff} = 2.84C^{1/2}; \text{ gives } \mu_{eff} = 2.236.$$

The 'spin only' formula;

$$\mu_{eff} = [n(n + 2)]^{1/2}; \text{ gives } \mu_{eff} = 2.83.$$

'n' in this case corresponds to two free spins per mole according to the stoichiometry of the salt i.e. $[CPP]^{2+}[(TCNQ)_4]^{2-}$.

For CPP-$TCNQ_4$ the evidence obtained from spectroscopic analysis and from the analysis of the TCNQ bond lengths indicates that the mean charge on the TCNQ lattice does not differ significantly from 2- within the stoichiometric unit.

The low experimental value for μ_{eff} compared to that calculated suggests a spin quenching which may be attributed, in part, to antiferromagnetic ordering of spins. If these interactions were absent then the susceptibility would follow the Curie law, $\chi = C/T$.

The susceptibility at high temperatures reflects a spin system in which the spins interact only weakly with each other. The evidence for partial localisation of spins on specific TCNQ sites indicated from calculations made using the TCNQ bond lengths shows that TCNQs (B) and (B$'$) possess

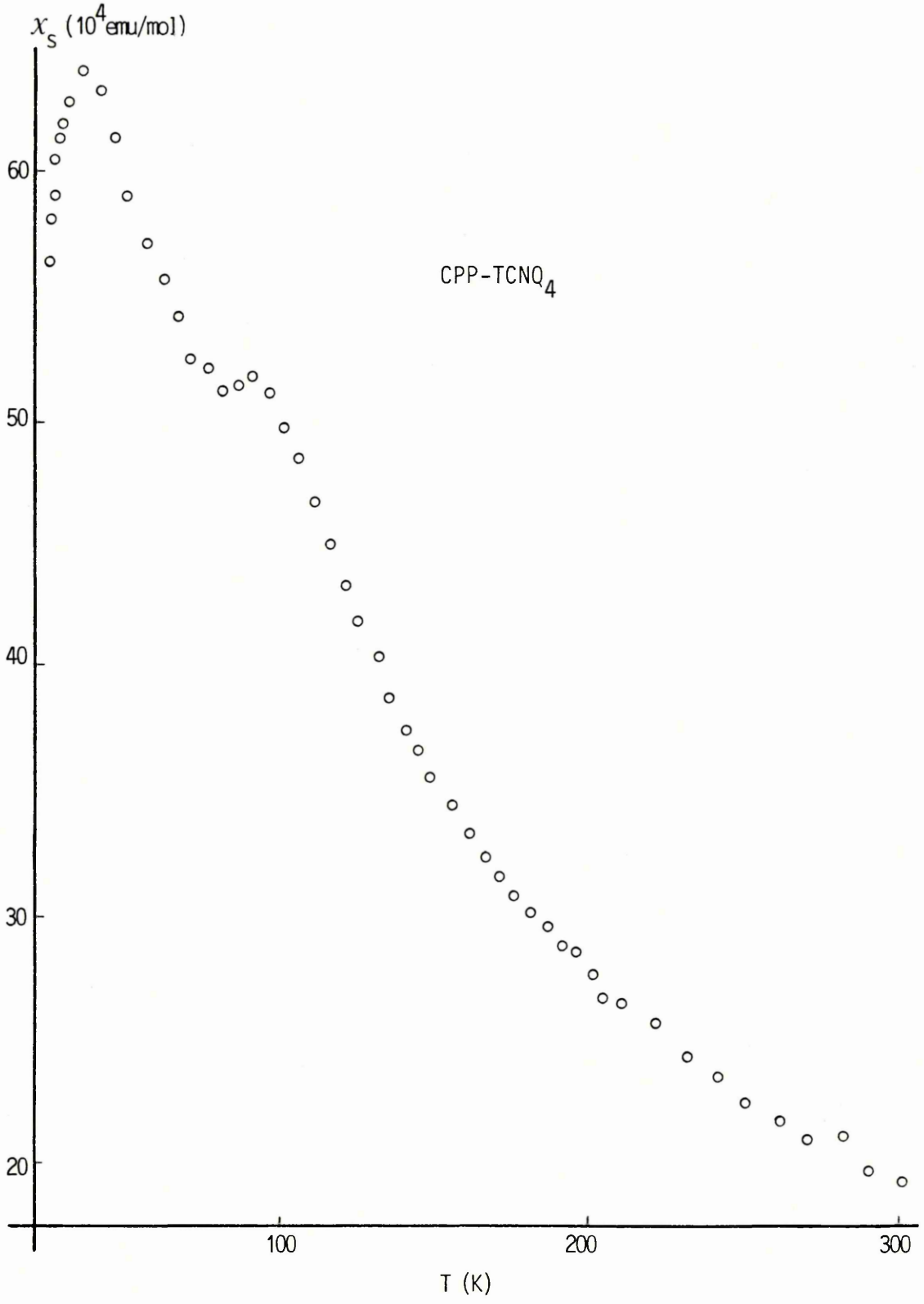

FIGURE 3.46 : The susceptibility, corrected for core diamagnetism versus temperature of CPP-TCNQ$_4$

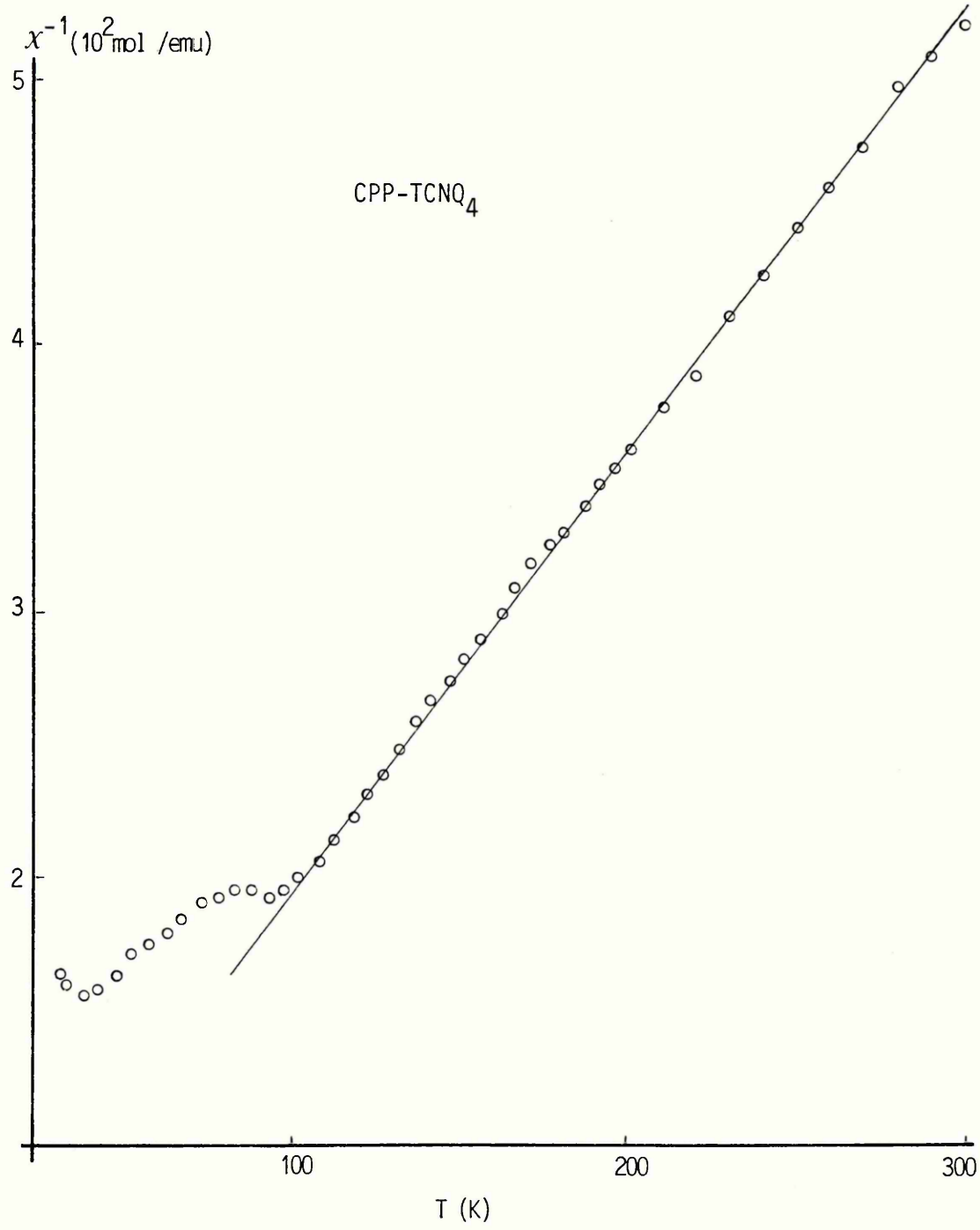

FIGURE 3.47 : The reciprocal susceptibility versus temperature for CPP-TCNQ$_4$

the highest charge (Ø.6 e on each). These moieties are adjacent in the stack and the strongest spin interaction may occur between spins on these sites. However, the overlap between TCNQ (B) and TCNQ (B′) is only minimal [Figure 3.44 (b)]. Since J decreases with spin separation this poor overlap will minimise the interaction. The overlap between TCNQ (A) and TCNQ (A′) is of the favourable exocyclic double bond to ring type, but the mean charge on each moiety is calculated to be only Ø.3 e. Thus the exchange interaction between spins on these sites is likely to be only weak.

At 1ØØ K, the susceptibility exhibits a weak cusp. Below 1ØØ K the susceptibility varies as $\chi = C \exp(-J/kT)$. The semilog plot of Figure 3.48 (overleaf) is linear in the range 25 to 1ØØ K. The interpretation of the susceptibility in this region can only be made tentatively since it has been found (Sections 3.3-3.5) that the susceptibility of species obeying a Curie law have an appreciable contribution at these temperatures.

The electrical and magnetic properties of CPP-$TCNQ_4$ are given in Table 3.9 (p 184). The log normalised conductivity versus reciprocal temperature plot is shown in Figure 3.49 (p 179). The conductivity varies as;

$$\sigma = \sigma_o \exp(-E_A/kT)$$

and the salt may be classed as a small band gap semiconductor with the gap arising from the periodic distortion of the TCNQ lattice.

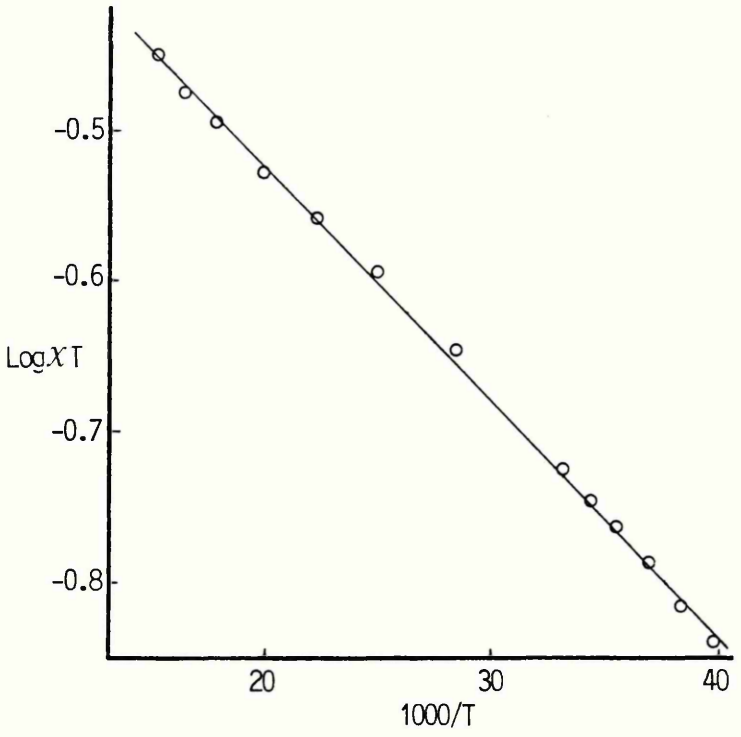

FIGURE 3.48 : The low temperature susceptibility of CPP-$TCNQ_4$

In contrast to the isostructural series discussed in sections 3.1 to 3.5 the cation lattice in CPP-$TCNQ_4$ is ordered and metallic behaviour has not been observed in either this salt or its para-substituted congeners, the conductivities of which are listed in Table 3.7.

Cation	σ (300K) (Scm^{-1})
1,1'-Diphenyl-4,4'-bipyridinium	0.07
1,1'-Bis-(p-methylphenyl)-4,4'-bipyridinium	0.2
1,1'-Bis-(p-fluorophenyl)-4,4'-bipyridinium	0.06
1,1'-Bis-(p-iodophenyl)-4,4'-bipyridinium	0.3
1,1'-Bis-(p-thiocyanophenyl-4,4'-bipyridinium	0.007

TABLE 3.7: The electrical properties of compacted pellets of microcrystalline samples of 1,1'-diphenyl-4,4'-bipyridinium$(TCNQ)_4$ and para-substituted congeners of CPP-$TCNQ_4$

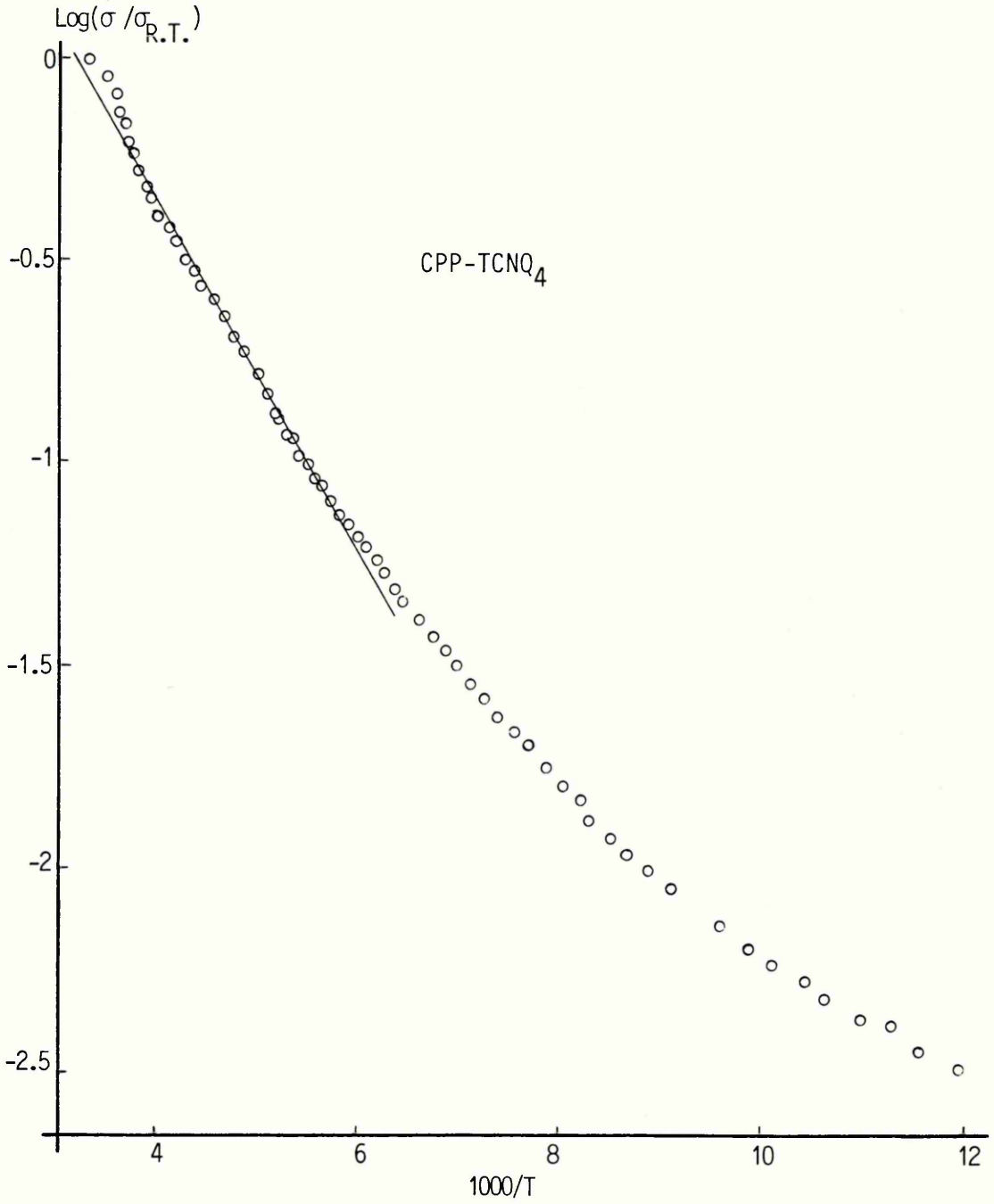

FIGURE 3.49 : Log normalised conductivity versus reciprocal temperature for CPP-$TCNQ_4$

Semiconductive behaviour and a well defined gap are features which are common to salts of 1,1-diaryl-4,4-bipyridinium dications and in all these salts the cation lattice is ordered.

In contrast, the series of TCNQ salts of the cations DRPE-DRPA-DRPP, possess a disordered cation lattice. Channels in between the TCNQ sheets can accommodate cations which vary in size from 1,2-bis-(4-pyridinium)ethane ($C_{12}H_{14}N_2$) to 1,3-bis-(n-propyl-4-pyridinium)propane ($C_{19}H_{28}N_2$). The adaptability is possibly due to the flexibility of the cations in this series and leads to the suggestion that the 1,1-diary-4,4-bipyridinium dications are too rigid to be accommodated in the narrow, disordered cation channels.

3.6.3: 1,1-Dimethyl-4,4-bipyridinium $(TCNQ)_3$, $(DMBP)(TCNQ)_3$.

The structure of $(DMBP)(TCNQ)_3$ has been determined by Ashwell and Wallwork[227] and general views of the structure are shown in Figure 3.5Ø (reproduced from figure 1 in reference 227).

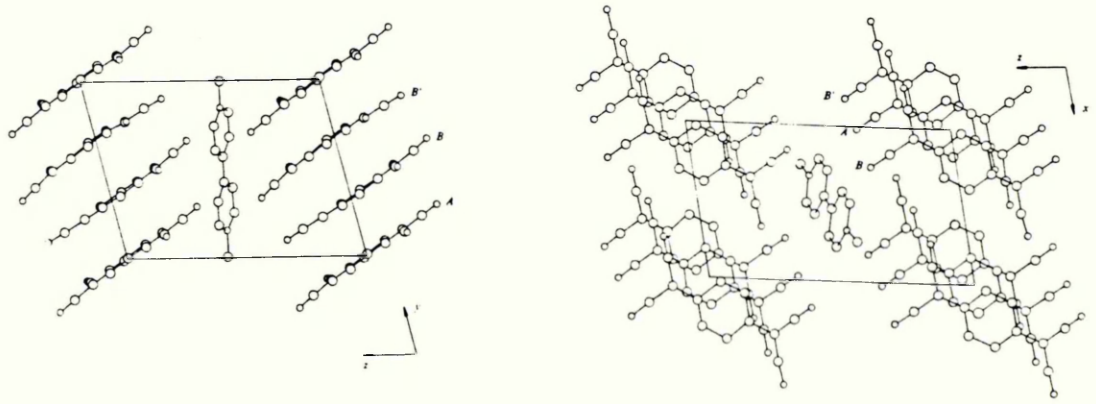

FIGURE 3.5Ø : The structure of $(DMBP)(TCNQ)_3$

The TCNQs are stacked plane to plane in stoichiometric groups of three. There is a favourable exocyclic double bond to ring overlap between adjacent TCNQs in each triad but there is no direct overlap between triads. The mean interplanar spacing between TCNQs within the triad is 3.16 Å. The central molecule of the triad TCNQ(A), makes the closest contact to the cation (see Table 3.6) and the charge is partially localised on this moiety. The mean charges on TCNQ(A) and TCNQ(B), calculated by the method of Flandrois and Chasseau, are 0.96 e and 0.61 e, respectively.

The electrical properties of $(DMBP)(TCNQ)_3$ are given in Table 3.9 (p 184). The log σ versus reciprocal temperature plot (Figure 3.51, overleaf) is linear in the range 200 to 300 K. The conductivity measured along the b axis varies as;

$$\sigma = \sigma_{o} \exp(-E_A/kT)$$

The salt thus possesses a well defined gap giving rise to semiconductive behaviour. The gap arises from the structural non-uniformity in spacing and overlap of TCNQs.

The conductivity transition seen at 178 K is reproducible upon thermal recycling and is possibly the result of a structural transition at this temperature. DSC studies confirm the transition temperature.

The conductivity of the salt is anomalously high if the conduction process is considered to occur mainly along the distorted columns (the b axis). In fact it has been shown by Ashwell and Wallwork[227] that the TCNQ lattice possesses

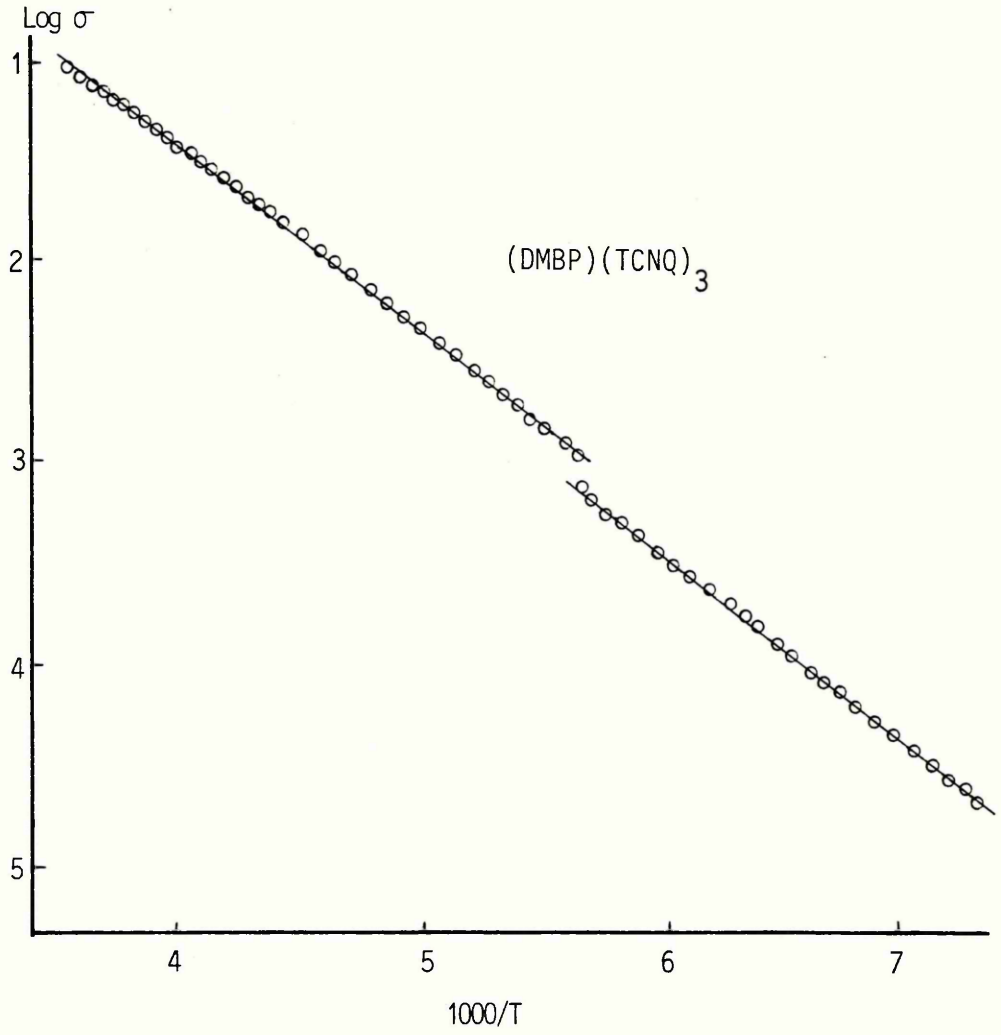

FIGURE 3.51 : Log conductivity versus reciprocal temperature of $(DMBP)(TCNQ)_3$

several short contacts (<3.4Å) between triads. These contacts are listed in Table 3.8 .

C(2i)-N(2ii)	3.3Ø5(5)	C(12i)-C(18iv)	3.377(6)
C(3i)-N(2ii)	3.332(5)	C(13i)-N(6iv)	3.372(7)
C(9i)-N(6iii)	3.372(6)	C(14i)-N(6iv)	3.222(7)
C(11i)-C(11iv)	3.333(6)		

Symmetry code : (i) x,y,z ; (ii) 1-x,y,z ;
(iii) x+1,y,z ; (iv) x,1-y,z

Table 3.8 : Short inter-triad contacts (<3.4Å) in (DMBP)(TCNQ)3 (For atom numbering, see figure 3.52 below)

The moderate conductivity in this salt may be attributed to the relatively strong interactions arising from these close contacts between triads. It might be expected on these considerations that the electrical properties would be less anisotropic, however, the conductivity along the a and c axes has not been determined.

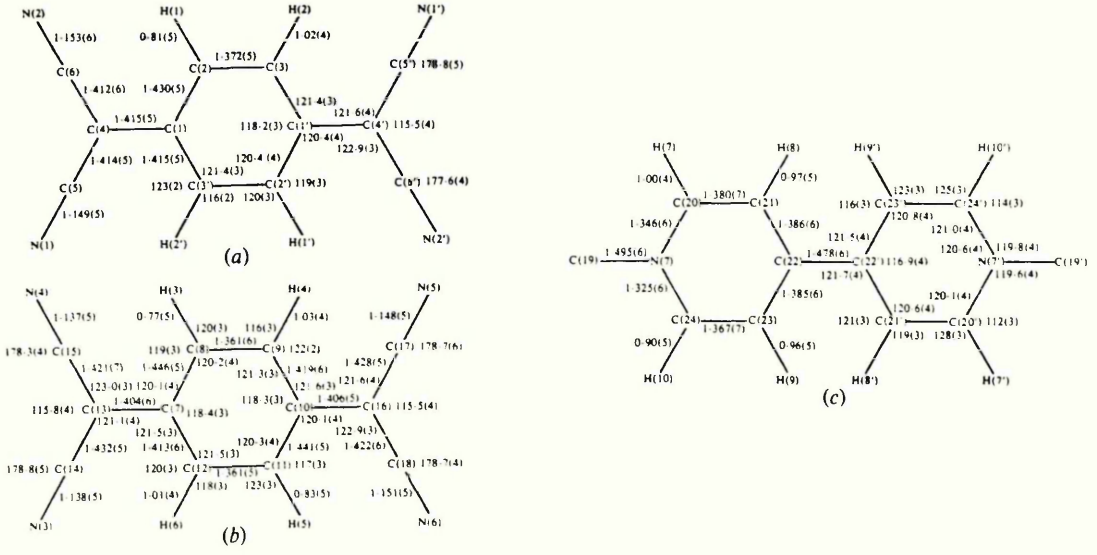

FIGURE 3.52 : Molecular dimensions of (a) TCNQ(A), (b) TCNQ(B) and (c) the DMBP cation in $(DMBP)(TCNQ)_3$ (after reference 227)

SALT	$\sigma_{R.T.}(Scm^{-1})$	$E_A(eV)$	Magnetic Susceptibility
CPP - $TCNQ_4$	0.1	0.1 (150-300K)	Curie-Weiss, (T >100K) Weakly Activated Susceptibility (T >100K) J = 0.003eV
$(DMBP)(TCNQ)_3$	1	0.15 (200-300K)	

TABLE 3.9 : The electrical and magnetic properties of TCNQ salts at 1,1'-bis-(p-cyanophenyl)-4,4-bipyridinium, CPP, and 1,1-dimethyl-4,4-bipyrdinium, DMBP.

3.7: 1:2 TCNQ Salts of Dialkyldiphenylphosphonium Cations

The crystal structures of $(Et_2Ph_2P)(TCNQ)_2$ (ref.241) and $(Me_2Ph_2P)(TCNQ)_2$ (ref.56) are of particular interest. In the former complex, the TCNQs form homologous columns with a regular, short interplanar spacing which is in contrast to the related alkyl triphenylphosphonium[87,230] and tetraphenylphosphonium[231] salts where the TCNQ lattice is distorted with stoichiometric periodicity. The structure of $(Me_2Ph_2P)(TCNQ)_2$ is of interest since there is evidence of a distortion at room temperature, of a regular TCNQ stack.

A general view of the structure of $(Me_2Ph_2P)(TCNQ)_2$ is presented in Figure 3.53. The cation lattice is represented as open circles in the figure which depict the position of the phosphorous atoms. The phenyl rings and methyl groups have been omitted for clarity. The cation lattice is disordered and the phenyl rings and methyl groups adopt two orientations distributed randomly throughout the lattice. The cations are interleaved between the TCNQ sheets which are arranged parallel to the bc plane. As with the series discussed in Sections 3.1-3.5, the disorder in the cation lattice assists the homologous stacking of TCNQs. Figure 3.54 depicts the structure projected along a. The TCNQs form columns parallel to b with adjacent TCNQs overlapping in the favourable exocyclic double bond to ring manner. The mean interplanar spacing between TCNQs is 3.28 Å. This is the average crystallographic spacing, however, it should be noted

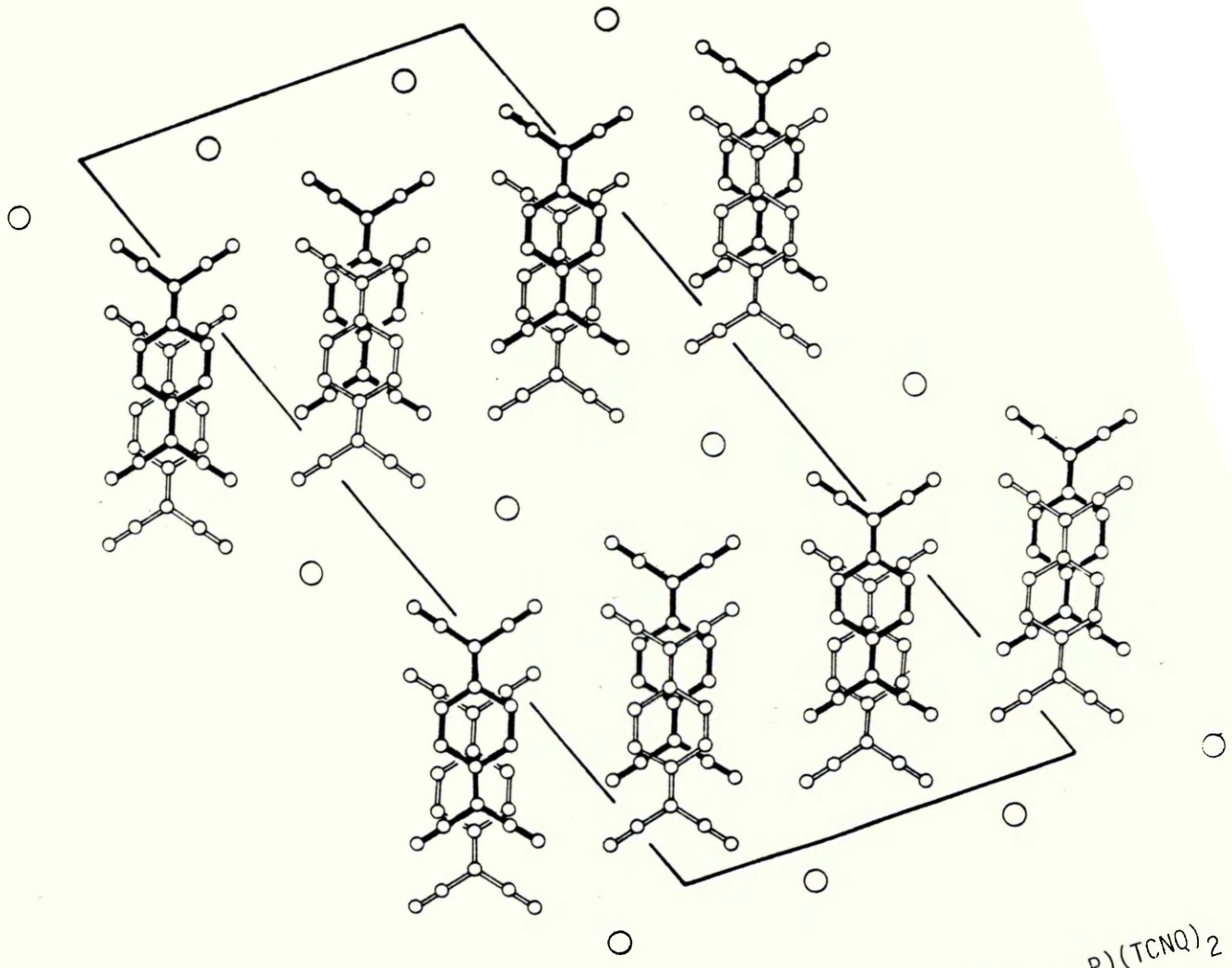

FIGURE 3.53 : A general view of the structure of $(Me_2Ph_2P)(TCNQ)_2$

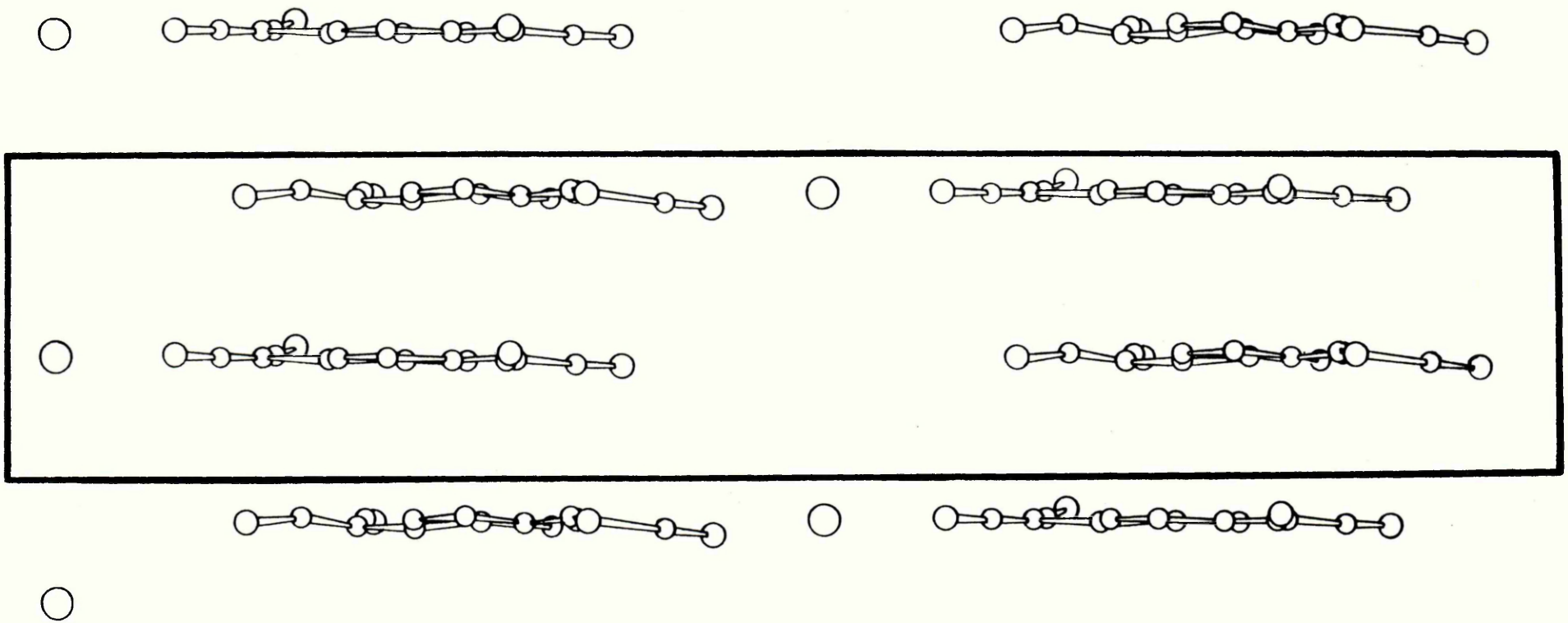

FIGURE 3.54 : The structure of $(Me_2Ph_2P)(TCNQ)_2$ projected along a

that the X-ray oscillation photographs show two sets of layer lines for crystals mounted about b. They show strong layer lines corresponding to a d-spacing of 6.56 Å and weak layer lines corresponding to a d-spacing of 13.1 Å.

The layer lines are commensurate and suggest that the spacing is not uniform but that there is an incipient distortion with a tendency towards formation of diads at lower temperatures. Similar sets of lines have been observed previously in, for example, TTF-TCNQ[232] and its substituted congeners[233,234].

The electrical and magnetic properties of $(Me_2Ph_2P)(TCNQ)_2$ are given in Table 3.10 (p 199). The conductivity along b the needle axis of this salt in the range 180 to 300 K varies as $\sigma = \sigma_o \exp(-E_A/kT)$ where E_A = 0.2 eV. The plot of log normalised conductivity versus reciprocal temperature is linear in this range but shows curvature below 180 K (see Figure 3.55, overleaf). This curvature at lower temperatures is assigned to an extrinsic mechanism. Above 300 K, (although not shown in the figure) the conductivity follows a weaker temperature dependence but the conductivity maximum, characteristic of quasi-one-dimensional metallic behavior has not been reached and the crystals begin to decompose at about 330 K.

The proposal of an incipient distortion at room temperature in this salt as suggested by the X-ray work may be related to the apparent conductivity transition around 300 K. Thus the activation gap observed below room temperature may originate

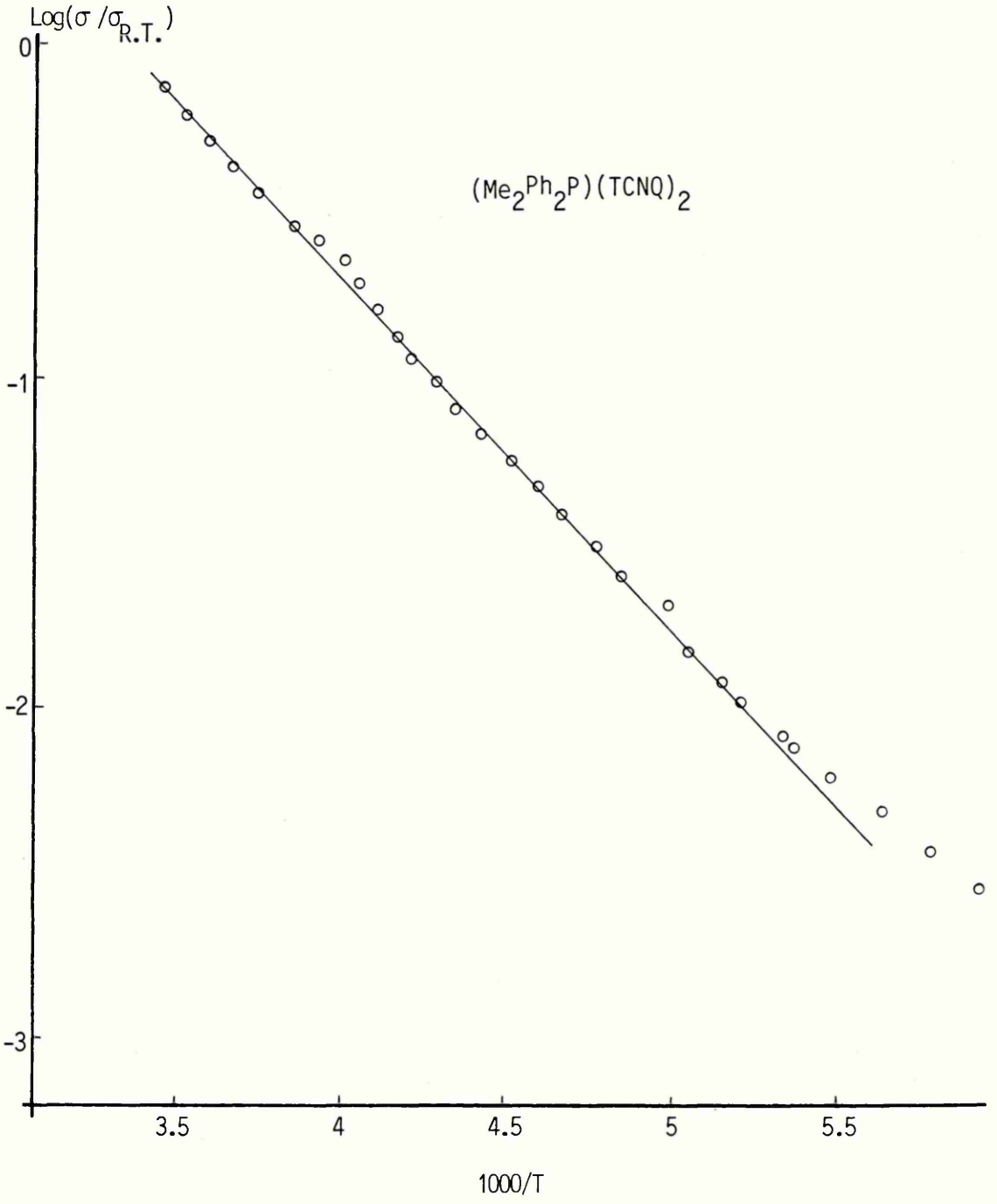

FIGURE 3.55 : Log normalised conductivity versus reciprocal temperature for $(Me_2Ph_2P)(TCNQ)_2$

in the lattice distortion proposed to exist at these temperatures. Above 300 K, the lattice is regular and the gap may be renormalised to zero. Problems presented by decomposition at elevated temperatures preclude a more rigorous description of the conductivity above 300 K.

The structure of $(Et_2Ph_2P)(TCNQ)_2$ has been determined[241] and the weak layer lines characteristic of a lattice distortion have not been observed. In this salt, the cation lattice is ordered and the TCNQs stack in homologous columns. This is an unusual observation since in all other N-quaternary salts having an ordered counterion lattice the TCNQ lattice shows non-uniformity of spacing and, with a few exceptions, of overlap. The suggestion has been made[229] that the effects of the bulky ethyl and phenyl groups are to effectively screen the positive potential on the phosphorous ions from the TCNQ lattice, thereby reducing the more commonly observed inter-lattice Coulomb coupling in ordered salts. The closest contact between the TCNQ moiety and the positive charge on the phosphorous atom is 4.28 Å and no contact between the anion and cation columns is significantly shorter than the sum of the van der Waals radii.

The electrical properties of $(Et_2Ph_2P)(TCNQ)_2$ are given in Table 3.10 (p 199). The moderate conductivity (1 to 10 Scm^{-1} at room temperature) and low activation energy (0.04 to 0.06 eV) are consistent with the homologous stacking of TCNQs. The differences in the electrical properties between this salt and the dimethyl analogue highlight the structural

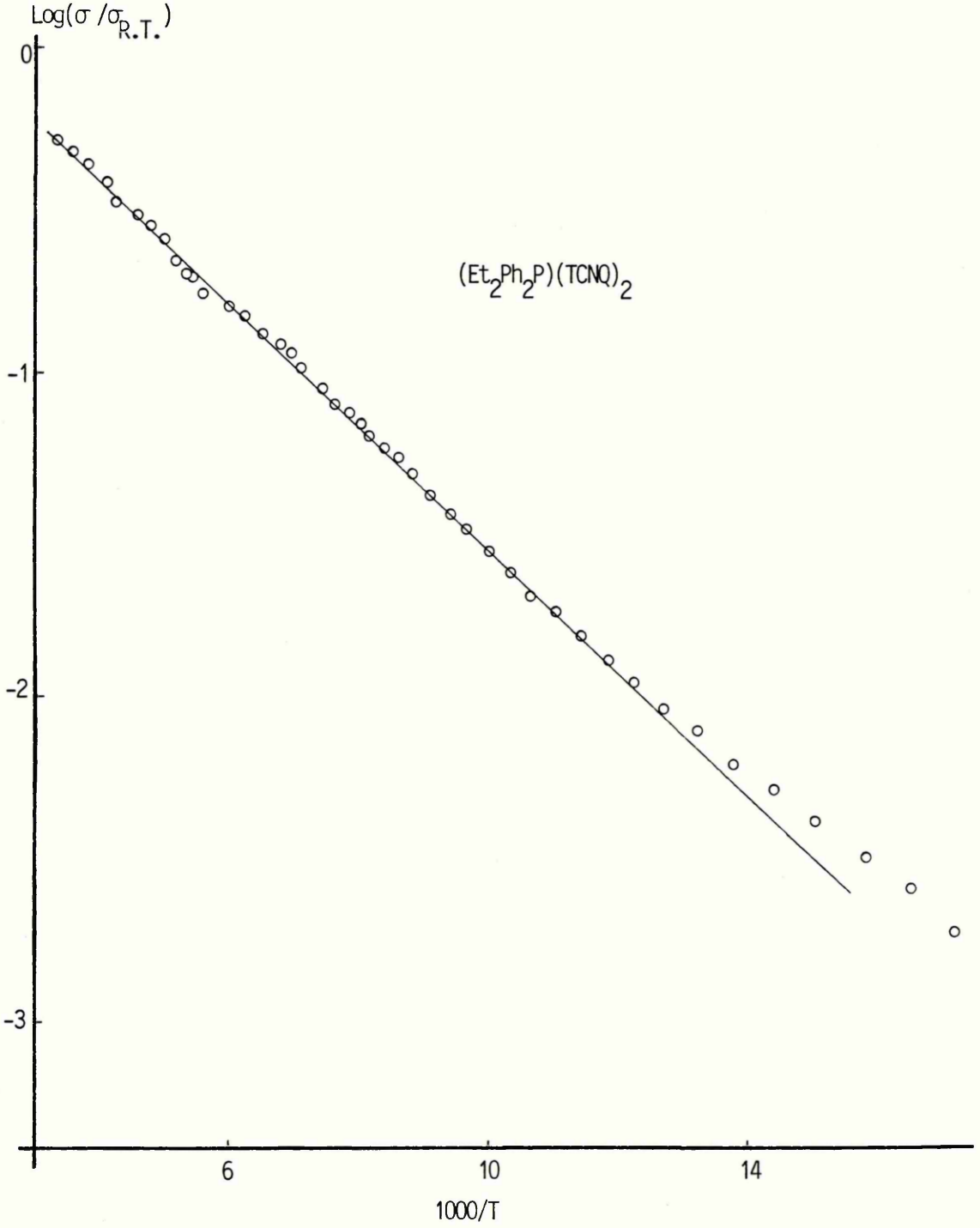

FIGURE 3.56 : Log normalised conductivity versus reciprocal temperature of $(Et_2Ph_2P)(TCNQ)_2$

differences between these salts. In the dimethyl analogue the TCNQ lattice is not regular below room temperature and the relatively large gap (E_A = Ø.2 eV) is possibly due to the non-uniformity of spacing.

The magnetic properties of the salts are given in Table 3.1Ø. The temperature dependence of the magnetic susceptibility of $(Me_2Ph_2P)(TCNQ)_2$, (Figure 3.57) exhibits a broad maximum centered at about 22Ø K. The susceptibility varies exponentially with temperature, the semilog plot, log χT versus reciprocal temperature being linear in the range 11Ø-3ØØ K (Figure 3.58). The slope is equivalent to J = Ø.Ø18 eV. The zero field splitting lines observed in the esr spectrum[229] for this salt at low temperatures (T = 11Ø K) are consistent with a suggestion that the spins are partially localised at these temperatures. Zero field splitting lines have been observed in $(MePh_3P)(TCNQ)_2$ and in $(MePh_3A_s)(TCNQ)_2$ below 173 K and are attributed to the dipolar interaction of two localised spins of a triplet[2Ø6]. At higher temperatures the doublets coalesce as a result of mutual spin exchange between spins of the triplet state.

The magnetic susceptibility of $(Et_2Ph_2P)(TCNQ)_2$ exhibits a weak temperature dependence and passes through a maximum at 11Ø K (Figure 3.59). The slope of the log χT versus reciprocal temperature plot, shown in Figure 3.6Ø is equivalent to Ø.ØØ89 eV. This is in excellent agreement with the value of J determined by the esr method[229] which gives J = Ø.ØØ92 eV.

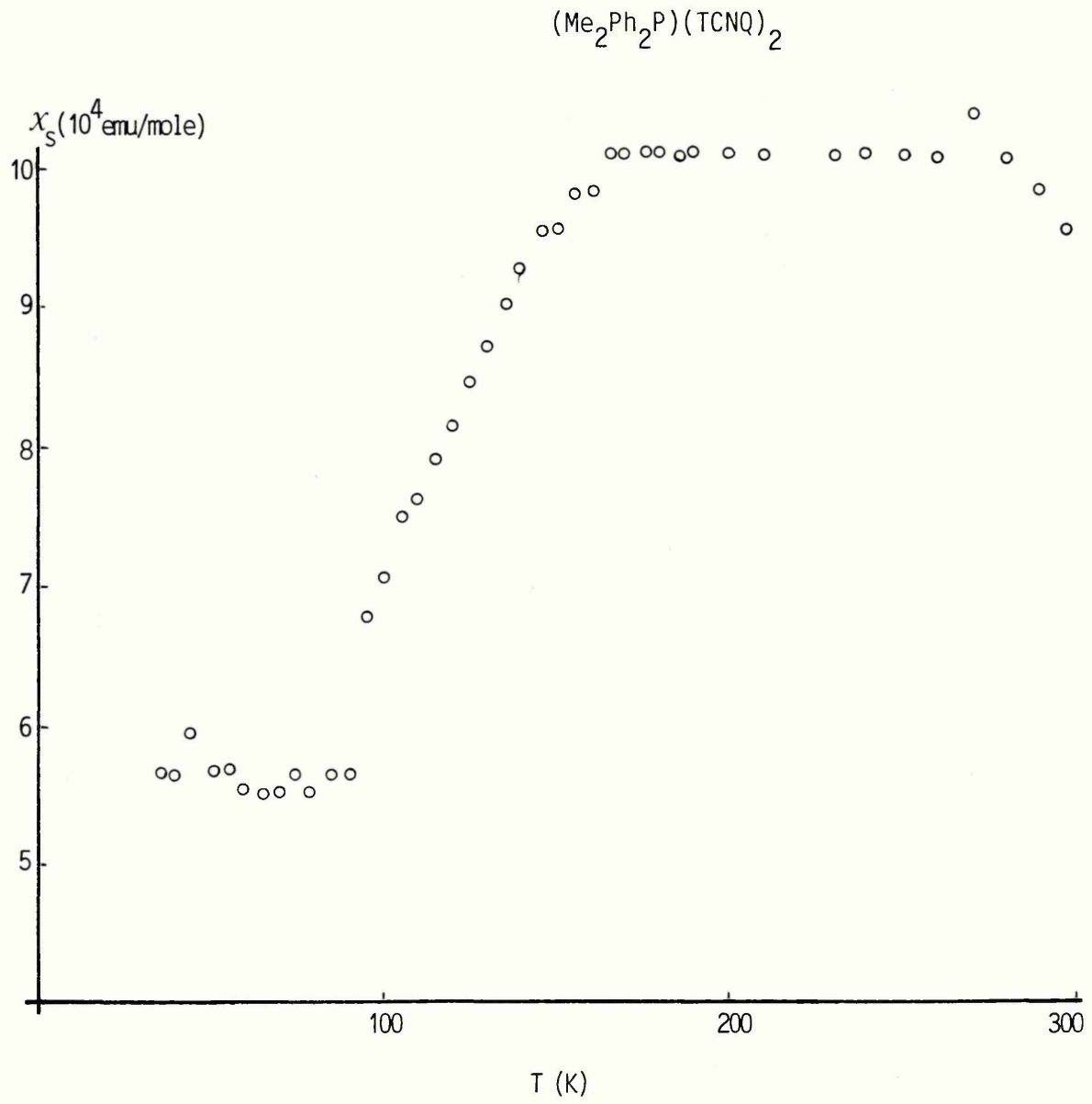

FIGURE 3.57 : The susceptibility, corrected for core diamagnetism versus temperature of $(Me_2Ph_2P)(TCNQ)_2$

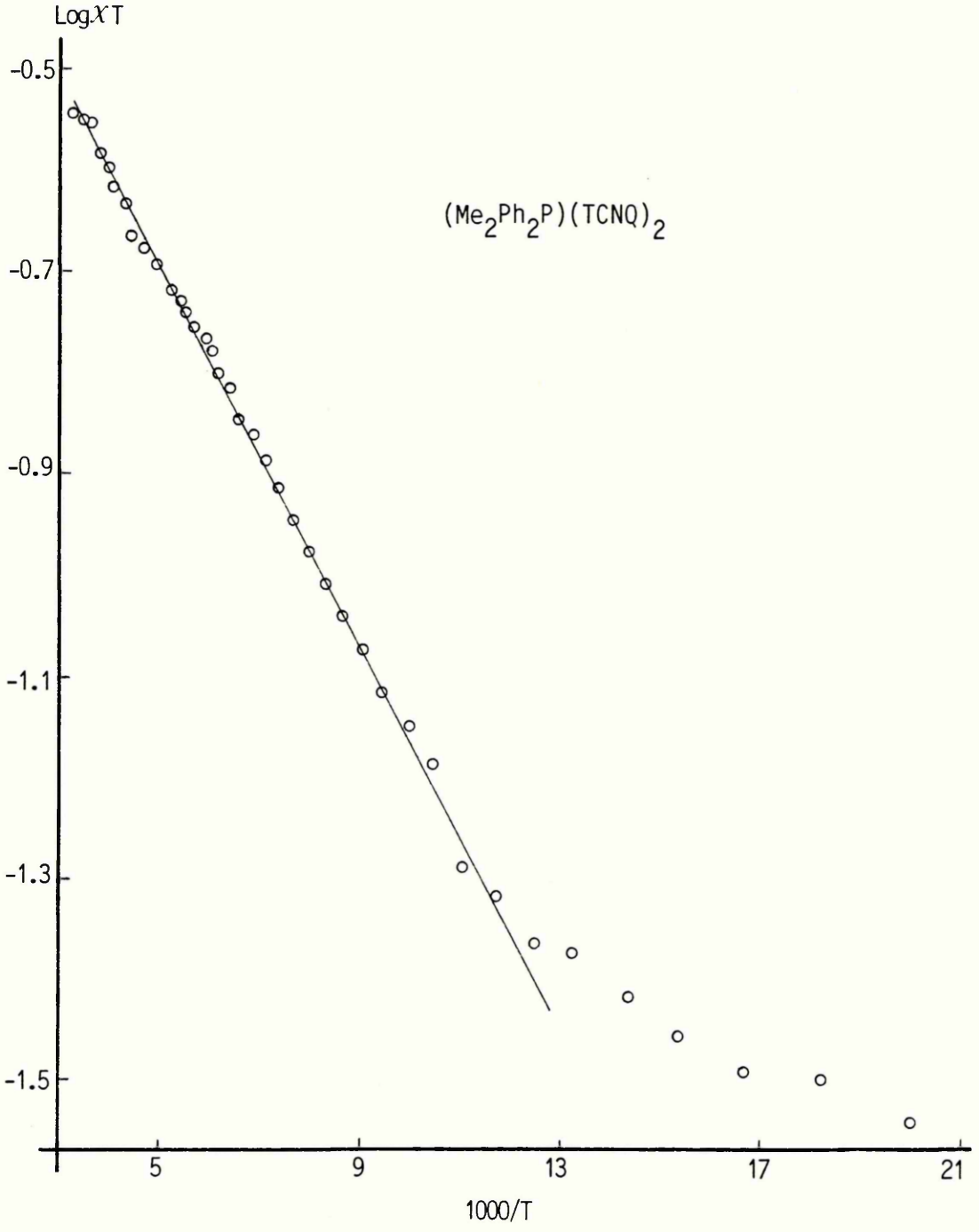

FIGURE 3.58 : The product of susceptibility and temperature versus reciprocal temperature of $(Me_2Ph_2P)(TCNQ)_2$

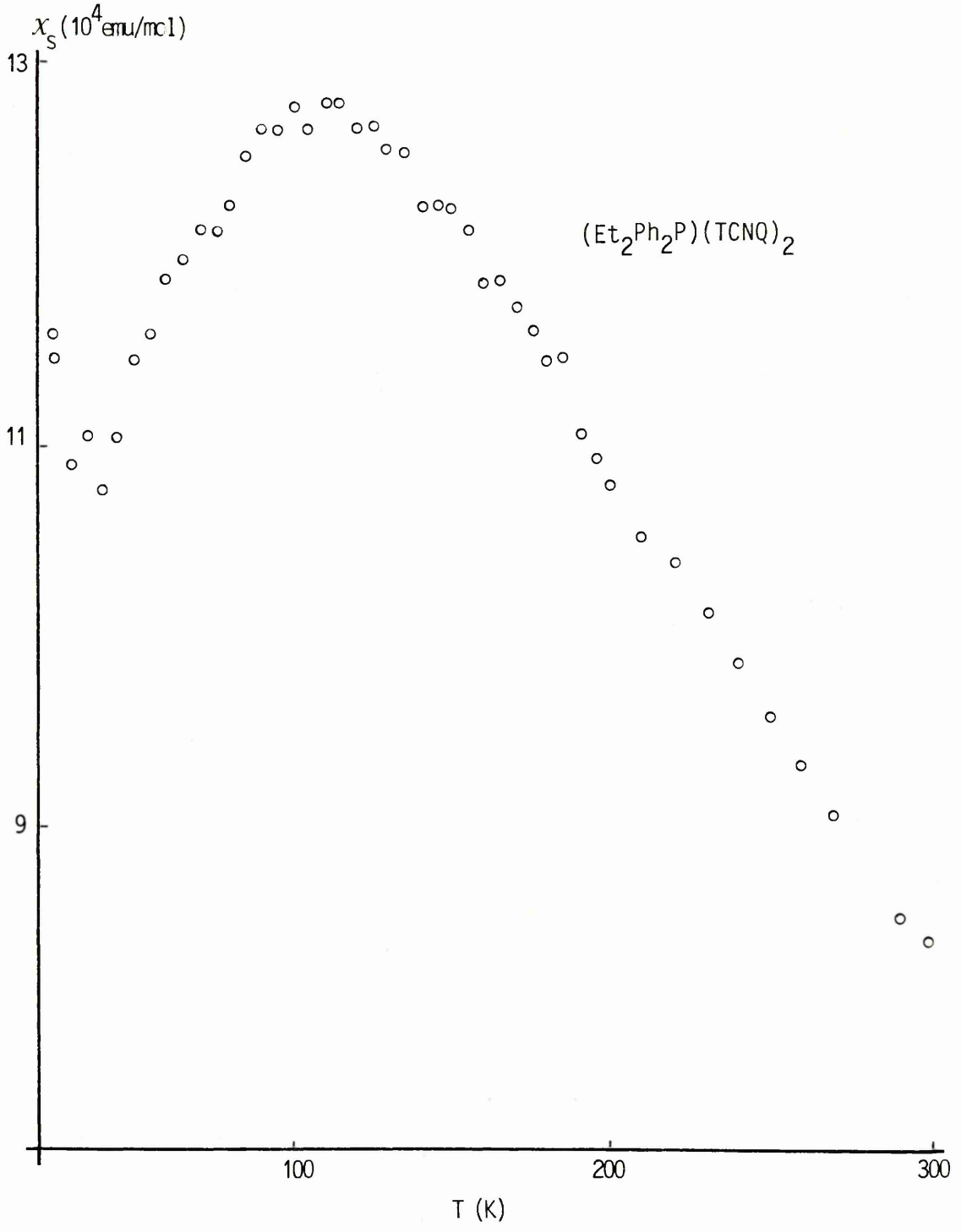

FIGURE 3.59 : The susceptibility, corrected for core diamagnetism versus temperature for $(Et_2Ph_2P)(TCNQ)_2$

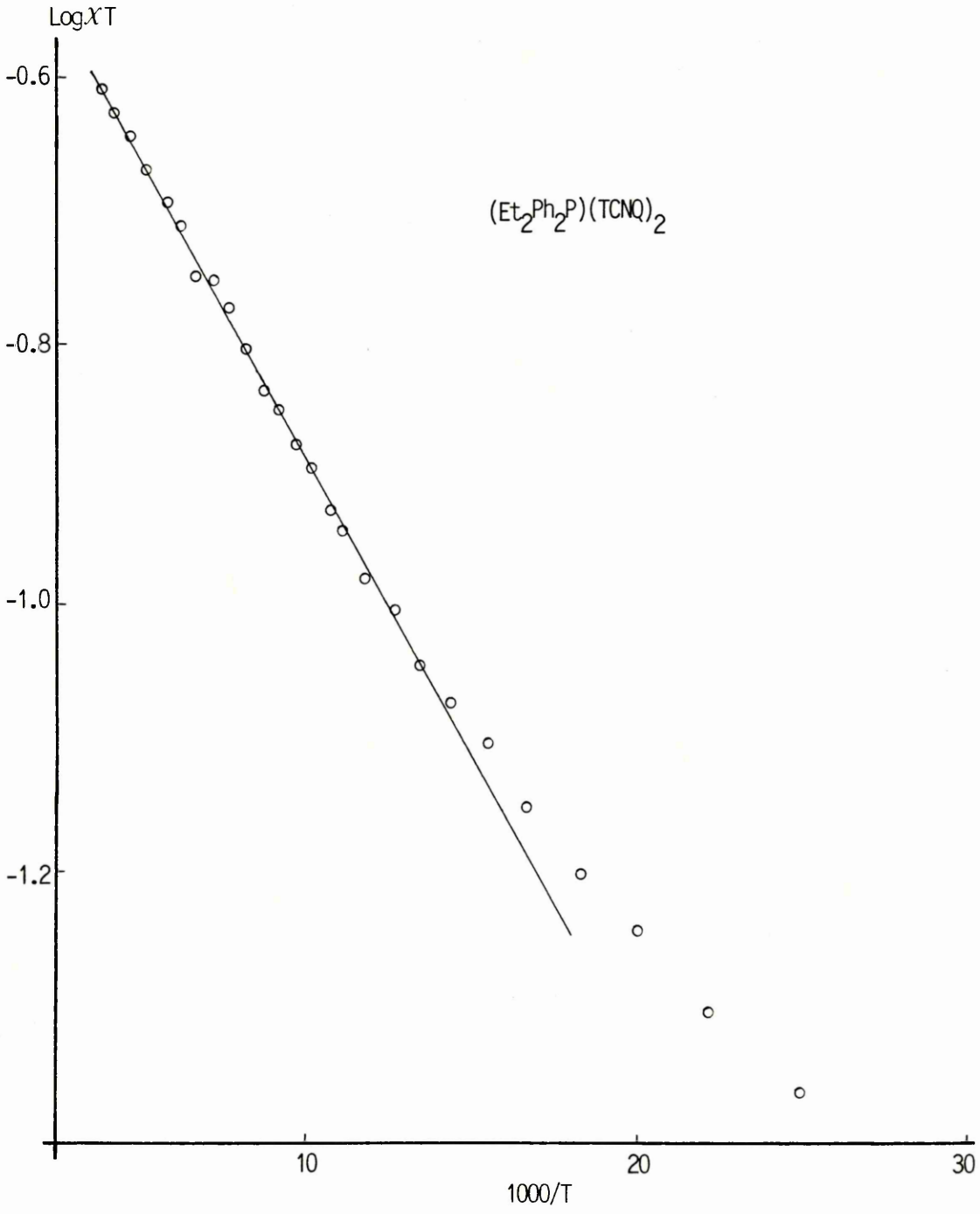

FIGURE 3.60 : Log of the product of susceptibility and temperature versus reciprocal temperature for $(Et_2Ph_2P)(TCNQ)_2$

The temperature dependence of susceptibility for $(Et_2Ph_2P)(TCNQ)_2$ is similar to that observed in the salts discussed in Section 3.5. In the 1:5 salts, the slopes of the plots, log χT versus reciprocal temperature are all equivalent to approximately Ø.Øle$V$ and the susceptibility maximum occurs between 11ØK and 14ØK.

The absolute paramagnetic susceptibility at 3ØØK for $(Et_2Ph_2P)(TCNQ)_2$ is approximately half that of the dication 1:5 salts. This is consistent with the expectation that the spin concentration per mole for this monocation 1:2 salt would be half that of the dication 1:5 salts, assuming that the spin quenching due to antiferromagnetic interactions is similar in $(Et_2Ph_2P)(TCNQ)_2$ and the 1:5 salts. The esr susceptibility at low temperature shows no zero field splitting lines which suggests that mutual spin-exchange still occurs to low temperatures and that the spins are delocalised and mobile.

In the light of this evidence the Bulaevskii treatment[219] may be confidently applied to the susceptibility results and the values of $a(\gamma)$, γ , $\Delta(\gamma)$ and J are given in Table 3.1Ø. These compare very closely with the corresponding values obtained for the 1:5 salts (Table 3.5, p 145).

The spin system may therefore be described as a system of delocalised excitons with a weakly alternating exchange interaction. A triplet excited state lies about Ø.Øle$V$ above the singlet ground state. It is of interest that the

TCNQ lattice in the 1:5 salts consists of homologous columns of TCNQs with exocyclic double bond to ring overlap of adjacent molecules. This is the type of stacking which exists in $(Et_2Ph_2P)(TCNQ)_2$ and the similarities in the magnetic properties between this salt and those of the 1:5 series may be attributed, at least in part, to these similarities of structure.

SALT	$\sigma_{R.T.}$ (Scm^{-1})	Ea(eV)	Magnetic Properties
$(Me_2Ph_2P)(TCNQ)_2$	0.02-0.05	0.2-0.22 (180-300K)	Activated. J = 0.02eV Localised excitons
$(Et_2Ph_2P)(TCNQ)_2$	1 - 10	0.04-0.06 (90-300K)	Weak temperature dependence Delocalised excitons $a(\gamma)$ = 0.24, γ = 0.68 $\Delta(\gamma)$ = 0.50, J = 0.018eV

TABLE 3.10 : The electrical and magnetic properties of 1:2TCNQ salts of dialkyl-diphenyl phosphonium cations.

4 : Summary and Conclusions

This investigation of a series of salts some of which are isostructural has allowed a direct correlation to be made between the electrical and magnetic properties of the salts with their stoichiometries and with the degree of disorder in the counter ion lattice.

The cation lattice disorder plays an important role in the stabilisation of homologous stacks of TCNQ which, when combined with non-integral charge per site, the actual value of which is largely determined by the stoichiometry, confers, at least, a moderate conductivity in these salts and in some salts, metallic character. An important exception to this proposal has been seen in the moderately conductive salt $(Et_2Ph_2P)(TCNQ)_2$ in which the TCNQs form regular stacks and the cation lattice is ordered.

In stabilising a regular TCNQ stack the electrostatic interstack interactions must be minimised. In the disordered isostructural series of salts, the inherent disorder in the cation lattice smears out the positive potential to prevent periodic coupling of the anion and cation chains, whereas in $(Et_2Ph_2P)(TCNQ)_2$ the electrostatic interactions are thought to be suppressed by steric conditions. In this salt the bulky ethyl groups and phenyl rings of the cation prevent close P^+ to $TCNQ^-$ contacts.

The degree of disorder in the isostructural series of salts

has been shown to be of primary importance in determining the trend in the electrical properties for the series (Sections 3.1 - 3.5) but it cannot be easily quantified. The weak layer lines seen in the oscillation photographs however, have intensities which qualitatively reflect this property. Since these lines are attributed to the disordered hydrated cation lattice, their relative intensity among the salts may reflect the relative degree of cation disorder, which may, in turn, be correlated with the electrical properties.

In the 1:4.5 salts, these lines weaken in intensity and in some cases are no longer observable when the crystals are annealed. This weakening in intensity of the lines is correlated with an increase in disorder in the cation lattice. It is important to note that the degree of disorder in annealed crystals of these salts may be the highest for the series and that in these salts metallic behaviour has been seen.

In contrast to these lines and to those seen for the 1:4 and 1:3 salts, the lines seen in the oscillation photographs of $(DPPP)(TCNQ)_5(H_2O)$ are more numerous, of greater intensity and possess some structure. This strongly suggests that the cation lattice in this salt is partially ordered. The conductivity of this salt and that of its isostructural and isostoichiometric congeners, is appreciably lower (by up to four orders of magnitude) than the conductivity of the other salts in the isostructural series.

The alloy salts discussed in section 3.2 have moderate to high conductivities and one member of the group has recently been found to be metallic. In accordance with the correlations shown above, the electrical properties of these salts are consistent with the existence of a highly disordered cation lattice with the additional disorder due to a random occupation of neutral, or monoquaternised, base in the lattice sites.

The salts discussed in Section 3.6, possess ordered structures and the periodic coupling of the anion and cation chains causes a distortion of the TCNQ lattice. As a consequence, these salts have relatively low conductivities.

The rigidity of the cations is in part responsible for the ordering. The principal structural difference between the cations of Section 3.6 which form ordered salts and those discussed in the preceeding sections (3.1 - 3.5) which form disordered salts is that these latter cations possess a bridging group between the pyridinium rings. The flexibility that this lends to the cations allows the formation of disordered structures by the adaptability of the cations in occupying the narrow disordered channels between sheets of TCNQ. It is this adaptability which allows the stoichiometry of the series to be varied from between 1:2 and 1:5, (dication : TCNQ) depending on the length of the cation.

The conductivity of the 1:5 salts exhibit temperature dependences which are inconsistent with models in which the

conductivity is simply activated. The salts are described as zero-gap non-metals, possessing a strong temperature dependence of the carrier mobility. There has been a suggestion that the conduction is by optical phonon assisted hopping among localised states where the experimental temperature range is such that the hopping process is not simply activated.

The excellent reproducibility in the conductivity results for the 1:5 salts suggests that the unusual temperature dependence of conductivity is an intrinsic property of these salts but suggestions as to its origin remain tentative. This type of behaviour is not a property of the isostructural series as a whole. The interpretation of the conductivity of the 1:4 and 1:3 salts, for example, is in terms of a definite gap in the electronic density of states in contrast to the proposal of a zero gap in the 1:5 salts. It is reasonable to propose that the gap in these salts arises from Coulomb correlations. This can be readily understood in the 1:4 salts in which ρ is commensurate (ρ = Ø.5). As discussed in Section 1.2.3, the energy cost of conduction in such systems is incurred in overcoming the nearest neighbour Coulomb interaction, V_1.

In salts in which ρ is incommensurate, the relatively strong interactions, V_1 and U (the on-site Coulomb repulsion) are avoided and the conductivity may be high (see, for example, Table 1.4, p 36). Thus in the 1:4.5 salts, where the charge per site may deviate from a commensurate value, Coulomb

correlations should not be the dominant determinants of the conductivity.

An interpretation of the conductivity of the 1:3 salts on the basis of the commensurability of ρ or within the framework of the mobility model applied to the 1:5 salts, cannot be satisfactorily made. In these salts, the cation lattice contains an appreciable concentration of unquaternised base and the degree of occupancy of such species determines ρ. Spectrophotometric and magnetic susceptibility measurements, suggest that ρ may be incommensurate which would imply a very low, or zero Coulomb gap. Since these salts are isostructural with those of the 1:5 series it might be expected that the zero gap mobility model would apply to the conductivity. If this were so, the characteristic negative curvature would be seen in the log σ versus reciprocal temperature plots throughout the range 100 - 300K. In fact these plots are linear for the 1:3 salts, at least at high temperatures, which suggests that an intrinsic gap exists.

These uncertainties in the interpretation of the conductivity results highlight the difficulties in unambiguously assigning models of conduction to organic salts.

The magnetic susceptibility studies have provided insights into the nature of the state of the electron systems in the salts.

Within the isostructural series (Sections 3.1 - 3.5) the

magnetic susceptibility may be related to the spin concentration, which is usually determined by the stoichiometry of the salts assuming that the degree of charge transfer, donor to acceptor, is similar between them. It has been clearly shown that the separation of spins determines the magnitude of the exchange interaction, J, a principle which is expected on theoretical grounds. Since the series is isostructural, a relationship should be observed between ρ, as a measure of the spin concentration, and J. Thus in the isostructural series, ρ follows the the trend:

$$1{:}4 > 1{:}4.5 > 1{:}5 > 1{:}3$$

which is in excellent agreement with the observed trend in the exchange interaction between isostoichiometric groups.

The 1:3 salts in the series are unusual since the inclusion of unquaternised base in the cation lattice reduces ρ from its expected value. These salts are Curie - Weiss paramagnets, that is, the spin-spin interactions are relatively weak. Although the exchange interaction has not been calculated for these salts, it may be stated that $J < 0.02$ eV (the interaction in the 1:5 salts) and therefore the position for these salts in the trend given above is justified.

The interpretation of the susceptibility for the organic alloy $(DHPE\ Cl)_{0.3}(DPE)_{0.7}(TCNQ)$ remains ambiguous. The salt exhibits a small, temperature independent paramagnetism. The conductivity is moderate and recent studies of the temperature dependence suggest that the salt may be metallic.

The susceptibility may therefore, be interpreted as the Pauli susceptibility of a metallic system. A calculation of the bandwidth is in reasonable agreement with those previously made for organic metals. It should be noted however that problems associated with attempting to assign Pauli behaviour to organic conductors are frequently encountered[175,176,178,183]. In Section 3.4 for example, the magnetic susceptibility of the metallic form of (DEPE)$(TCNQ)_{4.5}(H_2O)x$ exhibits a weak temperature dependence instead of the Pauli susceptibility which might be expected for a metallic system.

The diamagnetism of the simple salt (DHPA)$(TCNQ)_2$ reflects the very strong antiferromagnetic interaction between spins that would be expected as a result of the short inter-site spacing and unit charge on each site. The electron system is completely spin quenched.

The interpretation of the dynamics of the spin systems in many salts of the isostructural series has been made on the assumption of a system of delocalised exitons. This assumption is based, in this work, on the inapplicability of models which invoke localised spins. More rigorous evidence for the degree of localisation can only be obtained from esr studies on these salts. At present the esr susceptibility of the salts discussed in Sections 3.3 - 3.5 have not been determined and thus the assignment of a delocalised exciton model may be made only tentatively.

The low temperature esr spectrum of $(Et_2Ph_2P)(TCNQ)_2$ does not show zero field splitting lines and the spin system in this salt may be described as consisting of delocalised triplet excitons. The value of J determined by esr is in excellent agreement with that found in this work, by static susceptibility measurements. Thus, the assignment of the Bulaevskii model of delocalised spins to the susceptibility in the salt may be made with greater confidence. It is of interest that the structural characteristics of this salt are not dissimilar to those of the isostructural series of salts for which a delocalised exciton model was assigned only tentatively. It would be of value to study the esr susceptibility of these salts to see if the structural features may be related to the existence of delocalised spin systems.

The correlation of structural characteristics with magnetic properties has been possible in one salt of a series possessing ordered structures, discussed in Section 3.6. It has been shown that an analysis of the TCNQ bond lengths may be used to identify partial localization of charge on specific TCNQ sites. In knowing the crystal structure and the location of regions of high spin density it has been possible to explain the observed susceptibility in terms of these spatial considerations. Thus in CPP-$TCNQ_4$, for example, the poor overlap between neighbouring sites of high spin density results in a relatively low exchange interaction.

REFERENCES

1. D.D. Eley, Science Journal (Dec.1967) pp 61-65.

2. See for example; Physics and Chemistry of the Organic Solid State Vol.1. Eds. D.Fox, M.M. Labes, A. Weissberger - Interscience (Wiley) London, 1963.

3. D.S. Acker, R.J. Harder, W.R. Hertler, W. Mahler, L.R. Melby, R.E. Benson and W.E. Mochel, J.Am. Chem. Soc, **82**, 6408, (1960).

4. L.R. Melby, R.J. Harder, W.R. Hertler, W.Mahler, R.E. Benson and W.E. Mochel, J.Am. Chem. Soc., **84** 3374, (1962).

5. W.J. Siemons, P.E. Bierstedt and R.G. Kepler, J. Chem. Phys.,**39**, 3523 (1963).

6. R.G.Kepler, P.E.Bierstedt and R.E.Merrifield, Phys.Rev.Lett.**5**, 503 (1960).

7. R.G.Kepler, J.Chem.Phys.,**39**, 3528, (1963).

8. L.B.Coleman, S.K.Khanna, A.F.Garito, A.J.Heeger and B.Morosin, Phys.Lett., **42A**, 15, (1972).

9. F.Sanz and J.J.Daly J.Chem.Soc. Perkin II, 1146, (1975).

10. H.Kobayashi, F.Marumo and Y.Saito, Acta Cryst., **B27**, 373, (1971).

11. D.J.Dahm, P.Horn, G.R.Johnson, M.G.Miles and D.J.Wilson J.Cryst.Mol.Struct., **5**, 27, (1975).

12. G.J.Ashwell, I.Diaconu, D.D.Eley, S.C.Wallwork and M.R.Willis, Z.Naturforsch, **34a** 1-5, (1979).

13. W.A.Little, Phys.Rev. **134**, No.6A, A1416,(1964).

14. J.P.Ferraris, D.O.Cowan, V.V.Walatka and J.Perlstein,J.Am.Chem.Soc., **95**, 948,(1973).

15. L.B.Coleman, M.J.Cohen, D.J.Sandman, F.G.Yamagishi, A.F.Garito and A.J.Heeger, Sol.St.Comm. **12**, 1125, (1973).

16. R.Comes. Chemistry and Physics of One-Dimensional Metals **25** NATO Advanced Study Institutes Series (B-Physics) Plenum Press, N.Y. Ed. H.J.Keller, (1977).

17. C.W.Chu, J.M.E.Harper, T.H.Geballe and R.L.Greene, Phys.Rev.Lett.**31**, 1491,(1973).

18. J.A.Perlstein, J.P.Ferraris, V.V.Walatka and D.O.Cowan, Am.Inst.Phys.Conf.Proc. **10**, 1494, (1973).

19. T.J.Kistenmacher, T.E.Phillips and D.O.Cowan, Acta Cryst., **B30**, 763, (1974).

20. S.Etemad, Phys.Rev.B **13**,2254, (1976).

21. J.P.Ferraris, T.O.Poehler, A.N.Bloch and D.O.Cowan, Tet.Lett. **27**, 2552, (1973).

22. T.E.Phillips, T.J.Kistenmacher, A.N.Bloch, J.P.Ferraris and D.O.Cowan, Acta Cryst.,**B33**, 422,(1977).

23. C.S.Jacobsen, K.Mortensen, J.R.Andersen and K.Bechgaard, Phys.Rev. B **18**, 905, (1978).

24. K.Bechgaard, T.J.Kistenmacher, A.N.Bloch and D.O.Cowan Acta Cryst. **B33**, 417, (1977).

25. R.L.Greene, J.J.Mayerle, R.Shumacher, G.Castro, P.M.Chaikin and S.Etemad Sol.St.Comm **20**, 943, (1976).

26. A.N.Bloch, D.O.Cowan, K.Bechgaard, R.E.Pyle, R.H.Banks and T.O.Poehler Phys.Rev.Lett. **34**, 1561, (1975).

27. T.E.Phillips, T.J.Kistenmacher, A.N.Bloch and D.O.Cowan J.Chem.Soc.Chem.Comm. 334, (1976).

28. C.S.Jacobsen, K.Mortensen, J.R.Andersen and K.Bechgaard, Phys.Rev.B **18**, 905, (1978).

29. J.R.Andersen, C.S.Jacobsen, G.Rindorf, H.Soling and K.Bechgaard, J.Chem.Soc.Chem.Comm., 883, (1975).

30. K.Bechgaard, C.S.Jacobsen, K.Mortensen, H.J.Pedersen and N.Thorup, Sol.St.Comm., **33**, 1119, (1980).

31. L.I.Buravov ZhETF, **20**, 457, (1974).

32. G.Keryer in Proc.Int.Conf. on Quasi I-D.Conductors Pt.1 Dubrovnik 1978 (Springer-Verlag, Berlin 1979).

33. J.B.Torrance, J.J.Mayerle, K.Bechgaard, B.D.Silverman and Y.Tomkievicz, Phys.Rev.B, **22**,4960, (1980).

34. R.Somoano, V.Hadek, S.P.S.Yen, A.Rembaum and R.Deck, J.Chem.Phys. **62**, 1061, (1975).

35. A.W.Hanson Acta Cryst.B**24**, 768 (1968).

36. H.Kobayashi Bull.Chem.Soc.Jap **47**(b), 1346, (1974).

37. D.Chasseau Thesis, University of Bordeaux, France, (1979).

38. L.R.Melby Can.J.Chem. **43**, 1448, (1965).

39. C.J.Fritchie Acta Cryst. B**2Ø**, 892, (1966).

4Ø. A semiconductive phase of NMP-TCNQ consisting of mixed stacks has been discussed by B Morosin Acta Cryst. B**32**, 1176, (1976).

41. A.Bosch and B. Van Bodegom Acta Cryst. **B33**, 3Ø13, (1977).

42. T.Sundaresan and S.C.Wallwork Acta Cryst. **B28**, 491, (1972).

43. G.J.Ashwell, Mol. Cryst. Liq. Cryst., **91**, 359, (1983)

44. G.J.Ashwell and C.M.Care, Phys.Stat.Sol., (a), **81**, 557, (1984)

45. H.Kobayashi, Y.Ohashi, F.Marumo and Y.Saito Acta Cryst. **B26**, 459, (197Ø).

46. A.Brau and J.P.Farges, Phys.Stat.Sal. **61**, 257, (1974).

47. K.Ukei and I.Shirotani Commun.Phys. **2**, 159, (1977)

48. I.F.Schegolev Phys.Stat.Sol. (a), **12**, 9, (1972).

49. L.I.Buravov, D.N.Fedutin and I.F.Schegolev Sov.Phys. JETP, **32**, 612, (1971).

5Ø. R.P.Shibaeva and V.I.Ponomarev Sov.Phys.Cryst. **2Ø(2)**, 183, (1977).

51. G.J.Ashwell, D.D.Eley, R.J.Fleming, S.C.Wallwork and M.R.Willis Acta Cryst. **B32**, 2948, (1976).

52. G.J.Ashwell, D.D.Eley and M.R.Willis Nature, **259**, 2Ø1, (1976).

53. G.J.Ashwell, Phys.Stat.Sol. **86**(b), 7Ø5, (1978).

54. G.J.Ashwell, D.D.Eley, S.C.Wallwork, M.R.Willis, G.D.Welch and J.Woodward Acta Cryst. **B33**, 2252, (1977).

55. G.J.Ashwell, Nature, **29Ø**, 686, (1981).

56. G.J.Ashwell, D.W.Allen, G.H.Cross, D.A.Kennedy and I.W.Nowell Sol.St.Comm. **43**, 731, (1982).

57. M.Konno and Y.Saito Acta Cryst. **B31**, 2007, (1975).

58. M.Konno, T.Ishii and Y.Saito Acta Cryst. **B33**, 763, (1977).

59. I.Shirotani and H.Kobayashi, Bull.Chem.Soc.Jap. **46**, 2595, (1973).

60. N.Sakai, I.Shirotani and S. Minomura, Bull.Chem.Soc.Jap.**45**, 3314, (1972).

61. B.Van Bodegom, J.L.de Boer and A.Vos Acta Cryst. **B33**, 602, (1977).

62. C.J.Fritchie and P.Arthur Acta Cryst. **B21**, 139, (1966).

63. R.J.van der Wal and B van Bodegom Acta Cryst. **B34**, 1700, (1978).

64. H.Kobayashi Acta Cryst. **B34**, 2818, (1978).

65. H.Kobayashi, T.Danno and Y.Saito Acta Cryst. **B29**, 2693, (1973).

66. G.P.Saakyan, R.P.Shibaeva and L.O.Atovmyan Sov.Phys.Dokl **17**, 1138, (1973).

67. V.F.Kaminskii, R.P.Shibaeva and L.O.Atovmyan Zh.Strukt.Khimii **14**, 700, (1973).

68. V.F.Kaminiskii and R.P.Shibaeva Sov.Phys.Cryst. **21**, 653, (1976).

69. R.P.Shibaeva, V.F.Kamisskii and L.O.Atovmyan Zh.Strukt.Khimii **15**, 720, (1976).

70. D.Chasseau, J.Gaultier and C.Hauw C.R.Acad.Sci.Fr **274**, C,1434, (1972).

71. in reference 74, p55.

72. T.Sundaresan and S.C.Wallwork Acta Cryst. **B28**, 3507, (1972).

73. J.B.Torrance Acc.Chem.Res. **12**, No.3, 79, (1979)

74. L. van Bodegom Thesis, University of Groningen (1981).

75. D.Chasseau, J.Gaultier, C.Hauw and J.Jaud C.R.Acad.Sci.Fr.**276**, 661, (1973).

76. J.P.Farges, H.Grassi, A.Brau and P.Dupuis Phys.Stat.Sol. **55**, 89, (1979).

77. D.Castagne, P.Dupuis, J.Neel and A.Filhal Abstracts IV Int.Symp.Org.Sol.St.Bordeaux (1975).

78. M.Konno and Y.Saito Acta Cryst. **B30**, 1295, (1974).

79. H.Afifi, F.M.Abdel-Kerim, H.F.Aly and A.A.Shabaka, Z.Naturforsch **33a**, 344, (1978).

80. P.Richard, J.C.Zanghi, J.F.Guedon and N.Hota Acta Cryst. **B34**, 788, (1978).

81. A.Hoekstra, T.Spoelder and A.Vos Acta Cryst. **B28**, 14, (1972).

82. M.Almeida, L.Alcacer and S.Oostra Phys.Rev.B, **30**, 2839, (1984)

83. M.Przybylski, A.Graja, A.Rajchel, M.Gawron and T.Borowiak Acta Phys. Pol. **A56**, 67, (1978).

84. M.Przybylski and A.Graja, Physica **104B**, 278, (1981).

85. G.W.Crabtree, K.Douglas Carlson, L.N.Hall, P.Thomas Copps, H.H.Wang, T.J.Emge, M.A.Beno and J.M.Williams Phys.Rev.B **30**, 2958, (1984)

86. T.Sundaresan and S.C.Wallwork Acta Cryst. **B28**, 3065, (1972).

87. A.T.McPhail, G.M.Semenuik and D.B.Chesnut J.Chem.Soc.A, 2174, (1971).

88. Y.Iida, M.Kinoshita, A.Kawamori and K.Suzuki Bull.Chem.Soc.Jap. **37**, 764, (1964)

89. T.Sundaresan and S.C.Wallwork Acta Cryst. **B28**, 2474, (1972).

90. G.J.Ashwell, D.D.Eley, N.J.Drew, S.C.Wallwork and M.R.Willis Acta Cryst. **B34**, 3608, (1978).

91. G.J.Ashwell, D.D.Ely, A.Harper, A.C.Torrance, S.C.Wallwork and M.R.Willis Acta Cryst. **B33**, 2258, (1977).

92. M.Konno and Y.Saito Acta Cryst. **B29**, 2815, (1973).

93. G.J.Ashwell, G.H.Cross, D.A.Kennedy, I.W.Nowell and J.G.Allen J.Chem.Soc. Perkin Trans II, 1787, (1983).

94. G.J.Ashwell, J.G.Allen, G.H.Cross and I.W.Nowell, Phys.Stat.Sol. (a) **79**, 455, (1983).

95. A.Andrieux, P.M.Chaikin, C.Duroure, D.Jerome, C.Weyl and K.Bechgaard J.Phys. (Fr) **40**, 1199, (1979).

96. C.S.Jacobsen, K.Mortensen, J.R.Andersen and K.Bechgaard Phys.Rev. B **18**, 905, (1978).

97. K.Bechgaard, C.S.Jacobsen, K.Mortensen, H.J.Pedersen and N.Thorup, Sol.St.Com. **33**, 119, (1980).

98. D.Jerome, A Mazaud, M.Ribault and K.Bechgaard J.Phys.Lett (Fr.) **41**, L-95, (1980).

99. M.Ribault, J.P.Pouget, D.Jerome and K.Bechgaard C.R.Acad.Sci.(Paris) **291**, B145, (1980).

100. S.S.Parkin, M.Ribault, D.Jerome and K.Bechgaard J.Phys.C **14**, 5305, (1981).

101. R.C.Lacoe, S.A.Wolfe, P.M.Chaikin, F.Wudl and E.Aharon-Shalom Phys.Rev. B. **27**, 1947, (1983).

102. K.Andres, F.Wudl, D.B.McWhan and A.L.Stevens Phys.Rev.Lett., **45**, 1449, (1980).

103. K.Bechgaard, K.Carneiro, F.B.Rasmussen, M.Olsen, G.Rindorf, C.S.Jacobsen, H.J.Pedersen and J.C.Scott J.Am.Chem.Soc. **103**, 2440, (1981).

104. F.Wudl, E.Aharon-Shalom, D.Nalewajek, J.V.Waszczak, W.M.Walsh, L.W.Rupp, P.M.Chaikin, R.Larve, M.Burns, T.O.Poehler, J.M.Williams and M.A.Beno J.Chem.Phys., **76**, 5497, (1982).

105. H.J.Keller, D.Nothe, H.Pritzkow, D.Dehe, M.Werner, R.A.Harms, P.Koch and D.Schweitzer Chemica Scripta, **17**, 101, (1981).

106. S.S.P.Parkin, E.M.Engler, R.R.Schumacher, R.Lagier, V.Y.Lee, J.C.Scott and R.L.Greene Phys.Rev.Lett, **50**, 270, (1983).

107. N.Thorup, G.Rindorf, H.Soling and K.Bechgaard Acta Cryst. B**37**, 1236, (1981).

108. S.S.P.Parkin, M.Ribault, D.Jerome and K.Bechgaard J.Phys.C **14**, L-445, (1981).

109. T.Sundaresan and S.C.Wallwork Acta Cryst.**B28**, 1163, (1972).

110. R.P.Shibaeva and L.O.Atovmyan J.Struct.Chem. **13**, 514, (1972).

111. A.W.Hanson Acta Cryst. **B19**, 610, (1965).

112. I.Goldberg and U.Schmueli Acta Cryst. B**29**, 421, (1973).

113. H.Kuroda, I.Ikemoto, K.Yakushi and K.Chikaishi Acta Cryst. **A28**, suppl. 515, (1872).

114. R.Foster, Organic Charge TransferComplexes, Academic Press, London and New York, Appendix Table 1, (1969).

115. M.J.Cohen, L.B.Coleman, A.F.Garito and A.J.Heeger Phys.Rev.B **10**, 1298, (1974).

116. D.E.Schafer, F.Wudl, G.A.Thomas, J.P.Ferraris and D.O.Cowan Sol.St.Comm. **14**, 347, (1974).

117. D.Zosel, H.Ritschel and H.Hamel Phys.Stat.Sol. **32**, K75, (1969).

118. R.E.Peierls, Quantum Theory of Solids (Oxford University Press, Oxford, New York 1955) p.108.

119. H.Frohlich, Proc.R.Soc.London Sec. **A223**, 296, (1955).

120. C.Coulon, S.Flandrois, P.Delhaes, C.Hauw and P.Dupuis Phys.Rev.B **23**, 2850, (1981).

121. S.Kagoshima, Jap.J.App.Phys. **20**, 1617 (1981).

122. S.Barisic Phys.Rev. B **5**, 932, (1972).

123. R.Comes, M.Lambert, H.Launois and H.Zeller Phys.Rev. B**8**, 571, (1973).

124. T.W.Thomas and A.E.Underhill Chem.Soc. Rev.**1**, 99, (1972).

125. M.J.Minot and J.H.Perlstein Phys.Rev.Lett. **26**, 371, (1971).

126. S.Etemad, E.M.Engler, T.D.Schulz, T.Penney and B.A.Scott Phys.Rev. B **17**, 513, (1978).

127. G.J.Ashwell Phys.Stat.Sol. (b) **109**, K89, (1982).

128. This salt was previously reported [52,55] to have a stoichiometry of 1:4 which was later found to be erroneous.

129. G.J.Ashwell Mol.Cryst and Liq.Cryst. **86**, 1887, (1982).

130. K.Kamaras, G.Mihaly, G.Gruner and A.Janossy, J.Chem.Soc.Chem.Comm. (comm 736), 974, (1978).

131. L.Zuppiroli and S.Bouffard J.Phys.(Fr.) **41**, 291, (1980).

132. J.C.Scott, H.J.Pedersen and K.Bechgaard Chem.Sci. **17**, 55, (1981).

133. J.C.Scott Mol.Cryst.Liq.Cryst. **79**, 49, (1982).

134. K.Chiang, M.J.Cohen, P.R.Newman and A.J.Heeger Phys.Rev.B **16**, 5153, (1977).

135. S.Bouffard, M.Ribault, R.Brusetti, D.Jerome and K.Bechgaard J.Phys. C **15**, 2951, (1982).

136. J.Friedel and D.Jerome Contemp.Phys. **23**, 583, (1982).

137. J.P.Pouget, R.Monet, R.Comes, K.Bechgaard, J.M.Fabre and L.Giral Mol.Cryst. Liq.Cryst. **79**, 129, (1982).

138. D.Jerome and H.J.Schultz, Extended Linear Chain Compounds Vol.2, Ed. J.S.Miller (N.Y. Plenum Press, 1981).

139. A.Andrieux, H.J.Shultz, D.Jerome and K.Bechgaard Phys.Rev.Lett.**43**, 227, (1979).

140. J.R.Cooper, D.Jerome, S.Etemad and E.M.Engler Sol.St.Comm.**22**, 257, (1977).

141. R.L.Greene and E.M.Engler Phys.Rev.Lett.**45**, 1587, (1980).

142. A.Rembaum, A.M.Hermann, F.E.Stewart and F.Gutmann J.Phys.Chem. **73**, 513, (1969).

143. S.Mazumdar and A.N.Bloch Phys.Rev.Lett. **50**, 207, (1983).

144. J.B.Torrance N.Y. Acad.Sci. **313**, 210, (1978) Synthesis and Properties of Low-Dimensional Materials Eds. J.S.Miller and A.J.Epstein.

145. S.Megtert, J.P.Pouget and R.Comes in Molecular Metals NATO Conference Series VI: Material Science Ed. W.E.Hatfield (Plenum, N.Y., 1979) p 87.

146. M.E.Hawley, T.O.Poehler, T.F.Carruthers, A.N.Bloch, D.O.Cowan and T.J.Kistenmacher. Bull. Am.Phys. Soc. **23**, 424, (1978).

147. J.B.Torrance and B.D.Silverman Phys.Rev. B**15**, 788, (1977).

148. A.A.Ovchinnikov. Sov.Phys. JETP **37**, 176, (1973).

149. A.J.Epstein, E.M.Conwell and J.S.Miller in 'Synthesis and Properties of Low-D. Materials' Eds. J.S.Miller and A.J.Epstein N.Y. Acad. Sci. **313**, 183, (1978)

150. M.Przybylski Acta Phys. Pol. **A56**, 517, (1979).

151. G.J.Ashwell, D.D.Ely, S.C.Wallwork and M.R.Willis, Proc.Roy.Soc. A **343**, 461, (1975).

152. V.A.Johnson and K.Lark-Horowitz Phys.Rev. **92**, 226, (1953).

153. M.A.Shaikh Sol.St.Comm. **33**, 991, (1980).

154. G.Croteau, A.A.Lakhani and N.K.Hota Sol.St.Comm. **40**, 741, (1981).

155. J.P.Farges and A.Brau Phys.Stat.Sol. (b) **64**, 269, (1974).

156. A.Brau and J.P.Farges Phys.Stat.Sol.(b) **61**, 257, (1974).

157. A.N.Bloch, R.B.Weismann and C.M.Varma Phys.Rev.Lett. **28**, 753, (1972).

158. V.K.S.Shante Phys.Rev.B **16**, 2597, (1977)

159. D.Kuse and H.R.Zeller Phys.Rev.Lett. **27**, 1060, (1971).

160. M.J.Rice and J.Bernasconi J.Phys.(Fr) **3**, 55, (1973).

161. P.M.Lenahan and T.J.Rowland Phys.Rev.B **23**, 752, (1981).

162. R.C.Lacoe, G.Gruner and P.M.Chaikin Sol.St.Comm. **36**, 599, (1980).

163. A.Bosch and B.Van Bodegom Acta Cryst. **B33**, 3013, (1977).

164. see for example 'An Introduction to Solid State Physics and It's Applications'. R.J.Elliott and A.F.Gibson (MacMillan, London, 1982) pp300-305.

165. J.P.Farges, A.Brau and F.Gutmann Phys.Chem.Solids **33**, 1723, (1972).

166. A.J.Epstein, S.Etemad, A.F.Garito and A.J.Heeger Phys.Rev.B **5**, 952, (1972).

167. G.J.Ashwell, D.D.Eley, N.R.Willis and J.Woodward, JCS FARADAY TRANS II, 1785, (1975).

168. S.Etemad, T.Penney, E.M.Engler, B.A.Scott and P.E.Seiden Phys.Rev.Lett. **34**, 741, (1975).

169. R.P.Groff, A.Suna and R.E.Merrifield Phys.Rev.Lett. **33**, 418, (1974).

170. M.Weger, B.Horowitz and H.Gutfreund Phys.Rev.B **12**, 1086, (1975).

171. A.N.Bloch, D.O.Cowan, K.Bechgaard, R.E.Pyle and R.H.Banks Phys.Rev.Lett. **34**, 1561, (1975).

172. D.Allender, J.W.Bray and J.Bardeen Phys.Rev.B **9**, 119, (1974).

173. H.J.Shultz, D.Jerome, A.Mazaud, M.Ribault and K.Bechgaard J.Phys. Paris **42**, 991, (1981).

174. L.B.Coleman, J.A.Cohen, A.F.Garito and A.J.Heeger Phys.Rev.B **7**, 2122, (1973).

175. L.N.Bulaevskii, A.V.Zvarykina, Yu.S.Karimov, R.B.Lyubovski and I.F.Shchegolev. Sov.Phys. JETP **35** (2), 384, (1972).

176. J.Ameill, P.Delhaes, S.Flandrois and H.Strzelecka. Sol.St.Comm. **39**, 55, (1981).

177. G.J.Ashwell Phys.Stat.Sol. (a) **81**, 361, (1984).

178. T.Sugano, T.Ohta and H.Kuroda Chem.Phys.Lett. **34**, 164, (1975).

179. J.H.Perlstein, J.P.Ferraris, V.W.Walatka, D.O.Cowan and G.A.Candela. Electron Transport and Magnetic Properties of New Highly Conducting Charge Transfer Complexes, AIP Cont.Proc.(USA) No.10 Pt2, 1494, (1972).

180. J.Woodward, PhD Thesis, University of Nottingham (1976).

181. S.Etemad, PhD Thesis, University of Pennsylvania (1972).

182. J.C.Scott, H.J.Pedersen and K.Bechgaard Phys.Rev.Lett. **45**, 2125, (1980).

183. J.C.Scott, A.F.Garito and A.J.Heeger Phys.Rev. B **10**, 3131, (1974).

184. Y.Tomkiewicz, A.R.Taranko and J.B.Torrance Phys.Rev.Lett. **36**, 757, (1976).

185. Y.Tomkiewicz, B.Welber, P.E.Seiden and R.Schumaker Sol.St.Comm. **23**, 471, (1977).

186. Y.Tomkiewicz, A.R.Taranko and R.Schumaker Phys.Rev. B, **16**, 1380, (1977).

187. A.A.Bright, A.F.Garito and A.J.Heeger Phys.Rev. B **10**, 1328, (1974).

188. D.B.Tanner, C.S.Jacobsen, A.F.Garito and A.J.Heeger Phys.Rev.Lett. **32**, 1301, (1974).

189. P.A.Lee, T.M.Rice and P.W.Anderson Phys.Rev.Lett. **31**, 462, (1973).

190. A.J.Epstein, S.Etemad, A.F.Garito and A.J.Heeger Phys.Rev. B **5**, 952, (1972).

191. S.K.Khanna, E.Ehrenfreund, A.F.Garito and A.J.Heeger Phys.Rev. B **10**, 2205, (1974).

192. M.Ribault, G.Benedeck, D.Jerome and K.Bechgaard J.Phys.Lett. **41**, L397, (1980).

193. D.U.Gubser, W.W.Fuller, T.O.Poehler, D.O.Cowan, M.Lee, R.S.Potember, La Y.Chiang and A.N.Bloch Phys.Rev. B **24**, 478, (1981).

194. H.Schwenk, K.Neumair, K.Andres, F.Wudl and E.Aharon-Shalom Mol.Cryst. Liq.Cryst. **79**, 277, (1982).

195. P.Delhaes, S.Flandrois, G.Keryer and P.Dupuis Mat.Res.Bull. **10**, 825, (1975).

196. J.R.Cooper, M.Miljak and B.Korin Chemica Scripta **17**, 79, (1981).

197. L.C.Isett Phys.Rev. B **18**, 439, (1978).

198. I.F.Shchegolev Phys.Stat.Sol. **12**, 9, (1972).

199. W.G.Clark, J.Hammann, J.Sanny and L.C.Tippie, Proc.Int.Conf. on 1-D Cond., Dubrovnik, (1978), Springer Verlag, Lecture Notes in Physics, **96**, 255, (1979).

200. M.Miljak, B.Korin, J.R.Cooper, K.Holczer and A.Janossy J.Phys. **41**, 639, (1980).

201. L.C.Tippie and W.G.Clark Bull.Am.Phys.Soc. **23**, 431, (1978).

202. L.C.Tippie and W.G.Clark Phys.Rev. B **23**, 5846, (1981).

203. L.J.Azevedo and W.G.Clark Phys.Rev. B **16**, 3252, (1977).

204. G. Theodorou and M.H.Cohen Phys.Rev.Lett. **37**, 1014 (1970).

205. A.N.Bloch, R.B.Weisman and C.M.Varma Phys.Rev.Lett. **28**, 753, (1972).

206. D.B.Chesnut and W.D.Phillips J.Chem.Phys. **35**, 1002, (1961).

207. H.Kainer, D.Bijl and A.C.Rose-Innes Naturwissenschaften **41**, 303, (1954).

208. D.Bijl, H.Kainer and A.C.Rose-Innes J.Chem.Phys. **30**, 765, (1959).

209. L.N.Bulaevskii Sov.Phys. JETP **17**, 684, (1963).

210. T.Hibma, Thesis, University of Groningen (1974).

211. A.Rembaum, V.Hadek and S.P.S.Yen, J.Am.Chem.Soc. **93**, 2532, (1971).

212. see for example The Magnetic Properties of Matter, J.Crangle (Edward Arnold, 1977).

213. T.Cvitas and N.Kalley J.Chem.Ed., **54**, 530, (1977).

214. G.J.Ashwell, S.C.Wallwork and P.J.Rizkallah Mol.Cryst. Liq.Cryst. **91**, 359, (1983).

215. D.J.Sandman J.Am.Chem.Soc. **100**, 5230, (1978).

216. G.J.Ashwell Phys.Stat.Sol. (b) **109**, K89, (1982).

217. see for example M.Dugay and J.Roustan Int.J. of Quantum Chem., **XVIII**, 1057 (1980).

218. M.Lequan, R.M.Lequan, P.Batail, J.F.Halet and L.Ouhab Tet.Lett. **24**, 3107, (1983).

219. G.J.Ashwell, J.G.Allen, E.P.Goodings, D.A.Kennedy and I.W.Nowell Phys.Stat.Sol. (a), **75**, 663, (1983).

220. G.J.Ashwell, D.D.Eley, N.J.Drew, S.C.Wallwork and M.R.Willis Acta.Cryst. **B33**, 2598, (1977).

221. P.S.Flandrois and D.Chasseau Acta.Cryst. B**33**, 2744, (1977).

222. R.E.Long, R.A.Sparks and K.N.Trueblood Acta.Cryst. **B18**, 932, (1965).

223. P.M.Chaikin and G.Beni Phys.Rev.B **13**, 647, (1976).

224. G.J.Ashwell Phys. Stat. Sol.(a), **83**, 669, (1984)

225. D.B.Chesnut and P.A.Arthur J.Chem.Phys. **36**, 2696, (1962).

226. J.C.Bonner and M.E.Fisher Phys.Rev A **135**, 640, (1964).

227. G.J.Ashwell and S.C.Wallwork Acta.Cryst. **B35**, 1648, (1979).

228. Redetermination of the structure of reference 89

229. G.J.Ashwell, S.Jansen, M.T.Jones and C.H.L.Kennard Phys.Stat.Sol. (a) **80**, 127, (1983).

230. R.J.Fleming, M.A.Shaikh, B.W.Skelton and A.H.White Aust. J. Chem. **32**, 2187, (1979).

231. P.Goldstein, K.Seff and K.N.Trueblood Acta.Cryst. **B24**, 2815, (1968).

232. G.Shirane, S.M.Shapiro, R.Comes, A.F.Garito and A.J.Heeger Phys.Rev. B**14**, 2325, (1976)

233. T.J.Kistenmacher, T.E.Phillips, D.O.Cowan, J.P.Ferraris and A.N.Bloch Acta.Cryst. B**32**, 539, (1976).

234. S.Megtert, J.P.Pouget and R.Comes, Ann.N.Y.Acad.Sci. **313**, 234, (1978).

235. J.R.Cooper Phys. Rev. B **19**, 2404, (1979)

236. D.Emin Adv.Phys. **24**, 305, (1975)

APPENDIX I: Fractional Positional Parameters, Bond Distances and Angles of $[DHPA][TCNQ]_2$

TABLE 1

Final fractional positional parameters ($\times 10^4$) with e.s.d.s in parentheses.

	x	y	z
C(1)	2629(1)	3280(2)	3971(1)
C(2)	2926(1)	4414(2)	4570(1)
C(3)	3326(1)	3781(2)	4999(1)
C(4)	3466(1)	1966(2)	4854(1)
C(5)	3166(1)	825(2)	4274(1)
C(6)	2762(1)	1461(2)	3852(1)
C(7)	2219(1)	3969(2)	3522(1)
C(8)	2099(1)	5811(3)	3623(1)
C(9)	1916(1)	2939(2)	2893(1)
C(10)	3897(1)	1347(3)	5241(1)
C(11)	4202(1)	2485(3)	5800(1)
C(12)	4056(1)	-386(3)	5011(1)
C(13)	1098(1)	1607(3)	7281(1)
C(14)	851(1)	3144(3)	7367(1)
C(15)	413(1)	3261(2)	6919(1)
C(16)	241(1)	1772(2)	6396(1)
C(17)	499(1)	258(3)	6326(1)
C(18)	126(1)	4912(2)	7017(1)
N(1)	2000(1)	7310(3)	3696(1)
N(2)	1663(1)	2160(3)	2367(1)
N(3)	4450(1)	3415(3)	6246(2)
N(4)	4185(1)	-1791(3)	4814(2)
N(5)	919(1)	223(2)	6761(1)

TABLE 2

Bond distances (Å) and angles (°), with standard deviations in parentheses, of the TCNQ moiety.

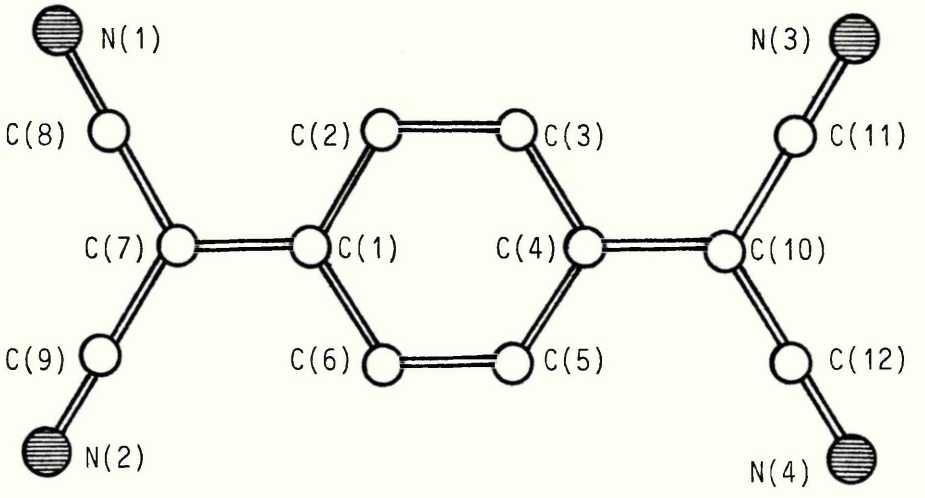

(a) Distances

C(1)--C(2)	1.427(2)	C(7)--C(8)	1.423(3)
C(1)--C(6)	1.419(2)	C(7)--C(9)	1.416(2)
C(1)--C(7)	1.411(2)	C(8)--N(1)	1.156(3)
C(2)--C(3)	1.363(2)	C(9)--N(2)	1.151(2)
C(3)--C(4)	1.427(2)	C(10)-C(11)	1.415(3)
C(4)--C(5)	1.421(2)	C(10)-C(12)	1.412(3)
C(4)--C(10)	1.419(2)	C(11)-N(3)	1.148(3)
C(5)--C(6)	1.370(2)	C(12)-N(4)	1.149(3)

(b) Angles

C(2)--C(1)--C(6)	117.5(1)	C(1)--C(7)--C(8)	121.3(2)
C(2)--C(1)--C(7)	120.3(1)	C(1)--C(7)--C(9)	123.4(2)
C(6)--C(1)--C(7)	122.1(1)	C(8)--C(7)--C(9)	115.1(2)
C(1)--C(2)--C(3)	121.3(2)	C(7)--C(8)--N(1)	179.4(2)
C(2)--C(3)--C(4)	121.1(2)	C(7)--C(9)--N(2)	177.5(2)
C(3)--C(4)--C(5)	117.7(1)	C(4)--C(10)-C(11)	121.7(2)
C(3)--C(4)--C(10)	121.0(2)	C(4)--C(10)-C(12)	121.1(2)
C(5)--C(4)--C(10)	121.3(2)	C(11)-C(10)-C(12)	117.0(2)
C(4)--C(5)--C(6)	121.0(2)	C(10)-C(11)-N(3)	179.4(2)
C(1)--C(6)--C(5)	121.4(2)	C(10)-C(12)-N(4)	179.3(2)

TABLE 3

Bond distances (Å) and angles (°), with the standard deviations in parentheses, of the DHPA dication.

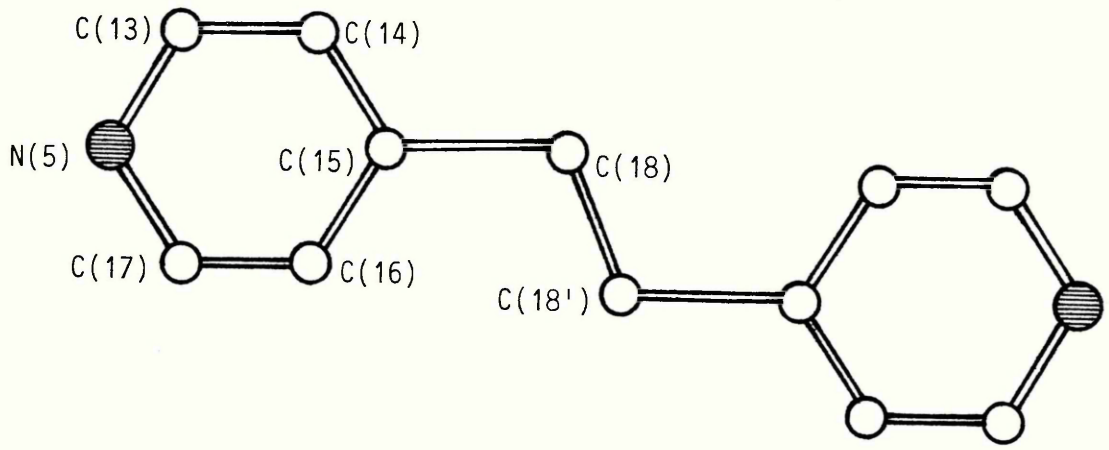

(a) Distances

C(13)-C(14)	1.363(3)	C(15)-C(18)	1.502(3)
C(13)-N(5)	1.333(3)	C(16)-C(17)	1.365(3)
C(14)-C(15)	1.392(3)	C(17)-N(5)	1.336(3)
C(15)-C(16)	1.389(2)	C(18)-C(18')	1.549(4)

(b) Angles

C(14)-C(13)-N(5)	119.7(2)	C(15)-C(16)-C(17)	120.3(2
C(13)-C(14)-C(15)	120.1(2)	C(16)-C(17)-N(5)	119.4(2
C(14)-C(15)-C(16)	117.9(2)	C(15)-C(18)-C(18')	
C(14)-C(15)-C(18)	121.8(2)	C(13)-N(5)--C(17)	122.6(2
C(16)-C(15)-C(18)	120.4(2)		

APPENDIX II: BASIC Programme used for Processing of Raw Dat

CONDAT I

```
10    OPEN 2,4,0
40    LETK = 0
50    DIM R(125)
60    DIM T(125)
72    PRINT "WHAT IS THE DATE"
73    INPUT F$
75    PRINT "WHAT IS THE RUN CODE"
76    INPUT C$
80    PRINT "ENTER THE ROOM TEMP RESISTANCE"
85    INPUT A
87    LET A = A * 1000
92    PRINT "ENTER - 1 WHEN FINISHED"
95    FOR L = 1 TO 125
97    PRINT "TEMP"
100   INPUT T(L)
105   IFT(L) = -1 THEN 130
107   PRINT "RESISTANCE"
110   INPUT R(L)
115   IF R(L) = -1 THEN 130
117   LET R(L)* 1000
120   LETK = K + 1
```

```
125  NEXT L
130  PRINT "ARE YOU READY FOR A PRINTOUT"
137  INPUT B$
140  IFB$ = "NO" THEN 210
145  PRINT "WHAT IS THE COMPOUND UNDER STUDY"
150  INPUT M$
154  GOSUB 250
155  PRINT #2, F$, "RESULTS FOR" M$, "CODE" C$, "RES (300K)
IS" A
156  PRINT #2, "TEMP(K)", "RES(OHMS)", "1000/T", "NORM COND",
"LOG  N.C."
180  FOR L = 1 TO K
185  LET S = A/R(L)
190  LET C = LOG(S)/LOG(10)
195  PRINT 2, T(L), R(L), 1000/T(L), S,C,
200  NEXT L
225  PRINT "END OF PROGRAM" : GOTO 700
240  REM:ALLOCATE PROBE PDS TO LINEAR V VS T PLOT
250  FORL = 1 TO K
260  IFT(L) = >0.248 THEN IFT(L) < = 18.560 GOTO 360
270  IFT(L) = >18.561 THEN IFT(L) < = 39.76 GOTO 370
280  IFT(L) = >39.77 THEN IFT(L) < 60.23 GOTO 380
290  IFT(L) = >60.231 THEN IFTL(L) < = 80.27 GOTO 390
300  IFT(L) = >80.271 THEN IFT(L) < = 100 GOTO 400
310  IFT(L) = >100.001 THEN IFTL(L) < = 119.4 GOTO 410
320  IFT(L) = >119.401 THEN IFT(L) > = 138.5 GOTO 420
330  IFT(L) = >139.501 THEN IFT(L) > = 153.933 GOTO 430
340  PRINT "OUT OF RANGES" T(L)
```

```
350  NEXT L
355  RETURN
357  REM:CALCULATE TEMPERATURES FROM PROBE PDS.
360  LET T(L) = T(L)* 2.2936 + 30.6312 : GOTO 350
370  LET T(L) = T(L)* 2.3587 + 29.4262 : GOTO 350
380  LET T(L) = T(L)* 2.5 + 22.525 : GOTO 350
390  LET T(L) = T(L)* 2.439 + 26.2988 : GOTO 350
400  LET T(L) = T(L)* 2.5394 + 19.264 : GOTO 350
410  LET T(L) = T(L)* 2.5773+ 15.468 : GOTO 350
420  LET T(L) = T(L)* 2.6178 + 10.6437 : GOTO 350
430  LET T(L) = T(L)* 2.6568 + 5.2404 : GOTO 350
700  END
```

APPENDIX III: Abbreviations and Full Names of Donors and Acceptors Referred to in the Text

DONORS

Ad	Acridinium
BAd	Benzacridinium
BEDt	Bis-ethylenedithiolo-tetrathiafulvalene
DBuPE	1,2-Bis(N-n butyl-4-pyridinium)ethylene
DEPA	1,2-Bis(N-ethyl-4-pyridinium)ethane
DEPE	1,2-Bis(N-ethyl-4-pyridinium)ethylene
DEPP	1,3-Bis(N-n propyl-4-pyridinium)propane
DHPA	1,2-Bis(4-pyridinium)ethane
DHPE	1,2-Bis(4-pyridinium)ethylene
DMBP	N,N'-dimethyl-4-bipyridinium
DMM	dimethylmorpholinium
DMPA	1,2-Bis(N-methyl-4-pyridinium)ethane
DMPE	1,2-Bis(N-methyl-4-pyridinium)ethylene
DMPP	1,3-Bis(N-methyl-4-pyridinium)propane
DPPE	1,2-Bis(N-n propyl-4-pyridinium)ethylene
DPPP	1,3-Bis(N-n propyl-4-pyridinium)propane
Et_2Ph_2P	diethyldiphenylphosphonium
HMTSF	hexamethylene tetraselenafulvalene
HMTTF	hexamethylene tetrathiafulvalene
MEM	methylethylmorpholinium
Me_2Ph_2P	dimethyldiphenylphosphonium
Morph.	morpholinium
NEQn	N-ethylquinolinium
NMAd	N-methylacridinium
NMePy	N-methylpyridinium
NMP	N-methylphenazinium
NMQn	N-methylquinolinium
NPrQn	N-propylquinolinium
Qn	quinolinium
TEA	triethylammonium
TMA	trimethylammonium
TMPD	N,N,N',N'-tetramethyl-p-phenylenediamine
TMTSF	tetramethyltetraselenafulvalene
TMTTF	tetramethyltetrathiafulvalene
TSF	tetraselenafulvalene
TTF	tetrathiafulvalene
t-TTF	trimethylene-tetrathiafulvalene
MeEt-t-TTF	methyl-ethyl-trimethylene-tetrathiafulvalene
TTT	tetrathiatetracene

ACCEPTORS

DMTCNQ	dimethyltetracyano-p-quinodimethane
TCNQ	tetracyano-p-quinodimethane
$TCNQF_4$	tetrafluorotetracyano-p-quinodimethane

APPENDIX IV: Statement of Postgraduate Studies Undertaken

The Author Has;

(a) Completed a computing course for BASIC programming

(b)Participated in research colloquia and conferences and has presented a colloquium on his own work

(c) Attended post-graduate solid state lectures

(d) For a full reading list see references on pages 208-220 in main text